Unravelling cylindromas: A molecular dissection of CYLD defective tumours.

Neil RAJAN

A 069190780

Thesis submitted to the University of Newcastle upon Tyne for the degree of Doctor of Philosophy

March 2011

Institute of Human Genetics

University of Newcastle upon Tyne

Acknowledgements

This work is dedicated to the families with *CYLD* mutations, who generously donated tissue samples for research.

Funding was obtained from the North East Skin Research fund, the Newcastle Hospital Trustees, Breakthrough Breast Cancer Research and the Medical Research Council.

The transition from the clinic to the lab was made easier by members of the Crucible, Sieber-Blum, Peters and Ashworth labs. I am grateful to my supervisors and mentors for the interesting discussions and guidance. In particular, James Langtry for dermatological and surgical training, John Burn and Alison Trainer for clinical genetics training, Maya Sieber-Blum for molecular and laboratory training and Alan Ashworth for vision and project direction. I am indebted to my colleagues at the Institute of Human Genetics, Dermatological Sciences, and Breakthrough Breast Cancer Research for helpful discussions and protocols.

Finally, I am grateful for the encouragement and support of friends and family, especially Annie and Oliver.

Declaration

I performed the work described in this thesis, with the exception of the array CGH assay and SNP assay and analysis, for which I am indebted to Alan Mackay's and Charles Mein's labs respectively.

Abstract

Patients with germline mutations in the tumour suppressor gene *CYLD* develop multiple cutaneous tumours on the head and neck; historically this has been termed “turban tumour” syndrome. Cylindromas and spiradenomas, hair follicle related tumours seen in this syndrome, cause significant clinical morbidity. Here we characterise the clinical phenotype of these patients, utilising tumour mapping to determine the location of tumours in mutation carriers from two large pedigrees. We demonstrate the disease often affects sites outwith the head and neck, and that androgen stimulated hair follicles are particularly vulnerable to tumour formation. The impact of this disease is severe, with 1 in 4 carriers of this gene undergoing complete scalp removal. To improve this outcome, we performed whole genome profiling of CYLD defective tumours, characterising genomic and transcriptomic changes to determine targetable signalling pathways. High resolution analysis using whole genome array based comparative genomic hybridisation and single nucleotide polymorphism analysis suggest that loss of heterozygosity at the *CYLD* locus may be the only change required for tumour phenotype. Gene expression profiling highlighted transcriptomic similarity between cylindromas and spiradenomas. Three-dimensional reconstruction *in silico* from serial sections of tumours demonstrated contiguous growth between cylindromas and spiradenomas, in support of this finding. In both tumour types, dysregulated tropomyosin receptor kinase (TRK) signalling was found. Consistent with this, was the finding that TRKB and TRKC protein was overexpressed selectively in the tumour samples, demonstrated on a tissue microarray. Therapeutic utility of targeting this pathway was demonstrated by reduced viability of CYLD defective primary cell cultures in the presence of TRK inhibitors. These preliminary data support the use of TRK inhibitors as a therapeutic strategy in severely affected *CYLD* mutation carriers.

Prizes associated with this work

- Poster prize - Medical Research Society (London 2011).
- Highly commended prize 2010 MRC Max Perutz Science Writing Award (London 2010).
- Best oral presentation in the dermatopathology section at the British Association of Dermatologists meeting (Manchester 2010).
- Registrar's Prize for the best oral presentation by a trainee in dermatology at the British Society of Investigative Dermatology (Edinburgh 2010).
- Best oral presentation in the clinico-pathological cases section at the British Association of Dermatologists meeting (Glasgow 2009).

Publications associated with this work

Abstracts

- Rajan N, Burn J, Langtry JAA, Sieber-Blum M, Lord CJ, Ashworth A. Loss of organisation in CYLD defective tumours is associated with reduced DKK2 expression. *Br J Dermatol* 2011; **164**: 900-938.
- Rajan N, Elliott R, Lord CJ, Clewes O, Burn J, Sieber-Blum M, Ashworth A. Dysregulated tropomyosin receptor kinase (Trk) signalling in CYLD mutant tumours. *J Invest Dermatol* 2010; **130s2**: s76.
- Rajan N, Elliott R, Lord CJ, Burn J, Sieber-Blum M, Ashworth A Advances in the development of new therapies for CYLD mutation carriers: Targeting Trk. *J Med Genet* 2010;**47:** s26.
- Rajan N, Gillinder K, Lord C, Langtry JAA, Burn J, Ashworth A, Chaudhury B, Sieber-Blum M. Unravelling cylindromas: insights into appendageal tumour patterning from patients with truncating CYLD mutations. *Br J Dermatol* 2010; **163s1**: 90-100.
- Rajan N, Lord CJ, Clewes O, Burn J, Sieber-Blum M, Ashworth A. Dysregulated tropomyosin receptor kinase (Trk) signalling in CYLD $^{trunc/trunc}$ tumours. *Br J Dermatol* 2010; **163s1**: 8-11
- Rajan N, Bourn D, Roberts C, Langtry JAA, Burn J. A review of seven U.K. pedigrees with CYLD mutations: Clinical implications for mutation carriers. *Br J Dermatol* 2009; **161(s1**):13–20.
- Rajan N, Powell H, Langtry JAA, Carmichael A, Bourn D, Burn J. Two novel CYLD mutations associated with Brooke-Spiegler syndrome *Br J Dermatol* 2009; **161(s1**):21–69.
- N Rajan, JAA Langtry, P Chapman, A Trainer, J Burn. Familial cylindromatosis, Brooke-Spiegler syndrome and multiple famililal trichoepithiliomas: Tumour mapping of 26 patients with CYLD mutations suggest androgen stimulation may play a role in tumourigenesis. *J Invest Dermatol 2008;* **128(s1):**s34.

Papers

- Rajan N, Burn J, Langtry J, Sieber-Blum M, Lord CJ, Ashworth A. Loss of tumour patterning in a cutaneous appendageal tumour syndrome is associated with loss of DKK2 expression. *J Pathol.* 2011; **224**: 309-21.
- Rajan N, Elliott R, Clewes O, Mackay A, Reis-Filho JS, Burn J, Langtry J, Sieber-Blum M, Lord CJ, Ashworth A. Dysregulated TRK Signalling is a Therapeutic Target in CYLD Defective Tumours. *Oncogene* 2011 May 9 (Epub ahead of print).
- Rajan N, Langtry JAA, Ashworth A, Roberts C, Chapman P, Burn J, Trainer AH. Tumor mapping in two large multigeneration families with *CYLD* mutations: Implications for patient management and tumor induction*. Arch Dermatol*. 2009; **145**: 1277-84.
- Rajan N, Trainer AH, Burn J, Langtry JAA. Familial Cylindromatosis and Brooke-Spiegler Syndrome: A review of current therapeutic approaches and the surgical challenges posed by two affected families. *Derm Surg* 2009; **35**: 845-52.

Abbreviations

3D	Three dimensional
Ab	Antibody
aCGH	Array based comparative genomic hybridization
alpha 1 ACT	Alpha 1 anti chymotrypsin
AT	Annealing temperature
ATP	Adenosine triphosphate
BAC	Bacterial artificial chromosome
BCC	Basal cell carcinoma
BCL	B-cell lymphoma protein
BDNF	Brain derived neurotrophic factor
BPE	Bovine pituitary extract
BSS	Brooke-Spiegler syndrome
Cd	Cluster of differentiation
cDNA	Complementary DNA
CEA	Carcinoembryonic antigen
CK	Cytokeratin
CPCC	Cylindroma primary cell culture
Ct	Cycle threshold
CTNNB1	Beta-catenin
CYLD	Cylindromatosis tumour suppressor gene
DAP	DASL assay pool
DAPI	4',6-diamidino-2-phenylindole
DASL	cDna-mediated Annealing, Selection, Extension, and Ligation
DMBA	7,12-Dimethylbenz(a)anthracene
DKK	Dickoppf
DMEM	Dulbecco's modified eagle medium
DMSO	Dimethyl sulfoxide
DNA	Deoxyribonucleic acid
dNTPs	Deoxynucleotide triphosphates
DSO	downstream-specific oligonucleotide
EDA1	Ectodysplasin-A
EDAR	Ectodysplasin-A receptor
EDRADD	Ectodysplasin-A receptor-associated adapter
EDTA	Ethylenediaminetetraacetic acid
ERK	Extracellular signal-regulated kinase
FC	Familial cylindromatosis
FIBRO	Fibroblast primary cell culture
FOXE1	Forkhead box protein E1

GFP	Green fluorescent protein
GLI	Glioblastoma protein
H+E	Haematoxylin and eosin
HeLA	Cercival cancer cell line
HEK293	Human embryonic kidney cell line
HEPES	4-(2-hydroxyethyl)-1-piperazineethanesulfonic acid
HMFG	Human milk fat globulin
IKB	Inhibitor of kappa beta
IKK	IKB kinase
JNK	C-Jun N-terminal kinase
K63	Lysine 63
KSFM	Keratinocyte serum free media
LB	Lysogeny broth
LEF1	Lymphoid enhancer-binding factor-1
LNCap	Androgen-sensitive human prostate adenocarcinoma cells
LOH	Loss of heterozygosity
MFT	Multiple familial trichoepitheliomas
NBCCS	Naevoid basal cell carcinoma syndrome
NEMO	Nf-kappa-b essential modulator
NFkB	Nuclear factor kappa-light-chain-enhancer of activated B cell
NGF	Nerve growth factor
NT3	Neurotrophin 3
NTRK	Neurotrophic tyrosine kinase
OCT	Optimal cutting temperature compound
PAGE	Polyacrylamide gel electrophoresis
PBS	Phosphate buffered saline
PC3	Prostate cancer cell line
PCC	Primary cell culture
PCR	Polymerase chain reaction
pERK	Phosphorylated ERK
PFA	Paraformaldehyde
PMSF	Phenylmethylsulfonyl fluoride
Poly-HEMA	Poly(2-hydroxyethyl methacrylate)
RNA	Ribonucleic acid
SDS	Sodium dodecyl sulfate
SH3	Src – homology domain 3
SHH	Sonic hedgehog
SNP	Single nucleotide polymorphism
TBST	Tris-buffered saline tween-20
TNF	Tumour necrosis factor
TPA	tetradecanoyl phorbol acetate,
TRAF	TNF receptor-associated factor

TRK	Tropomyosin receptor kinase
USO	Upstream-specific oligonucleotide
UVR	Ultraviolet radiation

List of Tables

List of Figures

1 Chapter 1: Introduction

1.1 Background

Cylindroma tumours represent an intriguing model to explore cutaneous tumour biology. Patients who inherit a tendency to develop multiple cylindroma tumours have been described since 1842 by Ancell and are termed to have familial cylindromatosis (FC- OMIM 132700) (Welch, Wells et al. 1968). These tumours have a predisposition to the face and scalp, and surgery often leaves disfiguring scars. In some patients, when the tumours form a confluent mass termed a “turban tumour” the entire scalp must be removed (O'Blenes, Lee et al. 2010).

Figure 1 Multiple cylindromas form a confluent mass on the scalp.

The locus of the gene that is mutated in patients with FC was identified by classical linkage analysis to chromosome 16q (Biggs, Wooster et al. 1995). Five years later, the gene, termed *CYLD*, was found by positional cloning and sequenced (Bignell, Warren et al. 2000).

CYLD was subsequently shown to encode an ubiquitin hydrolase enzyme that negatively regulated the NFκB pathway (Trompouki, Hatzivassiliou et al. 2003). It was postulated that constitutively activated NFκB signalling, recognised to be important in proliferation and apoptosis resistance, was likely to confer the tumour phenotype seen in CYLD defective tumours (Brummelkamp, Nijman et al. 2003; Kovalenko, Chable-Bessia et al. 2003; Trompouki, Hatzivassiliou et al. 2003). Non-surgical treatments became a possibility when CYLD was found to negatively regulate TRAF2 and TRAF6, members of the NFκB signalling pathway that were upstream of aspirin's point of action at IKK (Yin, Yamamoto et al. 1998). Such medical treatments are an attractive, unexplored avenue, particularly as the tumours are easily accessible, allowing for topical or intralesional delivery of these agents with potentially fewer systemic side-effects. However, a clinical trial with topical salicylic acid only demonstrated a modest result in a small number of tumours (Oosterkamp, Neering et al. 2006), prompting a search for alternative therapeutic agents.

Inspired by the prospect of non-surgical treatments, an unbiased whole genome approach was adopted for this work, characterising the genomic and transcriptomic changes seen in "CYLD defective" tumours. This was feasible as I had access to fresh tumour tissue, collected from *CYLD* mutation carriers undergoing routine surgery to control tumour burden. Here, we describe the results of a detailed molecular dissection of this intriguing tumour syndrome, highlighting novel targetable pathways and insights into non-melanoma skin cancer.

1.2 An overview of hair follicle biology

Patients with FC develop tumours at hair bearing sites, and the hair follicle and its related structures are thought to contain the cell of origin of these tumours (Massoumi, Podda et al. 2006). The hair follicle and its associated structures represent a mini organ within the skin (Figure 2).

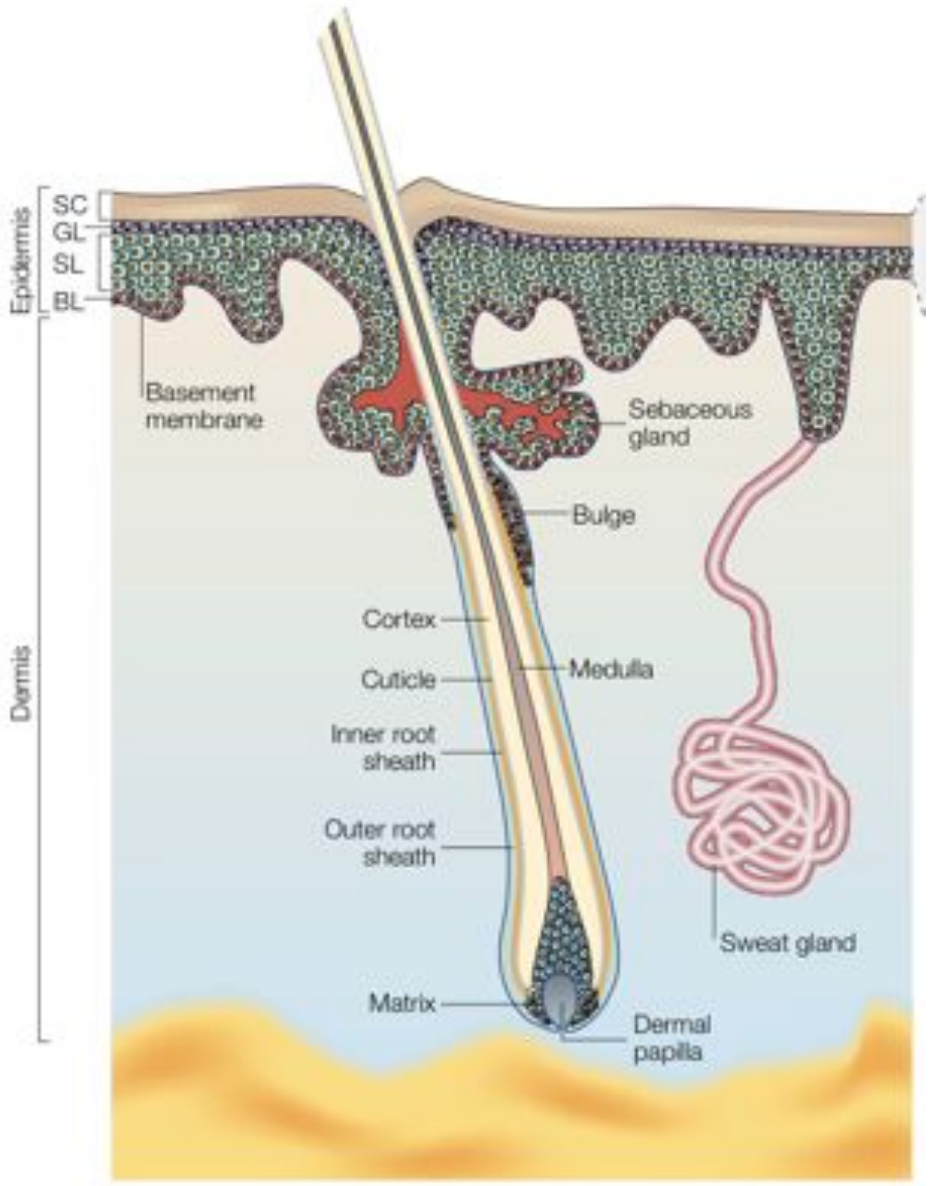

Figure 2 The hair follicle and related structures.

Key: SC – stratum corneum, GL – granular layer, SL, spinous layer, BL – basal layer. The hair follicle, originating from the epidermis, consists of several layers, as indicated in the diagram. At the bottom of the follicle is the hair bulb, made from proliferating matrix cells. The dermal component of the hair follicle is the dermal papilla, which consists of specialized mesenchymal cellssurrounded by hair matrix cells. Adapted from Fuchs et al.(Fuchs and Raghavan 2002)

The components of this organ include: the hair follicle, the sebaceous gland (responsible for sebum production) and the apocrine gland (responsible for scent, found at particular body sites such as the axilla). The eccrine gland is distinct but found closely associated with hairs, and is important for thermoregulation. Aspects of hair biology pertinent to the study of CYLD defective tumours include hair development, the cyclic nature of hair follicle growth and the maintenance of this structure by stem cell compartments.

1.2.1 Hair development

Murine hair biology parallels human hair biology and has been useful for understanding the contributory effects of different structures and genes towards hair development (Schmidt-Ullrich and Paus 2005). Hair structures are formed following interaction of ectodermal (epidermis) and mesenchymal (dermis) layers. The first sign of embryonic hair formation is the development of a placode at the interface of these two layers. The epidermis at this site is then committed to the formation of a hair follicle. Using transgenic mice, the details of the interplay of complex signalling networks between dermis and epidermis that commit these cells towards a hair follicle fate have begun to be understood (Figure 3). Central to the formation of a placode is Wnt signalling, highlighted by the lack of hairs demonstrated in a mouse overexpressing Wnt inhibitor DKK1 (Andl, Reddy et al. 2002). Another key pathway, NFκB signalling, is thought to influence the type of mouse hair seen. Mice that have mutations in *Eda*, *Edar* and *Edaradd*, important in NFκB signalling, have been shown to develop a reduced number of hairs, and only one type of hair, awl hair, is seen (Schmidt-Ullrich, Aebischer et al. 2001).

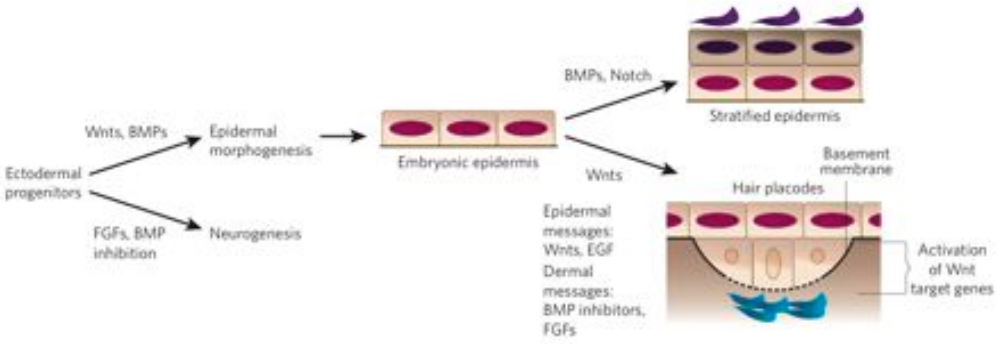

Figure 3 Hair follicle specification of epidermal fate. Epidermal cells that are responsive to Wnt signalling in the embryonic epidermis respond to dermal BMP inhibitory signals to form a hair placode.

Additional dermal messages further instruct the placode to form the hair follicle. Adapted from Fuchs *et al.* (Fuchs 2007).

Following the development of the placode, the mesenchymal dermal papilla is then encapsulated by ectodermal hair follicle. This structure, termed a peg, grows to invade the dermis, a process dependent on SHH signalling. The hair subsequently matures and different components including layers of the hair shaft, sebaceous glands and innervation are then seen to form.

1.2.2 The hair cycle

After the follicle is formed, the hair cycles through phases of growth (anagen), rest (catagen), shedding (telogen) and renewal, mimicking some of the processes that occur during embryogenesis (Figure 4). In humans, hairs from different body sites have intrinsic mechanisms that influence the length of each phase of this cycle, with the regulation of duration of anagen being key for hair length. These mechanisms have been shown to be maintained independent of site by respective hair follicles following hair transplantation experiments in humans (Orentreich 1959).

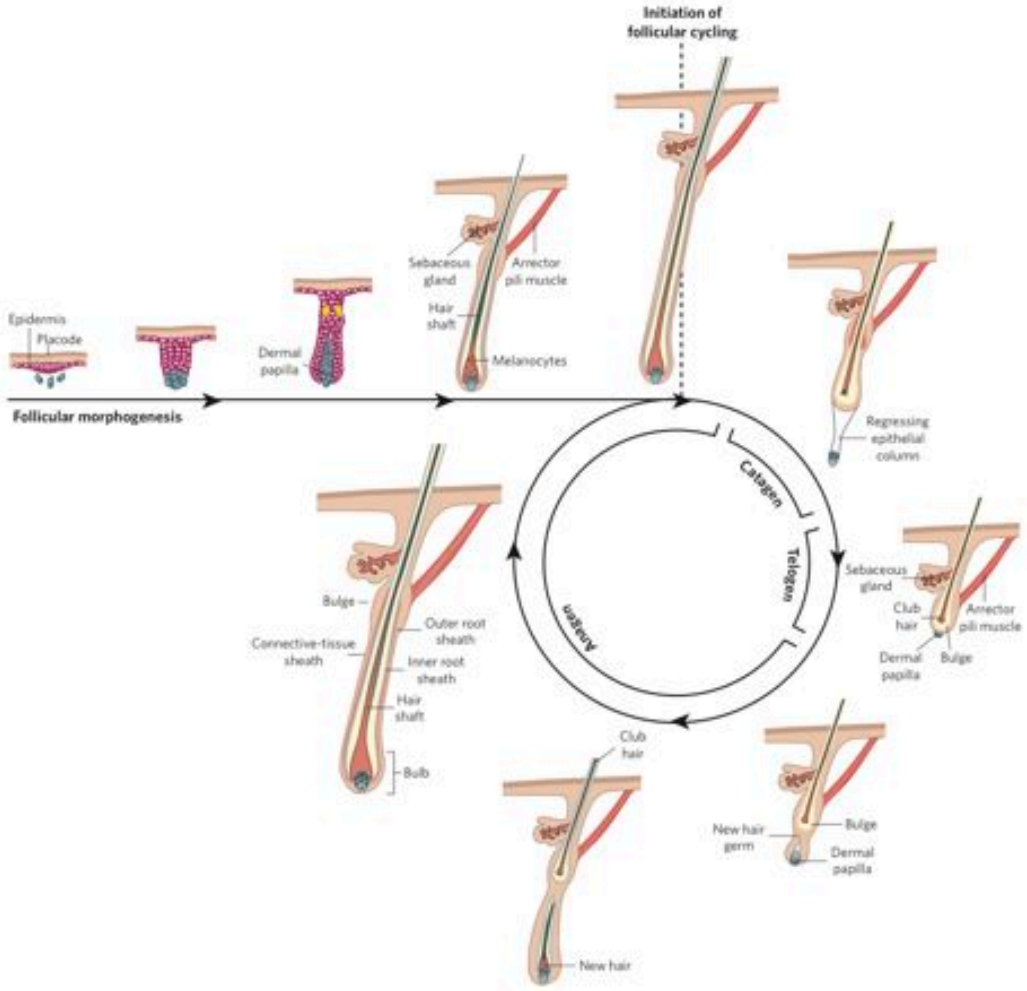

Figure 4 The hair cycle. The hair follicle is a cycling structure in adult life, undergoing phases of growth (anagen), rest (catagen) and shedding (telogen). Adapted from Fuchs *et al* (Fuchs 2007).

Recent data has highlighted the role of genes (*CLOCK and BMAL1*) that are influenced by diurnal variation may influence the length of these cycles, and hence account for seasonal variations in hair growth (Lin, Kumar et al. 2009).

1.2.3 Hair follicle stem cells

In adult life, compartments of stem cells maintain the hair follicle. Stem cell compartments of slow cycling cells that both self renew and give rise to transit amplifying cells are of interest in skin cancer as they are a prime site for accumulating mutations that may be responsible for tumour formation (Perez-Losada and Balmain 2003). Cells from the hair follicle bulge in mice are thought to be the reservoir of stem cells that contribute to the new transit amplifying cells needed for hair growth. These cells interact with the dermal

papilla to form a new hair follicle. In mouse whiskers, migration of stem cells along the outer root sheath to the papilla are thought to facilitate the formation of a new hair, and hence stem cells can also be demonstrated at this site (Oshima, Rochat et al. 2001). The bulge is likely to contain a mixture of multipotent cell types, with for example, cells of neural crest origin demonstrated at this site (Hu, Zhang et al. 2006). Recent wound healing experiments using *LGR6* transgenic mice for fate mapping, demonstrate the formation of labelled new hairs and all the structures in the skin from a region above the hair bulge, highlighting this as the niche for the most primitive stem cells (Snippert, Haegebarth et al. 2010). Stem cell compartments are thought to also exist in sebaceous glands, following retroviral mediated *lacz* labelling and lineage tracing experiments in mice (Ghazizadeh and Taichman 2001).

1.2.4 Differential sensitivity of human hairs to hormonal stimulation

In humans, hairs at different body sites demonstrate a growth response following puberty. Humans are thought to be, in an ontological sense, nude apes, and are distinct in the acquisition of secondary sexual hair at this time. The change from fine vellus hair to coarse hair as well as increased length is thought to be mediated by androgen stimulation, and highlights the heterogeneity of hair types seen in humans (Randall 2008). Furthermore, there is the paradoxical observation that androgen stimulation is important in hair loss, as seen in male pattern balding, highlighting the differential effect of androgen stimulation (Randall, Hibberts et al. 2000). Apart from hair growth, hair follicles at some body sites become inflamed at puberty, with the development of acne. This can include the chest and back in addition to the face. Acne and the sites of development of secondary sexual hair are hence markers of androgen sensitive hair follicles

In summary, human hair formation and growth is complex. Perturbation of the homeostatic mechanisms that maintain normal growth may result in tumour formation. CYLD defective tumours represent an interesting model to gain insight into molecular changes seen in the putative context of hair follicle cells.

1.3 Clinical and histopathological features of CYLD defective tumours

1.3.1 Clinical features

FC is an autosomal dominant predisposition to multiple tumours thought to derive from the hair follicle (Massoumi, Podda et al. 2006). Cylindromas are not exclusively seen in FC however (Figure 5). Brooke and Fordyce described a distinct, inherited disfiguring disease, predominantly resulting in nasolabial and facial hair follicle tumours – multiple familial trichoepitheliomas, with which cylindromas are sometimes seen (MFT- OMIM 601606) (Welch, Wells et al. 1968) . An overlap between FC, where cylindromas predominate and MFT, where trichoepitheliomas are the main tumour, occurs in Brooke-Spiegler syndrome (BSS- OMIM 605041). Patients with BSS may also develop other hair follicle related tumors such as eccrine spiradenomas, syringomas and milia. The common finding of cylindroma tumours in all three syndromes was recently corroborated by detection of germ-line mutations in *CYLD* in all three conditions (Young, Kellermayer et al. 2006). These data suggest that the three recognised inherited tumour syndromes in which cylindromas are seen may represent a phenotypic spectrum (Figure 5).

The majority of tumours in seen in *CYLD* mutation carriers are on the head and neck, however some are seen on the back and the pubic region (Rajan, Langtry et al. 2009). The tumours vary in size, the smallest being approximately a centimeter in diameter, and the largest between 10-15 centimeters in diameter. The three commonest CYLD defective tumours seen are cylindromas, spiradenomas and trichoepitheliomas. Cylindromas are typically pink nodules often found in the scalp. They may have telangiectatic vessels overlying them and are often slow growing tumours. Trichoepitheliomas are small skin coloured (usually 2-5mm) papules commonly seen on the nose or upper lip. Eccrine spiradenomas have a dusky blue appearance, particularly if the overlying skin is atrophic. It is intriguing that all three tumour phenotypes can arise in the same patient, as are the processes that may influence the presentation of the different tumour phenotypes.

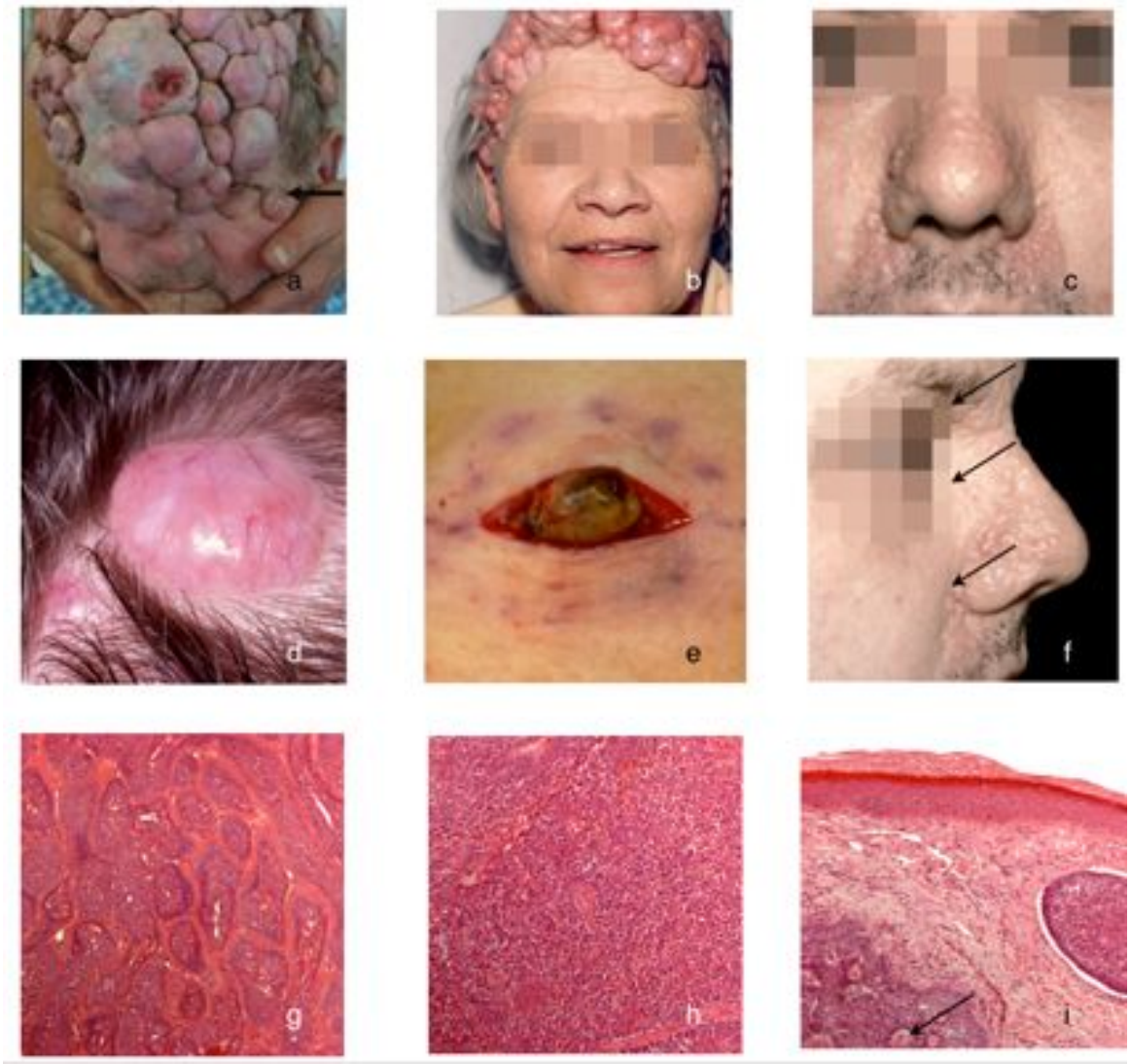

Figure 5 Clinical and histological features in CYLD mutation carriers.
Exemplary cases of (a) familial cylindromatosis, (b) Brooke-Spiegler syndrome and (c) multiple familial trichoepitheliomas. (d) Cylindroma tumour, (e) Spiradenoma at surgery and (f) trichoepitheliomas (arrowed). Haematoxylin and eosin staining of (g) cylindroma tumour displaying classical “cylinder shaped” islands of cells, separated by abnormal basement membranes. (h) Diffuse sheet of basophilic cells as seen in spiradenoma. (i) Two islands of trichoepithelioma tumour, with early abortive hair cysts (arrowed)

Apart from the disfiguring appearance these tumours have, they can be highly symptomatic. Larger tumours, tumours at pressure sites, and tumours that are subject to repeated trauma can ulcerate and bleed. Eccrine spiradenomas are typically painful tumours, and the pain associated with this is not well reported in the literature (Kazakov, Soukup et al. 2005). Occlusion

of the external auditory canal by tumours can cause conductive hearing loss, a favoured site for trichoepitheliomas and cylindromas (Wolf, Gluckman et al. 1985).

Beyond the skin, there is an association between patients with inherited cylindromas and salivary gland adenocarcinoma, which shares remarkable histological similarity (Jungehülsing, Wagner et al. 1999). Isolated reports exist of breast carcinoma (Sandbank and Bashan 1978) and lung cylindroma (Vernon, Olsen et al. 1988) in patients with MFT and BSS respectively. It would appear that the patients are not otherwise predisposed to developing common cancers, suggesting that the expression of CYLD as a tumour suppressor gene is crucial at the hair follicle. Malignant change of cylindromas and eccrine spiradenomas are reported and metastasis described, but is unusual despite the profuse number of lesions, suggesting genomic stability in these tumours (Gerretsen, van der Putte et al. 1993; Volter, Baier et al. 2002).

1.3.2 Histological features

Cylindromas, spiradenomas and trichoepitheliomas are histologically distinct (Figure 5 g-i). Cylindromas are so called, as the histological arrangement of the tumour cells is reminiscent of multiple stacked cylinders seen in cross section. Peripheral cells are basophillic and are arranged in a palisading fashion, whilst central cells in these islands are paler and larger. Each island is surrounded by a thick hyaline basal membrane. In between the islands of cylindroma, thin bands of stroma are sometimes seen. Occasional, ductal structures are seen in the central areas of cylindroma. Immunohistochemical analysis has demonstrated the presence of different cytokeratins in these distinct areas (Meybehm and Fischer 1997). These features are summarised in Figure 6. Cylindromas have been shown to express cytokeratins relating to the hair follicle, including cytokeratin 6 and 14. Certain cytokeratins, seen in eccrine ducts including cytokeratin 17 and 18 have also been noted. Some authors demonstrate malformed eccrine ducts containing foci of cylindroma and spiradenoma tumour, suggesting that these structures may contain the cell of origin of these tumours (Meybehm and Fischer 1997). The presence of keratins associated with these different structures, prompted debate as to the true structure of origin of cylindromas. Recent data demonstrating CYLD

expression in the IRS of the hair follicle, has swayed the debate back to a pluripotent cell in the hair follicle (Massoumi, Podda et al. 2006). Apart from distinct cytokeratins profiles, collagen deposition is disordered. The thick hyaline basal membrane has been shown to be rich in collagen 4, 6 and 7. There is also increased laminin 5 adjacent to the peripheral basophilic cells (Tunggal, Ravaux et al. 2002).

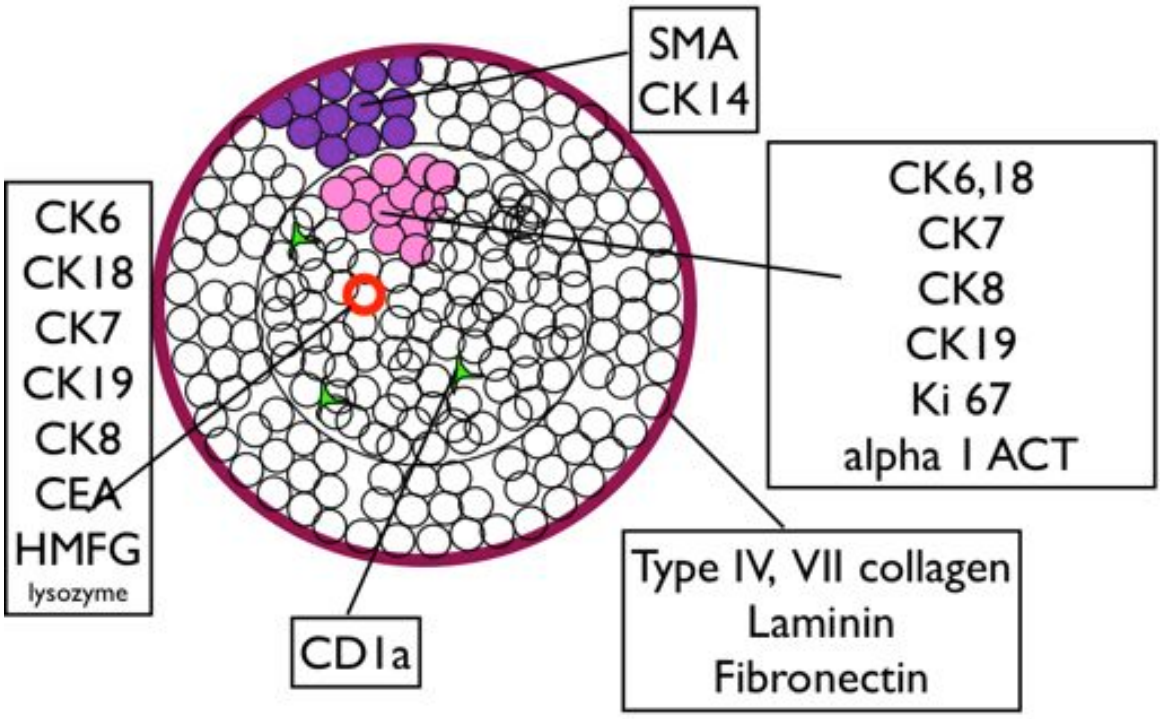

Figure 6 Immunohistochemical characterisation of cylindromas.
A cartoon representing one island of cylindroma cells, highlighting the patterns of immunohistochemical staining typically seen in different regions. Colour key : Magenta -hyaline membrane; Purple – peripheral palisading cells, ; Pink – central paler cells; Red – ductal structures; Green – dendritic cells.

Spiradenomas share similar cytokeratin markers as well as differentiation markers as cylindroma (Meybehm and Fischer 1997). Spiradenomas appear as basophilic nodules that are well circumscribed. Cells are arranged in sheets or are sometimes seen in a trabeculated pattern. Darker cells are seen in the periphery, with paler cells seen in the centre. Cystic structures are sometimes seen. The proliferative marker Ki67 is seen in the central, paler cells in both cylindroma and spiradenoma.

Cylindroma tumours have been reported to be more severe in women (Rajan, Langtry et al. 2009). Hormone receptors such as oestrogen and progesterone receptor staining has been performed and shown to be negative in 3 cases of cylindroma (Albores-Saavedra, Heard et al. 2005). Another group however demonstrated positivity of oestrogen receptor and progesterone receptor in 2 out of 3 cases of spiradenoma, as well as androgen receptor positivity in 1 out of 3 cases examined (Kariya, Moriya et al. 2005). These data are of limited use in interpreting the role of hormone stimulation in cylindroma growth due to the small numbers.

Immunohistochemical analysis has also highlighted other cells within the tumours. A finding in some spiradenomas is the presence of lymphocytes distributed among tumour cells (Kazakov, Thoma-Uszynski et al. 2009). Furthermore, dendritic cells have been seen within the tumour mass (Tellechea, Reis et al. 1995). The contribution of these cells to tumorigenesis remains to be clarified.

1.4 Genetic changes associated with development of CYLD defective tumours

The discovery of *CYLD* has allowed for assessment of correlation between human *CYLD* mutation type and clinical phenotype. *CYLD* maps to chromosome 16q21 and has a 56kb genomic footprint. The transcript comprises 20 exons of which the first 3 are non-coding, with a resulting cDNA transcript of 2.87Kb. Interestingly, the majority of the heterozygous germ-line mutations identified in cylindroma families have mapped to the 3' end of the gene. No significant correlation has been seen between mutation type and phenotype seen (Saggar, Chernoff et al. 2008). These mutations are typically single base changes or deletions, resulting in frameshift mutations, splice site mutations, nonsense or missense mutations. The majority of mutations result in premature termination codons and predict translated truncated proteins that have reduced catalytic activity (Saggar, Chernoff et al. 2008)(Figure 7).

CYLD defective tumours adhere to Knudson's two hit hypothesis (Knudson 1971) with loss of the wildtype allele of CYLD in 70% of tumours examined, in keeping with other tumour suppressor genes (Bignell, Warren et al. 2000; Leonard, Chaggar et al. 2001).

The consequence of loss of functional CYLD in this scenario may be informed by CYLD structure. The CYLD protein is 956 amino acids long and has a molecular weight of 107 kDa. A shorter isoform 953 amino acids long exists, and is a result of alternative splicing of exon 7. There are 4 identified functional motifs which include three cytoskeleton-associated-protein–glycine conserved (CAP-GLY) domains, a SH3-binding domain, four finger-like metal binding domains and two ubiquitin carboxy-terminal hydrolase (UCH) catalytic domains. The longer isoform is expressed ubiquitously, whilst the shorter isoform is expressed in all tissues except the kidney. In the hair follicle, CYLD is expressed in the inner root sheath (Massoumi, Podda et al. 2006).The ubiquitous expression contrasts with the largely restricted development of tumours to the skin. The mechanism behind such tissue tropism is intriguing and undetermined but has been described in other germline mutations in tumour suppressor genes such as *BRCA* (Monteiro 2003).

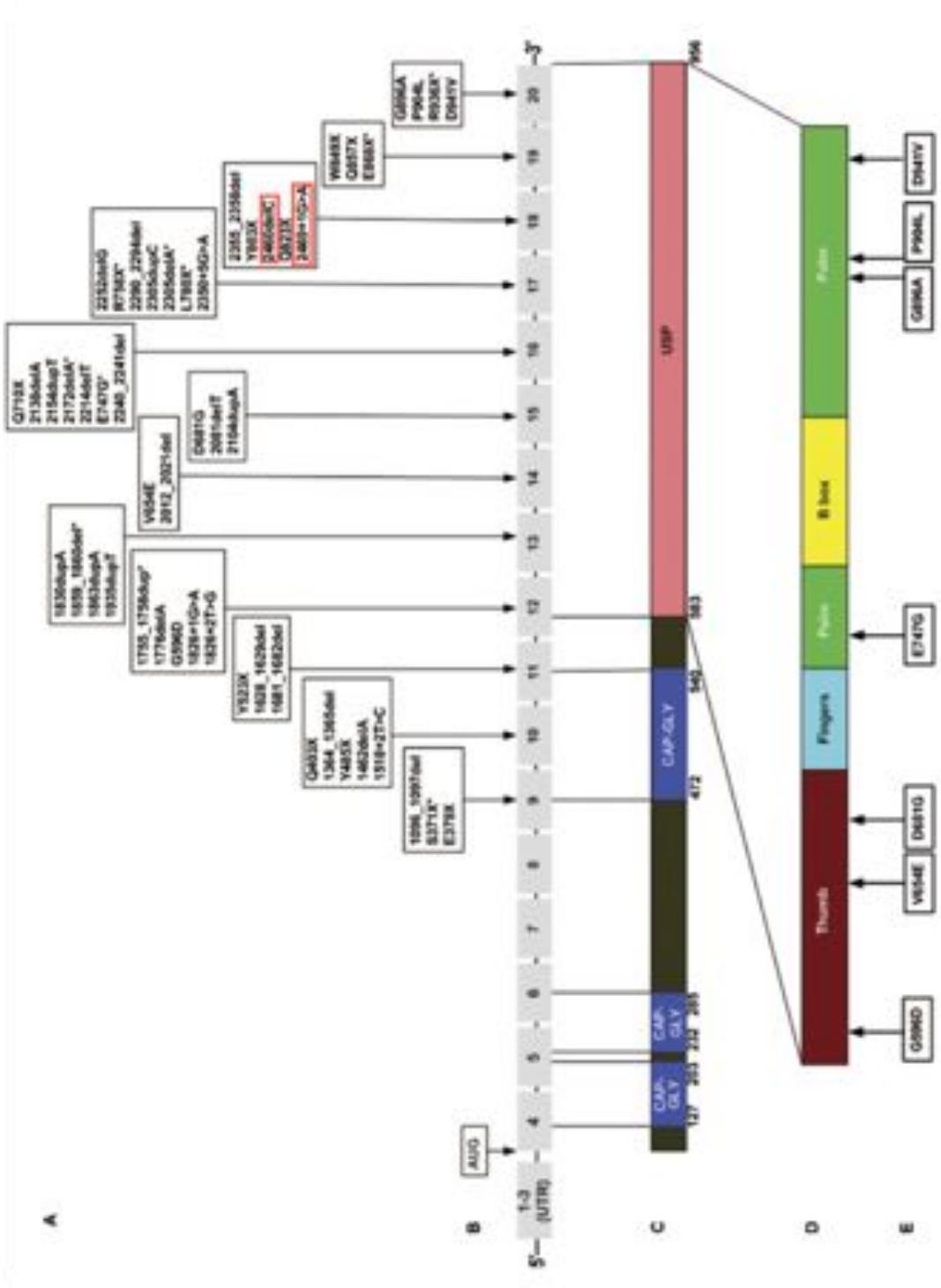

Figure 7 The mutation spectrum seen in *CYLD* mutation carriers.

CYLD encodes an ubiquitin hydrolase containing three CAP-GLY domains and a catalytic ubiquitin hydrolase domain, within which the human mutations cluster. Newcastle families are highlighted in red. Key A – Reported *CYLD* mutations, B – Exons, C- CYLD protein domains, D- CYLD ubiquitin hydrolase domain, E- missense mutations highlighted within the hydrolase domain. Adapted from Toro *et al. (Blake and Toro 2009)*

1.5 CYLD function

CYLD is an ubiquitin hydrolase enzyme. Polyubquitination is a post translation modification associated with targeting protein to the proteasome for degradation. This is catalysed by three enzymatic steps, involving ubiquitin activating enzyme (E1), ubiquitin conjugating enzyme (E2) and finally ubiquitin-protein ligase (E3) that links the ubiquitin polypeptide to the target protein (Chen 2005). Linkage of ubiquitin polypeptide by the lysine 48 residue has been shown to target a protein for proteasome degradation, whilst proteins tagged with polyubiquitin chains linked together by lysine 63 are involved in DNA repair and signal transduction (Kerscher, Felberbaum et al. 2006). Recently further work has suggested monoubiquitination to be responsible for endocytosis and transcriptional regulation (Chen 2005). Hydrolases such as CYLD have the opposite function. *CYLD* encodes an ubiquitin hydrolase that cleaves lysine 63 (K63) linked ubiquitin chains (Brummelkamp, Nijman et al. 2003; Kovalenko, Chable-Bessia et al. 2003; Trompouki, Hatzivassiliou et al. 2003). K63 tagging of proteins is increasingly recognised to have a role in cancer (Yang, Zhang et al. 2010). CYLD contains a B-box domain, which confers specificity for K63 linked ubiquitin chains, removal of which alters processes such as signal transduction and receptor endocytosis (Komander, Lord et al. 2008). Signalling pathways that are regulated by K63 ubiquitination are likely to be perturbed by the loss of functional CYLD, and are detailed below (Figure 8).

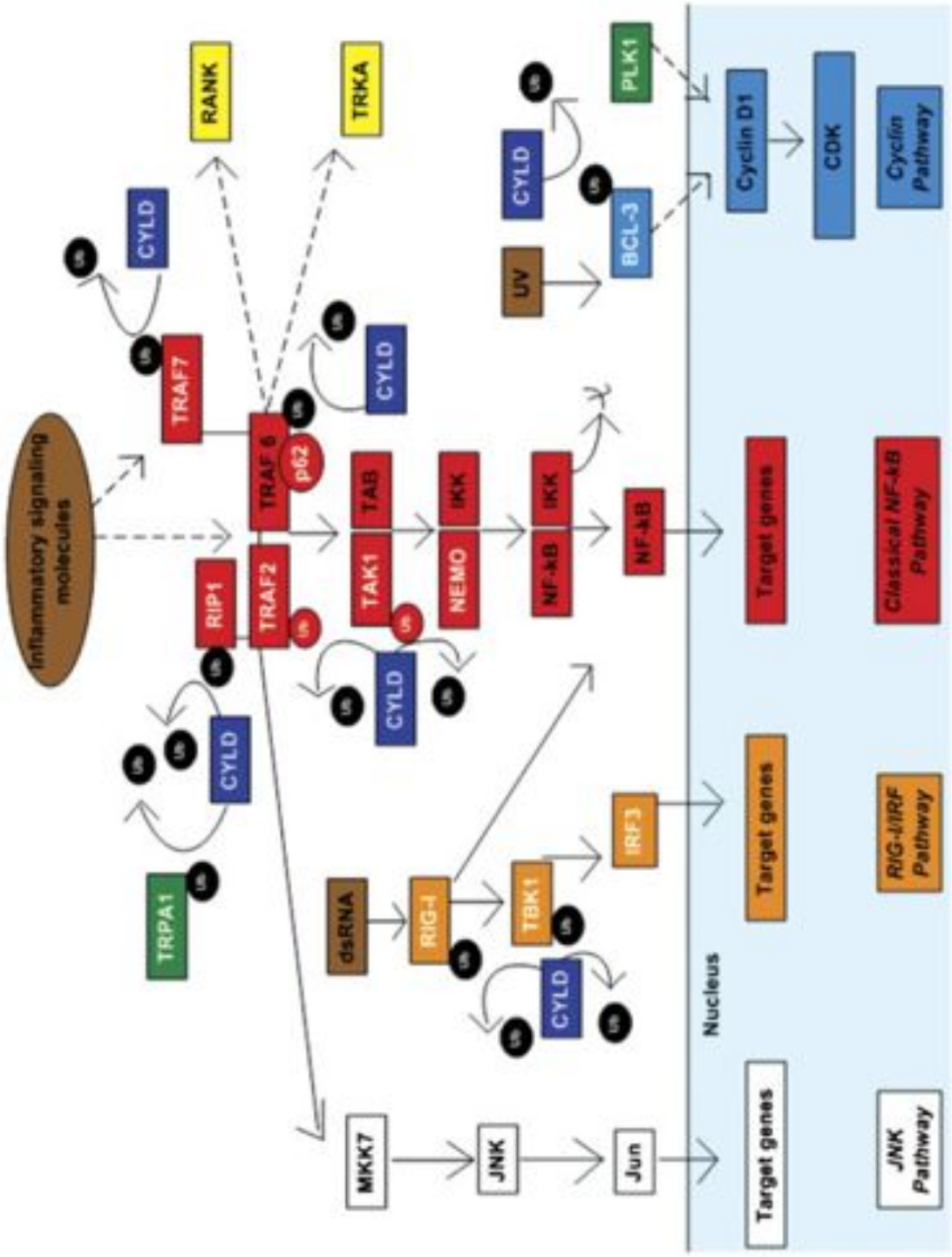

Figure 8 CYLD interacting partners and signalling pathways.

Key: CYLD – dark blue, K63 ubiquitin chains – black spheres, K48 ubiquitin chains – red spheres, straight arrows with solid lines – direct effect or interaction, straight arrows with dotted lines - indirect effect or incompletely characterised effect, curved solid arrows – deubiquitination. CYLD removes ubiquitin chains from proteins involved in several signalling pathways recognised to be important in cancer and immunity, such as NFkB, JNK, RIG-1/IRF and Cyclin pathways. (Adapted from Toro et al.(Blake and Toro 2009)

1.5.1 CYLD is a negative regulator of NFκB and JNK signalling

Loss of CYLD was discovered to result in upregulation NFκB in a RNA interference screen of ubiquitin hydrolase enzymes (Brummelkamp, Nijman et al. 2003). There are five members of the NFκB family, namely p65/RelA, Rel B, c-Rel, p52/p100 and p50/105. The importance of this pathway in tumourigenesis is highlighted by the discovery that many cancers exhibit disturbances in signalling pathways that activate NFκB. This may relate to its role in regulating genes that control inflammation, the immune response, or cell death (Chen and Goeddel 2002) .

NFκB is normally found in the cell cytoplasm, where it is kept inactive by inhibitor (IκB) proteins. Upon stimulation by proteins such as tumour-necrosis factor alpha (TNF-α) or interleukins, TNF receptors signal to intracellular adapter proteins known as TRAFs. These proteins have a variety of effects, one of which is to activate the IkB kinase (IKK) complex. IKK in turn phosphorylates IκB, leading to its polyubiquitination and degradation. NFκB is then released from its repressor and is free to move into the nucleus, where it transcribes a variety of genes that facilitate cell proliferation (Massoumi 2006). CYLD binds NEMO (IKKγ), a regulatory component of the IKK complex, and has been shown to deubiquitinate attached K63 polyubiquitin chains. CYLD also deubiquitinates TRAF2 and TRAF6, which is upstream of IKK. IKK activation is thus inhibited and NFκB remains in the cytoplasm (Kovalenko, Chable-Bessia et al. 2003). These results imply that under normal conditions CYLD is involved in downregulating NFκB signalling at a point upstream of IKK activation.

c-Jun NH_2 terminal kinase (JNK) is a member of the MAP kinase family, and is also activated following upstream activation of members of the TRAF family such as TRAF 2 and TRAF 6. The biological functions of JNK are diverse and include regulation of immune and inflammatory responses, cell growth, apoptosis and tumour formation (Manning and Davis 2003). Reiley *et al.* showed a preferential activation of JNK rather than IKK following knockdown by CYLD siRNA knockdown in HeLa cells and HEK293 cells stimulated with TNF (Reiley 2004), in contrast with previous overexpression studies (Kovalenko, Chable-Bessia et al. 2003). JNK activation is shown to be

negatively regulated by CYLD in response to CD40, TNF, IL-1β and LPS, whilst IKK activation is negatively regulated by CYLD only in response to specific stimulation with LPS and IL-1β rather than TNF. These data demonstrate the JNK signalling pathway as a downstream target of CYLD and suggest a receptor-dependent role of CYLD in regulating the IκB kinase pathway.

TAK1, a ubiquitin dependent kinase in the NFκB pathway, also interacts with CYLD. CYLD negatively regulates TAK1 mediated stimulation of IKK and hence activation of NFκB (Reiley, Jin et al. 2007). TAK1 also plays a role outwith the NFκB pathway, as it phosphorylates and activates MKK6 and MKK7, leading to the activation of p38 and JNK kinase pathways which may also contribute to pathogenesis (Reiley 2004; Liu, Xie et al. 2006).

CYLD has been shown to negatively regulate BCL3, preventing its nuclear entry where it forms a dimer with p50/p52, resulting in transcription of genes involved in proliferation including cyclin D1 (Massoumi 2006). NFκB in its active form is usually a heterodimer, with a transactivation and a transcription domain. Massoumi *et al.* demonstrated that a transcriptional co-activator, BCL3 could form a heterodimer with p52 (that contains a transactivation domain) to transcribe cell proliferation genes such as cyclin D1 (Massoumi 2006). CYLD was shown to co-localise with and negatively regulate BCL3, by retaining it in its inactive form in the cytoplasm. Massoumi *et al.* postulate that the different family members of NFκB modulate different effects, with p50/p65 being responsible for activation of immune responses and inflammation, whilst p52/BCL3 may be responsible for tumourigenesis.

1.5.2 CYLD is a negative regulator of Wnt signalling

CYLD has recently been shown to regulate Dishevelled, a member of the Wnt signalling pathway (Tauriello, Haegebarth et al. 2010). CYLD knockdown results in upregulation of canonical Wnt signalling, with nuclear beta-catenin demonstrated in cylindroma tumour cells. This data is of interest as Wnt signalling has been shown to be pathogenic in other hair follicle tumours, such as pilomatrixoma (Chan, Gat et al. 1999).

1.5.3 CYLD is a regulator in the cell cycle

Recent data has shown that CYLD plays a role in cells entering mitosis. CYLD was found as part of a siRNA screen that was designed to identify genes whose downregulation resulted in delayed mitotic entry or defective spindle checkpoint function (Stegmeier, Sowa et al. 2007). CYLD RNAi in HeLa produced cells that accumulated prior to mitosis and had normal interphase nuclear morphology. CYLD's deubiquitinating activity was shown to be important for regulation of cell cycle function, with a catalytically inactive CYLD mutant (C601A) failing to cause the premitotic arrest phenotype.
CYLD protein levels were also shown to vary in the cell cycle using lysate from synchronised cells. CYLD levels are low during G1, accumulate during S phase and subsequently degrade at the end of mitosis. This is characteristic of other substrates of the anaphase promoting complex such as PLK1 and Cyclin B. Interestingly, CYLD has been shown to interact with PLK1 , which was detected on a proteomics screen using a mass spectrophotometry approach. These data suggests CYLD may deubiquitinate a regulator of mitotic entry and may function in the same pathway as PLK1. This raises the paradox in this model that CYLD is a tumour promoter, rather than a tumour suppressor. The authors speculate that CYLD's role in the cell cycle may vary between tissue types and may be less critical in tissues where other deubiquitinating enzymes afford redundancy. Alternatively, they suggest the benign nature of cylindromas may be due to the cell cycle arrest resulting from the loss of CYLD compensating for the antiapoptotic constitutively activated NFKB also seen.
CYLD has been shown to inhibit Aurora-B, an important protein in the cell cycle, independently of its deubiquitinase activity. This kinase, which is important in cytokinesis and cell proliferation, has elevated activity in human cancer (Katayama, Brinkley et al. 2003). The authors speculate that the tumour- suppressing function of CYLD might be attributed at least partly to its inhibition of Aurora-B activity.

1.5.4 CYLD is a regulator of the innate immune response

Tight regulation of CYLD itself may be important in regulating the innate immune response. CYLD degradation has been shown to be mediated by

IKKγ phosphorylation. Lysates from a Jurkat cell line deficient in IKKγ (JM4.5.2), demonstrated the presence of a phosphorylated CYLD band, that was lost following over expression with IKKγ. Using CYLD mutants harbouring serial truncations, the site at which CYLD was phosphorylated was narrowed to between amino acids 420 and 446. Site-specific mutations of two serine pairs inhibited phosphorylation of CYLD within this region. CYLD phosphorylation by IKKγ inactivates it's ubiquitin hydrolase activity, which may serve as a mechanism that allows accumulation of ubiquitinated TRAF2 and hence sustained NFKB and JNK signalling in response to TNF and other infective stimuli.

Conversely in the context of attenuating the innate immune response to bacterial infections, CYLD is overexpressed as a consequence of peptidoglycan induced TLR2 signalling. An autoregulatory mechanism for the tight regulation of TLR stimulation is mediated via deubiquitination of TRAF6 and TRAF7, which results in negative regulation and attenuation of the NFκB/p38 mediated induction of immune and inflammatory responses (Yoshida, Jono et al. 2005). CYLD also regulates aspects of the host response to viral infections, by inhibition of the interferon regulatory factor 3 (IRF3) signalling pathway by acting as a negative regulator of retinoic acid-inducible gene 1 (RIG-1), a cytoplasmic viral RNA sensor (Friedman, O'Donnell et al. 2008) The putative mechanism is thought to be via CYLD deubiquitination of RIG-I and the IKK-related kinases IKKε/TBK1, kinases that phosphorylate IRF3.

1.5.5 Other putative targets and functions of CYLD

Beyond its role as tumour suppressor, CYLD also has roles in regulating immunity, microtubule assembly, spermatogenesis and calcium ion channel regulation (Reiley, Zhang et al. 2006; Stokes, Wakano et al. 2006; Stegmeier, Sowa et al. 2007; Wright, Reiley et al. 2007; Gao, Huo et al. 2008). CYLD has been shown to deubiquitinate K63 linked ubiquitin chains from TRKA, modulating TRKA receptor endocytosis and signalling (Geetha, Jiang et al. 2005). How perturbation of these pathways by loss of functional CYLD may contribute to tumour formation is not yet clear. The signalling pathways CYLD are involved with are summarised in Figure 8.In addition to knowledge of

CYLD function from *in vitro* models, transgenic animal models have been developed that highlight the tissues in which CYLD defects result in disease pathogenesis.

1.6 *CYLD* transgenic models

1.6.1 Murine models

To further define the function of this interesting tumour suppressor gene, mouse models have been developed, which show markedly different phenotypes. Crucially, none of them develop cylindromas, indicative of the fact that mouse hair follicle biology is not a perfect model to study human disease. Human and murine *CYLD* share 94% sequence homology at the transcript level however, and should elucidate CYLD function in humans. CYLD deficient mouse models with complete loss of CYLD expression do not develop spontaneous tumours, but show an increased susceptibility to cancer. This includes an increased susceptibility to chemical carcinogen induced cutaneous tumours (Massoumi 2006) as well as colorectal tumours following dextran sulphate induced colitis (Zhang, Stirling et al. 2006). Mice expressing truncated *CYLD* mutations that mimic human mutations in contrast, are not viable beyond a few hours after birth (Ermolaeva, Sebban et al. 2006; Trompouki, Tsagaratou et al. 2009). This difference in the two phenotypes is intriguing and suggests that further work is required to understand genotype-phenotype correlations. Intriguingly, a null mouse with a conditional deletion of exon 7 that abrogates the TRAF2/NEMO binding site is viable, suggesting a dominant negative effect mediated by this binding site may account for the perinatal lethal phenotype.

Apart from increased susceptibility to tumour formation, CYLD deficient mice (both complete knockouts and exon 7 deletions), demonstrate several immunological defects. These defects include the lack of maturation of T-cells, hyperproliferative T and B cell responses following stimulation and hyperplasia of the lymphoid tissue, summarised in Table 1.

CYLD TRANSGENIC MICE PHENOTYPES				
AUTHOR	**KO**	**GROSS PHENOTYPE**	**CANCER SUSCEPTIBILITY**	**IMMUNOLOGICAL FEATURES**
Massoumi	Exon 4 deletion	Null normal phenotype.	Mutation increases likelihood of squamous proliferation (not cancer *per se*), following DBMA and TPA treatment. Number of papillomas increases from wt, to het to null.	Not described
Reiley	Exon 1 deletion	No description of abnormalities of mouse phenotype.	Not described	Fewer mature CD4 and CD8 thymocytes and peripheral T cells. Hyperproliferative T cell responses, and abnormal B cell responses.
Zhang	Exon 2-3 deletion	Null - normal at birth. Changes in the organs of 10-month-old null mice, include marked lymphoid hyperplasia of the thymus and lymphoid inflammatory infiltrates in numerous tissues including the liver, spleen, lungs, and salivary glands.	Null mice were more susceptible to induced colonic inflammation and showed a dramatic increase in the incidence of tumors compared with controls in a colitis-associated cancer model.	Normal T cell ratios
Mosialos	Exon 9 deletion	Nulls die at P1, are smaller in size and have a kinked tail. Lungs are immature and fail to inflate.	Not described	Not described
Hovelmeyer	Exon 7 deletion	No gross changes; a short splice variant of *CYLD* is excessively expressed, and the mice are viable	Not described	A dramatic expansion of mature B lymphocyte populations in all peripheral lymphoid organs occurs in this strain.
Ashworth (unpublished data)	Exon 19	Nulls die at P1 from generalised inflammatory changes, are smaller in size and have subtle tail abnormalities. Increased numbers of hair follicles seen in nulls.	Hets develop liver tumours after 6 months.	Not described
Courtois	Truncated *CYLD* knockin	Perinatal lethal	Not described	Not described

Table 1 *CYLD* transgenic mice phenotypes.

1.6.2 Drosophila model

Human and Drosophila *CYLD* share 45% sequence homology. Drosophila has an analogous NFκB pathway (IMD –Immune deficiency pathway), in which proteins similar to the mammalian counterparts of NFKB are seen. Drosophila *CYLD* has deubiquitinating activity; the conservation of this domain may afford further insight into CYLD biology. The key phenotype seen in null flies are altered fat body morphology, increased survival against starvation and increased susceptibility to bacterial infections (Tsichritzis, Gaentzsch et al. 2007).

The lack of cylindromas in *CYLD* transgenic models has limited the use of these models for drug discovery. Intriguingly a GLI1 overexpressing mouse has been described, where cylindromas, trichoepitheliomas and basal cell carcinomas were seen. Whilst the cylindromas seen in this model have not arisen following mutations in *CYLD*, the model highlights the possibility of SHH signalling playing a role in CYLD defective tumours (Nilsson, Undèn et al. 2000). Equally, molecular insights gained from CYLD defective tumours may inform the pathogenesis of BCC.

1.7 *CYLD* mutations in sporadic human cancers

Apart from cylindromas, other cancers that lack functioning CYLD or have reduced expression of CYLD include hepatocellular and colonic carcinoma (Hellerbrand, Bumes et al. 2007), multiple myeloma (Annunziata, Davis et al. 2007; Jenner, Leone et al. 2007; Keats, Fonseca et al. 2007), lung cancer (Zhong, Fields et al. 2007), prostate cancer (Kikuno, Shiina et al. 2008) and malignant melanoma (Massoumi, Kuphal et al. 2009). In multiple myeloma, loss of heterozygosity (LOH) at 16q, the genomic location of the *CYLD* gene, is an indicator of poor prognosis and is associated with reduced overall survival (Jenner, Leone et al. 2007). Both deletions involving the locus of *CYLD* resulting in reduced copy number, as well as biallelic events, comprising a 16q deletion with mutations within the coding exons of *CYLD* in the remaining allele have been shown (Demchenko, Glebov et al. 2010). Overexpression of NFκB target genes has been demonstrated in myeloma consistent with the proposed role of CYLD (Jenner, Leone et al. 2007). Apart

from genetic changes resulting in reduced CYLD expression in cancer, epigenetics have also been shown to play a role. CYLD expression is reduced in non-small cell lung cancer cell lines, a process mediated by histone deacetylation (Zhong, Fields et al. 2007). In prostate cancer cell lines (LNCap and PC3) CYLD expression is increased following phytoestrogen mediated demethylation and acetylation and is associated with reduced NFκB activity, suggesting methylation as method of repressing CYLD (Kikuno, Shiina et al. 2008). The reduced expression of CYLD contributing to tumorigenesis in cancers beyond cylindromas is in keeping with its role as a tumour suppressor gene.

1.8 Present treatment of *CYLD* mutation carriers

CYLD mutation carriers undergo repeated surgery to control tumour burden. These procedures can culminate in complete scalp removal. Taken together with the disfiguring and painful nature of these tumours, and the impairment of function, the development of non-surgical therapies is indicated. The discovery that CYLD negatively regulated the NFκB pathway upstream of aspirin's putative point of action raised the possibility of non-surgical treatments. The concept of treating cylindromas with aspirin is an appealing one. Aspirin is cheap and has a well-known safety profile. Cylindromas are easily accessible and topical application, as well as transcutaneous delivery or intralesional injections are feasible to achieve sufficient tissue concentrations. Aspirin competitively inhibits ATP binding to IKK-beta and hence reduces IKK's enzymatic activity (Yin, Yamamoto et al. 1998). As a CYLD independent weak inhibitor of IKK, aspirin can compensate for the activation of IKK seen in CYLD depleted cells. This was shown in HeLa cells subjected to siRNA *CYLD* knockdown, where the resistance to TNF induced apoptosis was overcome by the addition of aspirin. However, topical application of salicylic acid only had a modest effect in *CYLD* mutation carriers, with complete remission seen in only two tumours after prolonged daily treatment (Oosterkamp, Neering et al. 2006).This prompted the development of this work, which has an overarching aim to use an unbiased approach to discover targetable pathways using rare tumour samples from *CYLD* mutation carriers.

The aims of this project are:

1. Characterisation of the distribution and histological features of CYLD defective tumours in germline *CYLD* mutation carriers
2. Identification of the key regulatory pathways, abrogation of which are associated with formation of CYLD defective tumours.
3. Functional studies of disrupting such pathways in primary cell culture models derived from CYLD defective tumours.

2 Chapter 2: Materials and methods

2.1 Patient selection and tissue collection

2.1.1 Ethical approval

Appropriate approval from the local ethical review board was obtained (REC 06/1059) and written informed consent was obtained from patients.

2.1.2 Patients

Two large families with known germline mutations (Bignell, Warren et al. 2000) within the *CYLD* locus were identified for the assessment using a questionnaire and tumour mapping (see below). Family A has a frameshift mutation (c.2460delC), resulting in a premature termination codon, whilst Family B has a splice site mutation (c.2469+1G>A). In total, twenty-six affected individuals as determined by a dermatologist or geneticist were surveyed, of which eighteen were clinically examined . Eight unaffected relatives, five from family A and three from family B, provided blood samples to exclude the presence of a non-penetrant mutation. Patients provided blood samples from which genomic DNA was extracted.

In addition to patients from these pedigrees, further patients who were undergoing routine surgery to control tumour burden were identified. Surplus tissue from these patients, were used as described. These patients carried germline mutations that were c.2460delc, c.2469+1G>A and c.2290del5 (Accession No. NM_015247).

2.1.3 Tumour mapping and clinical disease impact assessment

A questionnaire was designed following a search for all publications in PubMed for the text: *CYLD*, cylindroma, Brooke-Spiegler syndrome, familial cylindromatosis, and multiple familial trichoepitheliomas. The phenotypes seen in *CYLD* knockout mice models and all clinical phenotypic data were collated into a clinical questionnaire. The questionnaire aimed to gather clinical data on patient signs and symptoms, disease severity, hormonal

therapy exposure in females, associated diseases and response to existing aspirin or NSAID therapy.

Due to the extensive geographical spread of the families, a template was designed, and affected members were asked to self-report the exact location of tumours. However, as the majority of patients lived in the North East of England, detailed examination of eighteen patients was performed to ensure corroboration. Tumour mapping done in the clinic corroborated well with the template data on the torso and face. Detailed location on the scalp was accurate when there were less than approximately ten tumours; accurate resolution was not possible when confluent tumours were present.

Eight affected patients, who were not examined due to geographical reasons, were interviewed by telephone. These patients self-reported lesion locations on a template and supplemented this subjective description with confirmatory digital photographic images. Histological reports were reviewed to confirm the nature of the tumours where available. The distribution of tumours on each patient was ultimately marked on a template and a composite image was created by overlaying the templates according to gender using Adobe Photoshop™.

2.1.4 Tumour sampling techniques

Patients who underwent routine surgery and had consented to the use of surplus tumour tissue for surgical procedures were included. Tumour locations were recorded at the time of surgery on a diagram used to map the location of the collected tissue. Tumour tissue was collected under sterile conditions at the time of operation, and depending on the intended use, was snap frozen in liquid nitrogen, fixed in PFA or placed in supplemented tissue culture medium that contained antibiotics (Transport medium).

2.2 Histochemical techniques

2.2.1 Tissue processing

Tissue used for standard haematoxylin and eosin staining, and immunohistochemical detection of proteins from tissue sections were fixed in 4% PFA for 4-12 hours depending on the dimensions of the tissue block. Specimens were then gently agitated and dehydrated in graded alcohols.

Specimens were then immersed in xylene, before being immersed in wax, and then finally placed in wax blocks.

2.2.2 Generation of custom tissue microarray

A custom made tissue microarray was made from single 2mm cores from representative tumour areas and was used to validate protein expression in tissue sections. The TMA contained 10 cylindroma samples, 4 spiradenoma samples and 2 trichoepithelioma samples. Cylindromas and spiradenomas were chosen from both scalp and torso, and trichoepitheliomas were from the face. 2mm cores of tumour samples were placed onto a piece of PCR film, which was cut to fit into a tissue processing mould. Molten wax was then poured into the mould, and allowed to cool. The PCR film was then removed.

2.2.3 Tissue sectioning

Tissue sections were cut using a microtome, typically at 5 μm thickness. Serial sections were cut and orientated on Superfrost Plus (VWR, UK) glass slides, which were sequentially labelled. Sections were floated on distilled water, warmed using a hotplate. Missing sections, where applicable, were noted. Surplus water was removed and the slides were baked overnight at 58°C. Slides were then cooled to room temperature.

2.2.4 Pre treatment of tissue sections

Slides were incubated in a warm oven at 60°C for 30 minutes, prior to being dewaxed in fresh xylene twice. Tissue sections were rehydrated in graded alcohols, and then finally immersed in distilled water, prior to the applications below.

2.2.5 Haematoxylin and eosin staining

Rehydrated sections on glass slides were transferred from distilled water to haematoxylin solution for 25 seconds, immersed for 5 seconds in distilled water, and then immersed in bluing solution for 10 seconds. After a brief 5 second immersion in water, slides were then immersed in eosin solution for 30 seconds. The slides were then dehydrated in graded alcohols, immersed in two changes of xylene, and then coverslipped using DPX mounting media.

2.2.6 Fluorescent indirect immunohistochemistry

Tissue sections were transferred from distilled water into sodium citrate buffer (pH 6.0), and antigen retrieval was performed using a pressure cooker for 7 mins. This was done to unmask antigenic epitopes that may have been masked following the cross linking of proteins following PFA fixation. Slides were then cooled to room temperature, and washed once in PBS. Slides were marked with a membrane pen (ImmEdge Hydrophobic Barrier pen - H-4000, VECTOR Industries) , with care taken not to allow the sections to dry out. Sections were then blocked in serum free protein block (X0909, DAKO UK) for ten minutes, before incubation with primary antibodies diluted in antibody diluent (Background Reducing S3022, DAKO UK), at concentrations specified below in Table 2. After an hour incubation, slides were gently washed in PBS thrice, before incubation with secondary antibodies at a dilution of 1:200, and DAPI (SIGMA, UK) at a dilution of 1:10000 (1mg/ml stock solution). After a further hour incubation, slides were washed thrice in PBS, and then mounted using Vectashield Hardset Mounting Medium (H-1400, VECTOR Industries). Fluorescent staining was visualised using a UV Zeiss Axioimager microscope, and images captured using a monochrome digital camera connected to a computer running Zeiss Axiovision 4.7 software (Zeiss, UK).

2.2.7 Indirect immunohistochemistry utilising DAB visualization

Tissue sections were transferred from distilled water into sodium citrate buffer (pH 6.0), and antigen retrieval was performed using a pressure cooker for 7 mins. Slides were then cooled to room temperature, and washed once in PBS. Slides were marked with a membrane pen (ImmEdge Hydrophobic Barrier pen - H-4000, VECTOR Industries) , with care taken not to allow the sections to dry out. Tissue sections were then blocked with peroxidase blocking agent (DAKO, UK) and then incubated with primary antibodies as indicated in Table 2 Concentration of antibodies used for immunohistochemistry for 1 hour at room temperature. Tissue sections were then washed in phosphate buffered saline and probed with secondary polymer linked HRP-conjugated antibodies for 30 minutes (DAKO, UK), and staining was visualized with 3,3'-Diaminobenzidine (DAB). Haematoxylin

(SIGMA, UK) was used as a nuclear counterstain. Colour photomicrographs were captured using a Zeiss Axioplan microscope, coupled to a colour digital camera connected to a computer running Zeiss Axiovision 4.7 software (Zeiss, UK).

Table 2 Concentration of antibodies used for immunohistochemistry.

Primary Antibody	Concentration of 1˚Ab	Secondary antibody	Concentration of 2˚Ab
CK6 (Abcam)	1:200	Anti mouse FITC (Jackson)	1:200
CK14 (Abcam)	1:200	Anti mouse FITC (Jackson)	1:200
CK17 (Abcam)	1:200	Anti mouse FITC (Jackson)	1:200
SMA (Abcam)	1:200	Anti rabbit FITC (Jackson)	1:200
Beta Catenin (BD)	1:50	DAKO Mouse Polymer HRP	N/A
BCL2 (Cell Signalling)	1:200	DAKO Rabbit Polymer HRP	N/A
TRKA (Cell Signalling)	1:200	DAKO Rabbit Polymer HRP	N/A
TRKB (Cell Signalling)	1:200	DAKO Rabbit Polymer HRP	N/A
TRKC (Cell Signalling)	1:200	DAKO Rabbit Polymer HRP	N/A
Phospho ERK (Cell Signalling)	1:200	DAKO Rabbit Polymer HRP	N/A
LEF1 (Cell Signalling)	1:200	DAKO Rabbit Polymer HRP	N/A

2.2.8 3D reconstruction of CYLD defective tumours

Formalin fixed paraffin embedded tissue was serially sectioned at 5 μm thickness. Tissue sections were subject to routine haematoxylin and eosin staining, and then photographed using Zeiss Axioplan microscope coupled to a Nikon D300 camera with a 50mm objective. Images were acquired using a 5x microscope objective. Alignment was performed manually using Amira software (V4.0 – Visage Imaging), allowing accurate overlap of serial sections. Artificial colour labels were applied to individual cylinders of tumour cells, allowing tracking of cylinders through the tumour block. Surface rendering of the ensuing columns of tumour cells and virtual flythrough examination was performed within Amira software.

2.2.9 Morphometric analysis of tumours

Photomicrographs were taken of the tissue sections that encapsulated the sections used for transcriptomic profiling. Tissue sections were subject to routine haematoxylin and eosin staining, and then photographed using Zeiss Axioplan microscope coupled to a Nikon D300 camera with a 50mm objective. These images were stitched together in Adobe Photoshop™ CS3. Each island of tumour cells was then highlighted by tracing around the periphery on a new layer in Adobe Photoshop. This layer, which contained circular shapes of different sizes, was then analysed in Image J (v1.64b - NIH) to determine the size of each island. A threshold size of 10,000 square pixels was used as the threshold at which tumour islands lost a circular pattern of organisation. The number of islands that fell on either side of this threshold was then determined as a proportion of the total number of islands in that sample. This measure of proportion of each sample's level of organisation was then correlated with the 3000 selected transcripts across 25 samples where morphometric analysis was technically adequate Spearman's coefficient was used to determine the statistical significance, with a value of $p<0.05$ taken to be significant.

2.3 Molecular Techniques

2.3.1 Extraction of RNA

Care was taken during the preparation of RNA to keep the working area and instruments free of RNAse contamination. This was achieved by wiping work surfaces and equipment with Diethylpyrocarbonate (DEPC)-ethanol or RNAse Zap (Ambion, UK), wearing disposable gloves wiped with DEPC-ethanol and using aerosol resistant tips.

Total RNA was extracted as per the Trizol (Invitrogen, UK) protocol. Samples were incubated at room temperature in 800μl for 5 mins to allow complete dissociation of nucleoprotein complexes after which 0.2ml of chloroform (Sigma, UK) per 800μl Trizol was added and the microfuge tubes shaken vigorously by hand for 15 secs. Samples were incubated at room temperature

for 2 mins and then centrifuged at 12000 rcf for 15 mins at 4˚C. The upper colourless aqueous phase containing the total RNA was carefully transferred to a fresh tube. Total RNA was then precipitated from the aqueous phase by adding 0.5ml isopropyl alcohol combined with 0.5 μl glycogen (Ultra Pure Glycogen - Invitrogen, UK). Samples were then incubated at room temperature for 10 mins and centrifuged at 12000 rcf for 10 mins at 4˚C. The supernatant was removed taking care not to disturb the total RNA pellet which was then washed with 1ml of 75% ethanol. The sample was vortexed briefly prior to centrifugation at 7500 rcf for 5mins at 4˚C. The supernatant was removed and the pellet air-dried on the bench for 5 mins. The total RNA pellet was then resuspended in 20μl DEPC-dH2O and stored at -20˚C.

2.3.2 Elimination of genomic DNA from total RNA preparation

Contaminating genomic DNA was removed from the above total RNA preparations by the addition of 0.2U DNaseI, RNAse free (Promega) per 20μl resuspended total RNA and incubating the mix for 5mins at 37˚C. The reaction was stopped by the addition of EDTA, pH 8.0 at a final concentration of 20mM.

2.3.3 Extraction of genomic DNA

Trizol was used as it was feasible to perform extraction of DNA from the microdissected samples after the RNA isolation stage described above was complete. Any remaining aqueous phase was aspirated, before 300μl of 100% ethanol was added. This was mixed and allowed to stand at room temperature for 3 minutes. The tube was then centrifuged at 2000 rcf for 5 minutes at 4˚C, and the supernatant was removed. The remaining DNA pellet was washed in a 0.1M sodium citrate with 10% ethanol solution, left at room temperature for 30 minutes and then spun down at 2000 rcf at 4˚C for 5 mins. This was repeated once, and the pellet was washed in 75% ethanol before being spun down again. The ethanol was aspirated, the pellet air dried, and then resuspended in 8mM sodium hydroxide. This was titrated with HEPES to a final pH of 8.

2.3.4 Isolation of genomic DNA from whole blood

Genomic DNA from peripheral blood was extracted using the QIAGEN whole blood kit according to manufacturer's protocol. In brief, cells are lysed in buffers that provide immediate denaturation of proteins such as nucleases, histones, and DNA-binding proteins. Under the pH and low-salt conditions provided by the buffer, DNA binds to the QIAGEN resin in the column while other cell constituents such as proteins, carbohydrates, and metabolites flow through. Purified DNA is eluted in high-salt buffer, and precipitated in isopropranol, before being resuspended in EB buffer.

2.3.5 Spectrophotometric determination of DNA and RNA concentration

DNA and RNA was quantified using a Nanodrop UV spectrophotometer (Nanodrop, UK). The ratio of the absorbance readings at 260nm and 280 nm (A260/A280) were calculated on the NanoDrop to provide an estimate of the purity of the DNA and RNA with respect to contaminants. A ratio of >1.8 was used as a threshold of a pure sample. Total RNA and DNA concentration was determined by measuring the absorbance at 260nm using the NanoDrop (Labtech International) spectrophotometer. An A260 reading of 1.0 is equivalent to about 40 µg/ml of RNA, and 50 µg/ml of DNA.

2.3.6 Microfluidic gel analysis of RNA integrity

RNA integrity analysis was performed using a chip based electrophoresis kit to confirm preservation of the 18S and 28S ribosomal bands, in accordance with the manufacturer's protocol (RNA 6000 Nano and Pico Chip kits; Agilent 2100 Bioanalyzer).

2.3.7 Synthesis of first-strand cDNA

cDNA was synthesized from total RNA using a Superscript III RT Kit (Invitrogen, UK) according to the manufacturers instructions. Reverse transcription of 100ng-5µg of total RNA was carried out in a 20µl reaction volume containing 100ng of random primers, 10mM dNTP mix, sterile distilled water, first strand buffer and DTT to a final concentration of 10mM. Reaction mixes were incubated at 25˚C for 2 minutes and then Superscript III RT was

added. The reaction was then incubated at 25˚C for ten minutes, 42˚C for 50 minutes and inactivated by heating to 70˚C for 15 minutes.

2.3.8 Primer design

Where primer design was not dictated by the need to incorporate endonuclease restriction sites, a Kozak sequence or to amplify the full coding sequence of a gene, the Perl primer v1.14 design program was used for both PCR and sequencing primers.

2.3.9 Primers for sequence verification of constructs

Sequencing primers were used to verify the sequence of CYLD. These were:

Table 3 *CYLD* cDNA sequencing primers.

Primer	Primer sequence (5'-3')	Position
pLEX MCS FWD	CACCAAAATCAACGGGACTT	-120
CYLD 2F	CTCCAAATAGACGTGGGC	642
CYLD 3F	GAGTGTGACGCAGGAAAGG	1190
CYLD 4F	GGCTGAAGTTAAGGAGAACC	1691
CYLD 5F	AGGCTGCATCAGGATTTACC	2275
CYLD 6F	CAGTGTCACTTCCCAAAGAC	2776

2.3.10 Primers for restriction enzyme cloning

Primers designed with restriction endonuclease sites were used to amplify CYLD. These included *Spe*I and *Age*I restriction sites. CYLD Forward 5' - GGC*ACTAGT*AGCATGAGTTCAGGCTTA - 3'; CYLD Reverse 5' – GGC*ACCGGT*TTATTTGTACAAACTCATTGT - 3'. (Restriction sites indicated in italics; underlined sequences represent the coding sequence of *CYLD*)

2.3.11 Primers for amplification of coding exons of CYLD and flanking regions

These primers were adapted from Saggar *et al*. (Saggar, Chernoff et al. 2008).

Table 4 *CYLD* exon amplification primers.

Forward Primer	5'-3' sequence	Reverse Primer	5'-3' sequence	AT °C
CYLD4F	GTATGTCTTTTAGCCCTTTT	CYLD4R	TGCATACAAATACACAGACA	55
CYLD5F	CCTAGAGTGAACCCCTTTTCC	CYLD5R	TTTGCAAGTAAATTGGTCCTAAAA	62
CYLD6F	TTTTGGAGGATTCTTTATGG	CYLD6R	AGAAATCACCACGAAAGAAC	60
CYLD7F	AACACATCCCCCTCCTCTTT	CYLD7R	ACCTTAAAGCCCAGCAATGA	50
CYLD8F	TTCCTTGTTTCTCTTCTATA	CYLD8R	ACATGTTCAGAAGTAATAGC	50
CYLD9F	CTTTGATGCTATATTGACTT	CYLD9R	TCTACTTATTCTGTTTCCAA	50
CYLD10F	TTGTGATGCCTATGAGAGTA	CYLD10R	TCAAAAAGCATATAATAGGG	55
CYLD11F	GGAGTGGTGAGAAAGGGTAT	CYLD11R	GCGTTGGCAAGAAATATATT	55
CYLD12F	GCATCAAAATACAAAAACAT	CYLD12R	CACAGTCATCCAGTTTCTCT	50
CYLD13F	CTTTACTTATTTTCCTCTTC	CYLD13R	ACATGAAGACAAGGTATAAA	55
CYLD14F	GCCTGAGTGATAGAGTGAGA	CYLD14R	TCATTATTCCACATCATCAA	55
CYLD15F	GAAAACTTGAAAACTGTGCT	CYLD15R	AGAGCCCTAAACAAATACAA	55
CYLD16F	TCTGTTGTTCTGACTATCCA	CYLD16R	GTGTTTCAAACTTTTCTCAG	55
CYLD17F	GTGGCTTATTGGTGTCCTCT	CYLD17R	GCCTTGGGAAATACTGTGTC	55
CYLD18F	GAGAGCTTAAGCAGATGGAA	CYLD18R	TAAACAGAAAAGGCAAAAGC	55
CYLD19F	ATTTAAATGATTCTCCTGCC	CYLD19R	TGTTGTCACCAGAATAATCC	55
CYLD20F	ATAAAATCACTGGCAAAAGG	CYLD20R	TCATCACCACAAAGACATCC	55

The annealing temperature for each primer pair in the reaction is indicated in the column "AT". Amplified PCR products were sequenced using the forward primer.

2.3.12 Polymerase chain reaction

All polymerase chain reactions (PCR) were setup in a dedicated laminar flow hood. PCR reactions carried out for the purpose of genotyping or amplification of the first strand from the reverse transcription of RNA were performed using *Taq* DNA Polymerase (Invitrogen, UK). The PCR reaction was carried out in a total volume of 50μl comprising the following: DNA template, 0.4mM dNTPs, 1μM forward primer, 1μM reverse primer, 10X *Taq* DNA Polymerase Buffer, 1.5mM MgCl2, 2U *Taq* DNA Polymerase and DEPC H20. All components were combined in sterile PCR tubes on ice using aerosol resistant tips. Amplification was performed in a thermal cycler using the following parameters: 95˚C for 3mins; 30-35 cycles of 30secs at 95˚C, 1min at the primer annealing temperature and 1min per kilobase of the desired product at 72˚C; a final 10min extension at 72˚C. Products were analysed on a 1-2.5% agarose gel, depending on size of the product.

PCR reactions carried out for the purpose of generating a cDNA product which incorporated specific restriction endonuclease sites at either end to facilitate cloning were performed using high fidelity polymerase. Phusion high-fidelity DNA polymerase (Finnzymes) with 5' ➞ 3' DNA polymerase activity and 3' ➞ 5' proofreading exonuclease activity was used. The PCR reaction was carried out in a total volume of 50μl comprising the following: DNA template, 0.2mM dNTPs, 0.5μM forward primer, 0.5μM reverse primer, 5X *Phusion HF* Buffer containing 1.5mM MgCl2 and 1U *Phu* DNA Polymerase. Amplification was performed in a thermal cycler using the following parameters: 98˚C for 1min; 30 cycles of 10 secs at 98˚C, 30 secs at the primer annealing temperature and 15-30 secs per kilobase of the desired product at 72˚C; a final 10min extension at 72˚C. Products were analysed on a 1% agarose gel prior to excision and purification.

2.3.13 Quantitative PCR

Total RNA was extracted from cylindroma primary cell cultures as described above, subject to DNAse digestion and then reverse transcribed using a Superscript III kit (Invitrogen, UK) according to manufacturers instructions. cDNA was then used for quantitative PCR with the following primers (5'-3)': (*GAPDH* F – ATGGGGAAGGTGAAGGTCG, *GAPDH* R – GGGGTCATTGATGGCAACAATA, *NTRK2* F – TGTTCAGCACATCAAGCGACA, *NTRK2* R – GCTCAGGACAGAGGTTATAGCAT, NTRK3 F TCCGTCAGGGACACAACTG, *NTRK3* R – GCACACTCCATAGAACTTGACA) with a SYBR green contain *Taq* polymerase master mix (Sigma, UK) , in an ABI 7900HT thermal cycler. Gene expression was normalised to GAPDH and comparisons in expression were made using the $2^{-\Delta\Delta CT}$ formula as the PCR reactions had similar efficiencies of amplification.

2.3.14 Agarose gel electrophoresis of DNA

PCR products generated for genotyping were visualised on 2% Tris-Acetate-EDTA (TAE) agarose gels. Gels contained ethidium bromide at a final concentration of 2µg/ml. DNA was mixed with 6X loading dye (Promega) to a final concentration of 1X prior to loading on an agarose gel. 1kb or 100bp ladder (Promega) was loaded alongside DNA samples to provide markers by which to ascertain the size of DNA fragments. Samples were run in 1X TAE Buffer at 25V until separation of the DNA fragments was achieved.

2.3.15 Gel extraction and purification of DNA

DNA fragments were extracted and purified using a QIAquick Gel Extraction Kit (Qiagen) according to the manufacturer's instructions. Briefly, 0.5-1µg of DNA was separated by electrophoresis on a 1% agarose gel. The fragment of interest was excised under UV light visualisation and transferred to a microfuge tube using a clean scalpel for each fragment. The agarose was dissolved by the addition of Buffer QG and heating to 50˚C for 10mins. For DNA fragments less than 500bp and greater than 4kb, isopropanol was added to the sample to increase the yield. The sample was then applied to a QIAquick spin column and centrifuged. The column was washed with Buffer QG to remove any trace of agarose, and then incubated for 5 minutes after the addition of Buffer PE to remove salts which may interfere with downstream ligations. Purified DNA was eluted from the column in 30µl Buffer EB.

2.3.16 DNA sequencing

DNA sequencing was performed using the Big Dye terminator sequencing method, performed by MWG/Eurofins. Plasmid DNA extracted using the QIAGEN Miniprep kit were sent with sequencing primers at the recommended concentrations. PCR products were purified using the QIAquick PCR cleanup kit according to manufacturer's instructions, before the sequencing primer (forward primer from amplification reaction) was added at the recommended concentration. When a novel mutation was detected in a sample from a patient, the sequencing reaction was repeated using the reverse primer for

the PCR reaction. Sequence data was viewed and aligned in Sequencher (v4.9 - http://www.genecodes.com)

2.4 Cloning

2.4.1 LB broth and agar

All cells were grown in 2X LB broth. This consisted 20g/L of LB-Broth-Lennox 10g/L peptone and 5g/l yeast extract. 15g/L agar was added for pouring plates.

2.4.2 Preparation of competent cells

E. coli DH5-alpha (Stratagene, UK) were streaked from a glycerol stock onto a LB agar plate and incubated at 37˚C overnight. A starter culture of 10ml LB without a selection antibiotic was then inoculated with a single colony and incubated overnight at 37˚C with shaking at 220rpm. 100ml of LB media was then inoculated with 1ml of starter culture and grown at 37˚C with vigorous shaking to an OD600 of 0.6. Cells were harvested by chilling the culture flask on ice for 10 mins and then pelleting the cells by centrifugation in a pre-chilled rotor at 6000rpm for 10mins. Cells were resuspended in 25mls of ice cold sterile 100mM $CaCl_2$ and incubated for 20 mins followed by centrifugation as above. The cells were then centrifuged as above and resuspended with 5ml of 100mM $CaCl_2$. 1ml of cold 100% glycerol was added. 100μl aliquots of competent cells were snap frozen in liquid nitrogen and stored at -70˚C. Prior to use the cells were tested to ensure a transformation efficiency of 107cfu / 1μg DNA.

2.4.3 Transformation of competent cells

A 100µl aliquot of *E. coli DH5-alpha* cells were defrosted on ice for 15 minutes. 2µl of the DNA was added and allowed to incubate for 15 minutes on ice. The cells were briefly heated to 42˚C for 45 seconds, and then returned to ice. The cells were then agitated at 220rpm for 1 hour. The cells were pelleted, and spread onto agar plates made with the relevant selective antibiotic, and incubated at 37˚C overnight.

2.4.4 Mini-preparation of plasmid DNA

A single colony of *E. coli DH5 Alpha* was picked from selective agar plates and used to inoculate 5ml of LB media plus the appropriate selective antibiotic. The *E. coli* were cultured overnight at 37˚C, 220rpm. A 1ml aliquot of the overnight culture was taken to make glycerol stocks and the remaining 4ml pelleted by centrifugation at 2100g (RCF) for 15 mins at 21˚C. Plasmid DNA was purified from the *E.coli* based on a modified alkaline lysis protocol using QIAprep Spin Miniprep Kits (Qiagen) as per the manufacturer's instructions for high-copy recombinant plasmids.

In summary, bacteria cells were lysed in Buffer P2 which contains NaOH-SDS. The cell lysate was then neutralised by the addition of Buffer N3. The high salt concentration of Buffer N3 precipitates cellular debris, enabling separation of the plasmid DNA which remains in solution by centrifugation. The plasmid DNA was then selectively adsorbed to the silica-gel membrane of the QIAprep column. The DNA was washed with Buffer PB and then Buffer PE to remove endonucleases and salts respectively. Purified plasmid DNA was eluted in 100 μl of Buffer EB and stored at -20˚C.

2.4.5 Glycerol stocks

1ml of a 5ml overnight bacterial culture was transferred to a microfuge tube and centrifuged at 13000rpm for 1min at room temp. The supernatant was discarded and the pellet resuspended in 0.5ml of 30% LB Glycerol. Glycerol stocks were stored at -80˚C.

2.4.6 Restriction enzyme digests

Restriction enzymes (Promega, UK) were used with the buffer supplied in single digests. The most compatible buffer for all enzymes was selected for double digests. 0.2μg of DNA was combined with 2μg Acetylated BSA, 10X RE Buffer to a final concentration of 1X and 5U restriction enzyme.

Where a restriction digest requiring two enzymes was necessary, and could be achieved using the same buffer, 5U of each enzyme were combined in a single reaction.

For all restriction digests, samples were incubated at the specified temperature for 3 hours before being resolved on an agarose gel.

2.4.7 Ligation reactions

DNA of vector and insert carrying restriction enzyme sites were subject to restriction digestion, and the products subject to agarose gel electrophoresis. The bands of interest were cut out from the gel, purified, and ligated in different ratios of vector to insert using a T4 DNA ligase (Fermentas). The ligation product was then used to transform competent cells, which were plated on antibiotic selective agar plates. Colonies were picked after a 16 hour incubation at 37°C, and cultured in selective LB media for 12-16 hours. DNA was extracted using the QIAGEN Miniprep kit, and subject to restriction digestion so as to cut the intended insert out of the vector to verify a successful ligation. Successful ligations were subject to DNA sequencing to ensure there were no mutations in the insert. Once sequence verified, the ligated product was amplified in *E.coli,* extracted using a QIAGEN Maxiprep kit and then used for experiments.

2.4.8 Generation of pLEX-CYLD

CYLD was amplified using a proofreading Taq polymerase, incorporating restriction sites *Spe*I and *Age*I, from pOTB7, obtained from the MGC clone library (MGC:19923; Geneservice, Cambridge). This product was TA-cloned into pCR2.1-TOPO (Invitrogen, UK kit K4500), and cut out using *Bam*HI and *Xho*I. None of these 4 sites were found within the *CYLD* cDNA. pLEX MCS, a lentiviral vector with a multiple cloning site incorporating unique restriction

sites *Bam*HI and *Xho*I was amplified in DH5alpha E.coli cells (Figure 9).

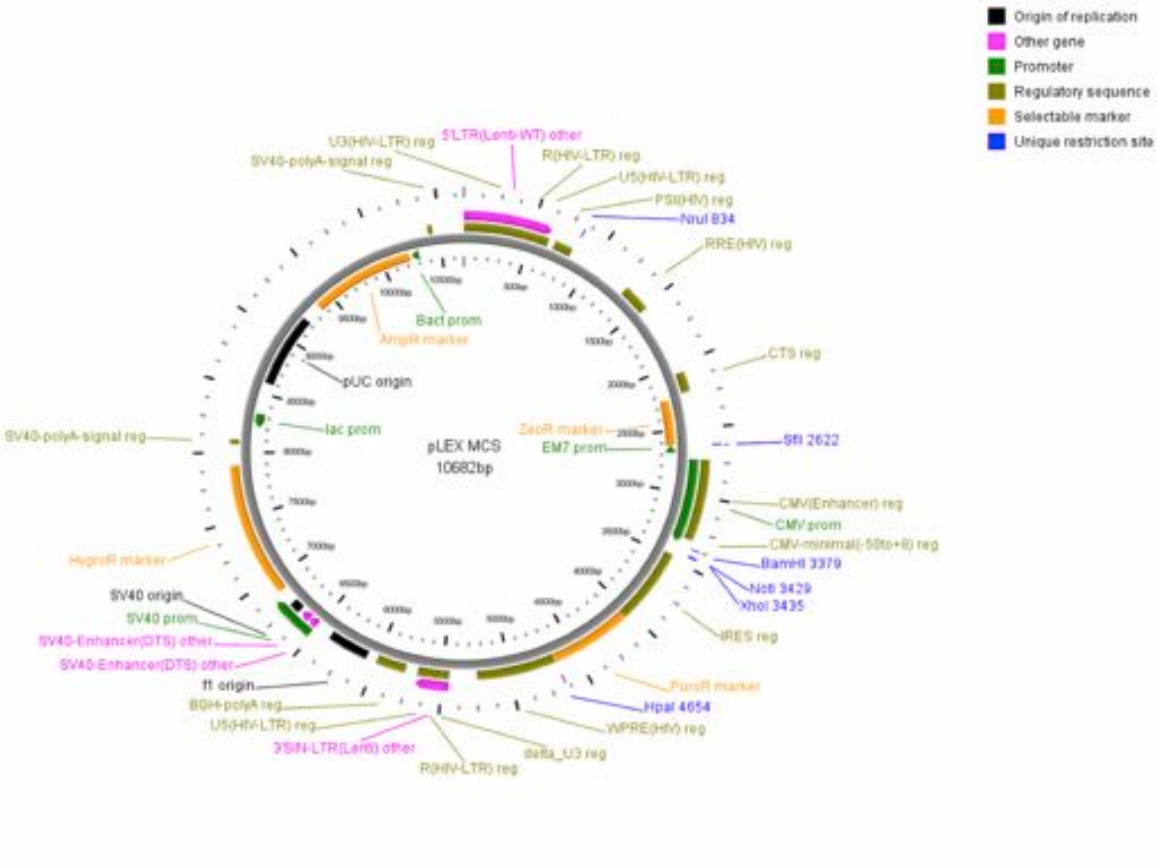

Figure 9 pLEX-MCS vector.

Both DNA products were cut with the restriction enzymes, before being purified on an agarose gel.

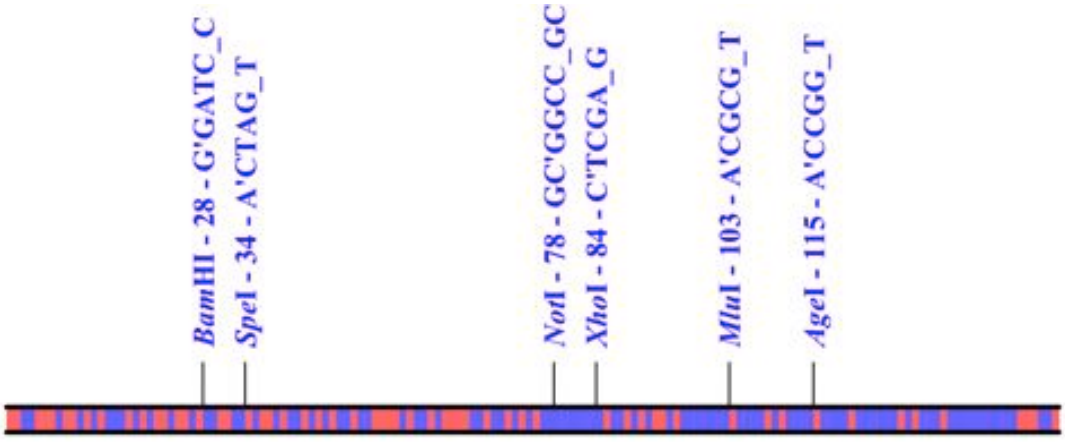

Figure 10 Multiple cloning site within pLEX-MCS.

DNA products were extracted from the agarose gel, and then the two products were ligated using a T4 DNA Ligase. To enrich for vectors that contained the

CYLD insert, a restriction digest was performed with *Not*I, which lay between the *Bam*HI and *Xho*I sites on the pLEX-MCS vector (Figure 10). The cut product was then transformed in competent cells, plated on selective agar and colonies were picked the next day. These colonies were allowed to grow for 6 hours in 200 µl of LB in a 96 well plate at 37°C on a shaker at 200 rpm. The cells were pelleted following centrifugation at 500 rcf for 5 mins at room temperature before sterile tips were dipped into the pellets and transferred into a 96 well plate for PCR screening. The recipient plate contained a PCR mastermix, with 10 µl per well, containing primers that amplified exons 16-18 of *CYLD* (5'-3': CYLD 16F =TCTGTTGTTCTGACTATCCA, CYLD 18R – TAAACAGAAAAGGCAAAAGC). This plate was then inserted into a 96 well thermal cycler, and following the PCR reaction, the products were run on an agarose gel. Colonies containing the *CYLD* insert were selected, and placed in selective LB (5mls) overnight. The extracted DNA was then subject to digestion with *BamH*I and *Xho*I to cut *CYLD* back out. Once confirmed, the pLEX-CYLD product was sequenced to verify the sequence and orientation of *CYLD*. This was then amplified in DH5 alpha cells, and used for lentiviral transfection of cylindroma primary cell cultures.

2.4.9 Lentiviral constructs

The following shRNA constructs were used for lentiviral mediated knockdown of the indicated genes in cylindroma primary cells, and were purchased from Openbiosystems (Thermo Scientific, UK). *DKK2*: V2LHS_198410 NM_014421 shRNAmir Hs Lentiviral pGIPZ RHS4430-98512097,V2LHS_214426 NM_014421 shRNAmir Hs Lentiviral pGIPZ RHS4430-98853869; *NTRK2*: V2LHS_63731 NM_001007097 shRNAmir Hs Lentiviral pGIPZ RHS4430-98842290, V2LHS_63734 NM_001018064 shRNAmir Hs, Lentiviral pGIPZ RHS4430-99159070; *NTRK3*: V2LHS_152393 NM_001012338 shRNAmir Hs Lentiviral pGIPZ RHS4430-98911610. For overexpression, pLEX-CYLD, generated as described, was used.

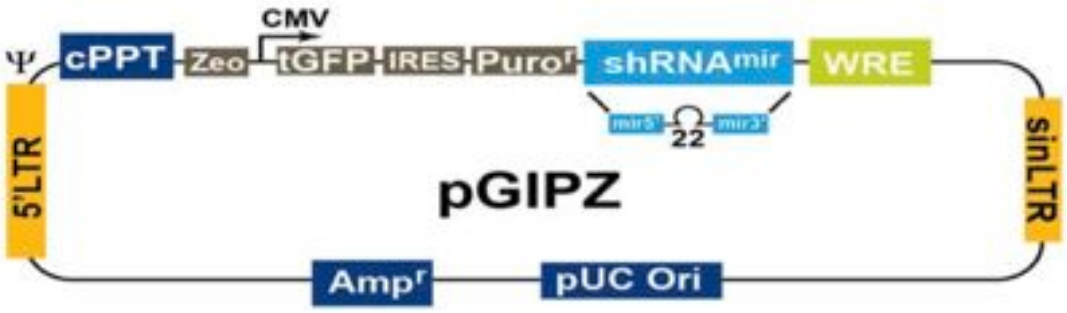

Figure 11 pGIPZ lentiviral vector.

Vector Element	Function
CMV Promoter	RNA Polymerase II promoter
cPPT	Central Polypurine tract helps translocation into the nucleus of non-dividing cells
WRE	Enhances the stability and translation of transcript c,
TurboGFP	Marker to track shRNAmir expression
IRES-puro resistance	Mammalian selectable marker
Amp resistance	Ampicillin (carbenicillin) bacterial selectable marker
5'LTR	5' long terminal repeat
pUC ori	High copy replication and maintenance of plasmid in E. coli
SIN-LTR	3' Self inactivating long terminal repeat
RRE	Rev response element
Zeo resistance	Bacterial selectable marker

Figure 12 Features of the pGIPZ vector.

2.4.10 Packaging of lentiviral vectors

Lentiviral vectors were used to deliver shRNA-targeting genes of interest to primary cells. To monitor transfection efficiency and allow for selection, the shRNA was linked via a bicistronic internal ribosomal entry site to both GFP and puromycin resistance genes. All work with lentiviral vectors and products were carried out in a Biosafety level 3 hood, under permission from the Health and Safety Executive. Lentiviral vectors were packaged using a mix obtained from Openbiosystems, containing the genes required to form the viral particles on 5 different vectors. A lipsomal transfection technique was used to transfect HEK-293T cells with a specified ratio of packaging mix vectors to the lentiviral vector carrying the shRNA. These cells were then grown for 48 hours, before the supernatant containing the viral particles was extracted. Polybrene (SIGMA, UK) was added to the culture medium (final concentration 4µg/ml) to optimize transfection efficiency and the packaged vectors were stored at - 80°C until use.

2.5 Microarray assays

2.5.1 Tumour microdissection for DNA and RNA extraction

All samples for microarray studies were snap frozen immediately after surgery. Tumour blocks were mounted in optimal cutting temperature compound and sectioned on a cryostat at 12 μm onto RNAse free Superfrost coated slides (VWR). All subsequent steps were performed in RNAse free solutions. Tissue sections were fixed in 100% ethanol at -20°C for 2 minutes and then washed in 70% DEPC treated ethanol and 50% DEPC treated ethanol for 2 further minutes. Sections were stained with crystal violet solution (Ambion, UK) for 40 seconds and then dehydrated in increasing concentrations of ethanol. Slides were then stored on dry ice until needle microdissection was performed. Microdissection was performed at 4°C using a Leica dissecting microscope. The dissected samples were placed directly into Trizol ® (Invitrogen, UK). Needle homogenisation was performed and the sample was frozen at -80°C until RNA and DNA extraction was performed.

2.5.2 Array CGH

The 32K BAC re-array collection (CHORI) tiling path aCGH platform was constructed at the Breakthrough Breast Cancer Research Centre, as described elsewhere (Marchio, Natrajan et al. 2008). This type of BAC array platform has been shown to be as robust as and to have comparable resolution with high- density oligonucleotide arrays. DNA labelling, array hybridisations and image acquisition were performed as described earlier (Turner, Lambros et al. 2010). aCGH data were pre-processed and analysed using an in-house R script (BACE.R) in R version 2.9.0 as previously described (Natrajan, Weigelt et al. 2009). After filtering polymorphic BACs, a final data set of 31544 clones with unambiguous mapping information according to the August 2009 build (hg19) of the human genome (http://www.ensembl.org) was smoothed using the circular binary segmentation (cbs) algorithm (Natrajan, Weigelt et al. 2009). A categorical analysis was applied to the BACs after classifying them as representing amplification (>0.45), gain (>0.08 and <0.44), loss (< -0.08 and >-0.44), deletion (<-0.45) or no-change according to their cbs-smoothed Log^2 ratio

values. aCGH data were deposited at ROCK (http://brcabase.icr.ac.uk/index.jsp), at URL: http://rock.icr.ac.uk/collaborations/Rajan/Cylindroma.

2.5.3 SNP analysis

Genomic DNA was extracted from microdissected tissue and assayed on an Illumina Sentrix Human Hap550 Genotyping BeadChip according to manufacturer's protocol. SNP array data were deposited at ROCK (http://brcabase.icr.ac.uk/index.jsp) , at URL: http://rock.icr.ac.uk/collaborations/Rajan/Cylindroma.

2.5.4 Restriction enzyme analysis to determine loss of heterozygosity

Polymerase chain reaction (PCR) was performed using primers (5'-3)' CYLD18F –GAGAGCTTAAGCAGATGGAA and CYLD 18R – TAAACAGAAAAGGCAAAAGC that flanked exon 18, and the PCR product was subject to restriction enzyme digestion using HpyCH4V (c.2460delc) and Sml I (c.2469+1G>A). Digested products were separated on an agarose gel and visualised using ethidium bromide on an ultraviolet transilluminator. LOH was determined by the absence of a band that corresponded with loss of the wild-type allele in both cases.

2.5.5 Gene expression profiling

The Illumina WG-DASL platform was used for each sample that allowed for monitoring of gene expression of 24,526 transcripts. This assay was selected as it was designed to reliably detect expression levels of partially degraded transcripts. Despite attempts to use fresh frozen microdissected tissue, the mean RIN of the RNA samples used was 2.3, warranting the use of this platform. 50ng of total RNA from each sample was used as per the supplied protocol. Briefly, total RNA was converted to cDNA using biotinylated oligo-dT18 and random nonamer primers. Two assay-specific oligonucleotides were designed to interrogate a single contiguous 50 nt sequence on each cDNA. Each of these oligonucleotides consisted of two parts: an upstream-specific oligonucleotide (USO) containing a 3" gene- specific sequence and a 5" universal PCR primer sequence (P1), while the downstream-specific

oligonucleotide (DSO) contained a 5' gene-specific sequence and a different 3' universal PCR primer sequence. The USOs and DSOs were designed with an average Tm of 65°C and 58°C, respectively and an average length of 22 and 20 nucleotides, respectively. Using this approach, a total of 24526 oligonucleotide pairs (probes) were designed and pooled, which together constituted the whole genome DASL assay pool (DAP), corresponding to 18626 unique genes, based on well-annotated content derived from the National Center for Biotechnology Information Reference Sequence Database (Build 36.2, Release 22)). The DAP was then annealed to the targeted cDNAs during a 16h incubation followed by enzymatic extension and ligation steps. Ligated products were PCR-amplified and labeled with a universal Cy3-coupled primer after which single-stranded labeled products were precipitated and then hybridized to whole genome gene expression BeadChips (Illumina Human 8 v3 chips). BeadChips were then scanned on a BeadArrayTM Reader using BeadScan software (v3.2), during which fluorescence intensities were read and images extracted. Scanned data were then extracted using Illumina Beadstudio software. Microarray gene expression profiles were deposited at Arrayexpress (www.ebi.ac.uk) at accession number E-MTAB-352.

2.5.6 Data normalisation and analysis

Raw gene expression values were normalised using quantile normalisation. Differential expression analysis was performed using Beadstudio software to detect significantly different expressed genes. Differences in signal values for each gene was scored with a differential score (DS). Bonferroni testing was performed to correct for multiple hypothesis testing, and the results were ranked in order of differential score with a differential score ranging from +374 to -374, with +/-65 corresponding to a p value cut off of <0.01. Signal values from genes that fulfilled this level of significance were then analysed.

2.5.7 Ingenuity pathway analysis of microarray data

Differentially expressed genes between CYLD defective tumours and perilesional control skin at a significance threshold of p<0.01 after correction

for multiple hypothesis testing using a Bonferroni post test correction were used for Ingenuity pathway analysis.

2.5.8 Gene set expression analysis of microarray data

Analysis was carried out using gene set expression analysis (GSEA). For this analysis, probe values (24526) were collapsed to gene symbols (18630), with the max probe value used for replicate probes. All tumours were compared to all controls. After filtering, 867 gene sets were used in the analysis. Gene sets were permutated 1000 times, before being ranked in order using a "difference of classes" metric, with a weighted enrichment statistic applied. 56 gene sets were significantly enriched at a nominal p-value of <0.01.

2.5.9 Methylation assay

Genomic DNA from the samples used for microarray analysis were assayed for methylation of the *DKK2* promoter using a quantitative PCR based assay (SA Biosciences, Qiagen UK). Samples were divided into 4 equal portions that were subject to restriction enzyme digestion with: a) controls without enzymes b) methylation sensitive enzymes c) methylation resistant enzymes d) methylation sensitive and resistant enzymes combined. Following a 16 hour period of digestion at 37°C, the samples were subject to quantitative PCR amplification with proprietary primers that amplified the promoter of DKK2. SYBR green was used to determine the amount of amplified DNA and the reaction was performed on ABI 7900HT machine. Ct values were obtained from all 4 separate reactions for each sample and used in accordance with the manufacturers formula to determine promoter hypermethylation.
(http://www.sabiosciences.com/support_manual.php?pfamily=dnamethylation)

2.6 Mammalian cell culture

All cell culture techniques were performed in vertical laminar flow cell culture hoods under sterile conditions. Culture media used is indicated in Table 5. Defined KSFM eliminated the requirement for bovine pituitary extract by inclusion of defined growth promoting additives including insulin, epidermal

growth factor and fibroblast growth factor. Cell lines were tested to exclude mycoplasma contamination. Standard tissue culture plastic was used (Iwaki UK), and this was coated with Type I collagen (Coating Matrix Kit R-011-K; Invitrogen, UK) at a concentration of 0.66 µl/cm^2 where indicated.

Table 5 Mammalian cell line cell culture media requirements.
(All items are from Invitrogen, UK; Product numbers are shown in brackets)

Tissue transport medium	**Cylindroma primary cell cultures**	**293HEK-T cells, Fibroblast culture medium**
100ml Ham's F-10 (22390-017)	500ml KSFM with supplement (10744-500**)**	500ml DMEM 1x High Glucose (21969-500)
25ml FBS (10100-139)	1ml Penicillin/Streptomycin (10,000:10,000) (15140-163)	50ml FBS (10100-139)
2ml Penicillin/Streptomycin (10,000:10,000) (15140-163)	5ml L-Glutamine (25030-024)	5ml Penicillin/Streptomycin (10,000:10,000) (15140-163)
1ml L-Glutamine (25030-024)	0.2ml Fungizone (15290-018)	5ml L-Glutamine (25030-024)
1ml Fungizone (15290-018)		1ml Fungizone (15290-018)

2.6.1 Thawing of cell lines

Cell lines were thawed rapidly by placing the vial containing a 1ml aliquot of cells, which had been frozen down in FBS and DMSO into a 37˚C water bath. The cells were then gently resuspended in appropriate medium, centrifuged, and the subsequent pellet resuspended in fresh medium to remove the DMSO. Cells were plated onto standard tissue culture flasks. The cells were then incubated in a 5% CO_2 incubator at 37˚C until almost confluent (usually 2 -3 days). Media was changed after 72 hours if the cells were not yet sufficiently confluent to passage.

2.6.2 Passage of mammalian cell lines

Cells were passaged every two to three days depending on how rapidly cells reached confluency. The existing culture media was aspirated off and the cells washed once with sterile PBS (Gibco). 4ml of sterile trypsin 0.5% (Gibco) was then added to each 75cm^2 cell culture flask, and the cells incubated for 5 – 15 mins at 37˚C in 5% CO_2 or until they had started to detach. The culture flask was then tapped sharply to dislodge any adherent cells or cell clumps. Cell concentration was determined using a haemocytometer to count the

number of cells/cm^3. Cells were then seeded into at a concentration appropriate to the size of the tissue culture vessel used. Where appropriate, an aliquot was frozen and stored in cryotubes at each passage using FBS and DMSO (9:1) as freezing medium.

2.6.3 Fibroblast primary cell culture

Perilesional dermis was dissected under a stereo microscope and cut into small pieces, before being cultured in 6 well tissue culture flasks. After 7-14 days, fibroblast cell cultures were established and passaged .

2.6.4 Growth of primary cells on tissue scaffold

Polystyrene tissue culture scaffolds were obtained from Reinnervate, UK. Scaffolds were rehydrated using graded ethanols, and then washed in PBS twice. Scaffolds were then coated with Type I collagen (Invitrogen, UK) before being washed in KSFM once. 1.5 – 3 million cylindroma primary cells were plated onto the scaffold in 250 µl of media, and placed in the incubator for 30 minutes. After this period media was gently added, and then changed every two days.

2.6.5 Characterisation of cell culture using immunocytochemistry

Cells were grown to 40- 60 % confluence in 6 well dishes in a 5% CO2 incubator at 37˚C for two days. The culture media was then removed, the cells washed once with PBS and fixed in 4% PFA for 10minutes at room temperature or methanol at –20˚C (20 – 60 minutes). Fixed cells were washed twice with PBS and used immediately.

Fixed cells were washed in PBS and then blocked with 2% Normal Goat serum. Cells were incubated in the primary antibody solution for at least 1-2 hours at room temperature. After three 10 minute washes with TBST at room temperature, the cells were incubated with fluorescent secondary antibodies mixed with TBST, in the dark for 30 - 60 mins. DAPI was used as a nuclear counterstain.

Table 6 Antibodies used for immunocytochemistry.

Primary Antibody	Concentration of primary Ab	Secondary antibody	Concentration of 2˚
CYLD (Ashworth)	1:200	Anti rat FITC (Jackson)	1:200
CK14	1:200	Anti mouse FITC (Jackson)	1:200
CK17	1:200	Anti mouse FITC (Jackson)	1:200
CK6	1:200	Anti mouse FITC (Jackson)	1:200
SMA	1:200	Anti rabbit FITC (Jackson)	1:200

No primary antibody was added to negative control cells, and each primary antibody was tested with both secondaries to exclude any non-specific cross reaction between antibodies. Finally, the cells were washed three times with TBST before carefully removing the chamber and seals from the slide. The cells were then mounted with a cover slip using Vectashield containing DAPI (Vector laboratories, UK). Images were captured with a UV Zeiss Axioimager microscope (Zeiss, Germany)

2.6.6 Primary cell transfection

Cells were grown to 50% confluence, and transfected with lentiviral particles in culture medium for 24 hours. Lentiviral transfection was performed with shRNA against TRKB, TRKC and DKK2 and compared to a non-silencing control (Openbiosystems, Thermo Scientific, UK). At this point media was replaced with KSFM, and cells grown for a further 48 hours. Transfection efficiency was found to be 80-100%, indicated by GFP positivity. Cells were then grown in puromycin selective media (4 µg /ml) for a further 72 hours, till all cells were GFP positive. Cells were maintained in KSFM for experiments, and monitored for maintenance of transfection using a UV microscope for GFP positivity.

2.6.7 Cell viability assay

Cell viability was assessed using a luminescent assay that generated a luminescent signal in proportion to the amount of ATP present (CellTiter-Glo, Promega, UK). The amount of ATP is directly proportional to the number of

cells present in culture. 4000 cells were plated out per well in a 96 well format in white tissue culture plastic plates with clear bases. After 96 hours, the luminescence was read using a Luminoskan plate reader (Thermo Scientific, UK). Luminescence was measured as luminescent units (RLU) and was tabulated in a spreadsheet. No cell controls were included to determine background luminescence. All conditions were performed in triplicate and experiments were repeated at least three times. Data was then normalised in Prism v5.0 (Graphpad, USA), with the mean value of 3 replicates of the control cells representing 100%, and 0 assigned as 0%. To minimize edge effects, only the central 60 wells were used, with remaining filled with PBS, as well as the inter well spaces.

2.6.8 3D cell viability assay

3D tissue culture scaffolds that were 4 weeks old were used. 2mm discs of the scaffold were punched out and placed in 96 well plates. Cells were grown for two weeks in triplicate in drug dilute in KSFM, with complete exchanges of drug and media every 48 hours. CellTiter-Glo was then added and luminescence was measured.

2.6.9 Drug assay

Cells were grown on 3D tissue culture scaffolds for 28 days, before being harvested and transferred to a 96 well format. Cells were grown in the following inhibitors, diluted in DMSO, with a final concentration of DMSO at 0.1%: K252a and Tyrphostin AG879, Salicylic acid (Sigma, UK), Lestaurtinib (Toronto Research Chemicals). Cells were maintained for 14 days, with exchanges performed every 2 days. The final concentration of DMSO was no greater than 0.1%, and this was used in drug free controls.

2.6.10 Colony forming assay

4000 transfected cells were plated per well in a 6 well tissue culture plate, coated with Type I collagen. Cells were grown 10- 14 days for the colony formation assay. Cells were fixed in 3.3% tricholoracetic acid, washed once and stained with 0.57% sulphorhodamine in 1% acetic acid for 30 mins. Cells were then washed in 1% acetic acid, dried and then scanned on a slide

scanner at 400% original size at 400 dpi. Images of the 6 well plates were then thresholded using Image J software (NIH – v1.64) and then colony counts and total cell area was determined. Data was then normalised in Prism v5.0 (Graphpad, USA), with the mean value of 3 replicates of the control cells representing 100%, and 0 assigned as 0%.

2.6.11 Cell cycle analysis using flow cytometry

Cells were trypsinised, resuspended in PBS and fixed by adding ice cold ethanol whilst gently vortexing the tube, until a final concentration of 70% ethanol was reached. Cells were fixed for 1 hour at 4° C. Cells were then pelleted and resuspended in Cystain Solution (Partech, UK) which stained the nuclear DNA with DAPI. Cells were stained for 1 hour in the dark at 4° C, before analysis on a FACS Canto II flow cytometer (Becton Dickson, UK) using a UV laser. Cells were analysed for total DNA content and a minimum of 10000 events were used for cell cycle data. All cell cycle data was analysed using Modfit (Verity Software House, USA)

2.6.12 Scratch assay

12000 transfected cells were plated in a collagen coated 12 well plate and grown to confluence. A linear scratch was made with a P10 pippette tip in the centre of the well. Cells were then maintained for 96 hours in media with 2.5% serum, to minimise the effects of proliferation on scratch closure. 5 fixed fields of view per scratch were photographed using a Nikon Biostation cell culture and imaging facility, and each condition was repeated in triplicate. Photographs were analysed in Image J (NIH – v1.64) and the size of the scratch remaining at 12 hour intervals was made. The experiment was repeated three times.

2.6.13 Anoikis assay

A 96 well tissue culture plate with clear-bottomed wells (Nun) was prepared such that half the wells were coated with Type I collagen (Invitrogen, UK) and the other half with poly-HEMA. Poly-HEMA was dissolved in 95% ethanol to a concentration of 50 mg/ml. Poly-HEMA was added to cell culture wells at a density of 5 mg/cm^2 and allowed to dry overnight, under sterile conditions in a laminar flow hood. 4000 transfected cells were plated per well in triplicate in

both conditions. After 96 hours, cell viability was measured using a luminescent assay (CellTiter-Glo, Promega, UK) in all wells, and the ratio of wells where cells were forced to grow in suspension was compared to the matched triplicate where they were allowed to grow in adherence. The proportion of surviving cells was compared across different gene knockdown conditions.

2.6.14 Apoptosis assay

4000 cells were plated in a 96 well format. The following day, TNF alpha was added at a concentration of 50 ng/ml, and cells were maintained for 4 hours. A luminescent assay that served as a readout of cleaved caspase 3 was used. This assay lysed cells, and released a luminescent signal in proportion to the available amount of cleaved caspase 3 (ApoGLO, Promega UK)

2.7 IMMUNOBLOTTING

2.7.1 Cell lysis

Cells were lysed in order to investigate expression of different receptors present on the cell surface or intracellular signalling molecules by western blotting. Cells were detached from the flask using Trypsin-EDTA and centrifuged in complete media. The pelleted cells were then resuspended in 1 ml ice cold sterile 1X PBS and centrifuged at 2,000 x g for five minutes at 4°C in a table top micro centrifuge. The pelleted cells were then resuspended in Lysis buffer ((65mM Tris ph7.5, 50mM NaCl, 5mM EDTA, 2% TritonX, 1% NP40, 0.5% Na deoxycholate, 1mM PMSF, 1mM Na Orthovanadate, 0.1% SDS), incubated on ice for 15 minutes then recentrifuged at 16 000 x g for 10 minutes at 4°C. Complete protease and phosphatase inhibitor cocktail tablets (Roche, UK) were used when making the lysis buffer.
The cells were lysed in buffer at a ratio of 40 μl lysis buffer per 50,000 cells. The supernatant was then removed and protein concentration determined using the BCA protein assay (Pierce, UK).

2.7.2 BCA protein assay

An aliquot of cell lysates were diluted to 1:20 dilution with distilled water, and added in a ratio of 1:8 to the prepared BCA assay solution (working reagent), made in accordance to the manufacturer's directions. Typically, 200µl of working reagent was added to 25µl of the diluted sample in a 96 well microplate. Duplicate wells were used for each sample. An albumin standard supplied with the kit was serially diluted with water and a constant proportion of lysis buffer and was included on the plate. The samples were then incubated at 37°C for 30 minutes, before absorbance at 562nm was determined using a plate reader. A standard curve was derived from the mean of the duplicate samples, and protein concentrations were interpolated using Prism software (v 5.0, Graphpad) , after curve fitting had been applied. The values were then corrected for the dilution factor and the protein concentration was normalised across samples for comparative analysis using SDS-PAGE and Western blotting.

2.7.3 Sodium Dodecyl Sulphate -Poly Acrylamide Gel Electrophoresis (SDS- PAGE)

Proteins were resolved using 8, 12, 15% acrylamide gels and BioRad mini-Protean apparatus. Stacking and resolving gels were made up as detailed Table 7. The appropriate percentage resolving gel was prepared, with the addition of N,N,N',N'-Tetramethylethylenediamine (Temed) and ammonium persulphate facilitating the polymerisation of the acrylamide. Before the gel had set it was poured into the apparatus to a level below that at which the gel comb sits. It was overlaid with isopropanol until set, which was then removed, and the stacking gel added. The gel comb was then inserted into the stacking gel so that when set, wells for sample loading were present.

Table 7 Components of hand-cast polyacrylamide gels.

Component	Stacking gel	8% gel	12% gel	15% gel
Acrylamide (30%)	4%	8%	12%	15%
Tris	0.125M pH6.8	0.375M pH8.8	0.375 MpH8.8	0.375M pH8.8
SDS	1 % (v/v)	1 % (v/v)	1 % (v/v)	1 % (v/v)
Temed	0.05% (v/v)	0.05% (v/v)	0.05% (v/v)	0.05% (v/v)
Ammonium Persulphate	0. 1 % (v/v)	0. 1 % (v/v)	0. 1 % (v/v)	0. 1 % (v/v)
Total volume	10 mls	10 mls	10 mls	10 mls

Protein samples were prepared for SDS-PAGE with addition of one quarter volume of 5X SDS-PAGE Laemmli buffer (50 mM Tris pH 6.8, 100 mM DTT , 2% (v/v) SDS, 10% (v/v) glycerol, 0.1% bromophenol blue, beta-mercaptoethanol (BME)) (Laemmli, 1970), boiled for five minutes and loaded onto a gel. This buffer and boiling causes the protein to reduce and denature as well as becoming coated with SDS, which generates a negative charge relative to the size of the protein. The negative charge then allows the protein to migrate towards the positive electrode. Molecular weight standards (Amersham GE) were run simultaneously to allow molecular weight characterisation of samples. Gels were run in SDS running buffer (192 mM glycine, 25 mM Tris, 0.1% (v/v) SDS) at 80-120V for approximately 45 minutes or until the dye reached the bottom of the gel.

2.7.4 Western blotting

Western blotting (wet blot method) was performed in order to specifically detect and visualise bands of protein using specific antibodies. SDS-PAGE gels were run as detailed in section 2.6. 1. Proteins were then blotted onto Immobilon P, 0.45 μm transfer membrane (Millipore). This membrane was pre washed with 100% methanol for five minutes, rinsed with ddH20 for one minute before being equilibrated in transfer buffer (192 mM glycine, 25 mM Tris, 20% (v/v) methanol) for five minutes before assembly of the blotting apparatus. The transfer buffer was chilled at 4°C for at least one hour before use.

Separated proteins were transferred using a BioRad mini-trans blot apparatus for one hour at 100 V. Constant cooling was applied to the blotting system throughout the hour through use of ice blocks and wet ice packing around the blotting apparatus. Following blotting, the membrane was transferred to blocking buffer (Tris buffered saline with Tween-20 (TBST) (50 mM Tris pH 7.4, 200 mM NACI, 0.1% (v/v) Tween-20 and 5% (w/v) dried non-fat milk (Marvel)) and incubated overnight at 4°C. Primary antibody was diluted, according to manufacturer's recommendations, in appropriate blocking buffer and applied to the blot in a sealed bag with end over end rotation for one hour at RT (Table 8). The blot was then washed with wash buffer TBS-T for three, 10 minute washes. The secondary antibody was then added, once again

being appropriately diluted in relevant blocking buffer, and rotated for one hour. The blotted membrane was then washed as previously described. Bands were visualised using enhanced chemiluminesence plus (ECL-PLUS) reagents (Amersham). For western blotting with ECL visualisation, horseradish peroxidase (HRP) conjugated secondary antibodies were used.

Table 8 Antibodies used for immunoblotting.

Primary Ab	Species primary Ab raised in	Concentration of primary Ab	Secondary antibody
CYLD (Ashworth)	Rat	1:250	Donkey anti-rat HRP (Jackson) 1:2000
B-actin (Santa Cruz)	Mouse monoclonal	1:20000	Sheep anti-mouse HRP (Amersham) 1:2000
BCL2 (Cell Signalling)	Rabbit	1:1000	Donkey anti-rabbit HRP (Amersham) 1:2000
TRKB (Cell Signalling)	Rabbit	1:1000	Donkey anti-rabbit HRP (Amersham) 1:2000
TRKC (Cell Signalling)	Rabbit	1:1000	Donkey anti-rabbit HRP (Amersham) 1:2000
DKK2 (Santa Cruz)	Rabbit	1:1000	Donkey anti-rabbit HRP (Amersham) 1:2000
phosphoERK (Cell Signalling)	Rabbit	1:1000	Donkey anti-rabbit HRP (Amersham) 1:2000
ERK (Cell Signalling)	Rabbit	1:1000	Donkey anti-rabbit HRP (Amersham) 1:2000

2.7.5 Enhanced chemiluminescence (ECL)

ECL is achieved through the oxidation of luminol by HRP in the presence of chemical enhancers. The blotted membrane was submerged in an equal volRPN2132) for one minute. The membrane was then covered with Saran wrap and exposed to Kodak Biomax MR auto radiographic film. Exposure time varied between 10 seconds and 30 minutes depending on signal strength, with overnight exposures also performed if the signal was particularly weak.

2.7.6 Stripping and re-probing of blotted membranes

Blotted membranes were occasionally stripped for re-probing with different antibodies, therefore making use of the same blotted samples more than once. Stripping was achieved by three 10 minute washes in stripping buffer, (65 mM Tris pH 8.0, 92 mM BME and 2% (v/v) SDS), which was pre warmed to 50'C in a water bath. The blot was then thoroughly rinsed with 1x PBS and stored in 1x PBS at 4°C until being re-probed. Storage of stripped blots did

not exceed two days. Following storage, the membranes were re-blocked either overnight at 4°C or for two hours at RT with constant agitation. Probing was then carried out as previously described.

3 CHAPTER 3: Phenotype characterisation of *CYLD* mutation carriers

3.1 Introduction

Heterozygous germline mutations within the *CYLD* gene locus have been identified as the cause of three clinically distinct dermatological phenotypes: FC, BSS and MFT (Bignell, Warren et al. 2000; Young, Kellermayer et al. 2006; Saggar, Chernoff et al. 2008). These conditions are unified by a predisposition to develop cylindromas. Although rare in the population, these disorders are associated with a high level of morbidity, which can impact greatly on the quality of life of the affected individual.

Cylindromas are purported to arise from hair follicle stem cells (Massoumi, Podda et al. 2006), a model supported by the numerous tumours seen on hair bearing sites. Ultraviolet radiation (UVR) has been suggested as the major predisposing factor for loss of heterozygosity (LOH) and tumour initiation (Massoumi 2006), based on the presence of face and scalp tumours. However, careful clinical mapping of the distribution of the tumours does not exist to support this hypothesis.

Transgenic *CYLD* knockout mouse models have been derived, which may help inform clinical phenotypes associated with germline *CYLD* mutations. The phenotypes seen in *CYLD* null mice include: an increased sensitivity to cutaneous squamous papilloma formation (Massoumi 2006); immunological defects involving T-cell maturation (Reiley, Zhang et al. 2006) and B-cell responses (Jin, Reiley et al. 2007); an increased predisposition to inducible colitis and colorectal tumour formation (Zhang, Stirling et al. 2006); and a protective effect against lethal *S. Pneumoniae* infections (Lim, Stirling et al. 2007). Altered immunity and susceptibility to cancer is yet to be clarified in humans.

Previous work (Table 9) investigating clinical phenotypes across multiple families has shown little phenotype-genotype correlation with regard to the position of a germline *CYLD* mutation and the tumours types seen in each family (Young, Kellermayer et al. 2006). We were interested in examining clinical phenotypes, tumour distribution, and the burden of disease associated with the diagnosis of germline *CYLD* mutations in two large multigenerational families. This information is a prerequisite for future accurate genetic counselling for individuals from such families.

3.2 Results

3.2.1 Penetrance of tumour phenotype

The pedigrees of two families are shown in Figure 13. They both demonstrate an autosomal dominant pattern of inheritance across 7 generations in family A with 34 out of 133 individuals being reported as affected, and 5 generations in family B with 16 out of 77 individuals being reported as affected. In total, 50 members of both families out of 210 were reported as clinically affected, 27 female and 23 male. This result is significantly less than would be expected with an autosomal dominant inheritance pattern and could be accounted for by either non penetrance of the mutation or a milder presentation of the condition which was under reported especially in the earlier generations. In particular, female IV-1 and male V-3 in family A, obligate carriers on family history for the *CYLD* mutation, were reported as unaffected. Neither of these patients were alive to confirm clinical status.

To address the possibility of non-penetrance within these families, we undertook *CYLD* mutation analysis in all available living affected individuals and contacted non-affected individuals to offer them testing within both families. 9 members of family A, in whom a diagnosis of BSS and FC had been made, were shown to have the familial mutation by sequencing. 5 unaffected members (age range 33-64) were shown not to have inherited the mutation. Family B were similarly examined, with 3 affected members with an FC phenotype, found to have the familial mutation and 3 unaffected members (age range 40-54) shown not to have the mutation.

Although numbers are small, we found no indication for non penetrance of either *CYLD* mutation. The unaffected obligate individuals present in this family most likely indicate a variation in *CYLD* mutation expression within family A.

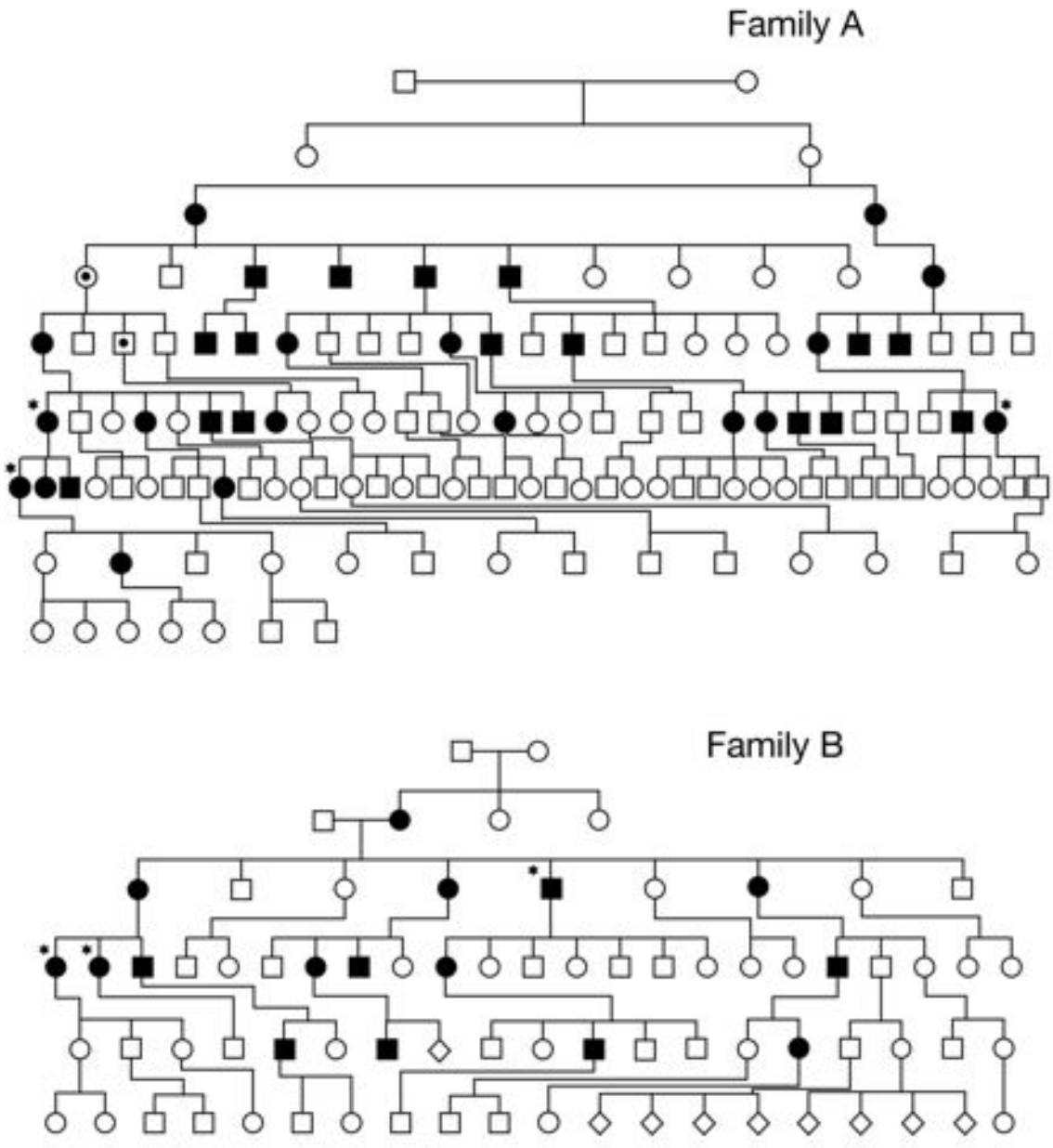

Figure 13 The pedigrees of family A (7 generations) and family B (5 generations).
Patients who have had their scalps removed indicated with a star, and the obligate carriers indicated by a dot.

3.2.2 Severity of phenotype and variety of expression

In our population, 5 female patients and 1 male patient developed severe scalp disease which necessitated entire scalp removal and repair with split

thickness skin grafts. The mean age for this was 55 (50-60) years. Patients who had undergone this procedure were all noted to have multiple tumours on the trunk and genital areas. Other markers of severity include use of wigs pre-operatively (23%) and painful tumours (52%).

Although there is the suggestion of clustering within the pedigree of individuals with a severe tumour burden, relatives of these patients were often noted to have only mild disease. These patients had a few tumours, that were only apparent on close inspection of the scalp. Conversely, one patient in family A (V-14), who had only three tumours on the face, fathered 4 children who each presented with more than 30 tumours on the face. In addition, unaffected obligate carrier V-3 had 9 affected progeny over three further generations, one of whom required total scalp removal.

3.2.3 Phenotype of the obligate carrier

In the course of analysis of another pedigree (Family C), we found a patient carrying germline mutations in *CYLD* that had milia as the only presenting feature (Figure 14). Milia are 1-2mm white papules in the skin that are thought to represent aborted hair follicles, and are a recognised feature of BSS.

A 65-year-old woman developed a few 0.5-1 cm diameter scalp cylindromas and milia on the forehead from the age of 20. Her 44-year-old son demonstrated facial milia only (black arrows). Three other relatives were reported to have tumours; two had scalp lesions and one had facial papules, but were unavailable for examination (Figure 15). We identified a canonical splice acceptor site mutation preceding exon 20 (c.2687-2A>G) in the proband and her son, which was absent in unrelated controls.

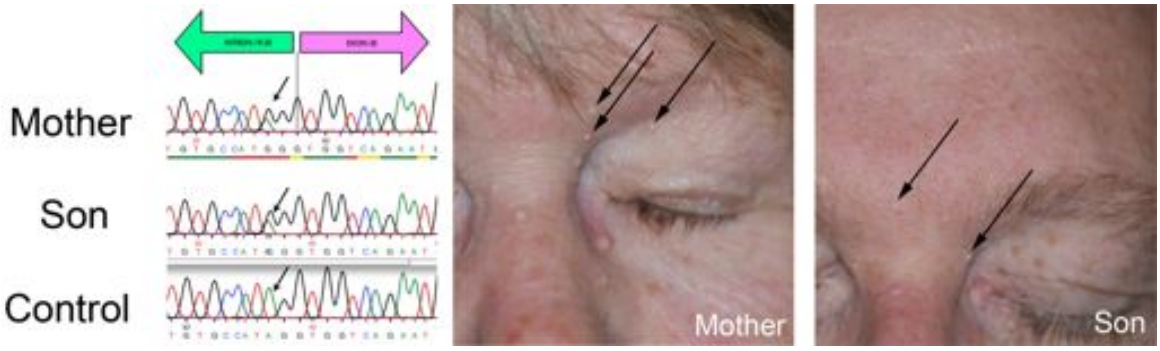

Figure 14 Phenotype of the obligate carrier.
65-year-old woman developed a few 0.5-1 cm diameter scalp cylindromas and milia on the forehead from the age of 20. Her 44-year-old son demonstrated facial milia only (black arrows).

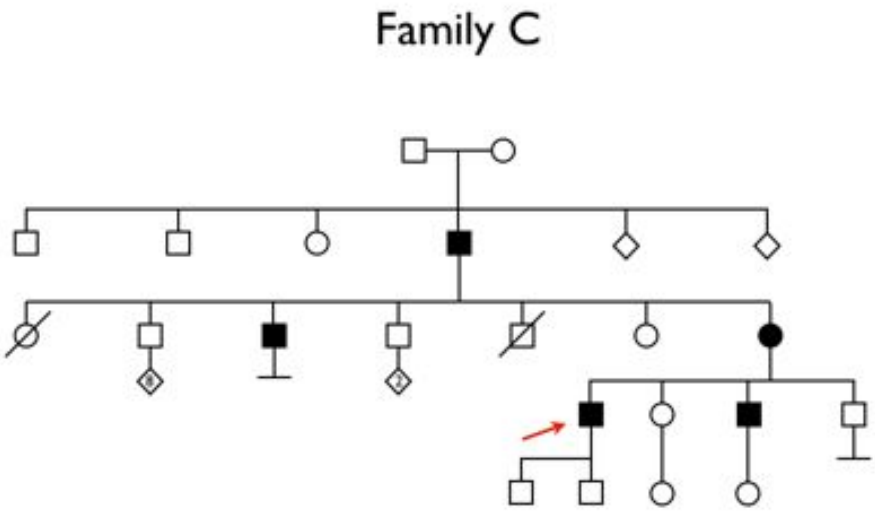

Figure 15 Pedigree with a genotyped obligate carrier.
The patient with milia is indicated with a red arrow

Table 9 Review of series of published pedigrees and correlation with genotype.

This table indicates: 1) The female preponderance described in the literature is based largely on small pedigrees, 2) The reported penetrance can vary between pedigrees 3) Where genotypes are available, there is no correlation with phenotype.

Author	Pedigree size	Proportion Affected	Affected Females	Affected Males	F:M ratio	Clinical Diagnosis	Genotype
Gerretsen	237	13%	19/119	11/118	1.71	BSS	NG
Rajan	133	26%	18/66	16/67	1.14	FC, BSS, MFT	2460delC
Welch	115	25%	15/51	14/64	1.34	BSS	NG
Rajan	77	21%	9/42	7/35	1.07	FC, MFT	2469+1G>A
Welch	67	16%	9/41	2/26	2.85	BSS	NG
Zheng G	36	56%	10/19	10/17	0.89	MFT	2822A>T
Saunders	32	25%	5/14	3/18	2.14	BSS	NG
Zhang G	29	31%	6/20	3/9	0.90	MFT	2272C>T
Salhi	29	45%	6/17	7/12	0.61	MFT	2104-2105 ins C
Young	24	46%	7/14	4/10	1.25	FC, MFT	2806 C>T
Liang	23	26%	4/10	2/13	2.60	MFT	2241_2242 del AG
Liang	20	30%	2/12	4/8	0.33	MFT	1826+2T>G
Hu	17	88%	7/8	8/9	0.98	MFT	2240A>G
Zhang X	15	60%	6/7	3/8	2.29	MFT	2355-2358 del CAGA,
Burrows	14	29%	3/6	1/8	4.00	BSS	NG
Zheng G	14	79%	7/9	4/5	0.97	MFT	1462delA
Zheng G	11	55%	5/9	1/2	1.11	MFT	2128C>T
Burrows	9	44%	3/4	1/5	3.75	BSS	NG
Fenske	9	33%	2/5	1/4	1.60	FC, MFT	NG
Bumgardner	8	50%	3/4	1/4	3.00	BSS	NG
Poblitez-Guirrrez	7	57%	3/4	1/3	2.25	BSS	2253 del G
Susanne	6	67%	1/3	3/3	0.33	FC	NG
Oiso	4	50%	1/2	1/2	1.00	FC	2272C>T

3.2.4 Tumour histology and distribution

We have summarised the clinical and tumour data in Table 10. The average age of onset of tumour formation was 16 years (range 8 - 30), consistent with tumour initiation occurring after adrenarche. In both families, the commonest site for the presenting tumour was the scalp. The clinically diagnosed tumour phenotypes were supported by histology in 10/26 patients.

Family A presented with classical scalp cylindromas, eccrine spiradenomas, trichoepitheliomas and milia. This wide variation in tumour type and clinical presentation in family A supported a clinical diagnosis of BSS within the majority of patients. However, some individuals with exclusively facial trichoepitheliomas, if seen in an isolated setting, would have been diagnosed with MFT.

In contrast, family B presented almost exclusively with cylindromas, supporting a diagnosis of FC in the majority of these individuals.

The detailed tumour distribution maps comprising in total 14 female and 12 male from both families were combined to produce composite maps (Figure 16). From these maps, it is clear that the tumours extend beyond the head and neck, with the trunk being involved in 69% of patients. The tumour distribution forms a “V-shaped” distribution on the trunk with tumours being more concentrated in the midline. Noticeably, tumours are highly concentrated on the hair bearing pubic and genital areas, with a relative absence on other areas of the body such as lower legs and axillary skin. Tumours were not seen on hairless areas of the body such as the palms and soles.

Table 10 Summary of clinical findings in our patient dataset.

						TUMOUR LOCATION				MARKERS OF SEVERITY		
Pt No.	Mutation	M/F	Onset (Yrs)	Tumour Type	Clinical Diag.	Scalp	Trunk	Pubic	Ear	Wig Use	Scalp Removed	Painful Tumour
1	2460	F	25	Cy	FC	+	+	+	+	+	+	+
2	2460	F	12	Cy,Es, Te	BSS	+	+	+	+	+	+	+
3	2460	F	15	Cy, Es, Te	BSS	+	+	+	+	+	+	+
4	2460	F	9	Cy,Es, Te	BSS	+	+	+	+	-	-	+
5	2460	F	8	Cy	FC	+	+	-	-	-	-	+
6	2460	F	15	Cy	FC	+	+	-	-	-	-	-
7	2460	F	25	Cy	FC	+	-	-	-	-	-	+
8	2460	F	12	Cy	FC	+	+	-	-	-	-	-
9	2460	F	11	Cy, Te, Mi	BSS	+	+	+	+	-	-	+
10	2460	F	13	Te	MFT	-	-	-	-	-	-	-
11	2460	F	12	Te	MFT	-	+	-	-	-	-	-
12	2460	M	15	Te	MFT	-	-	-	-	-	-	-
13	2460	M	12	Cy, Es	BSS	+	+	+	-	-	-	+
14	2460	M	30	Cy,Es, Mi	BSS	+	-	-	-	-	-	+
15	2460	M	15	Cy,Te	BSS	+	+	-	-	-	-	-
16	2460	M	NR	Cy,Te	BSS	-	-	-	-	-	-	-
17	2460	M	15	Cy	FC	+	+	-	-	-	-	NR
18	2469	F	18	Cy	FC	+	+	+	-	+	+	+
19	2469	F	18	Cy, Es	FC	+	+	+	-	+	+	+
20	2469	F	23	Cy	FC	+	+	+	+	+	-	+
21	2469	M	NR	Cy	FC	+	+	+	-	NR	+	NR
22	2469	M	17	Cy	FC	+	+	-	-	-	-	-
23	2469	M	16	Te	MFT	-	-	-	-	-	-	-
24	2469	M	NR	Cy,Te	FC	+	-	-	-	-	-	NR
25	2469	M	18	Cy	FC	+	+	+	+	-	-	-
26	2469	M	15	Cy	FC	+	-	-	-	-	-	-
		12M 14F	Avg 16	Total %		81%	69%	42%	27%	24%	23%	52%

Abbreviations: Cy- Cylindroma, Es - Eccrine Spiradenoma, Te- Trichoepithilioma, Mi - Milia, + Present, - Absent, 2460 - Family 1 (2460 del C), 2469 - Family 2 (2469+1 G>A), NR - Not Recorded

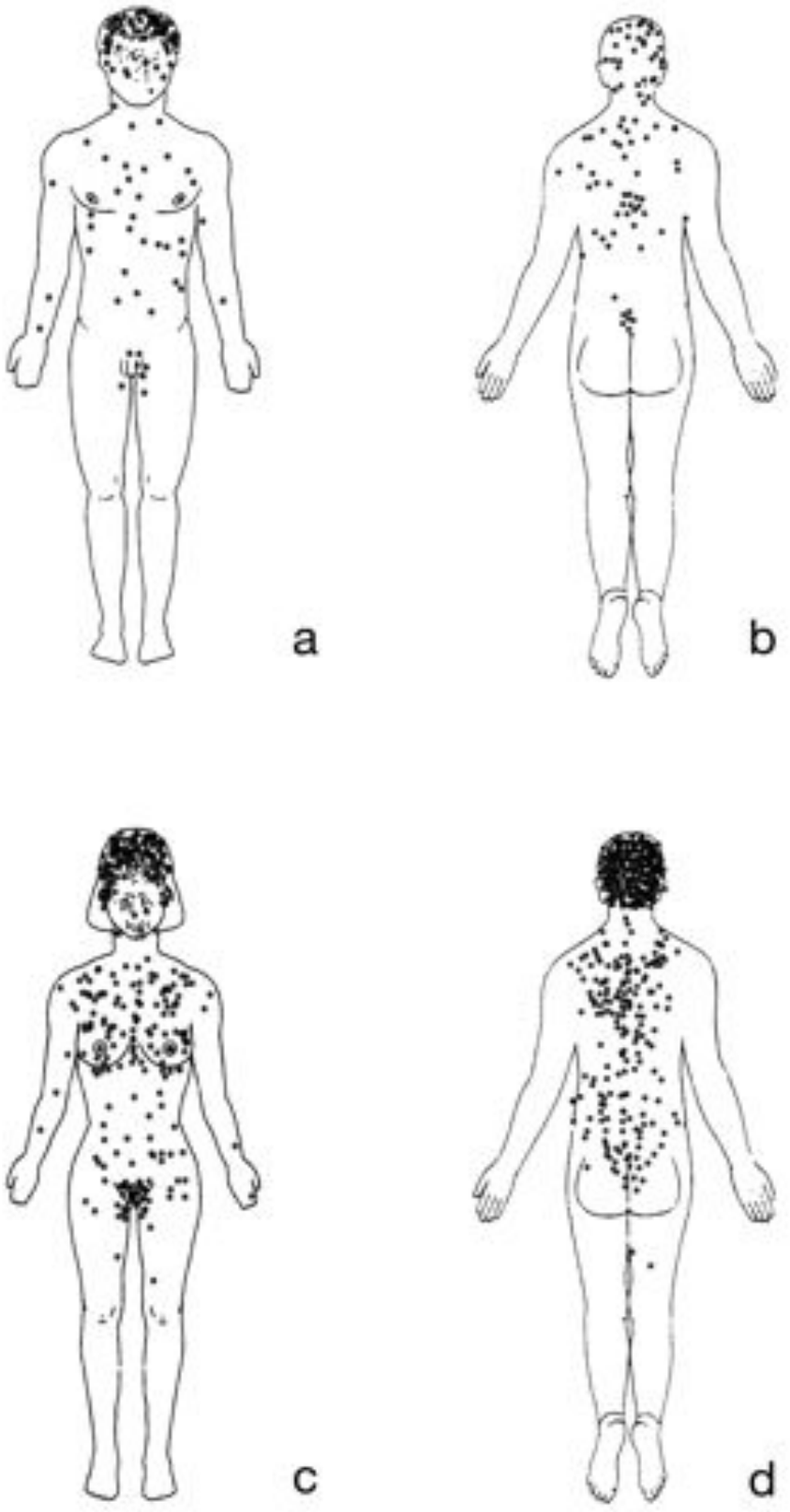

Figure 16 Tumor locations in 12 male and 14 female patients in the two families.

In addition, although not depicted on the tumour maps, patients with advanced scalp tumours (Family A: VI-1; Family B: IV-1, IV-2 and IV-3,)

showed a higher density of tumours over areas that are predisposed to androgenic alopecia (Hamilton, 1951) (Figure 17d). Although in these patients tumours did occur on the occipital and temporal scalp, they were smaller and not confluent, suggesting this to be a true predisposition, rather than one that was biased due to balding. Furthermore this distribution was also seen in female patients. Interestingly, one woman with severe disease reported an increase in number of tumours during pregnancy and also when hormone replacement therapy was started. As this had been previously noted anecdotally (Given, Pickrell et al. 1977), the remaining 13 affected females were directly questioned. No association was seen between presentation of tumours and hormonal exposure, as determined by delineating number of pregnancies, hormonal contraception, hormone replacement therapy and duration of menarche-menopause in other patients.

3.2.5 Impact on quality of life

Pain and disfigurement were commonly reported in individuals from both families as major signs and symptoms. Lesion-associated pain was a major complaint in over 50% of affected individuals, and attributed by the patient to both histologically confirmed cylindromas as well as spiradenomas. Whilst eccrine spiradenomas could be distinguished clinically as they were usually painful on light pressure and had a deep blue hue (Figure 17a), some painful cylindromas were also noted to have blue regions which correlated histologically with areas of spiradenomatous differentiation (Figure 18). This finding of regions within the same tumour showing spiradenomatous and cylindromatous patterns has been previously reported (Crain and Helwig 1961).

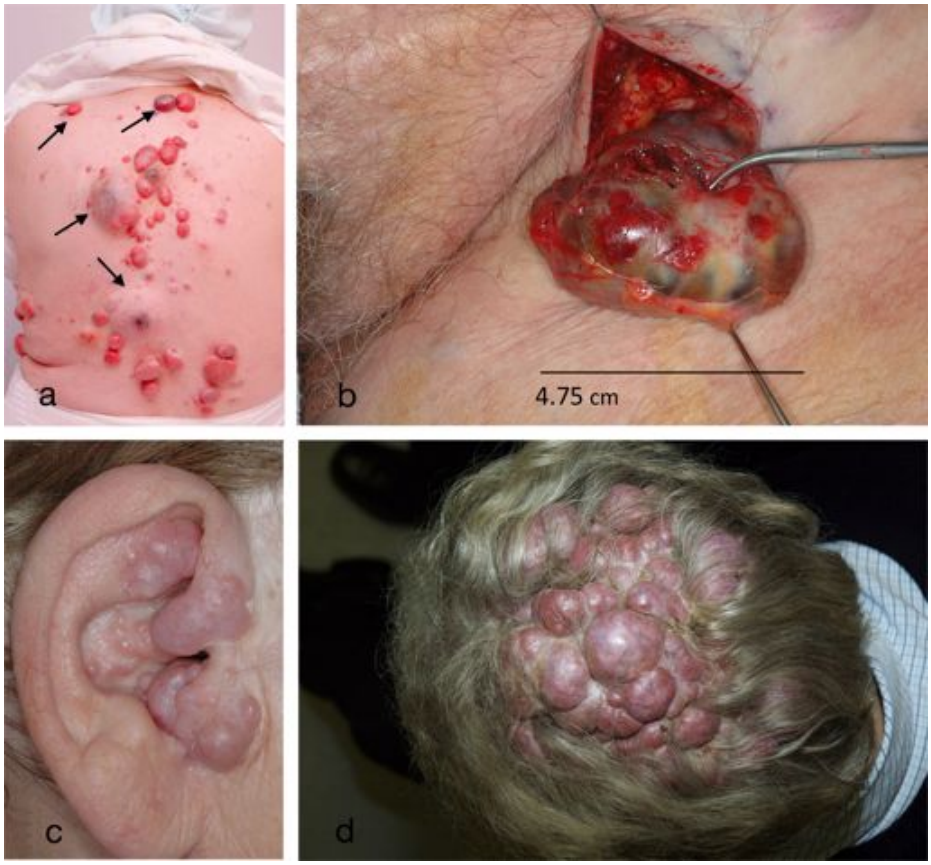

Figure 17 Typical CYLD defective tumours at different sites.
a) Midline distribution of tumors on back (spiradenomas arrowed); b) Pubic eccrine spiradenoma; c) Occluded ear canal resulting in conductive deafness; d) Scalp demonstrating larger confluent tumors clustering in areas predisposed to androgenetic alopecia.

Apart from pain, tumours on the back which were compressed during sitting or sleeping were susceptible to pressure necrosis, which caused problems due to ulceration and chronic discharge. Tumours in the pubic area were found in 42% of affected individuals and resulted in sexual dysfunction (Figure 17b). 27% of affected individuals were noted to have numerous confluent cylindromas in the ear canal resulting in a conductive deafness when occlusion of the ear canal occurred (Figure 17c).
Taken together, the impact on quality of life due to repeated surgery, scalp removal, painful tumours, deafness and sexual dysfunction appears to be underreported in the literature and a cause of major unaddressed morbidity within families.

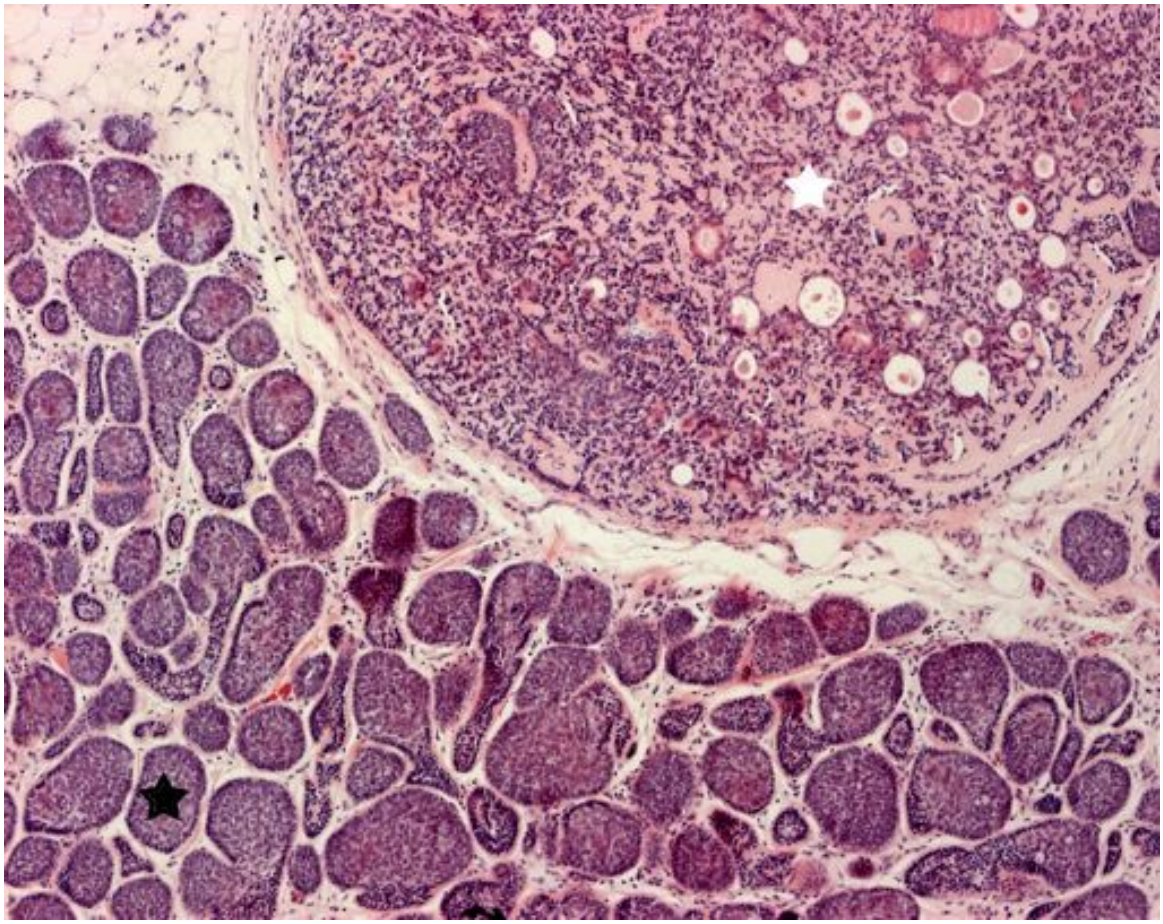

Figure 18 Spiradenocylindroma.
Haematoxylin and eosin stain displaying the characteristic pattern suggestive of cylinders in cross section which gave rise to the term cylindroma (lower left corner; black star), with an adjacent region (upper right corner; white star) within the tumor displaying a large ball of basophillic cells with areas of ductal differentiation, consistent with an eccrine spiradenoma (Original magnification 10x).

3.2.6 Associated co-morbidities

In keeping with a previously reported association (Jungehülsing, Wagner et al. 1999), one individual was also diagnosed with bilateral parotid gland tumours and underwent bilateral parotid surgical excision. (Family B: III-5). Unfortunately we were unable to obtain the histology report on these tumours. Due to the immunodysregulation observed in *CYLD* null mouse models, affected patients were also questioned as to symptoms associated with either an immunodeficiency or autoimmune phenotype. The results revealed no evidence of a predisposition to recurrent infections, autoimmune disease, colitis, infertility and non-cutaneous cancers. One patient reported vitilligo,

whilst other diseases reported included ischaemic heart disease and osteoarthritis.

3.3 Discussion

3.3.1 CYLD mutation carriers experience significant clinical morbidity

Here, we provide the most comprehensive study of the clinical features associated with germline heterozygous mutations within the *CYLD* gene locus.

In addition to the well recognised morbidity associated with face and scalp cylindromas in these families, we highlight that the tumour predisposition associated with this condition extends beyond the face and scalp affecting both the trunk and genital areas. These less well recognised sites of tumour formation can impact greatly on the quality of life experienced by these patients. Unless actively sought these complications may be under-diagnosed and not treated.

In our patient cohort, we found only a slight female preponderance of the disease. However, the impact of this disease appears to be more severe in females with 5 women, compared to only one male, undergoing entire scalp removal. Although clinical photographs support the underlying clinical severity that warranted this procedure, it is also feasible that the psychological impact and social disability has a greater impact on females.

Basal cell adenomas and adenocarcinomas of the parotid glands and minor salivary glands have been reported in association with this disorder (Jungehülsing, Wagner et al. 1999). In our families only one such case was reported, suggesting that this is an uncommon event in these families.

None of our patients developed any of the clinical features associated with the *CYLD* null ($CYLD^{null}$) mouse models (Massoumi 2006; Reiley, Zhang et al. 2006; Zhang, Stirling et al. 2006; Jin, Reiley et al. 2007; Lim, Stirling et al. 2007). Conversely, none of the $CYLD^{null}$ mice developed cutaneous cylindromas. This phenotypic difference may be due to the germline molecular heterozygosity found in the patients compared to the homozygote status of the $CYLD^{null}$ mouse models, and would suggest that either loss of

the second *CYLD* allele in humans is a rare event outwith the hair follicle or that somatic loss of the second *CYLD* allele in cells from other tissues may be non-viable. However, this explanation does not account for the observation that there is over-representation of mutations within the 3' end of *CYLD* gene in all published human cohorts ascertained on their predisposition to cutaneous tumours.

Thus, an intriguing alternative explanation for the phenotypic difference between $CYLD^{null}$ mice and the patients is that the human mutations represent hypomorphic alleles, which could potentially result in the production of a truncated protein with the potential for tissue-specific dominant negative pathogenic interactions. Evidence underpinning this theoretical possibility comes from recent murine models in which truncating mutations ($CYLD^{truncated}$) were engineered into the mCYLD locus. In direct contrast to the viable phenotype seen in the $CYLD^{null}$ models (Massoumi 2006; Reiley, Zhang et al. 2006; Zhang, Stirling et al. 2006; Jin, Reiley et al. 2007; Lim, Stirling et al. 2007), the $CYLD^{truncated}$ mouse models died shortly after birth (Ermolaeva, Sebban et al. 2006; Trompouki, Kontoyiannis et al. 2006). However, in humans, mechanistic data is still limited. In cylindroma tissue, a truncated form of the CYLD protein has not been visualised on immunohistochemistry despite the antibody recognising the N-terminus of the CYLD protein (Massoumi, Podda et al. 2006). In addition, the only heterozygous full *CYLD* gene deletion reported to date is in a 14-year-old girl with a large heterozygote chromosome deletion encompassing the *CYLD* locus (DECIPHER 2009). Although the preliminary report does not indicate the presence of cutaneous tumours, she is currently too young to exclude this as a possible future complication. Further work is necessary before precise mechanisms of the pathogenicity of the mutated *CYLD* locus can be formulated.

3.3.2 Tumour initiation

The pluripotent hair follicle stem cell as the probable cell of origin of cylindromas (Massoumi, Podda et al. 2006) is supported by our clinical data. The occurrence of multiple, different, rare (Harwood, McGregor et al. 2003) skin appendage tumours in these patients suggest tumours may arise from a

cell which is not fully committed to a lineage of differentiation. Furthermore, sites recognized to have an absence of hair follicles such as the palms and soles are spared. As the hair follicle stem cell compartment becomes better defined (Ohyama, Terunuma et al. 2006), it is to be hoped that the cell of origin of cylindromas will become clearer.

One key event in familial cancer tumourigenesis is loss of the wildtype allele in a previously heterozygous cell (LOH). Due to the high incidence of tumour formation on the face and scalp in patients with a *CYLD* mutation, it has been postulated that UVR associated DNA damage may be the main initiating factor in the development of cylindromas (Massoumi 2006; Massoumi and Paus 2007). Our data supports this hypothesis, as all patients have a tumour on the face or scalp, and the highest number of tumours is at these sites. In contrast however, we demonstrate a high incidence of genital and trunk cylindromas and spiradenomas in more than half of the affected patients. Tumours at lifelong light protected sites such as the pubic skin indicate that other mechanisms independent of UVR must play a role tumour initiation. There is further supportive data from a study of patients with nevoid basal cell carcinoma syndrome (NBCCS), where the cutaneous tumours are also thought to arise from hair follicles. This study (Goldstein, Bale et al. 1993) showed that patients with NBCCS (who carry *PTCH* mutations) have a disproportionately high proportion (59-65%) of tumours on the trunk, compared to the general population (9-12%) who present with basal cell carcinoma. There was no correlation to sun exposure behavior, (though numbers were small) and tumours were seen at genital sites as well as in highly pigmented skin types. Taken together, the distribution of skin tumours resulting from germline mutations in 2 known tumour suppressor genes suggest alternative, non-UVR mediated mechanisms of tumour induction are pertinent. One feature of human hair that may highlight such mechanisms is the differential sensitivity of follicles at different body sites to hormonal stimulation. Puberty highlights follicles that change from fine vellus hair to coarse hair in response to hormonal stimulation in some areas such as the beard area, axilla and pubic region. Another follicular response seen is acne, where hormonally driven proliferation of the opening of the hair follicle at certain sites results in comedones, inflammatory pustules and papules. The

detailed mapping of tumour distribution in our patient cohort demonstrates an increased incidence of tumours in areas associated with hormonally stimulated hair follicles such as the pubic hair and upper trunk. The distribution on the torso correlates well with the distribution of hair follicles affected by acne at puberty. The converse of this, a relative absence of tumours on unstimulated sites such as distal limbs, palms and mucous membranes is also seen. Further evidence that the tumours are more likely to arise from hair follicles that are hormonally stimulated come from the observation that the onset of tumours occurs after adrenarche (Welch, Wells et al. 1968), and the larger size and confluency of scalp tumours in areas predisposed to androgenic alopecia (male pattern balding is thought to reflect follicles that preferentially senesce following androgen stimulation (Bahta, Farjo et al. 2007)). Finally, recent preliminary data in mouse follicles has shown that CYLD may play a role in hair follicle cycling (K Moriwaki 2007). Whilst the precise mechanisms remain undetermined, the clinical data is supportive of hormonally sensitive hair follicles being vulnerable to LOH at the CYLD locus, leading to tumour induction.

3.3.3 Genetic counselling issues

The data we present here confirms that even within one family, mutations within the *CYLD* locus give rise to a wide variation of clinical phenotypes. More than 75 mutations have now been identified in *CYLD*, with the majority found towards the carboxyl terminus of the protein, the position of the catalytic residues of ubiquitin hydrolase (Massoumi and Paus 2007; Saggar, Chernoff et al. 2008; Blake and Toro 2009). Clustering around the catalytic residues of ubiquitin hydrolase suggests the loss of deubiquitinating activity is important for the development of a cutaneous phenotype. The poor genotype-phenotype correlation with regard to tumour histology, and wide variation in clinical expression that we demonstrate in our families has been noted by other authors (Young, Kellermayer et al. 2006; Zhang, Huang et al. 2006). In contrast, there have been families in China with up to 4 generations affected (Salhi, Bornholdt et al. 2004; Zheng, Hu et al. 2004)with predominantly MFT, where the same mutation in other populations have resulted in heterogenous phenotypes, highlighting the possibility of population-specific modifier genes.

This wide variation in clinical phenotype means that genetic counselling and prognostication in families with known CYLD mutations is not straight forward. Some mutation carriers may have milia as the only presenting feature, a finding that can be missed by professionals unfamiliar with cutaneous tumours. Milia are found in other genodermatoses (Berk DR 2010), and hence, can only be taken to be an indicator of *CYLD* mutation carrier status when another relative has either phenotypic features or a confirmed genotype. The presence of two obligate carriers in our pedigrees who were reported as unaffected by their relatives, but had severely affected children, underlines the importance of all 'at risk' individuals within a family being offered predictive testing if available or examined by a specialist with a prior knowledge of the condition.

A review of the literature places the oldest patient to develop a first tumour at 42 years (Martins and Bartolo 2000). Taken with our data of unaffected patients of the pedigree who were sequenced, this suggests that unaffected individuals in families that reach this age are unlikely to be carriers of a mutation (Biggs, Wooster et al. 1995). As most couples have children prior of this age, predictive testing for a known familial mutation rather than clinical examination of the 'at risk' individual would be required if reassurance concerning future or an ongoing pregnancy was requested. Our results also indicate the impact on the lives of future generations of affected individuals cannot be gauged by the clinical severity of previously affected individuals. Based on the variation seen in our European families, we suggest that the clinical diagnosis of BSS, MFT and FC have no prognostic, diagnostic or descriptive value and should be abandoned. Individuals found to have a germline *CYLD* mutation should be given the diagnosis of "CYLD cutaneous syndrome", as the eventual clinical phenotype may be uncertain. This nomenclature will also avoid confusion with regard to possible genetic heterogeneity.

3.4 Conclusions

The need for non-surgical approaches in the treatment of these families is emphasised by the repeated surgical procedures individuals in both families

underwent, the frequencies often only being restrained by available clinical resources.

Our current understanding of CYLD's function as a negative regulator of the NFκB pathway (Kovalenko, Chable-Bessia et al. 2003), highlighted a role for aspirin in the treatment of these patients (Brummelkamp, Nijman et al. 2003). However the clinical efficacy of aspirin in one trial of topical aspirin was limited, with only 2 out of 12 tumours showing complete remission after 24 weeks (Oosterkamp, Neering et al. 2006). This preliminary work however does suggest that further studies are required to analyse the dose, timing and efficacy of NFκB modifiying drugs, perhaps at an earlier stage of tumourigenesis or prophylactically in these patients. Furthermore, detailed molecular dissection of these tumours may yield other druggable pathways in this tumour syndrome.

Here, we highlight the wide variation in both clinical severity and tumour type present in multigenerational families with CYLD cutaneous syndrome. Significantly, the distribution of tumours suggest that hormonally sensitive hair follicles may be predisposed to tumour formation. Further understanding of the role of CYLD in regulating pathways such as NFκB may help develop non-surgical treatments of this devastating condition.

4 CHAPTER 4: 3D reconstruction and immunohistochemical characterisation of CYLD defective tumours

4.1 Introduction

Patients with germline mutations in the tumour suppressor gene *CYLD* develop multiple highly organised cylindromas (Figure 19 a,c). These tumours are so called as the tumour cells appear to be arranged in cylinders irrespective of which way the specimen is sectioned. Interestingly the same patients also develop poorly organised spiradenomas, which are clinically and histologically distinct (Figure 19 b,d). Spiradenomas, unlike the pink, painless cylindromas, are painful blue nodules and demonstrate poor architectural organisation. Occasionally patients develop features of both tumours within the same lesion (Figure 19 e). We found that in a study of two large pedigrees, that pain was a reported feature in 52% of affected patients, suggesting this may be a frequent event (Rajan, Langtry et al. 2009). The coexistence of both tumours in the same specimen has been thought to reflect a process of tumour maturation from one form to another, however a molecular mechanism has not been proposed (Michal, Lamovec et al. 1999). Further characterisation of these CYLD defective tumours therefore may provide insight into novel mechanisms that may explain the coexistence of these distinct tumours.

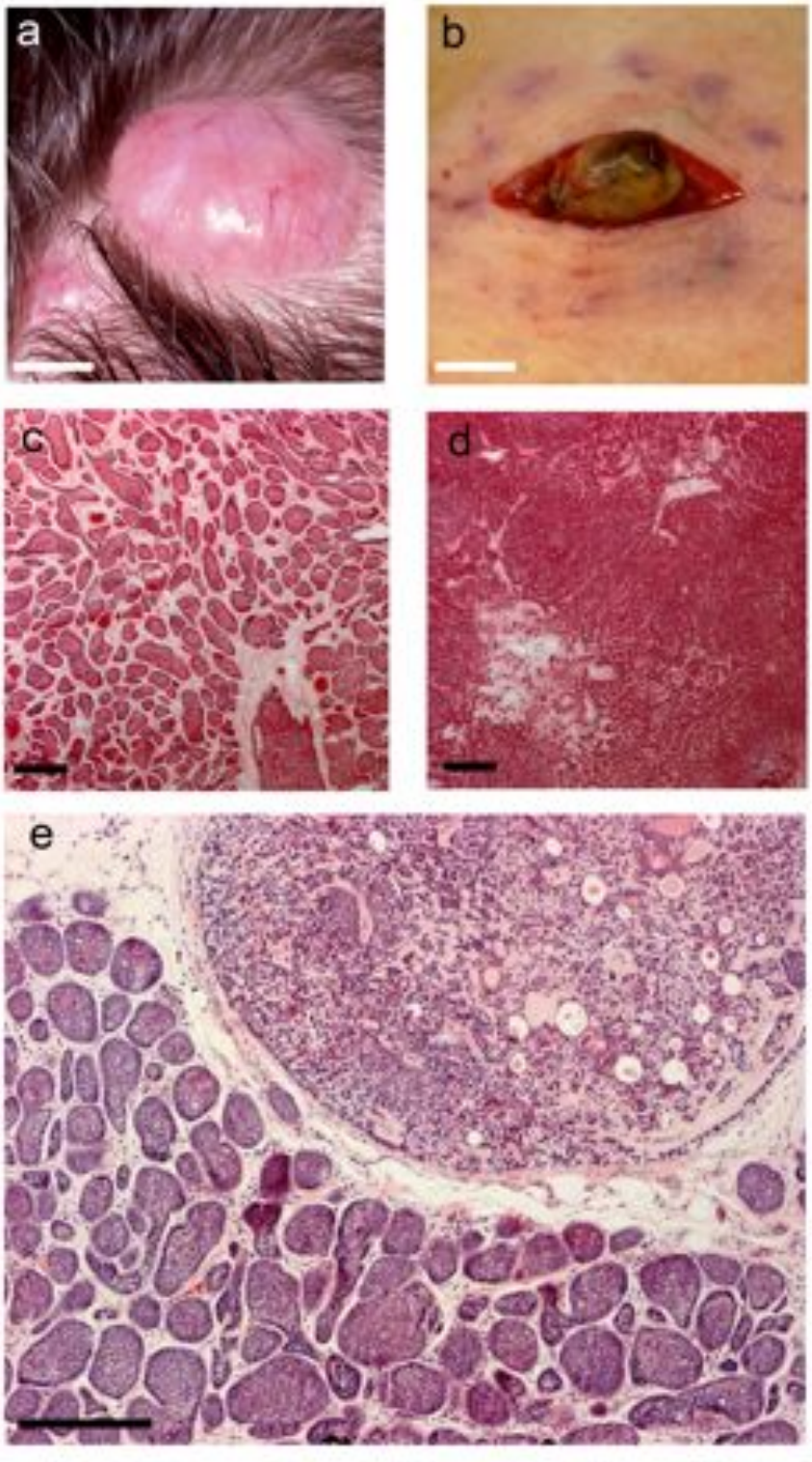

Figure 19 *CYLD* mutation carriers exhibit distinct clinical and histological tumour phenotypes. Patients with germline *CYLD* mutations develop (a) pink cylindromas on the scalp and trunk as well as (b) blue painful eccrine spiradenomas seen here at surgery. (c) Cylindroma tumours are highly organised with tumour cells arranged in cylinders, with basophilic cells at the periphery, and larger pale cells seen centrally. (d) Spiradenoma tumours are poorly organised, with areas of ductal differentiation and a lymphocytic infiltrate. (c-d. 5x original magnification) (e) Both tumour types are often seen

together in the same sample, giving rise to the term “spiradenocylindroma ”. (e. 20x original magnification). (Black scale bars indicate 100μm; white scale bars indicate 1cm.

4.2 Results

4.2.1 Cylindromas and spiradenomas represent extremes of a spectrum of tumour organisation

Cylindromas are highly organised, with tumour cells arranged in cylinders, which inspired the original naming of this tumour. To understand how this histological pattern is observed irrespective of how the tumour block is sectioned, we reconstructed 12 tumours *in silico* from serial sections. This allowed visualisation of the patterning of tumour cells in three dimensional (3D) space. Serial sections were taken at 5 μm thickness through tumour specimens, typically covering 750-1000 μm of the block. Standard staining was performed and photomicrographs were taken. Alignment of these images was performed manually using Amira software (V4.0 – Visage Imaging), allowing accurate overlap of serial sections. Artificial colour labels were applied to individual cylinders of tumour cells, allowing tracking of cylinders through the tumour block. Surface rendering of the ensuing columns of tumour cells and virtual flythrough examination was performed within Amira software.

This analysis demonstrated that cylindroma tumour cells grow contiguously, and form an interconnected network of cylinders, with branching and budding seen (Figure 20, Supplementary video 1 http://www.youtube.com/watch?v=95biz3YEDhU). Tracking of cylinders through the tumour block with different coloured labels demonstrated that all cylinders eventually connected to each other at some level in the tumour block. This was found to be the case in all twelve specimens examined. This finding of contiguous growth had prompted us to include tumours with mixed features of both cylindromas and spiradenomas. Spiradenocylindromas, a recognised feature in *CYLD* mutation carriers (Michal, Lamovec et al. 1999), have previously been suggested to represent a collision phenomenon, that is two adjacent tumours growing into each other (Goette, McConnell et al.

1982). However, personal clinical observation of *CYLD* mutation carriers revealed that cylindroma tumours can become painful over time and that this is often associated with a change in colour of the tumour from pink to blue, suggesting a spiradenoma focus developing within a preexisting cylindroma at least in some cases. 3D reconstruction of 4 spiradenocylindromas demonstrated that consistent with this clinical observation, they were also contiguous structures, with highly organised cylindroma growing in direct connection with poorly organised spiradenoma (Figure 21 and Supplementary video 2 http://www.youtube.com/watch?v=WcUSHk9NavI). We were able to observe a spiradenoma focus that links adjacent areas of cylindroma, suggesting an area that has transformed to spiradenoma, displacing the surrounding cylindroma columns. Finally, when reconstructed *in silico,* small spiradenomas (two out of twelve specimens) displayed an area that was highly organised, which may represent an initial cylindroma that had transformed into a spiradenoma (Figure 22 and Supplementary video 3 http://www.youtube.com/watch?v=NT7USIzcZPo). Methods to access to the video material, and the associated legends are detailed in Appendix A.

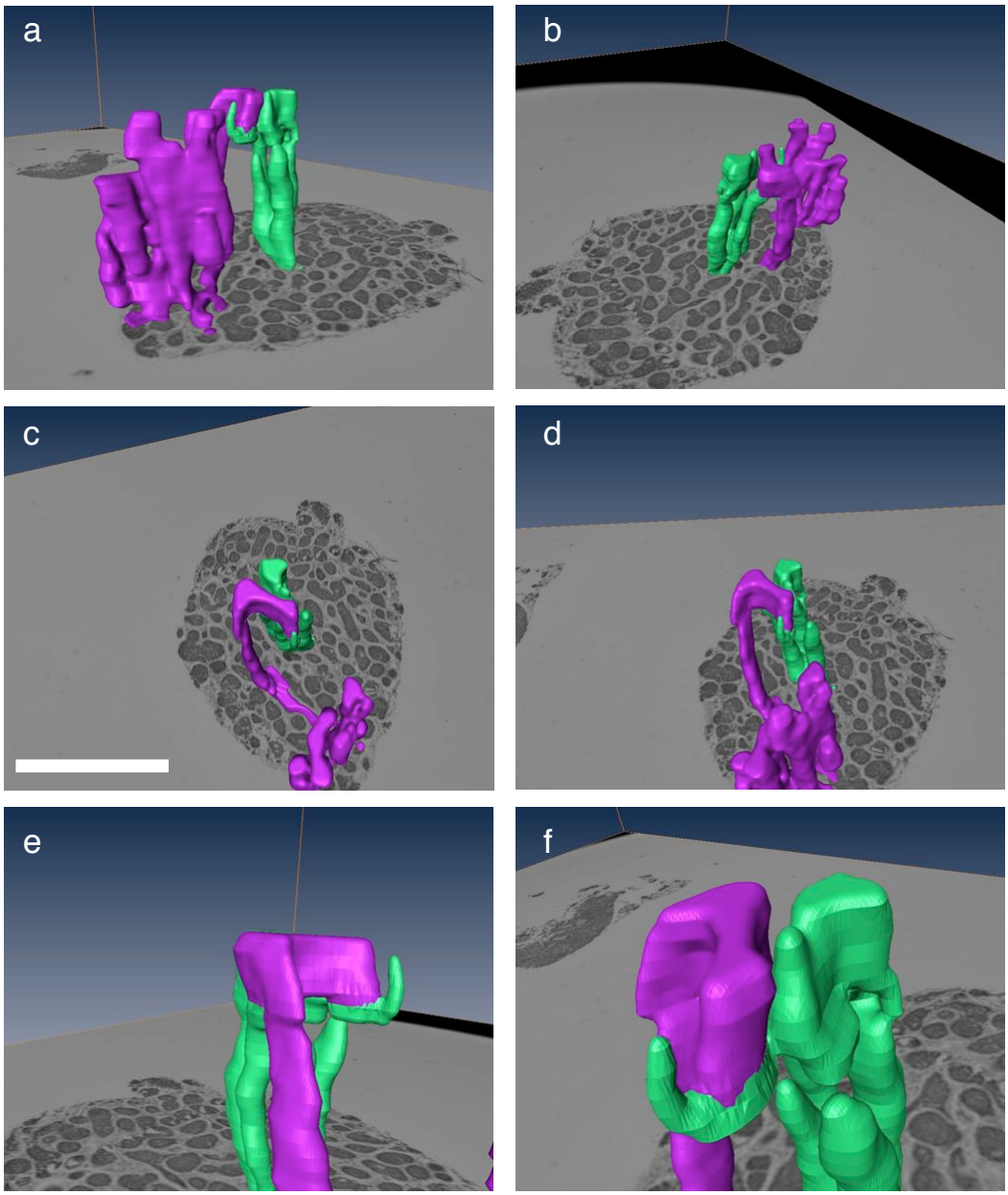

Figure 20 Cylindromas grow in a contiguous manner.
Paraffin embedded CYLD defective tumours were serially sectioned, typically at 5 μm thickness, stained with standard techniques and photographed. Images were aligned and tumour islands were traced through the ensuing "virtual block" *in silico.* Distinct artificial colours were applied when tumour islands were traced so that individual columns of tumour cells could be followed. (a-f) Cylindroma tumours were contiguous in growth, and each cylinder seen in cross section ultimately was connected to adjacent cylinders, a feature seen in other common hair follicle related tumours such as basal cell carcinoma. Here, a single cylinder of tumour cells was labelled in purple, and followed through the block, with all directly connecting cells labelled in the same colour. A similar process was performed on a distant island of tumour cells in green. The two separate columns of tumour cells are seen to connect higher up in the specimen. For clarity only two columns are shown, and only the first section is displayed. A video of a virtual flight through the green column via the demonstrated connection to the purple column is available (Supplementary video 1). Scale bars where shown indicate 1mm.

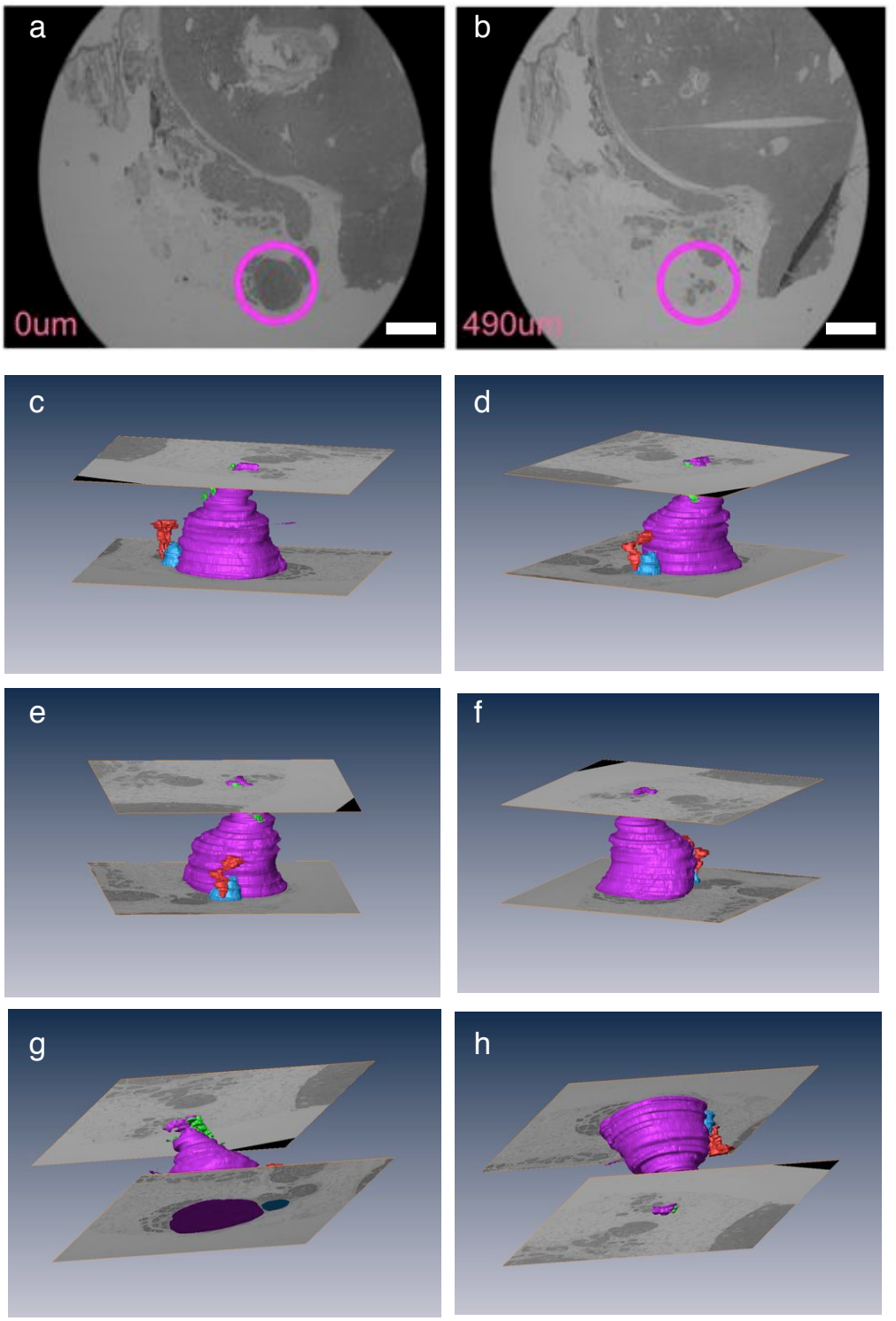

Figure 21 Spiradenocylindroma: Spiradenomas and cylindromas are part of the same tumour mass. (a-h) We also found that areas that were highly organised (cylindroma) were growing in direct connection with poorly organised areas (spiradenoma). We found areas in the tumour blocks that were disorganised at one level (a) that when followed through were organised further in the block (b), seen 490um apart in this example. When traced through, and labelled in purple, the two areas were part of the same column of tumour cells. Three further organised areas, labelled in red, blue and green were also connected to the purple mass. 2 sections are displayed (Original magnification 2.5x). A video of the

reconstructed spiradenocylindroma is available (Supplementary video 2). Scale bars where shown indicate 1mm.

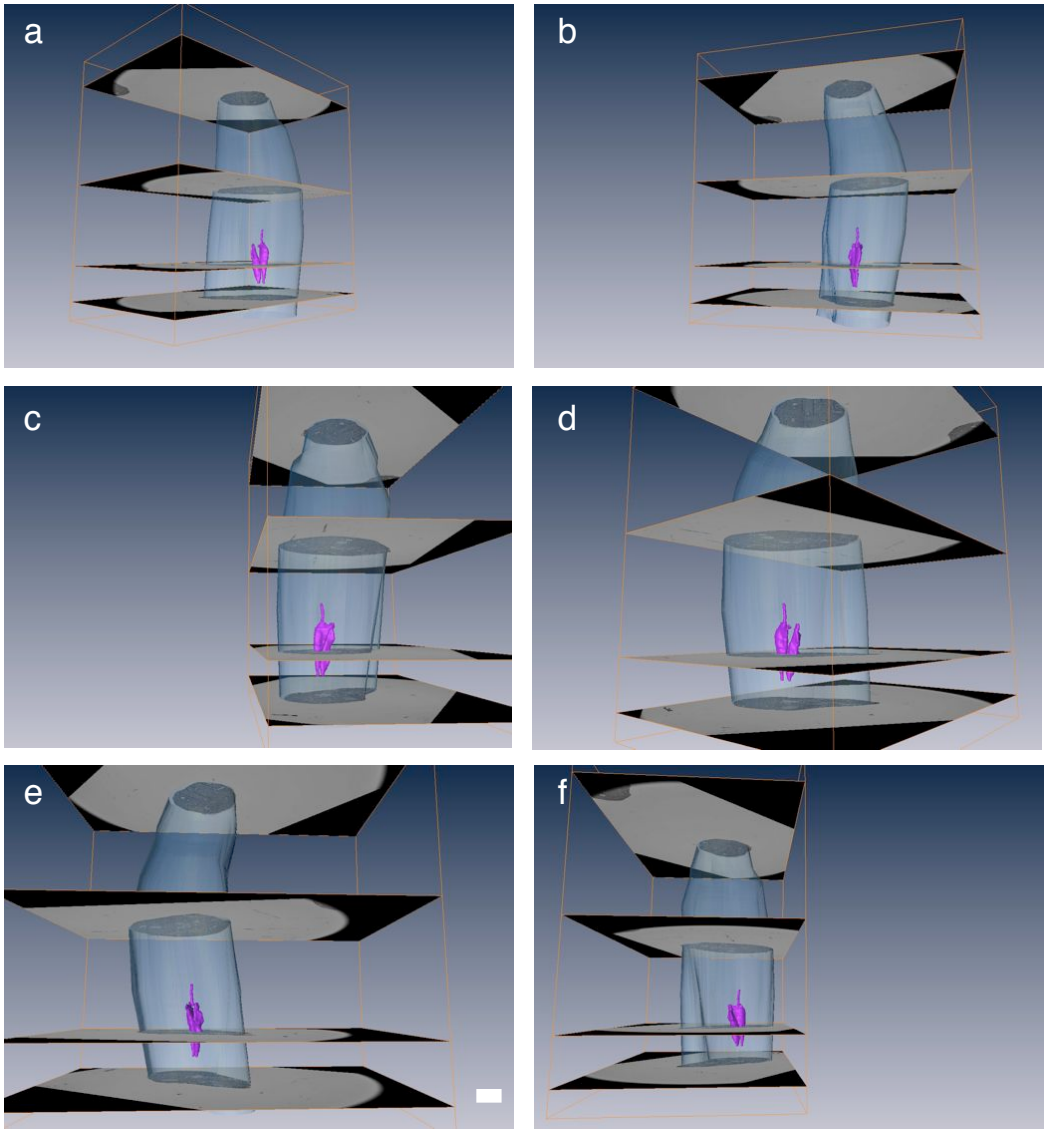

Figure 22 Spiradenoma with a central focus of cylindroma.
(a-f) Small spiradenomas sometimes displayed an area that was highly organised, that may represent the original organised focus of tumour cells. In this block, the small organised column of cells is shown in purple, and the surrounding disorganised mass of cells are shown in light blue. 4 sections are displayed. A video of the rotating reconstructed block is available (Supplementary video 3). Scale bars where shown indicate 1mm

4.2.2 Immunohistochemical characterisation of CYLD defective tumours

Characterisation of CYLD defective tumours has been previously performed highlighting expression of cytokeratins associated with the hair follicle and eccrine ducts (Meybehm and Fischer 1997). We validated these findings in tumours derived from our pedigrees, which formed the basis of using these markers to characterise primary cell cultures from these tumours. These findings are shown in Figure 23 below and were largely consistent between cylindromas and spiradenomas.

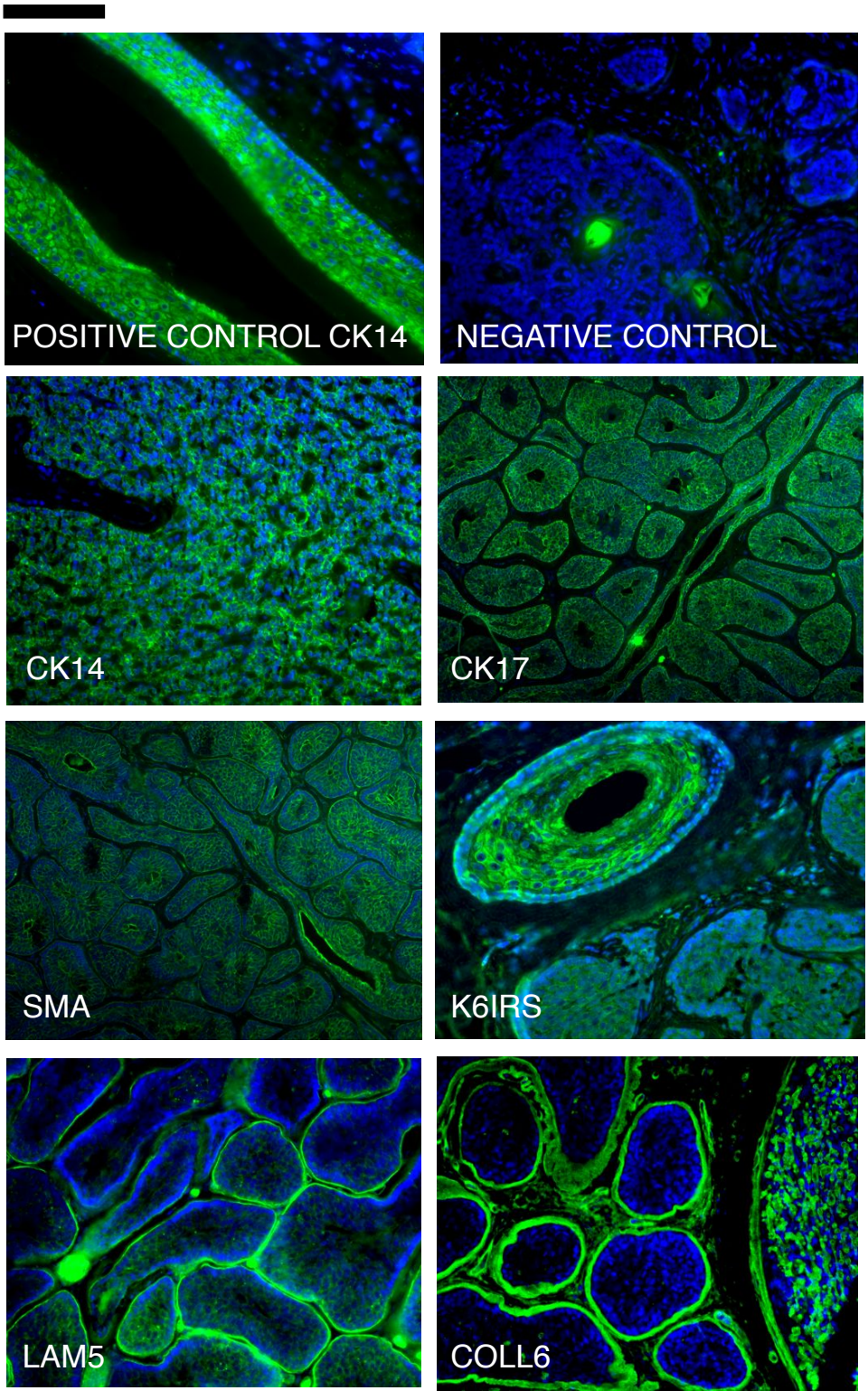

Figure 23 Indirect fluorescent immunohistochemical characterisation of CYLD defective tumours. Tissue sections underwent antigen retrieval, were probed with antibodies as indicated in the panels, and stained with FITC conjugated secondary fluorescent antibodies. DAPI was used as a nuclear counterstain. The outer root sheath of a hair follicle was used as a positive control (CK14), and no primary antibody sections were used as a negative control. Scale bar indicates100μm.

Other host-derived cells that may be present in these tumours were investigated. CD8 expressing lymphocytes in the tumour cells, were found in spiradenomas more than cylindromas (Figure 24a-b). This antibody however cross reacted with CK15, and whilst the cells that were CD8 positive had small dark nuclei consistent with lymphocytes, further validation with other lymphocytic markers are needed.

We chose to investigate the vascular supply of CYLD defective tumours, as the tumour size reached suggested that the tumour cells were likely to require a significant blood supply. We found that some cells as well as structures were CD31 positive (Figure 24c-d).

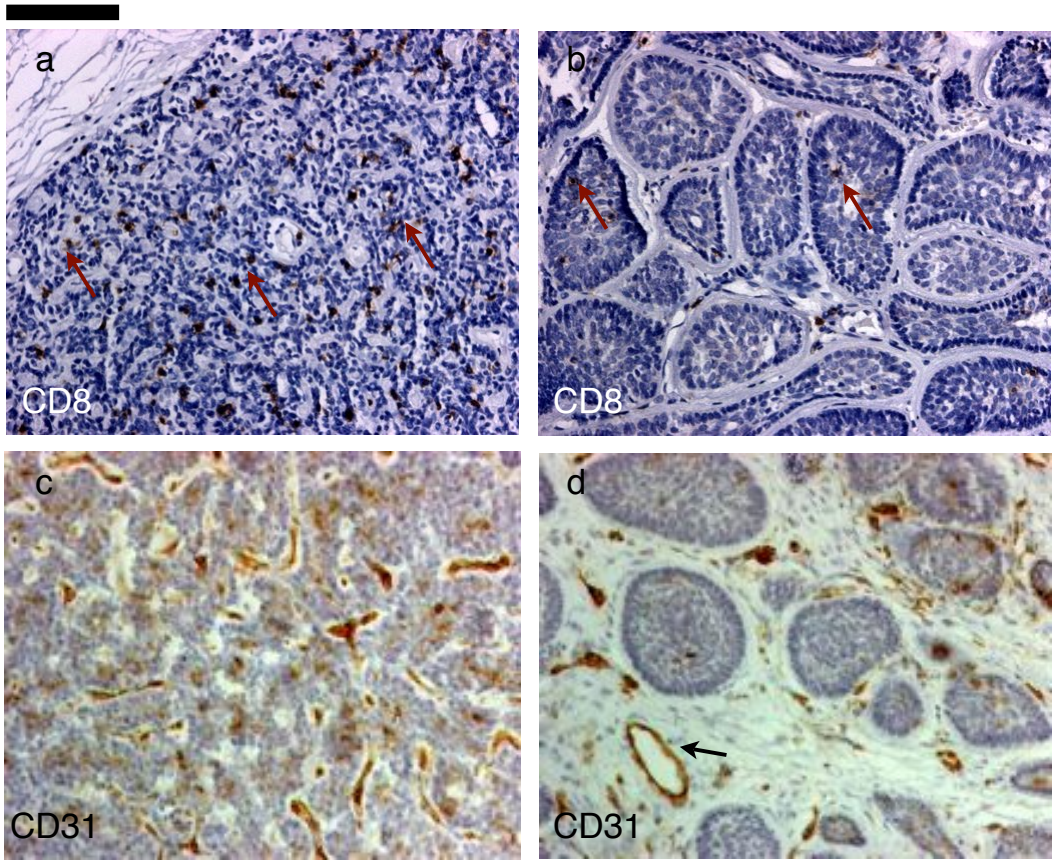

Figure 24 Lymphocyte and vascular markers are expressed in CYLD defective tumours.
Tissue sections underwent antigen retrieval, were probed with antibodies as indicated in the panels, and followed by secondary HRP antibodies. Protein expression was visualized using DAB. Haematoxylin was used as a nuclear counter stain. (a) A spiradenoma with multiple lymphocytes arrowed in red, with a cylindroma (b) with few lymphocytes seen. (c) CD31 positive channels seen within spiradenoma, and (d) occasionally amongst islands of cylindroma tissue. A blood vessel is arrowed (Scale bar indicates 100μm).

We chose to investigate the difference in proliferative index using Ki 67 staining in CYLD defective tumours. Spiradenomas and cylindromas both

demonstrated Ki 67 positivity in central paler cells, rather than peripheral basophilic cells (Figure 25a-b). Spiradenoma had more proliferative cells when compared to cylindroma (Figure 25c).

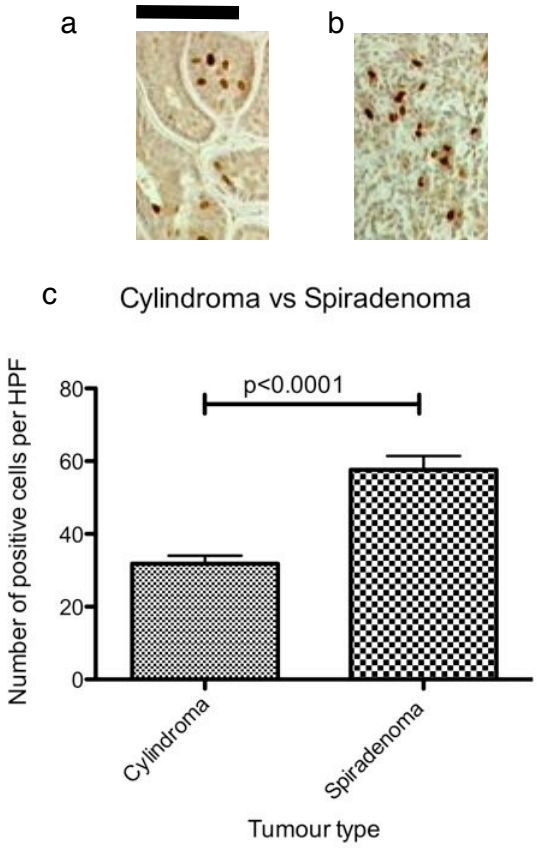

Figure 25 Spiradenoma has a greater proliferative phenotype than cylindroma.
Tumour sections on a custom-built tissue microarray underwent antigen retrieval, were probed with Ki 67 antibody and protein expression was visualized with a horseradish peroxidase/DAB system. Haematoxylin was used as a nuclear counterstain.(a) Cylindroma, (b) spiradenoma, (c) An increase in Ki 67 staining is seen in spiradenoma compared to cylindroma. Statistical significance was tested using a t-test ($p<0.0001$). Error bars indicate standard error of the mean. Scale bar indicates 100μm.

4.3 Discussion

CYLD defective tumours represent an intriguing model of cutaneous tumour biology. Highly patterned cylindromas and disorganised spiradenomas are seen to arise on the same patient and sometimes within individual specimens. Here, in keeping with these data, we show that cylindromas and spiradenomas represent extremes of a spectrum of tumour organisation.

We show that islands of cylindroma cells grow as contiguous structures, a finding consistent with the growth pattern found in sporadic hair follicle tumours such as basal cell carcinoma (Lang, McKelvey et al. 1987; Scheibe, Braumann et al. 2010). An extension of this concept is the finding that cylindromas and spiradenomas grow in direct connection with each other, which accounts for the recurrent finding that features of both tumours are found in the same specimen, termed spiradenocylindroma. Finally, we demonstrate that in small spiradenomas, a focus of organised cylindroma can be found within, growing in contiguity with the surrounding tumour. These data support a model where the default pattern of growth of the tumour cells once a "second hit" event such as LOH happens is a to grow in a tubular pattern. The tubular structure then buds and branches, and grows in a contiguous fashion, giving rise to a cylindroma. As this structure is folded to grow within the constraints of the mechanical forces exerted by surrounding tissue *in vivo*, sectioning of this folded structure results in cylinders seen irrespective of which way the tumour is sectioned. In spiradenoma, there is loss of patterning seen probably at an early stage, before the tumour has grown significantly and as we have demonstrated (Figure 22), a preexisting cylindroma can be demonstrated in smaller tumours. This loss of patterning is possibly mediated by a third molecular event, or “third hit”, giving the cells a proliferative or survival advantage. Ki 67 immunostaining supports an increase in proliferation in spiradenomas. In spiradenocylindromas, we propose loss of this tubular patterning within an established cylindroma happening at a later stage, resulting in the coexistence of the two tumour types in the same sample. These findings are summarised in this model (Figure 26).

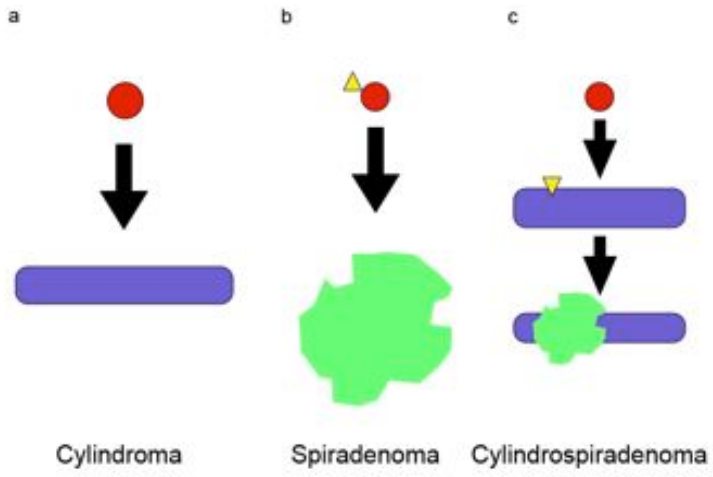

Figure 26 Cylindromas and spiradenomas represent extremes of a spectrum of tumour organisation. (a) Loss of heterozygosity in a putative pluripotent hair follicle cell results in exclusive expression of mutant CYLD, conferring a growth advantage for these cells, (indicated by the red sphere). The cells are restricted to a tubular growth pattern due, giving rise to a structure where growth by extension, branching and budding is feasible (indicated by the purple column). This structure when folded gives rise to the finding that the tumour cells are seen organised as cylinders irrespective of the way the tumour is sectioned. (b) Loss of patterning following a "third hit" (indicated by the yellow triangle), giving rise to a disorganised mass of tumour cells (indicated by the green mass), with no restriction to grow in a tubular pattern. (c) A late "third hit" event that results a tumour that has already grown as a cylindroma to develop a region that is poorly organised, a finding supported by clinical and pathological observations of the coexistence of two tumour types in the same specimen.

The demonstration of the two tumour types as part of a spectrum fits with the immunohistochemical characterisation demonstrating overlapping features between cylindromas and spiradenomas. In particular cytokeratin markers 6, 14 and 17 were seen in both tumour types, a finding corroborated by others (Meybehm and Fischer 1997). Interestingly, there was a difference in lymphocytic infiltration, seen predominantly in spiradenomas, suggesting the tumour milieu was different and may attract these cells. It would be interesting to further characterise these cells with other lymphocytic markers. The extent of vascular marker expression raises the possibility of extensive vasculature that could be targeted with anti angiogenic treatments, however further work in *in vivo* models is needed clarify the feasibility of this approach.

4.4 Conclusions

These data highlight the spectrum of tumour patterning seen in CYLD defective tumours. We demonstrate that cylindroma grows in a contiguous fashion. Furthermore we demonstrate coexistence of cylindroma and spiradenoma within the same tumour specimen, with areas that are highly organised growing in direct connection with areas that are disorganised. In keeping with these findings, we propose a model where a third hit may result in the loss of organised tubular growth. Mechanisms that may cause in this third hit are intriguing, and may be clarified by molecular profiling of these different tumour types.

5 CHAPTER 5: Molecular profiling of CYLD defective tumours

5.1 Introduction

CYLD mutant carriers develop hair follicle related tumours, of which cylindromas and spiradenomas grow to the largest size and have significant clinical impact. The presence of painful spiradenomas and truncal and genital tumours can have a significant impact on quality of life, as can the surgery used to remove lesions as this may culminate in entire scalp removal. As such, the development of non-surgical approaches to control tumour burden are required (Rajan, Langtry et al. 2009). Novel therapeutic approaches with inhibitors of the nuclear factor kappa beta (NFκB) pathway such as aspirin were proposed when *CYLD* was found to encode an ubiquitin hydrolase that negatively regulated this pathway (Brummelkamp, Nijman et al. 2003; Kovalenko, Chable-Bessia et al. 2003; Trompouki, Hatzivassiliou et al. 2003). However, initial clinical studies with topical salicylic acid demonstrated a significant response in only a small proportion of treated tumours (Oosterkamp, Neering et al. 2006). Therefore, a more detailed understanding of the molecular dysregulation caused by loss of functional CYLD is warranted and this may inform the development of novel therapeutic approaches.

Whole genome profiling of tumours, to assess the genetic and transcriptomic changes, is widely used in cancer biology to discover new druggable pathways. Indeed, the targeting of such pathways, with selected treatment of tumours dependent on the presence of specific driver mutations, has been shown to have a significant benefit in skin tumours such as melanoma. In this model, patients shown to carry a particular activating mutation (V600E) in BRAF, a tyrosine kinase, have been shown to have a clinical response to tyrosine kinase inhibitors targeting mutant BRAF. This response is not seen in patients with melanoma where the tumour does not have this mutation (Bollag, Hirth et al. 2010; Flaherty, Puzanov et al. 2010). CYLD defective tumours from patients with germline mutations in this tumour suppressor gene are uncommon. As existing technologies for transcriptomic profiling requires fresh frozen tissue with high quality RNA, this approach is difficult to adopt. I have been able to use this

approach with this tumour syndrome as I have access to fresh tumour tissue from patients undergoing routine surgery to control tumour burden. This allows for discovery of novel pathways in a human tumour model, independent of assumptions based on the previously described functions and ascribed roles played by CYLD. This is particularly important, as *CYLD* deficient mouse models with complete loss of CYLD expression do not develop cylindromas or spiradenomas. Apart from contributing to the discovery of targetable pathways for *CYLD* mutation carriers, such data would inform the pathogenesis of hair follicle tumours, as well as other tumours which are CYLD deficient.
Here, we have performed a detailed molecular analysis of tumours from patients with *CYLD* mutations, and highlight a novel targetable pathway in this cutaneous tumour syndrome.

5.2 Results

5.2.1 Cylindroma and spiradenomas tumours are genomically similar and stable

Fresh frozen tumours from patients with germline CYLD mutations were microdissected to isolate tumour cells and perilesional control cells. Genomic analysis of cylindroma and spiradenoma tissue was performed on 12 tumours and 7 perilesional skin samples using a 32K bacterial artificial chromosome (BAC) tiling path array (Natrajan, Weigelt et al. 2009). This BAC array platform has been shown to be as robust as, and to have comparable resolution with high density oligonucleotide arrays (Coe, Ylstra et al. 2007; Tan, Lambros et al. 2007; Gunnarsson, Staaf et al. 2008). Comparative genomic hybridisation was performed using DNA extracted from peripheral blood leukocytes from the same patient as the reference. No obvious regional genomic amplification or deletion was noted in 12 tumour samples (Figure 27). Moreover, no difference was seen between cylindromas (n= 7) and spiradenomas (n=5).

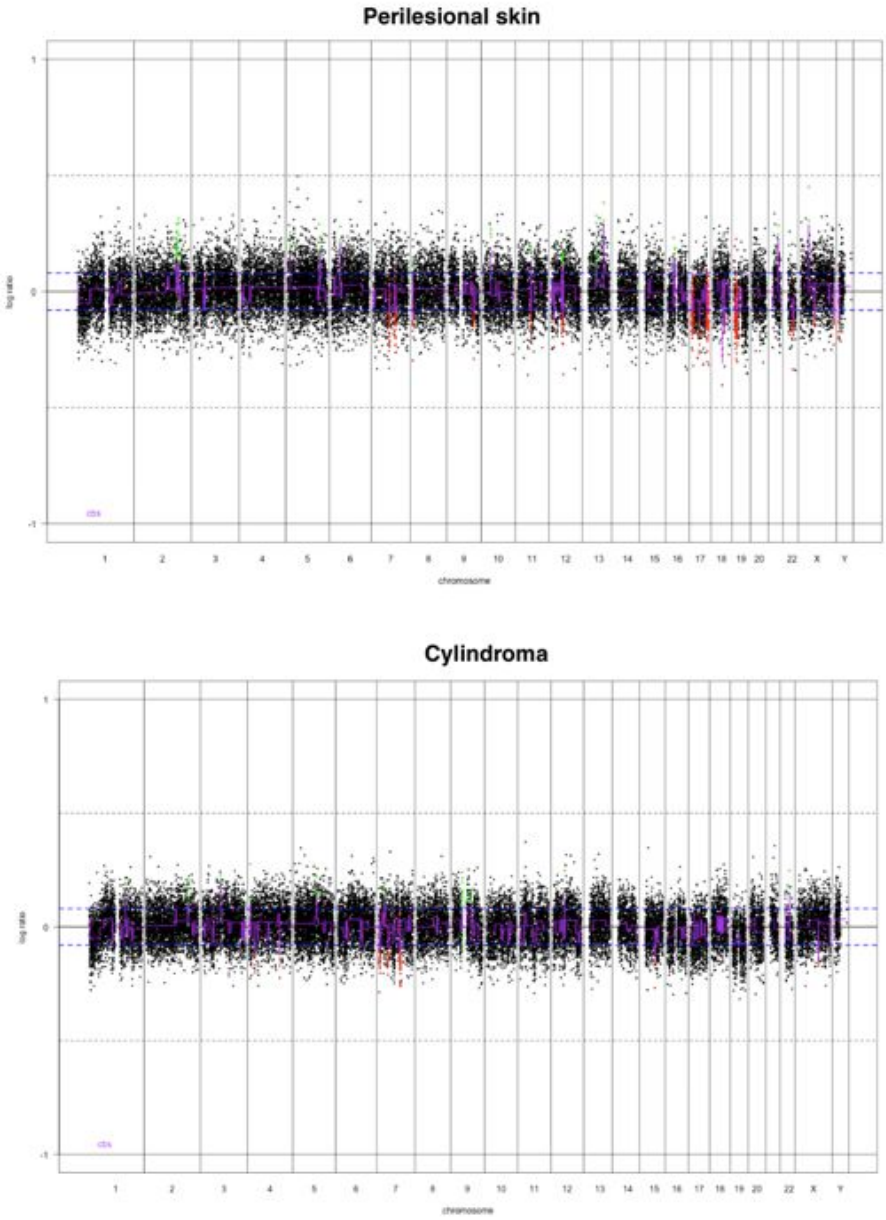

Figure 27 32K BAC tiling path array CGH of perilesional skin and cylindroma tumour.

Genomic DNA was extracted from microdissected tumours and control perilesional skin and competitively hybridised against patient matched peripheral lymphocyte DNA on a 32K BAC tiling path array. BACs categorised as displaying genomic gains or amplification are plotted in green and those categorised as genomic losses or deletion in red. Circular binary segmentation (cbs)-smoothed Log_2 ratios are plotted on the Y-axis in purple against each bacterial artificial chromosome (BAC) clone according to genomic location on the X axis. The threshold for a gain or loss is indicated by the blue dashed line (log_2 ratio > 0.08 or < -0.08) and the threshold for an amplification or deletion is indicated by the black dotted line (log_2 ratio > 0.45 or < -0.45). No significant copy number change was seen between tumours and perilesional skin; an indicative result for perilesional skin and a cylindroma tumour is shown.

Given the apparent absence of genomic copy number variation observed using BAC arrays, we went on to perform high resolution SNP typing using a 550K SNP array platform (Illumina, USA) on four further cylindroma tumours and one control sample. This revealed copy number silent LOH for the entire arm of chromosome 16q in all four tumours but no other significant changes (Figure 28, Figure 29).

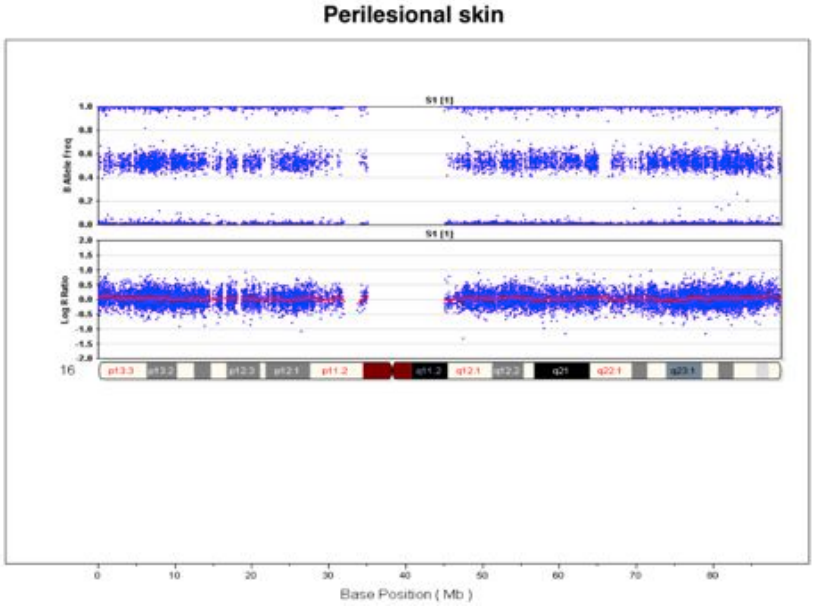

Figure 28 Perilesional skin SNP microarray analysis showing data from chromosome 16.

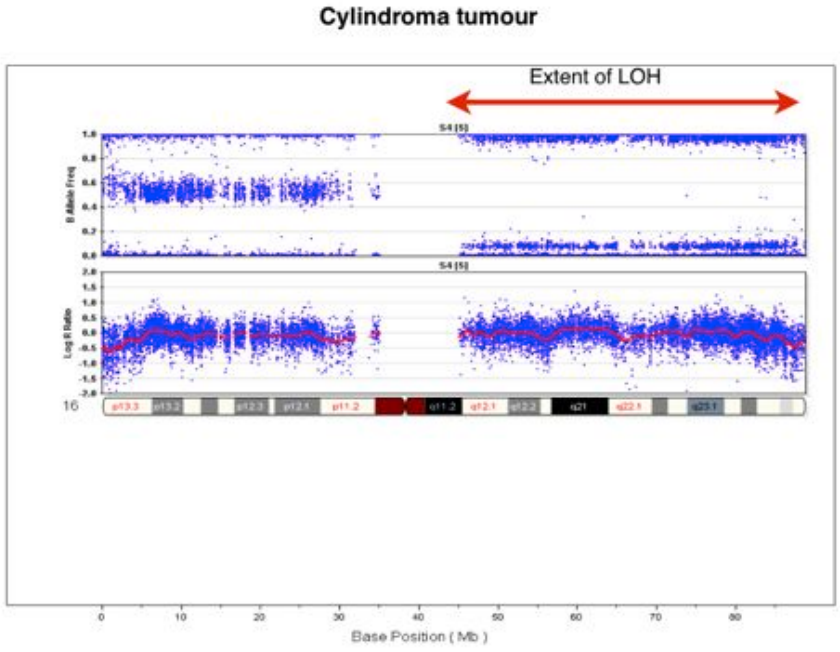

Figure 29 Cylindroma tumour SNP microarray analysis showing data from chromosome 16.
To examine for genomic changes at higher resolution, single nucleotide polymorphism (SNP) typing was performed using a 550K SNP array in a further 4 cylindromas. LOH was seen across the entire arm of chromosome 16q in all 4 samples, indicated by the red arrow.

LOH status at the site of the mutation was assessed in a further 27 tumours used in this study, which was possible as the genotype of each patient was known. LOH was assessed using genomic DNA from microdissected tumours by using restriction enzymes that specifically were unable to cut only the mutated allele in

each tumour. Polymerase chain reaction (PCR) amplification was performed using primers that flanked exon 18 (CYLD18F and CYLD18R) and the PCR product was subject to restriction enzyme digestion using enzymes chosen for pedigree specific mutations: *HpyCH4V* (c.2460delc) and *Sml* I (c.2469+1G>A). This revealed LOH at the site of the mutation in 75% of the 27 tumours, suggesting the mechanism resulting in LOH to be similar in the majority of tumours (Figure 30).

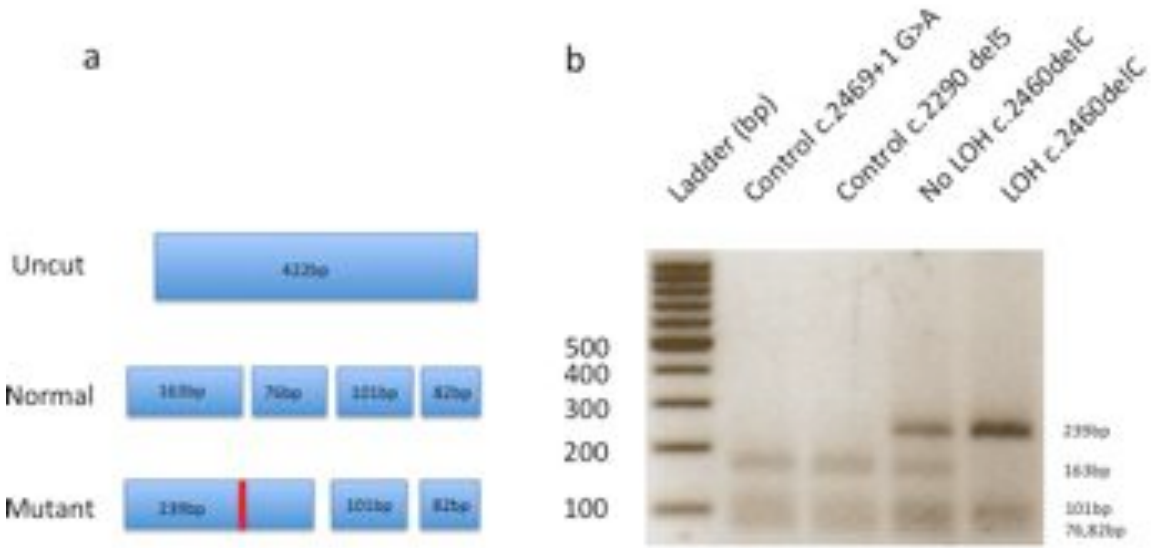

Figure 30 Restriction enzyme digest to determine LOH at c.2460delC.
PCR amplification of DNA from microdissected tissue of a region that was 422 bp in size was performed. These DNA products were subject to restriction digest and resolved on a 2% agarose gel. a) Restriction schematic - The enzyme used for this site (c.2460delc), *HpyCH4V,* would only cut the normal allele in 3 places, and the mutant allele in 2 places (lost restriction site following mutation shown as red line). b) Lane 1- 100bp ladder; each band is a 100bp increment. Lane 2 and 3 - Control DNA, resulting in 4 cut products (Sizes – 163bp, 101bp, 82bp and 76bp). Lane 4 shows presence of the normal allele, indicated by the 163bp band, which is digested by *HpyCH4V*, and the mutant allele (238 bp band), as well as the smaller producte, (101, 82 and 76bp) .Lane 5 - LOH resulting in only the mutant allele results the larger 239bp band, and the smaller 101 and 82bp bands, but not the 163bp and 76bp band. Resolution of the smaller products was not performed as this was not critical to the genotyping.

5.2.2 Transcriptomic analysis of CYLD defective tumours

Gene expression profiling was performed on total RNA extracted from 42 microdissected samples, consisting of 19 cylindromas, 9 spiradenomas, 4 trichoepitheliomas and 10 perilesional controls. A bead array platform (Illumina, USA) that is capable of assaying expression of 24,526 transcripts for each sample was used (April, Klotzle et al. 2009). Average signal values from replicate beads were summarised, log transformed, and normalised using quantile

normalisation across all samples (Workman, Jensen et al. 2002). Unsupervised clustering analysis of the individual transcriptomes (24526 probes) by Euclidean distance revealed close clustering of the majority of cylindroma and spiradenoma tissue, and distinct clustering of the perilesional skin and trichoepithelioma tissue (Figure 31). This was corroborated with clustering by an independent technique that used multiple bootstrapping to determine the robustness of the clusters. Clustering of transcriptomes using individual probes (24526) was employed and dissimilarity was measured using the correlation method using a statistical package (pvclust) (Suzuki and Shimodaira 2006). Clusters were maintained, however due to the small numbers of tumours used, statistical significance was seen between tumours and controls ($p<0.01$), but not between tumour subsets (Figure 32).

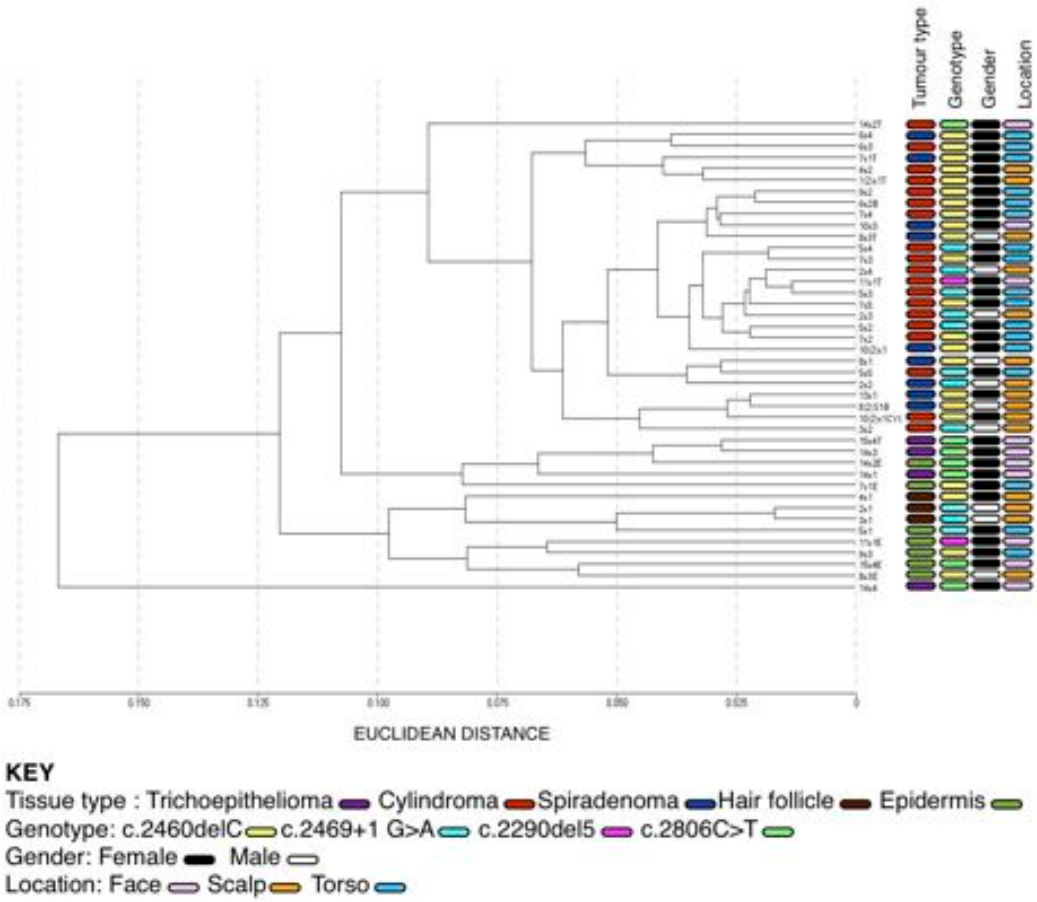

Figure 31 Clustering dendrogram of CYLD defective tumour and control transcriptomes.

Cylindromas and spiradenomas share similar transcriptomes, and cluster distinctly from trichoepitheliomas and perilesional control skin. Total RNA was extracted from 32 microdissected tumours and 10 perilesional controls and gene expression levels of 24526 transcripts for each sample were assayed. Unsupervised clustering of the 42 transcriptomes was performed, and cylindromas and spiradenomas clustered together, with trichoepitheliomas and perilesional skin clustering separately. No clustering by gender, genotype or tumour location was seen.

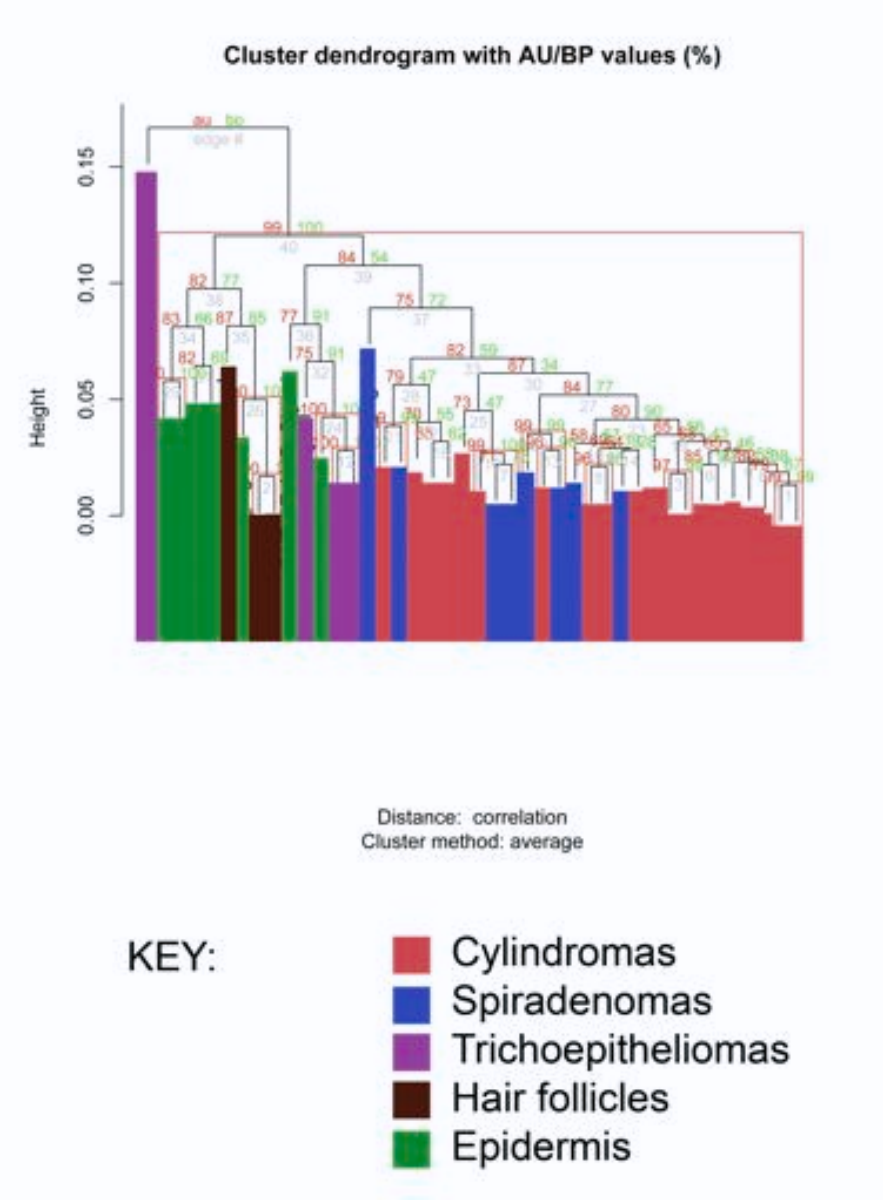

Figure 32 Stability of clusters of CYLD defective tumours.

Clustering analysis of transcriptomic data from CYLD defective tumours and control tissue. Clustering of transcriptomes using individual probes (24526) was employed and dissimilarity was measured using the correlation method using a statistical package (pvclust) (Suzuki and Shimodaira 2006). Clusters seen in Figure 31 were maintained, however due to the small numbers of tumours used, statistical significance was seen between tumours and controls ($p<0.01$), but not between tumour subsets. pvclust provides two types of p-values: AU (Approximately Unbiased – numbers in red) p-value and BP (Bootstrap Probability – numbers in green) value. AU p-value, which is computed by multiscale bootstrap resampling, is a better approximation to the true unbiased p-value than the BP value computed by normal bootstrap resampling. Numbers in grey are edge values.

The unsupervised clustering analysis was further corroborated by a supervised clustering analysis, allowing class comparison between cylindroma and spiradenoma tumours. 19 cylindromas and 9 spiradenomas were subject to significance of microarrays analysis (SAM), which showed no significant difference between the tumour types when standard criteria were applied (Figure 33). (Differentially expressed genes between the two groups had to pass a significance threshold of $p<0.01$ and 100 permutations of the data were analysed)

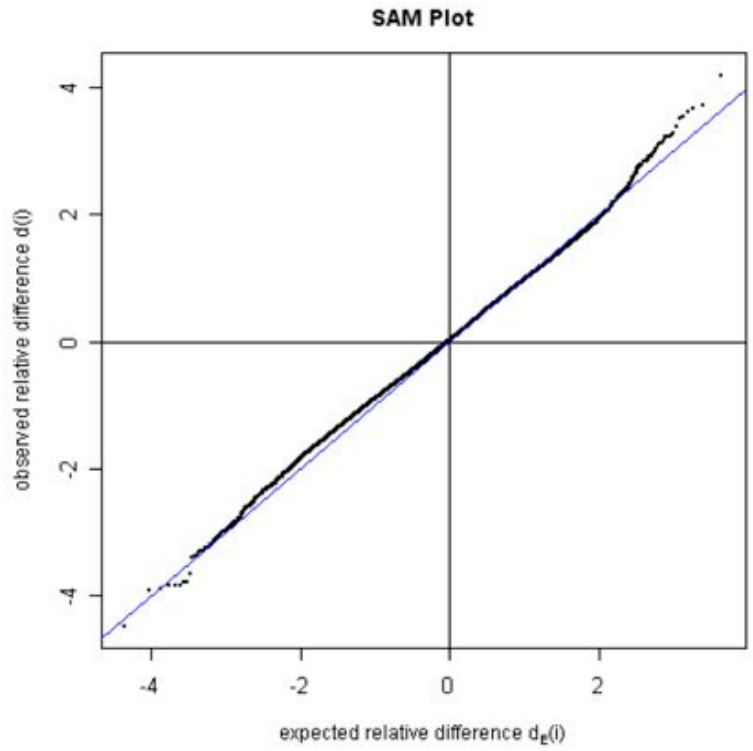

Figure 33 Supervised analysis of 19 cylindroma vs. 9 spiradenoma.
Supervised clustering comparing cylindromas and spiradenomas show no significant difference in transcriptomic profiles. Significance of microarrays analysis, a form of supervised clustering analysis was performed between 19 cylindroma and 9 spiradenoma samples, and showed no significant difference between samples types.

Given the genomic and transcriptomic similarity seen in cylindromas and spiradenomas, and our finding that they were extremes of a spectrum of tumour organisation, these were pooled and analysed against pooled controls to provide enhanced statistical robustness. Trichoepitheliomas were also included in this pool of CYLD defective tumours.

Quantitation of differential gene expression was determined using the bead array manufacturers' custom algorithm (Illumina custom method- Illumina Inc, 2009). The statistical significance of differential gene expression between tumours and samples was calculated as a differential score. This calculation incorporated the difference in signal values between the two groups compared, corrected for appropriate negative control bead values, and was corrected for multiple hypothesis testing using a Bonferroni post test. We used stringent thresholds for filtering genes, with only transcripts that were differentially expressed with a p value of < 0.01 included for subsequent analysis (n=4492).

Transcripts of proteins that were previously noted to be overexpressed in cylindromas were also present in a subset of 19 cylindroma tumours and supported the enrichment of cylindroma tissue following microdissection. These included numerous laminins (Table 11) (Tunggal, Ravaux et al. 2002), collagen 4 and 7 (Timpl, Fujiwara et al. 1984; Bruckner-Tuderman, Pfaltz et al. 1991) and cytokeratins (Tellechea, Reis et al. 1995; Meybehm and Fischer 1997) which were preferentially expressed in the tumours compared to perilesional epidermis. Upregulation of NFκB target genes (http://people.bu.edu/gilmore/nf-kb/target/index.html) was present as expected and served as an internal positive control. 19 cylindroma tumours were compared to all controls, and the NFκB target genes that were differentially expressed with a p-value of less than 0.01 were tabulated in Table 11.

To detect low level changes in gene expression between all tumours and all control tissue, gene set enrichment analysis (GSEA) was performed on data filtered at a threshold of p< 0.05 (Subramanian, Tamayo et al. 2005). This highlighted multiple gene sets that were involved in apoptosis (Figure 34) and genes that were common to these sets were found to be members of or target genes of NFκB and JNK signalling pathways (Figure 35). To validate this finding at the protein level, we demonstrated expression of p52 and Cyclin D1 in CYLD defective tumours (Figure 36)

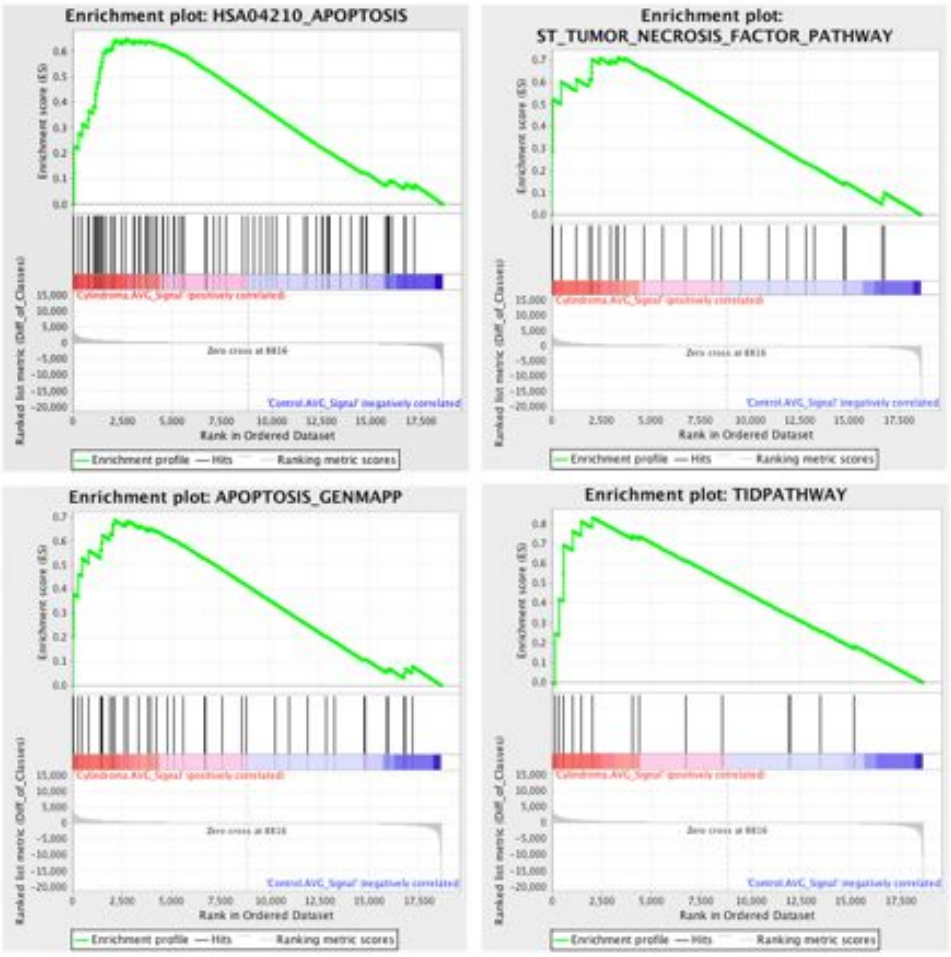

Figure 34 Gene set expression analysis of CYLD defective tumours.

Gene sets that modulate apoptosis are enriched in the tumour transcriptomes and contain NFκB target genes. Expression levels of 24526 genes from 32 microdissected tumours were pooled and compared against 10 pooled perilesional controls and subject to gene set expression analysis. Sets of genes recognised to modulate apoptosis were found to be enriched in the tumour sample. Leading edge analysis of these gene sets revealed NFκB target genes to be frequently present in these samples. A heat map of gene set HSA04210_APOPTOSIS is shown in Figure 35.

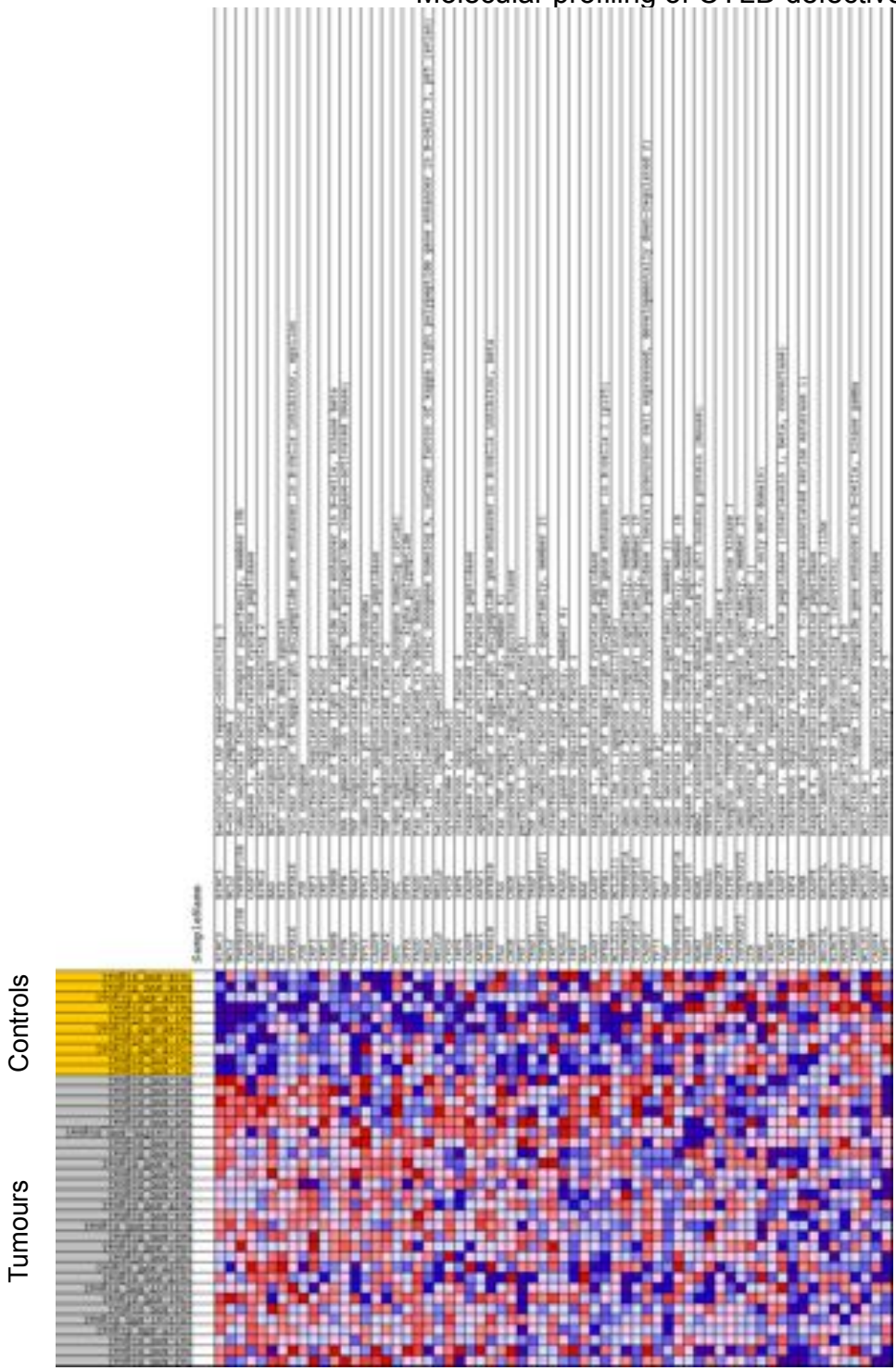

Figure 35 NFκB target genes are overexpressed in CYLD defective tumours.

Expression levels of 24526 genes from 32 microdissected tumours were pooled and compared against 10 pooled perilesional controls and subject to gene set expression analysis. Sets of genes recognised to modulate apoptosis were found to be overexpressed in the tumour tissue (see also Supplementary figure 1). A heat map of the members of one set (HSA04210_APOPTOSIS) is shown here, with overexpressed genes shown in red and underexpressed genes in blue. Overexpressed genes included several NFκB target genes.

Table 11 Upregulation of NFκB target genes in tumour tissue and markers confirming purity of cylindroma tissue following microdissection.

NFKB target genes that are upregulated in tumour tissue (p<0.01)		
Gene	**Fold change**	**Gene name**
SAA1	5.92	Serum amyloid a2
BCL2A1	5.74	BCL2-related protein a1
SAA2	4.58	Serum amyloid a2
BDNF	2.72	Brain-derived neurotrophic factor
OLR1	4.53	Oxidized low density lipoprotein (lectin-like) receptor 1
CD83	2.53	Cd83 molecule
TIFA	2.54	Traf-interacting protein with forkhead-associated domain
TF	2.77	Transferrin
CXCL10	2.67	Chemokine (c-x-c motif) ligand 10
HLA-G	3.44	Major histocompatibility complex, class i, g
RELB	2.36	V-rel reticuloendotheliosis viral oncogene homolog b
MYB	2.17	V-myb myeloblastosis viral oncogene homolog (avian)
Genes that are upregulated in tumour tissue that have been previously described to be overexpressed in cylindroma tumours (p<0.01)		
KRT18	1.74	Keratin 18
KRT13	4.6	Keratin 13
KRT8	3.71	Keratin 8 pseudogene 9; similar to keratin 8
KRT7	2.1	Keratin 7
LAMA1	4.14	Laminin, alpha 1
LAMA3	3.08	Laminin, alpha 3
LAMB3	2.79	Laminin, beta 3
LAMC2	1.86	Laminin, gamma 2
COL7A1	1.94	Collagen, type vii, alpha 1
COL4A1	1.5	Collagen, type iv, alpha 1
COL4A2	1.73	Collagen, type iv, alpha 2

NFκB target genes are overexpressed in 19 cylindroma tumours. Transcripts that were differentially expressed between tumours and perilesional controls were filtered with the criteria of a p value of less than 0.01. Transcripts that fulfilled this criteria were compared against known NFκB target genes and tabulated. The purity of tumour microdissection was supported by overexpression of transcripts in cylindroma tissue described previously in the literature.

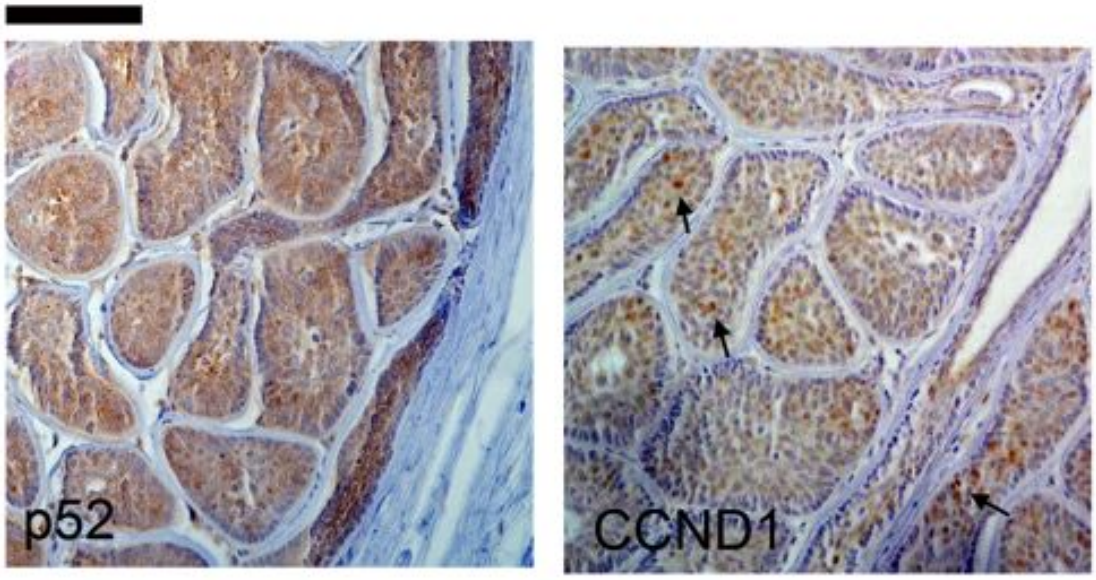

Figure 36 NFκB target genes, p52 and cyclin D1, are expressed in CYLD defective tumours. Cytoplasmic p52 and predominantly cytoplasmic cyclin D1 is seen. Occasional nuclear cyclin D1 is indicated with black arrows. Scale bar indicates 100μm.

5.2.3 TRK signalling is dysregulated in the CYLD defective tumour transcriptome

Fold change (FC) analysis (Table 12) revealed overexpression of several members of the TRK signalling pathway compared to perilesional tissue, namely, TRKC (FC = 4.75x), Neurotrophin 3 (FC=3.00x) and Neurotrophin 4/5 (FC=3.15x) in the tumour group when compared to perilesional skin.

Table 12 Fold change analysis of CYLD defective tumours compared against unaffected perilesional tissue.

Altered gene expression in a human CYLD defective model. Transcripts that were differentially expressed between tumours and perilesional controls were filtered with the criteria of a 4x fold change and p value of less than 0.01. Overexpressed transcripts are shown in red and underexpressed transcripts are shown in green.

Gene	Fold change	Gene name
FGF3	8.38	Fibroblast growth factor 3 (murine mammary tumour virus integration site (v-int-2) oncogene homolog) (FGF3), mrna.
APIN	6.74	Apin protein (APIN), mrna.
ABTB2	5.65	Ankyrin repeat and BTB (POZ) domain containing 2 (ABTB2), mrna.
IQCA	5.53	IQ motif containing with AAA domain (IQCA), mrna.
SAA1	5.13	Serum amyloid A1 (SAA1), transcript variant 2, mrna.
RPRM	5.07	Reprimo, TP53 dependent G2 arrest mediator candidate (RPRM), mrna.
RARB	5.06	Retinoic acid receptor, beta (RARB), transcript variant 1, mrna.
COL9A2	4.97	Collagen, type IX, alpha 2 (COL9A2), mrna.
USP6	4.84	Ubiquitin specific peptidase 6 (Tre-2 oncogene) (USP6), mrna.
IL17RB	4.83	Interleukin 17 receptor B (IL17RB), transcript variant 2, mrna.
RARB	4.82	Retinoic acid receptor, beta (RARB), transcript variant 2, mrna.
C1ORF61	4.82	Chromosome 1 open reading frame 61 (c1orf61), mrna.
BCL2A1	4.81	BCL2-related protein A1 (BCL2A1), mrna.
REPS2	4.76	RALBP1 associated Eps domain containing 2 (REPS2), mrna.
CPA6	4.70	Carboxypeptidase A6 (CPA6), mrna.
NTRK3	4.66	Neurotrophic tyrosine kinase, receptor, type 3 (NTRK3), transcript variant 3, mrna.
RAB6B	4.64	RAB6B, member RAS oncogene family (RAB6B), mrna.
LRRN5	4.59	Leucine rich repeat neuronal 2 (LRRN2), transcript variant 1, mrna.
FLJ45803	4.58	FLJ45803 protein (FLJ45803), mrna.
ARNT2	4.51	Aryl-hydrocarbon receptor nuclear translocator 2 (ARNT2), mrna.
EDAR	4.37	Ectodysplasin A receptor (EDAR), mrna.
KIAA1622	4.34	KIAA1622 (KIAA1622), transcript variant 1, mrna.
MIA	4.34	Melanoma inhibitory activity (MIA), mrna.
CLUL1	4.30	Clusterin-like 1 (retinal) (CLUL1), transcript variant 2, mrna.
DACT2	4.30	Dapper, antagonist of beta-catenin, homolog 2 (Xenopus laevis) (DACT2), mrna.
ADM2	4.25	Adrenomedullin 2 (ADM2), mrna.
SNX22	4.15	Sorting nexin 22 (SNX22), mrna.
ADAMTS18	4.12	ADAM metallopeptidase with thrombospondin type 1 motif, 18 (ADAMTS18), transcript variant 1, mrna.
LOC130940	4.10	Hypothetical protein BC015395 (LOC130940), mrna.
COL22A1	4.06	Collagen, type XXII, alpha 1 (COL22A1), mrna.
MMP7	4.02	Matrix metallopeptidase 7 (matrilysin, uterine) (MMP7), mrna.
ENPP6	4.00	Ectonucleotide pyrophosphatase/phosphodiesterase 6 (ENPP6), mrna.
C6ORF85	0.25	Chromosome 6 open reading frame 85 (c6orf85), mrna.
GRHL3	0.25	Grainyhead-like 3 (Drosophila) (GRHL3), transcript variant 1, mrna.
KRT10	0.24	Keratin 10 (epidermolytic hyperkeratosis; keratosis palmaris et plantaris) (KRT10), mrna.

ZD52F10	0.24	Dermokine (DMKN), transcript variant 2, mrna.
ZD52F10	0.24	Dermokine (DMKN), transcript variant 2, mrna.
TLCD1	0.24	TLC domain containing 1 (TLCD1), mrna.
MUC15	0.23	Mucin 15, cell surface associated (MUC15), mrna.
SLC19A3	0.23	Solute carrier family 19, member 3 (SLC19A3), mrna.
RP11-19J3.3	0.23	Centromere protein P (CENPP), mrna.
CPA4	0.23	Carboxypeptidase A4 (CPA4), mrna.
LGALS7	0.23	Lectin, galactoside-binding, soluble, 7 (galectin 7) (LGALS7), mrna.
ALDH3A1	0.22	Aldehyde dehydrogenase 3 family, membera1 (ALDH3A1), mrna.
XKRX	0.22	XK, Kell blood group complex subunit-related, X-linked (XKRX), mrna.
BNIPL	0.22	BCL2/adenovirus E1B 19kd interacting protein like (BNIPL), transcript variant 1, mrna.
ALDH3B2	0.21	Aldehyde dehydrogenase 3 family, member B2 (ALDH3B2), transcript variant 2, mrna.
ANXA8	0.21	Annexin A8-like 2 (ANXA8L2), mrna.
LOC144501	0.20	Hypothetical protein LOC144501 (LOC144501), mrna.
CST6	0.20	Cystatin E/M (CST6), mrna.
MICALCL	0.20	MICAL C-terminal like (MICALCL), mrna.
HOP	0.20	Homeodomain-only protein (HOP), transcript variant 3, mrna.
MAP2	0.20	Microtubule-associated protein 2 (MAP2), transcript variant 2, mrna.
GGT6	0.20	Gamma-glutamyltransferase 6 homolog (rat) (GGT6), mrna.
PSORS1C2	0.20	Psoriasis susceptibility 1 candidate 2 (PSORS1C2), mrna.
DCT	0.20	Dopachrome tautomerase (dopachrome delta-isomerase, tyrosine-related protein 2) (DCT), mrna.
SERPINB13	0.20	Serpin peptidase inhibitor, clade B (ovalbumin), member 13 (SERPINB13), mrna.
MAP2	0.20	Microtubule-associated protein 2 (MAP2), transcript variant 1, mrna.
TMEM79	0.19	Transmembrane protein 79 (TMEM79), mrna.
FGFR3	0.19	Fibroblast growth factor receptor 3 (achondroplasia, thanatophoric dwarfism) (FGFR3), transcript variant 1, mrna.
C14ORF29	0.19	Abhydrolase domain containing 12B (ABHD12B), transcript variant 2, mrna.
DSG1	0.19	Desmoglein 1 (DSG1), mrna.
KRT1	0.19	Keratin 1 (epidermolytic hyperkeratosis) (KRT1), mrna.
TRIM7	0.19	Tripartite motif-containing 7 (TRIM7), transcript variant 6, mrna.
SLC39A2	0.18	Solute carrier family 39 (zinc transporter), member 2 (SLC39A2), mrna.
FLJ10847	0.17	Solute carrier family 47, member 1 (SLC47A1), mrna.
CST6	0.17	Cystatin E/M (CST6), mrna.
LOC342897	0.16	Similar to F-box only protein 2 (LOC342897), mrna.
ATP13A4	0.16	Atpase type 13A4 (ATP13A4), mrna.
GPR115	0.15	G protein-coupled receptor 115 (GPR115), mrna.
UNC93A	0.15	Unc-93 homolog A (C. Elegans) (UNC93A), mrna.
SBSN	0.15	Suprabasin (SBSN), mrna.
LOC144501	0.14	Hypothetical protein LOC144501 (LOC144501), mrna.
TYRP1	0.14	Tyrosinase-related protein 1 (TYRP1), mrna.
GSDM1	0.14	Gasdermin 1 (GSDM1), mrna.
LOC130576	0.13	Hypothetical protein LOC130576 (LOC130576), mrna.
FLJ21511	0.13	Hypothetical protein FLJ21511 (FLJ21511), mrna.

C3ORF52	0.13	Chromosome 3 open reading frame 52 (c3orf52), mrna.
WFDC5	0.12	WAP four-disulfide core domain 5 (WFDC5), mrna.
SLC5A1	0.12	Solute carrier family 5 (sodium/glucose cotransporter), member 1 (SLC5A1), mrna.
MLANA	0.12	Melan-A (MLANA), mrna.
TGM5	0.11	Transglutaminase 5 (TGM5), transcript variant 1, mrna.
CYP3A5	0.10	Cytochrome P450, family 3, subfamily A, polypeptide 5 (CYP3A5), mrna.
AADACL2	0.10	Arylacetamide deacetylase-like 2 (AADACL2), mrna.
BPIL2	0.10	Bactericidal/permeability-increasing protein-like 2 (BPIL2), mrna.
CDSN	0.10	Corneodesmosin (CDSN), mrna.
K5B	0.10	Keratin 5b (K5B), mrna.
RDH12	0.09	Retinol dehydrogenase 12 (all-trans/9-cis/11-cis) (RDH12), mrna.
DSC1	0.08	Desmocollin 1 (DSC1), transcript variant Dsc1b, mrna.
TGM3	0.07	Transglutaminase 3 (E polypeptide, protein-glutamine-gamma-glutamyltransferase) (TGM3), mrna.
PPP2R2C	0.07	Protein phosphatase 2 (formerly 2A), regulatory subunit B, gamma isoform (PPP2R2C), transcript variant 2, mrna.
IL1F10	0.07	Interleukin 1 family, member 10 (theta) (IL1F10), transcript variant 2, mrna.
CA12	0.07	Carbonic anhydrase XII (CA12), transcript variant 1, mrna.
CCL27	0.07	Chemokine (C-C motif) ligand 27 (CCL27), mrna.
PLA2G4F	0.07	Phospholipase A2, group IVF (PLA2G4F), mrna.
K6IRS3	0.06	Keratin 73 (KRT73), mrna.

This finding was corroborated by connectivity mapping analysis (Lamb 2006) using Ingenuity Pathways Analysis (Table 13) (Ingenuity® Systems, www.ingenuity.com).

Table 13 Top canonical signalling pathways enriched in 32 CYLD defective tumours.
Top canonical signalling pathways enriched in 32 CYLD defective tumours when compared to 10 perilesional skin controls. The ratio of transcripts of genes seen to be overexpressed to all the transcripts in the named pathway are shown in the final column. Thyroid cancer signalling and TRK signalling share mutual TRK transcripts.

Ingenuity canonical pathway	P-value	Ratio
Thyroid Cancer Signalling	2.96E-04	10/166 (0.06)
Wnt/β-catenin Signalling	5.59E-04	8/140 (0.057)
Human Embryonic Stem Cell Pluripotency	1.26E-03	5/70 (0.071)
Neurotrophin/TRK	4.02E-03	5/71 (0.07)
Signalling Tyrosine Metabolism	7.28E-03	5/41 (0.122)

This highlighted the concerted overexpression of multiple members of the Neurotrophin/TRK signalling pathway in tumour tissue compared to control tissue. This finding was reflected in two pathways, namely, the "Thyroid Cancer Signalling" pathway and the" Neurotrophin/TRK " pathway which essentially contained transcripts related to the Neurotrophin/TRK signalling pathway. In addition to the transcripts detected by FC analysis above, TRKB, brain derived neurotrophic factor and PIK3R1, which encodes a regulatory subunit of PI3 kinase, a downstream mediator of TRK signalling, were elevated in expression (Figure 37).

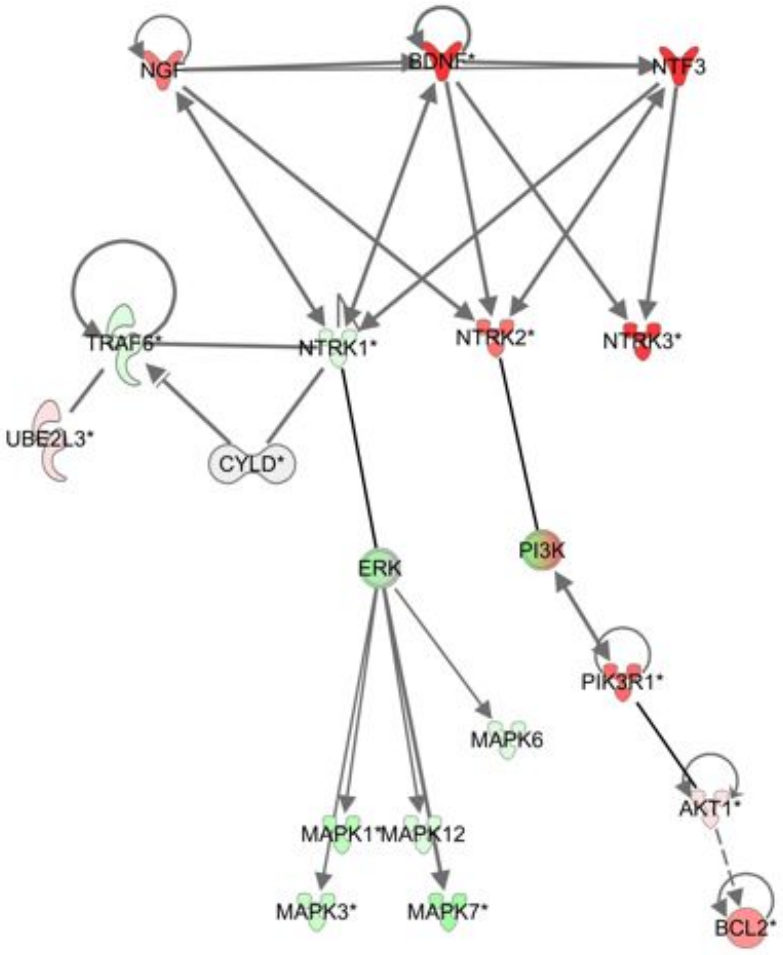

Figure 37 TRK signalling is dysregulated in cylindroma and spiradenoma tissue.
Expression levels of 24526 genes from 32 microdissected tumours were pooled and compared against 10 pooled perilesional controls, and genes that were differentially expressed (p value <0.01) were analysed using Ingenuity pathway analysis. Overexpressed transcripts are shown in red and underexpressed transcripts are shown in green. TRKB (*NTRK2*) and TRKC (*NTRK3*), members of the TRK signalling pathway, were overexpressed in tumour tissue compared to control samples. Expression of TRKA (*NTRK1*) however was reduced. Downstream members such as PI3K and AKT and BCL2 were also over expressed.

Moreover, TRKA, a previously described CYLD interacting protein (Geetha, Jiang et al. 2005), was found to be downregulated, whilst the cognate ligand nerve growth factor (NGF) was upregulated . No obvious changes in copy

number were found at the chromosomal location of the different TRK receptors and their respective cognate ligands suggesting that genomic amplification or deletion was not directly responsible for these changes in transcript level.

5.2.4 TRKB and TRKC proteins are overexpressed in human cylindromas and spiradenomas

The overexpression of TRKB and TRKC observed at the mRNA level was investigated at the protein level in CYLD defective tumours. A tumour tissue microarray (TMA) of CYLD defective tumours - cylindromas, spiradenomas, trichoepitheliomas and perilesional skin was constructed and protein expression assayed using immunohistochemical techniques. Expression of TRKB and TRKC was elevated in cylindroma, spiradenoma and to a lesser extent in trichoepithelioma tissue compared to perilesional skin (Figure 38). Strong membranous staining was apparent in cylindroma cells, whilst diffuse cytoplasmic staining was noted in overlying keratinocytes. TRKC expression was mainly noted over the basophilic peripheral cells in cylindroma islands, whilst TRKB overexpression was non-discriminatory within tumour islands (Figure 38). Quantification of membranous TRK expression was performed on each core of the TMA. A scoring scale, which assessed the intensity of membranous TRK staining and the proportion of tumour cells stained was used, (Figure 39), and the difference in expression between tumours and perilesional keratinocytes was found to be statistically significant ($p<0.05$) (Figure 39). Perilesional hair follicles were positive for TRKA and acted as positive controls, whilst perilesional epidermis was negative for TRKB and TRKC, acting as negative controls. Furthermore, cylindroma cells were strongly positive with antibodies against phosphorylated ERK (p44/42), a marker of active TRK signalling, mainly at the periphery of each tumour island. The antiapoptotic protein BCL2, a downstream target of TRK signalling, was also overexpressed in cylindroma tissue, showing strong perinuclear staining (Figure 38)

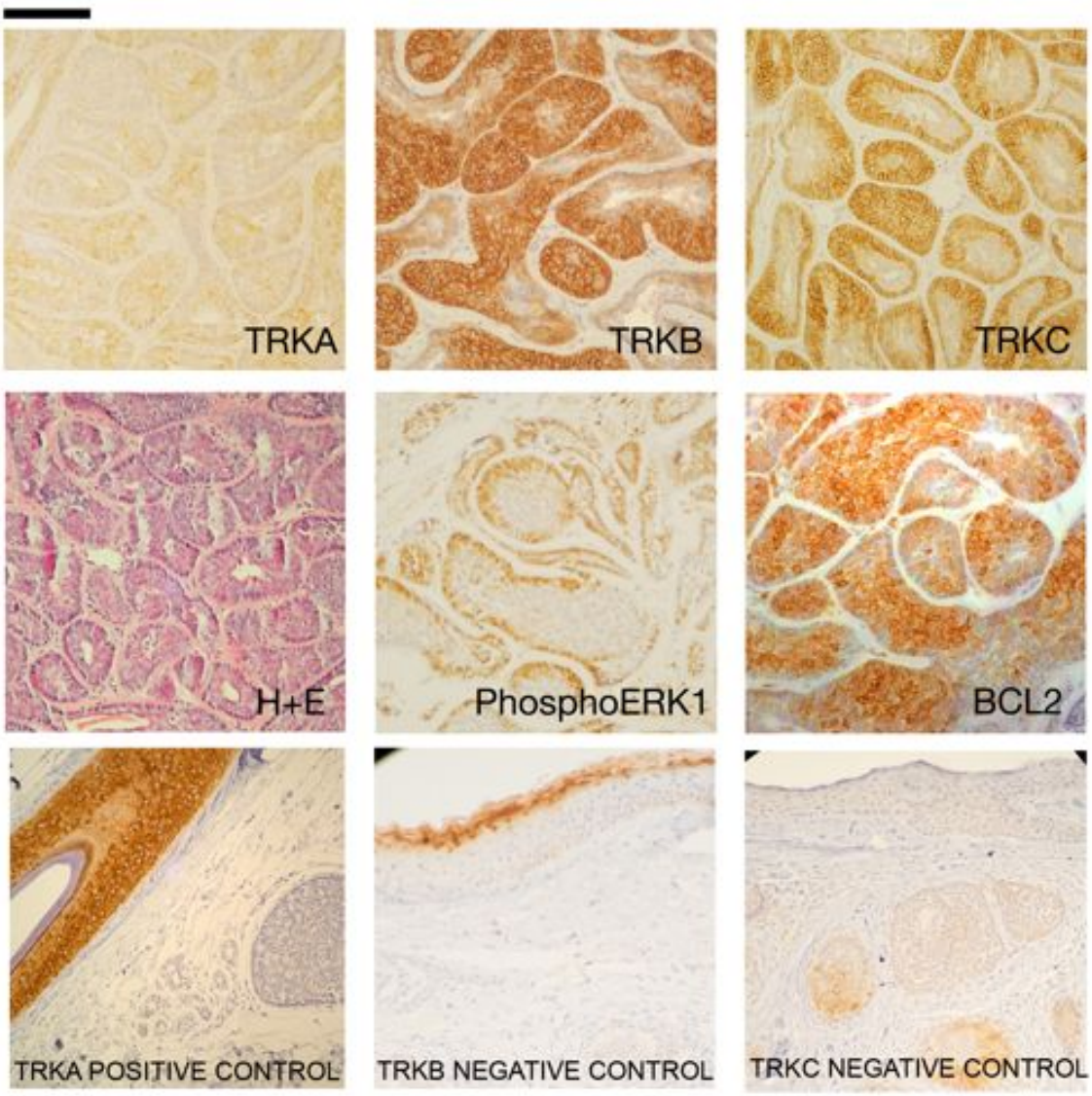

Figure 38 TRK immunostaining on a CYLD defective tumour microarray.
TRKB and TRKC proteins are over expressed in human cylindromas and spiradenomas. (**a**) Tissue microarrays of cylindromas and spiradenomas were probed with antibodies as indicated, and visualised using a horseradish peroxidase – diaminobenzene system, with haematoxylin used as a nuclear counterstain. Membranous TRKB and TRKC were overexpressed in the tumours, exemplified by the cylindroma tumours illustrated here. Patchy perinuclear TRKA staining was seen in some tumour cells. Expression of downstream targets phosphoERK and BCL2 was also seen. Perilesional anagen hair follicles acted as a positive control (TRKA) and perilesional epidermis was used as a negative control (TRKB and TRKC). Scale bars indicate 100μm; insets are shown to demonstrate specific membranous staining of TRKB and TRKC (2x enlargement of related image).

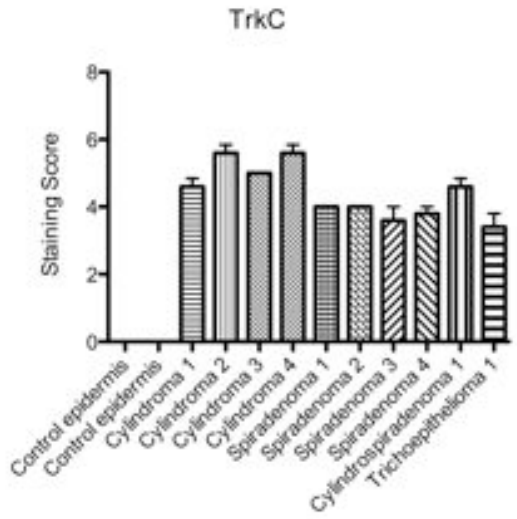

TrkC	Mean score and SEM	p value
Normal tissue (N=2)	0.0005 ± 0.0005	
Cylindroma (N=4)	5.350 ± 0.1500	< 0.0001
Spiradenoma (N=4)	3.850 ± 0.1094	< 0.0001
Cylindrospiradenoma (N=1)	4.600 ± 0.2449	< 0.0001
Trichoepithelioma (N=1)	3.400 ± 0.4000	0.0038

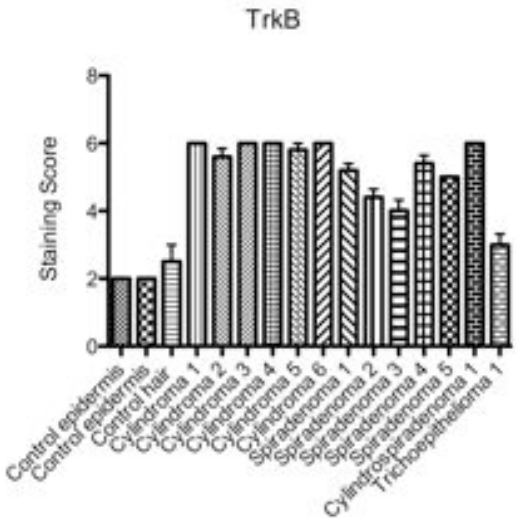

TrkB	Mean score and SEM	p value
Normal tissue (N=3)	2.125 ± 0.1250	
Cylindroma (N=6)	5.900 ± 0.05571	< 0.0001
Spiradenoma (N=5)	4.800 ± 0.1414	< 0.0001
Cylindrospiradenoma (N=1)	5.800 ± 0.2000	< 0.0001
Trichoepithelioma (N=1)	3.000 ± 0.3162	0.012

Staining
None - 0
Weak - 1
Strong, but not circumfrential -2
Strong and circumfrential - 3

Percentage of cells in HPF 63x
None -0
Less than 50% - 1
50-75% - 2
76-100% -3

Figure 39 Membranous TRKB and TRKC scores.

Membranous TRKB and TRKC is highly expressed in CYLD defective tumours. Membranous TRKC expression scores in cylindroma tumours compared to perilesional unaffected tissue. A custom tumour microarray was scored for membranous expression of TRKB and TRKC. Mean scores were grouped by tumour type and compared to the scores of unaffected perilesional tissue. Membranous immunostaining scores were made on all cores on the array, with p-values of the difference in score (t-test) between tumour and control indicated in the adjacent tables. Error bars indicate standard error of the mean.

5.2.5 Membrane-localised TRKC is overexpressed in sporadic basal cell carcinoma

Cutaneous appendageal tumours seen in CYLD mutation carriers share similarities in cytokeratin profiles with sporadic basal cell carcinoma (BCC), that in humans are thought to be also derived from the hair follicle (Donovan 2009). Dysregulation of several mutual oncogenic pathways are seen in cylindromas and BCCs. Wnt signalling is thought to play an oncogenic role in both, with expression of nuclear β-catenin demonstrated in both cylindromas (Tauriello, Haegebarth et al. 2010) and human basal cell carcinoma (Kriegl, Horst et al. 2009). Also, the Sonic hedgehog pathway, recognised to depend on such canonical Wnt signalling for cutaneous tumour formation (Hoseong Yang, Andl et al. 2008), is an important final common pathway in both tumours. In a murine model that overexpresses GLI1 (Nilsson, Undèn et al. 2000), tumours that had histological appearances that resembled both human basal cell carcinoma and cylindroma were seen. Diffuse light expression of TRK receptors has previously been noted in a small series of basal cell carcinoma using a pan TRK antibody (Chen-Tsai, Colome-Grimmer et al. 2004). Therefore, we went on to investigate if the membranous TRKB and TRKC overexpression we observed in CYLD mutant tumours was a feature that extended to sporadic skin cancers. We examined expression of TRK receptors in a human skin cancer TMA that included samples of squamous cell carcinoma (SCC; n=19), melanoma (MM; n=5) and basal cell carcinoma (BCC; n=23) using TRKA, TRKB and TRKC specific antibodies. Interestingly, membranous TRKC was overexpressed in 70% of BCC tumours (Figure 40), 5% of SCC but not melanoma. In some samples, TRKC staining was strongest at the invasive front where the tumour cells apposed stroma (Figure 41). No membranous TRKA staining was seen, however some perinuclear staining, a feature associated with activated TRKA signalling (Wu, Ramirez et al. 2007) and was seen in a 39% of cases of BCC and 16% of cases of SCC. TRKB staining was seen in the cytoplasm in 13% of cases of BCC only, where it was seen in a few cells, but not at the cell membrane.

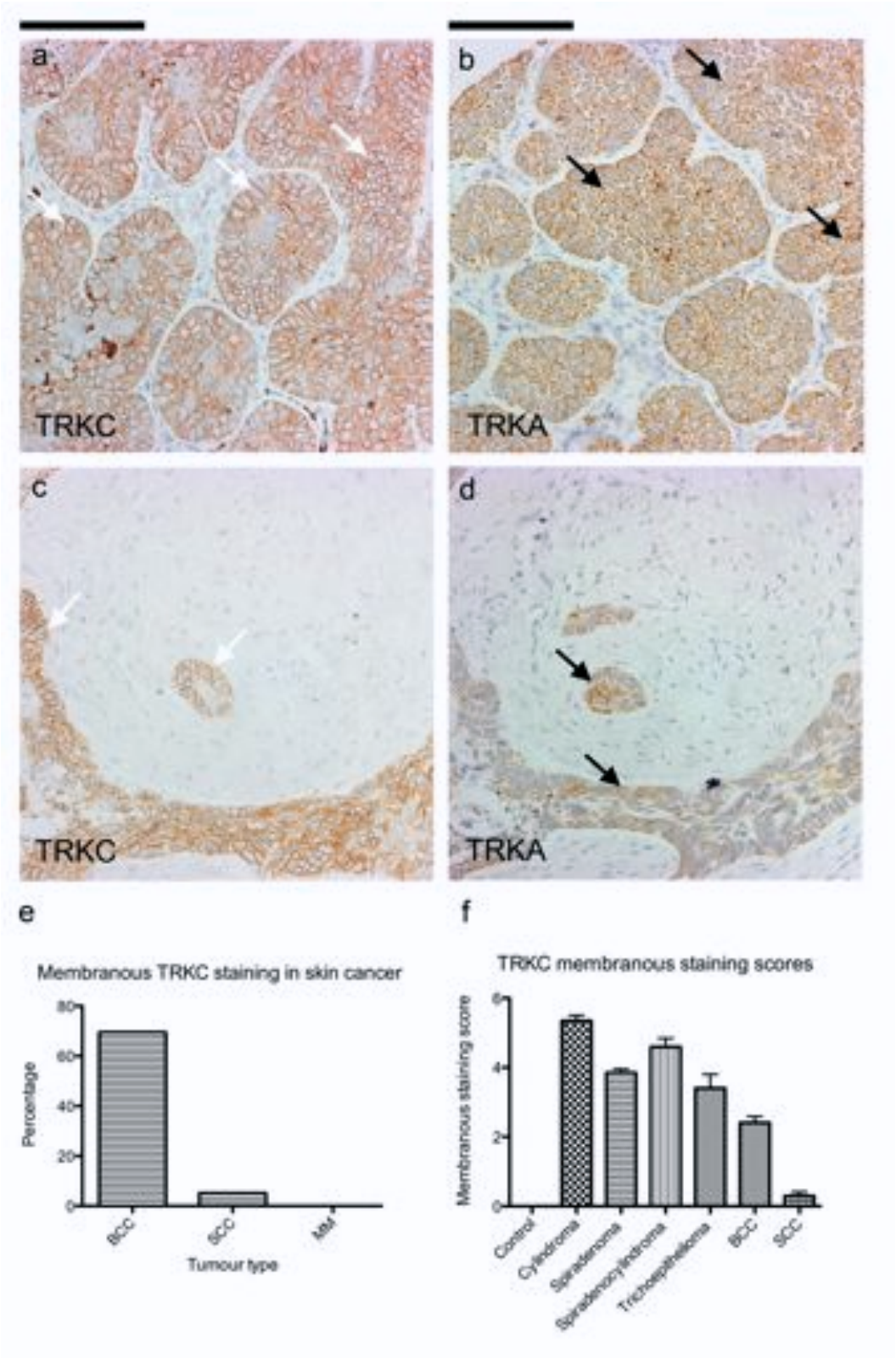

Figure 40 Membranous TRKC is overexpressed in basal cell carcinoma.

Membranous TRKC is overexpressed in basal cell carcinoma. A skin cancer tumour microarray with 23 BCCs, 19 SCCs and 5 malignant melanomas with two cores per case was immunostained with antibodies against TRKA, TRKB and TRKC. (a) Strong circumferential membranous immunostaining of TRKC is seen in 16 out of 23 cases (70%) of basal cell carcinoma on a tissue microarray, whilst there is an absence of membranous TRKA and TRKB staining. (c) One squamous cell carcinoma demonstrated

a similar pattern of staining. Malignant melanomas did not display membranous staining. (b,d) 39% of BCC and 16% of SCC also demonstrated perinuclear TRKA staining, and 13% of BCCs only demonstrated faint cytoplasmic TRKB staining. (e) Percentage of cases with membranous TRKC staining. (f) Mean membranous staining scores for TRKC were performed. Membranous TRKC staining is seen in 70% of BCC in this series, 5% of SCC, but not in malignant melanoma. Error bars indicate the standard error of the mean; Scale bars represent a distance of 100μm.

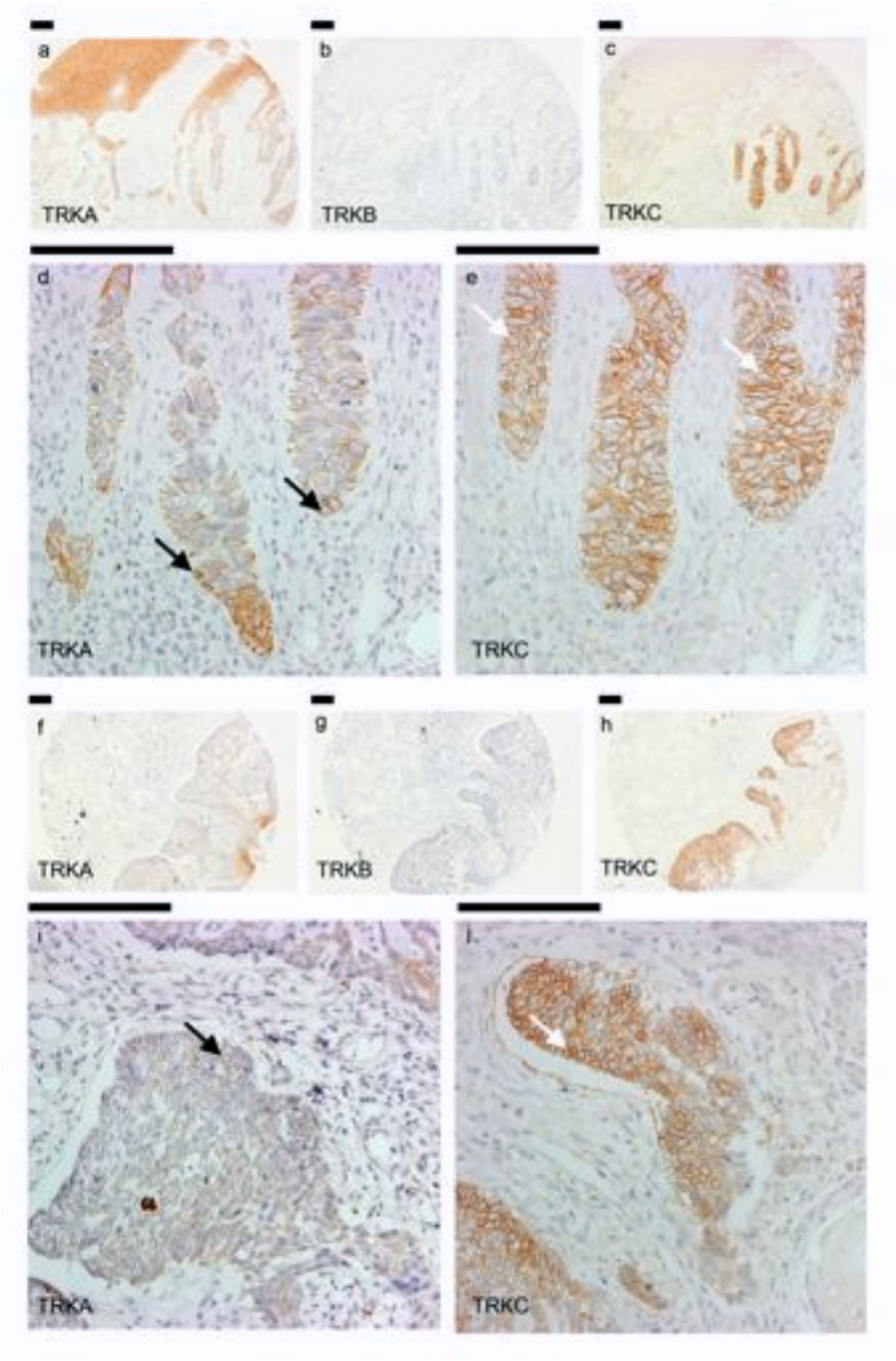

Figure 41 Membranous TRKC is seen in basal cell carcinoma predominantly at the invasive front adjacent to stroma.

Membranous TRKC is seen in basal cell carcinoma predominantly at the invasive front adjacent to stroma. A skin cancer tissue microarray containing 23 BCCs, 19 SCCs and 5 malignant melanomas with two cores per case was immunostained with antibodies against TRKA, TRKB and TRKC. (a-j) TRKA and TRKC staining varied across basal cell carcinoma tumour samples, with membranous TRKC seen at the invasive edge adjacent to stroma, indicated with white arrows (a,c,f and h) are enlarged in (d,e,i and j). TRKA staining was cytoplasmic, but predominantly perinuclear at the invasive front, indicated with black arrows. (a-c, f-h) were taken at 5x original magnification and (d-e, i-j) were taken at 20x original magnification. Scale bars represent a distance of 100μm.

5.2.6 Members of the Wnt/Beta-catenin signalling pathway are overexpressed in CYLD defective tumours

We were intrigued by the finding that Wnt/Beta-catenin signalling pathway was dysregulated in CYLD defective tumours and characterised this finding further (Table 13). We used Ingenuity Pathways Analysis (Ingenuity® Systems, www.ingenuity.com) to compare 24526 transcripts from 32 pooled CYLD defective tumours to 10 pooled perilesional tissue controls; differentially expressed transcripts with a significance level of <0.01 were included for analysis. Enrichment for transcripts that were components of the Wnt/Beta-catenin signalling pathway was seen (p=5.59E-04).

Fold change analysis was then carried out to highlight over and underexpressed transcripts associated with the Wnt/Beta-catenin signalling pathway in the tumour tissue (Table 14)

Table 14 Dysregulated Wnt/Beta-catenin pathway members and target genes in CYLD defective tumours.

Wnt/Beta-catenin pathway members and target genes that are overexpressed (Fold change>2) or underexpressed (fold change<0.5) in 32 CYLD defective tumours when compared to 10 perilesional skin controls. Only differentially expressed transcripts that attained a level of statistical significance of $p<0.05$ were included.

Gene	FC	Gene name
RARB	6.03	Retinoic acid receptor, beta
SOX10	4.48	SRY (sex determining region Y)-box 10
UBD	4.00	Ubiquitin D
MMP7	3.92	Matrix metallopeptidase 7 (matrilysin, uterine)
SOX8	3.66	SRY (sex determining region Y)-box 8
KREMEN2	3.49	Kringle containing transmembrane protein 2
CDKN2A	3.15	Cyclin-dependent kinase inhibitor 2A (melanoma, p16, inhibits CDK4)
DKK1	2.72	Dickkopf homolog 1
CTNNB1	2.59	Beta-catenin (cadherin-associated protein), beta 1, 88kda
SOX13	2.56	SRY (sex determining region Y)-box 13
SFRP1	2.47	Secreted frizzled-related protein 1
SOX11	2.23	SRY (sex determining region Y)-box 11
TCF3	2.20	Transcription factor 3 (E2A immunoglobulin enhancer binding factors E12/E47)
GSK3B	0.48	Glycogen synthase kinase 3 beta
WNT16	0.48	Wingless-type MMTV integration site family, member 16
PPP2R1B	0.43	Protein phosphatase 2 (formerly 2A), regulatory subunit A, beta isoform
CDH12	0.40	Cadherin 12, type 2 (N-cadherin 2)
GNAO1	0.38	Guanine nucleotide binding protein (G protein), alpha activating activity polypeptide O
CDH5	0.38	Cadherin 5, type 2 (vascular endothelium)
DKK2	0.38	Dickkopf homolog 2
SOX6	0.33	SRY (sex determining region Y)-box 6
WNT2B	0.32	Wingless-type MMTV integration site family, member 2B
WNT11	0.32	Wingless-type MMTV integration site family, member 11
SOX5	0.31	SRY (sex determining region Y)-box 5
WNT3	0.18	Wingless-type MMTV integration site family, member 3
WNT7B	0.14	Wingless-type MMTV integration site family, member 7B
PPP2R2C	0.05	Protein phosphatase 2 (formerly 2A), regulatory subunit B, gamma isoform

A network with transcripts related to the Wnt/Beta-catenin signalling pathway was developed to visually represent this data, with overexpressed transcripts indicated in red and underexpressed in green (Figure 42).

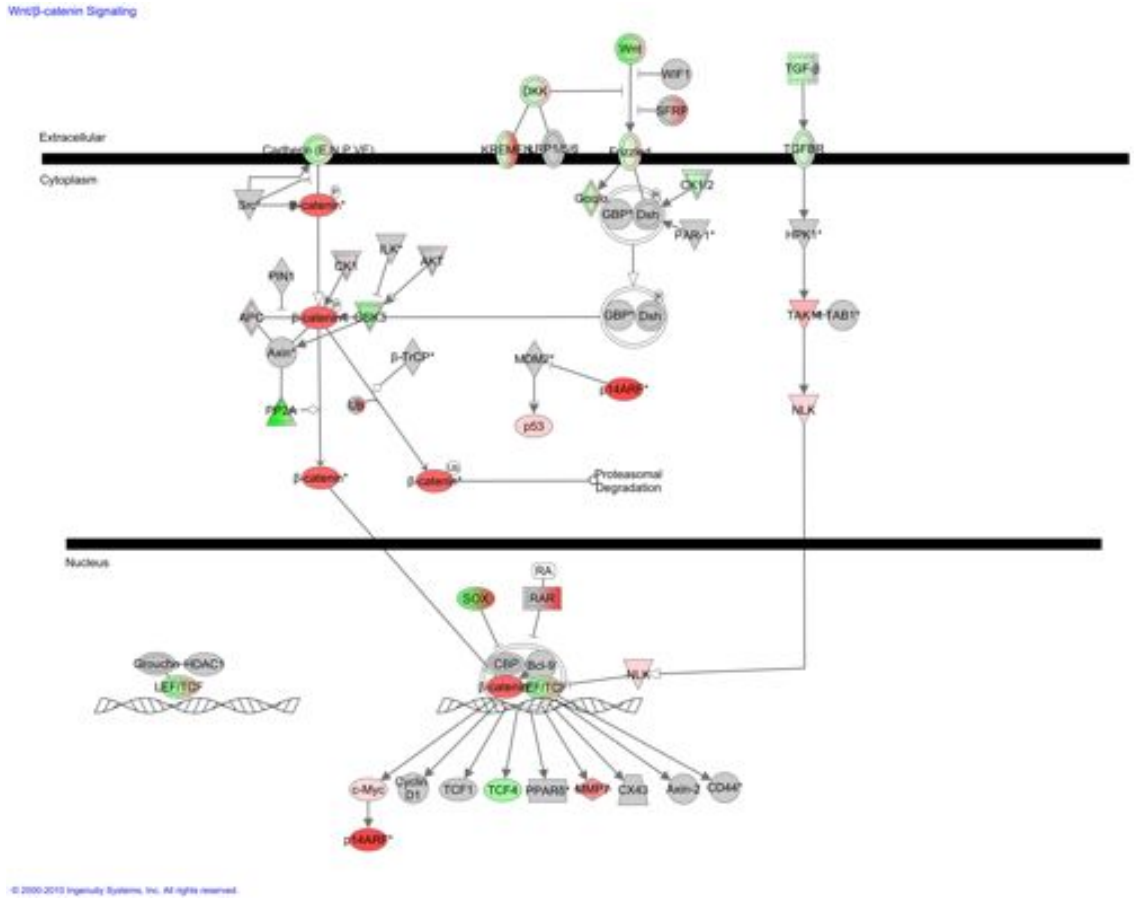

Figure 42 Members of the Wnt signalling pathway are overexpressed in CYLD defective tumours. Enrichment of Wnt/Beta-catenin signalling in CYLD defective tumours. 24526 transcripts from 32 pooled CYLD defective tumours were compared against 10 pooled perilesional tissue controls and a differentially expressed transcripts that attained a significance level of <0.01 were included for analysis. 5006 transcripts were subject to pathway analysis and transcripts related to the Wnt/Beta-catenin signalling pathway are visually represented here as overexpressed (red) and underexpressed (green). Groups of transcripts (eg; members of Frizzled) that had both under and overexpressed members are shaded as half red and half green.

To validate the finding of dysregulated Wnt/Beta-catenin signalling at the protein level, we examined nuclear beta-catenin expression in CYLD defective tumours. Nuclear beta-catenin was seen in cells at the periphery of islands, adjacent to stroma in cylindromas, affecting a minority of cells (Figure 43 a-b - indicated with black arrows). Other tumour cells predominantly displayed membranous beta-catenin at higher levels than perilesional epidermis. Trichoepitheliomas demonstrated a similar pattern to cylindromas (Figure 43c). Spiradenomas demonstrated nuclear beta-catenin both at the interface with stroma but also throughout the disorganised mass of tumour cells (Figure 43d) indicated with black arrows). This difference in nuclear beta-catenin suggested differential Wnt/Beta-catenin signalling in the two tumour types, prompting us to compare the two tumour type transcriptomes.

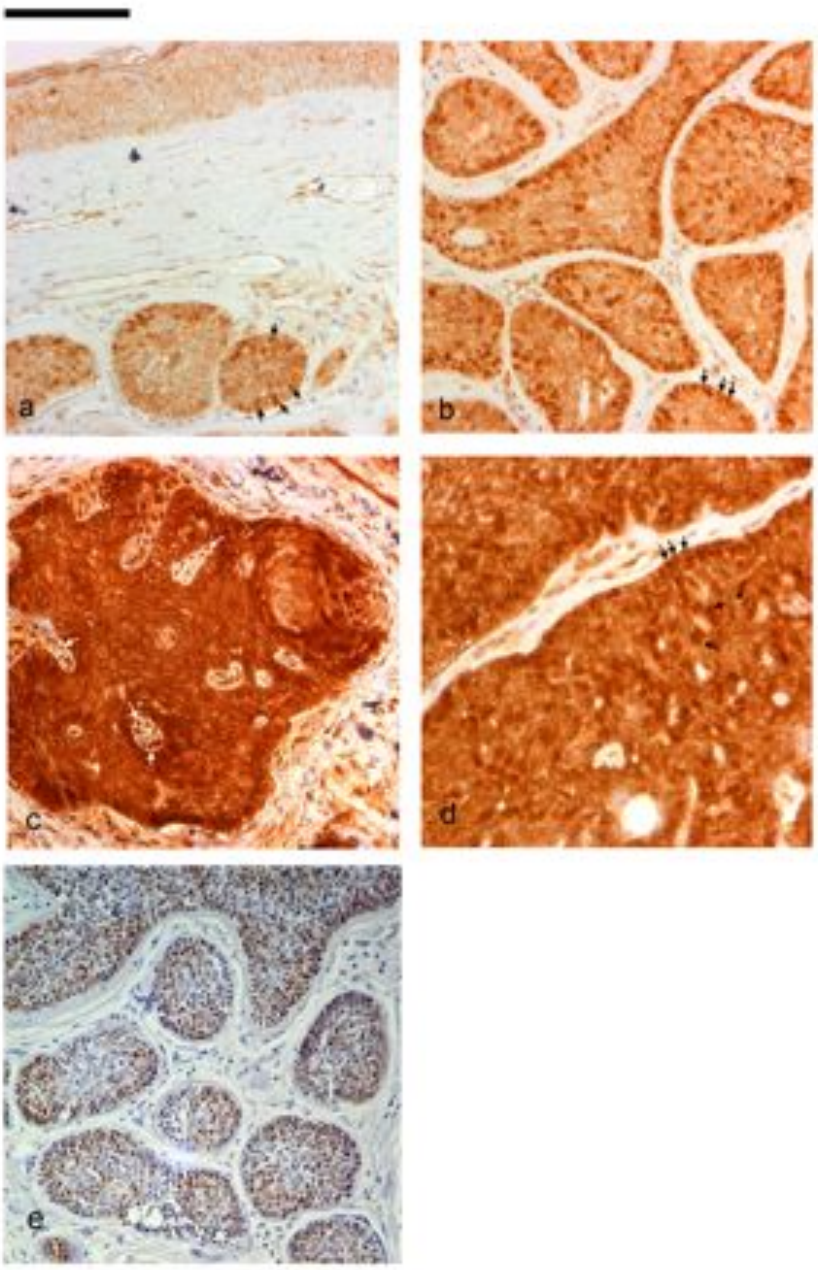

Figure 43 Nuclear beta-catenin and LEF1 expression in CYLD defective tumours.
Tumour sections on a custom-built tissue microarray underwent antigen retrieval, were probed with beta-catenin (a-d) and LEF1 (e) antibodies and protein expression was visualized with a horseradish peroxidase/DAB system. Haematoxylin was used as a nuclear counterstain. (a) Nuclear beta-catenin was seen in cells at the periphery of islands, adjacent to stroma in cylindromas, affecting a minority of cells (indicated with black arrows). Other tumour cells predominantly displayed membranous beta-catenin at higher levels than perilesional epidermis. (b) A cylindroma with sparse stromal tissue seen between islands demonstrated similar findings as the stromal rich sample seen in (a) (indicated with black arrows). (c) A trichoepithelioma demonstrating nuclear beta-catenin in the stromal cells (indicated with white arrows), with predominant overexpression of membranous beta-catenin in the tumour cells. (d) A spiradenoma demonstrating nuclear beta-catenin both at the interface with stroma but also through ought the disorganised mass of tumour cells (indicated with black arrows). (e) Nuclear LEF 1 is seen predominantly over peripheral cells in this cylindroma. Scale bar indicates 100μm.

5.2.7 Reduced expression of DKK2 is associated with increasing tumour disorganisation

To analyse genes that may be important in loss of tumour organisation in the transition of cylindromas to spiradenomas, we reanalysed transcriptomic data from 32 microdissected fresh frozen tumours. Our initial categorisation of tumours as cylindroma or spiradenoma was based on clinical and histological features of the tumour. However, detailed review of the histology revealed different levels of tumour organisation even within a cylindroma, making precise categorisation of organisation a challenge. To address this, we developed a novel method to quantify tumour organisation of each sample used for transcriptomic analysis. The first and last sections enclosing the microdissected sections used for profiling were stained using standard techniques. They were found to be similar over the 80-100 micron thickness of tumour they enclosed. A photomicrograph (Figure 44a) was taken and each tumour island of cells on each sample was traced out and a cartoon was developed (Figure 44b). The area of each island was measured, using an imaging programme (Image J v1.64, NIH - (Rasband)). A threshold size that correlated with loss of organisation was determined, and this was used to determine the proportion of each sample that was organized and disorganised (Figure 44c). 3000 selected transcripts associated with developmental patterning and cancer were correlated with level of organisation of 25 technically adequate samples. Of the 77 transcripts that had statistically significant correlations, the highest level of correlation was seen with DKK2 expression. DKK2 expression correlated inversely with disorganisation (Spearman's R value: -0.7612, 95% confidence interval (-0.8890 to -0.5234), p-value 0.000001) (Figure 44d). DKK2 was of interest given our previously noted finding of dysregulated Wnt/Beta-catenin signalling in CYLD defective tumours.

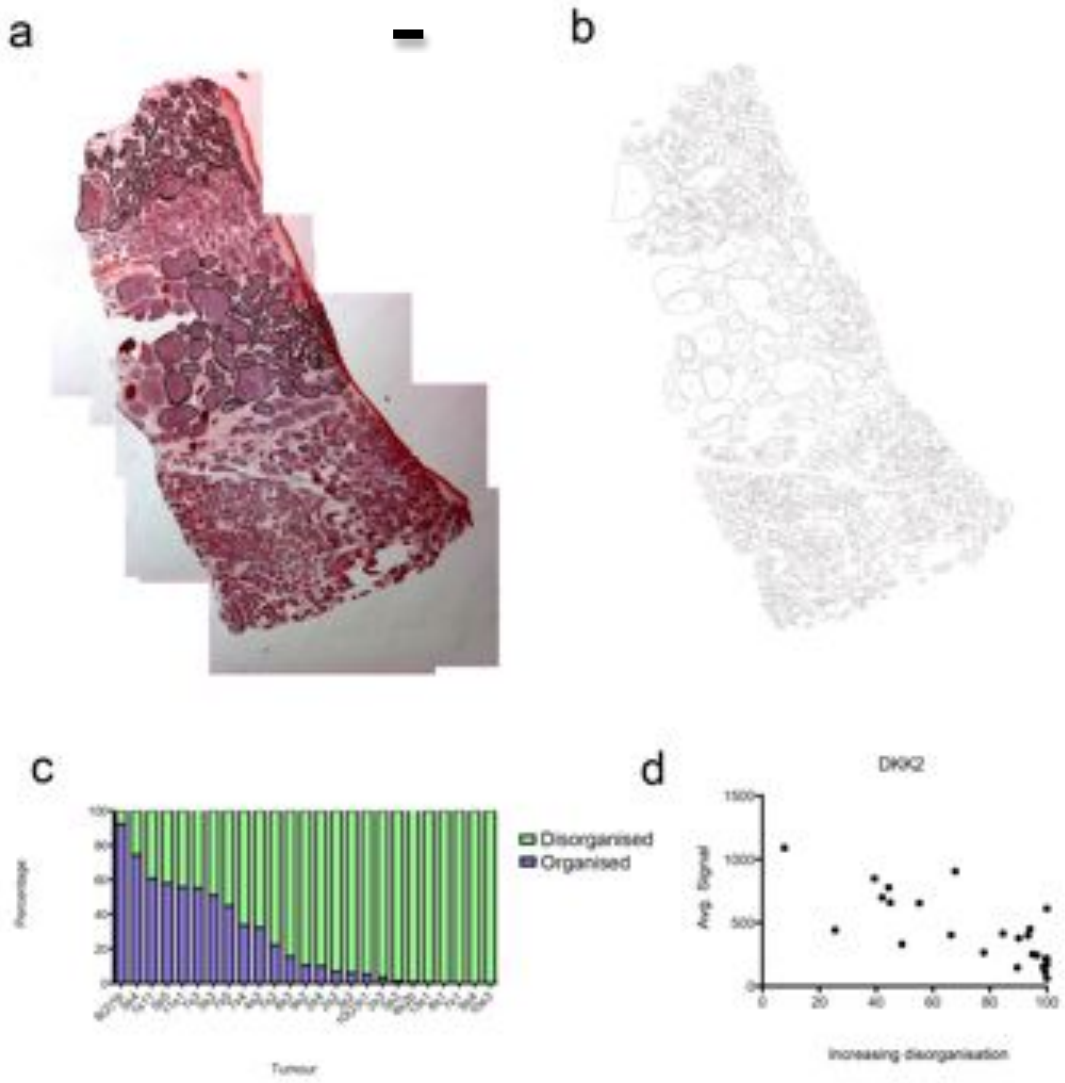

Figure 44 Reduced expression of DKK2 transcripts is associated with increasing disorganisation. 32 fresh frozen tumours were sectioned, microdissected and used for whole genome expression profiling. The first and last sections enclosing the sections used for profiling were stained and used to quantify level of tumour organisation. (a-b) A cartoon was developed by (a) tracing out each tumour island on each sample and the (b) area of each island was measured. Scale bar indicates 1mm. (c) A threshold size that correlated with loss of organisation was determined, and this was used to determine the proportion of each sample that was organised and disorganised. 25 samples were technically suitable for such quantification. (d) The gene expression profiles of 3000 selected genes were correlated with level of organisation and levels of DKK2 expression correlated inversely with organisation.

5.2.8 DKK2 promoter methylation correlates with reduced transcript level of DKK2 in the majority of CYLD defective tumours

Recently, methylation of the *DKK2* promoter has been described as a candidate mechanism to account for reduced expression of DKK2 in human renal cell and colorectal carcinoma (Sato, Suzuki et al. 2007; Hirata, Hinoda et al. 2009). Therefore we assessed *DKK2* promoter methylation status in this cutaneous tumour model. Promoter hypermethylation was assessed using a DKK2 targeted quantitative PCR based assay. Equal amounts of tumour DNA from each sample was subject to restriction digestion with methylation sensitive and methylation insensitive enzymes. Comparison of the ratio of amplification of the DKK2 promoter between these amounts allowed for assessment of extent of promoter hypermethylation. Genomic DNA from 13 microdissected tumours was included in the analysis. Percentage of promoter expression was found to inversely correlate with transcript levels ($r=-0.833$, $p=0.0041$), once 4 outliers were excluded (Figure 45), suggesting that this mechanism was not exclusive in altering DKK2 expression.

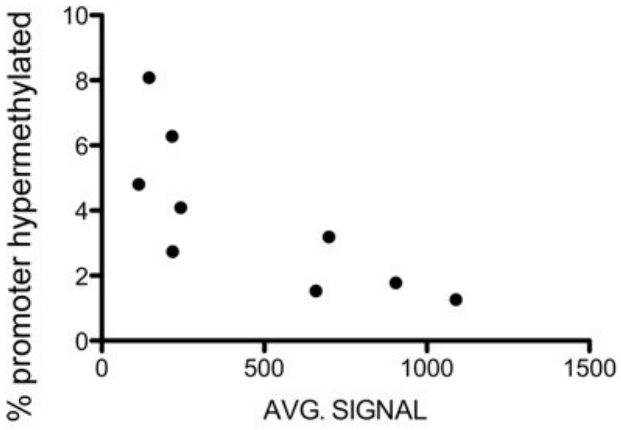

	% promoter hypermethylated
Number of XY Pairs	9
Spearman r	-0.8333
P value (one-tailed)	0.0041

Figure 45 Methylation status of the promoter of DKK2 in 9 tumours correlated with expression of DKK2 transcript.
Percentage of promoter hypermethylation was assessed using a DKK2 targeted quantitative PCR based assay that compared amplification between equal amounts of starting tumour DNA that was subject to restriction digestion with methylation sensitive and methylation insensitive enzymes. Percentage of promoter expression was found to inversely correlate with transcript levels (Spearman's R coefficient = -0.833, p=0.0041).

5.2.9 Reduction in DKK2 expression is associated with overexpression of transcripts associated with cancer and cell proliferation

The alteration in DKK2 levels associated with tumour organisation in CYLD defective tumours prompted us to conceptually reframe the cylindromas and spiradenomas as "DKK2 high" and "DKK2 low" tumours. We compared the pooled transcriptomes of 4 DKK2 "low" tumours against the transcriptomes of 4 DKK2 "high" tumours to characterise transcripts associated with reduction in DKK2 expression. We used Ingenuity pathway analysis, including genes that were differentially expressed with a fold change of 2 or greater and a level of statistical significance of $p<0.05$. Gene ontology analysis of these transcripts demonstrated that the highest scoring categories were associated with

"Cancer" (p value 2.43E-04 - 4.88E-02; 521 transcripts) and "Cellular Growth and Proliferation" (p value 3.59E-04 - 4.71E-02; 335 transcripts). The transcripts that were differentially expressed are listed in Table 15.

Table 15 Top ten over- and underexpressed transcripts in DKK2 "low" tumours (spiradenomas).

Gene	FC	Gene name
XRN2	19.25	5'-3' exoribonuclease 2
ID3	6.92	Inhibitor of DNA binding 3, dominant negative helix- loop-helix protein
MGC29506	5.40	Hypothetical protein MGC29506
PI3	5.33	Peptidase inhibitor 3, skin-derived
NOD1	5.22	Nucleotide-binding oligomerization domain containing 1
TNFAIP2	5.16	Tumour necrosis factor, alpha-induced protein 2
CYP4F12	5.06	Similar to cytochrome P450, family 4, subfamily F, polypeptide 12;
JAG2	4.93	Jagged 2
MS4A1	4.76	Membrane-spanning 4-domains, subfamily A, member 1
ELF3	4.75	E74-like factor 3 (ets domain transcription factor, epithelial-specific)
FLG	0.04	Filaggrin
SCGB2A2	0.06	Secretoglobin, family 2A, member 2
USP9Y	0.07	Ubiquitin specific peptidase 9, Y-linked
SPRR2E	0.08	Small proline-rich protein 2E
PIP	0.08	Prolactin-induced protein
RPS4Y1	0.08	Ribosomal protein S4, Y-linked 1
LAMC3	0.09	Laminin, gamma 3
SPRR1A	0.09	Small proline-rich protein 1A
ZFY	0.10	Zinc finger protein, Y-linked
GGCT	0.11	Gamma-glutamyl cyclotransferase

Network analysis of differentially expressed genes suggested that DKK2 low tumours had upregulated transcripts that included antiapoptotic BCL2. (Figure 46a). Notably Wnt/Beta-catenin pathway transcripts including APC were expressed at lower levels in DKK2 low tumours (Figure 46b).

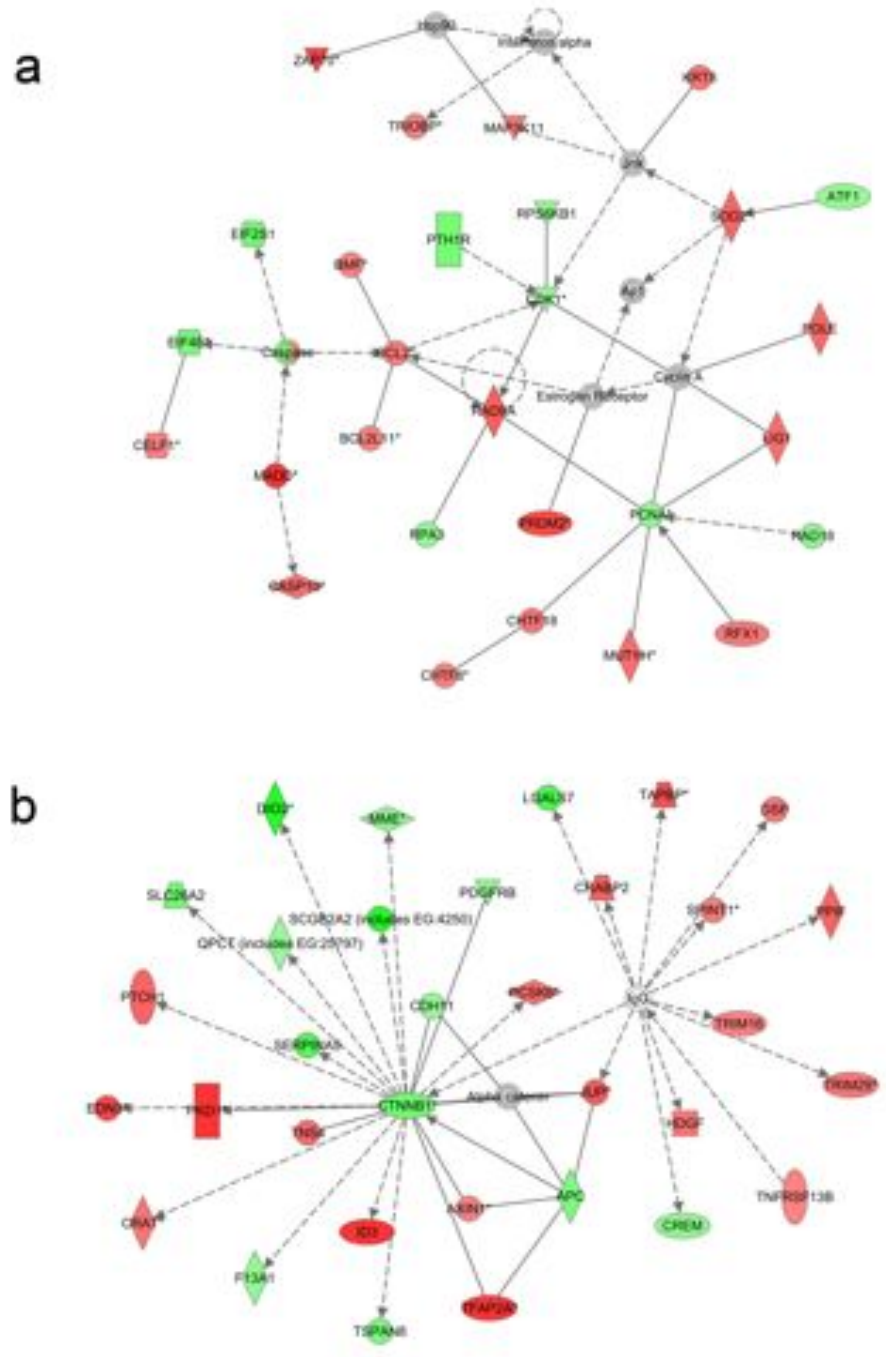

Figure 46 Reduction in DKK2 expression is associated with overexpression of transcripts associated with cancer and cell proliferation.

Comparison of the pooled transcriptomes of 4 DKK2 “low” tumours (spiradenomas) against the transcriptomes of 4 DKK2 “high” tumours (cylindromas) to characterise transcripts associated with reduction in DKK2 expression. (a) Network analysis of differentially expressed genes suggested that DKK2 low tumours had upregulated transcripts that included antiapoptotic BCL2, a TRK target gene highlighted previously by our group in CYLD defective tumours. (b) Notably Wnt/Beta-catenin pathway transcripts including APC were expressed at lower levels in DKK2 low tumours.

5.3 Discussion

CYLD mutation carriers face repeated, disfiguring surgery to control tumour burden, and in our study of two large pedigrees, up to one in four affected patients underwent total scalp removal (Rajan, Langtry et al. 2009). Painful eccrine spiradenomas, the development of conductive deafness caused by occlusive tumours in the ear canal and the risk of malignant transformation (Gerretsen, van der Putte et al. 1993) justify the development of non-surgical alternatives for this patient group. Here, we performed an unbiased approach using genomic and transcriptomic analysis of CYLD defective tumours.

We demonstrated that cylindroma and spiradenoma tumours were genomically similar and stable, with LOH at 16q found in the majority of tumours in this study. A level of LOH at 75% was demonstrable, in keeping with previous studies that performed assays using techniques capable of lower resolution analysis (Biggs, Wooster et al. 1995) (Biggs, Chapman et al. 1996) (Bignell, Warren et al. 2000).

We sought to clarify the genomic changes using high-resolution array CGH and confirmed that there were no significant changes seen in copy number between CYLD defective tumours (n=12) and perilesional skin (n=7). We also performed SNP genotyping of 4 cylindroma tumours and found that loss of heterozygosity was reserved to 16q. Interestingly, LOH analysis at the mutation site demonstrated the presence of the mutant allelle only in 75% of tumours. Taken together, the copy number neutral aCGH data, the presence of the mutant allelle only in the majority of tumours assayed by restriction enzyme analysis and the extent of LOH demonstrated in the SNP data support previous suggestions (Biggs, Chapman et al. 1996) that loss of 16q is key event in tumourigenesis and the lost arm is reduplicated by homologous recombination in the majority of tumours in this study. The genomic stability of cylindroma tumours we demonstrate may explain the benign, non-invasive nature of the tumours and the rare occurrence of transformation to malignancy (Gerretsen, van der Putte et al. 1993). Moreover, it raises the attractive possibility that genomically stable tumours may be less liable to the

acquisition of resistance mechanisms to novel therapeutics that arise through genomic diversity.

We detected upregulation of transcripts of TRKB and TRKC and their cognate ligands BDNF and NT3/NT4 in cylindroma and spiradenoma samples. This was of particular interest as CYLD, a deubiquitinase with K63 linked ubiquitin specificity, has previously been shown to deubiquitinate TRKA and inhibit its internalisation from the cell membrane and subsequent downstream signalling via the phosphatidylinositol-3-kinase (PI3K) pathway (Geetha, Jiang et al. 2005). Furthermore, recent studies have shown that BDNF is a NFκB target gene that may afford a neuroprotective role in astrocytes, supporting the finding that this TRK ligand is overexpressed by the cylindroma cells resulting in an autocrine loop (Saha, Liu et al. 2006). Validation of protein expression using TRK specific antibodies demonstrated strong membranous expression of TRKB and TRKC in cylindromas and spiradenomas, when compared to perilesional epidermis and hair follicles. Finally, downstream targets of TRK signalling such as phosphorylated ERK and BCL2 were overexpressed in the tumours.

TRK receptors have received considerable attention as mediators of neuronal growth, survival and maintenance (Huang and Reichardt 2001), and have been shown to be expressed in hair follicles (Adly, Assaf et al. 2005; Blasing, Hendrix et al. 2005). Their role in cancer was initially shown by uncommon oncogenic fusions involving C-terminal sequences of the NTRK1/NGF receptor gene with 5′ terminal sequences of various activating genes, such as TPM3, TPR and TFG in colon and papillary thyroid carcinoma (Martin-Zanca, Hughes et al. 1986; Butti, Bongarzone et al. 1995). Exploitation of the constitutively active prosurvival signalling that is usually restricted to neurons was thought to confer an advantage for the cancer cells. Recent advances in the understanding of complex signalling pathways involved in cancer (Luo, Solimini et al. 2009) has suggested that some neural derived cancer cells, such as neuroblastoma, may become dependent on TRK signalling for survival, independent of mutations in TRK (Matsumoto, Wada et al. 1995; Scala, Wosikowski et al. 1996). Subsequent demonstration of TRK expression

associated with a survival advantage in epithelial tumours including breast (Lagadec, Meignan et al. 2009), prostate (Weeraratna, Arnold et al. 2000), lung (Ricci, Greco et al. 2001), extended the role of TRK signalling to non-neural derived tumours. At a genomic level, we established that neither TRKB and TRKC amplification, nor that of BDNF and NT3/4 was demonstrated to account for the overexpression seen in cylindroma tumours, suggesting that CYLD dysfunction perturbs normal TRK homeostasis.

The differential expression of TRKA, TRKB and TRKC in these tumours is intriguing. Whilst TRKA is regulated by CYLD, the interaction of CYLD with TRKB and TRKC remains to be clarified. The low perinuclear expression of TRKA, but conversely the high membranous expression of TRKB and C suggests that not all TRKs are regulated by CYLD in the same manner. This has been shown to be true with other forms of ubiquitin modification including monoubiquitunation (Arévalo, Waite et al. 2006) or Lys48 polyubiquitination (Geetha, Jiang et al. 2005). Arévalo et al. demonstrated that an E3 ubiquitin ligase, Nedd4-2, associated with the TRKA receptor and was phosphorylated upon NGF binding whilst Nedd4-2 did not bind or ubiquitinate related TRKB receptors, due to the lack of a consensus PPXY motif. These results suggest that TRK receptors are differentially regulated by ubiquitination to modulate the survival of neurons (Arévalo, Waite et al. 2006). Interestingly, Geetha et al. have demonstrated that the scaffold protein p62 which facilitates the interaction between CYLD and TRKA, is able to bind to specific lysine residues on TRKB (Lys 811) and TRKC (Lys 602 and 815) and mutation of these sites disrupted downstream signalling (Geetha, Seibenhener et al. 2008). This suggests the possibility that CYLD could interact with TRKB and TRKC, but the precise mechanism of TRK specific homeostasis remains to be clarified.

We chose to investigate the expression of TRK in other human skin cancer models. The over expression of membranous TRKC in a high proportion of basal cell carcinoma is interesting. In sporadic BCC, LOH at 9p, the locus for *PTCH1*, has been found in the majority (93%) of basal cell carcinoma (Teh, Blaydon et al. 2005), whilst 16q, the locus for CYLD, appears rarely affected.

TRKC signalling in non melanoma skin cancer has not been characterised, but there are data from other models to support that TRK signalling could confer a proliferative advantage to cells where constitutively active SHH signalling following loss of functional PTCH could occur. Synergy between NT3, the cognate ligand for TRKC, and SHH has already been demonstrated in murine motorneurons where both are important for growth, and use of NT3 antibodies in this system reduces growth of these neurons (Dutton, Yamada et al. 1999) . TRKC also directly interacts with bone morphogenetic signalling receptors (BMPRI) in murine epithelial cells, and inhibits the tumour suppressor effects of BMP signalling (Jin, Yun et al. 2007) in a mouse colon cancer model. BMP and SHH signalling are tightly balanced, and BMP2, the ligand of BMPRI has been shown to oppose SHH mediated proliferation in murine cerebellar granular precursor cells via regulation of N-myc (Alvarez-Rodríguez, Barzi et al. 2007). Furthermore, BMP signalling is protective in cutaneous carcinoma, and a SMAD 4 conditional knockout expressed in murine keratinocytes has indeed shown to result in spontaneous squamous and basal cell carcinomas (Qiao, Li et al. 2006). It is hence conceivable that TRKC mediated inhibition of BMP signalling, on a mutated PTCH background in basal cell carcinoma may play a pathogenic role. The localisation of TRKC at the invasive margin of basal cell carcinoma tumour islands suggests that this role may be in invasion (Figure 41). The mechanism that results in TRKC overexpression in basal cell carcinoma however remains to be explored. However, TRK receptors may represent a novel therapeutic target both in tumours with loss of CYLD function but also for basal cell carcinoma, the commonest cancer in humans.

Beyond the use of this rare tumour syndrome to highlight targetable pathways in basal cell carcinoma, CYLD defective tumours represent an intriguing model of cutaneous tumour patterning. Highly patterned cylindromas and disorganised spiradenomas arise on the same genomic background and demonstrate homogeneity at the molecular level. We have shown that these two tumours are genomically similar, and share similar transcriptomic profiles, despite their histological and clinical differences. In keeping with these data, we show that cylindromas and spiradenomas represent extremes of a

spectrum of tumour organisation. Firstly, we show that islands of cylindroma cells grow as contiguous structures, a finding consistent with the growth pattern found in sporadic hair follicle tumours such as basal cell carcinoma (Lang, McKelvey et al. 1987; Scheibe, Braumann et al. 2010). Also, spiradenomas are shown to arise within and grow contiguously from preexisting cylindromas, accounting for the recurrent finding that features of both tumours are found in the same specimen, termed spiradenocylindroma. Finally foci of organised cylindroma are demonstrated within small spiradenomas.

The molecular changes that account for this variation of organisation may be explained by a model proposed below that incorporates the recent finding that loss of CYLD results in constitutively active Wnt/Beta-catenin signalling, via lack of regulation of Dishevelled (Tauriello, Haegebarth et al. 2010). CYLD defective tumours represent a cutaneous tumour model that has arisen on a background of abnormal Wnt/Beta-catenin signalling. We demonstrate nuclear beta-catenin in cells adjacent to stroma in cylindromas, and throughought the tumour mass in spiradenomas, suggestive of active signalling. By using morphometric analysis of tumour specimens, we were able to quantify the level of organisation of 25 CYLD defective tumours. Correlation analysis highlighted that reduced expression of DKK2, a negative regulator of Wnt/Beta catenin signalling, correlated with increasing disorganisation. DKK2 is one of four members of the DKK family, thought to negatively regulate Wnt/Beta-catenin signalling by binding to LRP (Katoh and Katoh 2007). Modulation of regulators of Wnt/Beta-catenin signalling has been shown to be associated with higher grades of malignancy in human tumours. Loss of expression of DKK family members has been described in cancers where Wnt/Beta-catenin signalling has been shown to be pathogenic, such as colorectal cancer, cervical cancer and breast cancer where such loss is mediated by epigenetic inactivation (Aguilera, Fraga et al. 2006; Lee, Yoon et al. 2008; Suzuki, Toyota et al. 2008). In renal cell carcinoma, epigenetic modification by methylation of *DKK2* has been recently shown to be associated with advanced tumour stages and reduced survival (Hirata, Hinoda et al. 2009). We demonstrate that *DKK2* promoter methylation positively

correlated with reduced DKK2 expression in the majority of tumour samples assayed. Epigenetic inactivation has an established pathogenic role in non melanoma skin cancer. Methylation of genes including *FOXE1* and *14-3-3 sigma* having been shown to play a pathogenic role in squamous cell carcinoma (Zhu, Xia et al. 2007; Venza, Visalli et al. 2010) and basal cell carcinoma (Lodygin, Yazdi et al. 2003). Methylation of Wnt inhibitors, whilst demonstrated in other tumours, has not been previously described in non-melanoma skin cancer. Our data extends the role of DKK2 beyond playing a role in hair follicle morphogenesis (Sick, Reinker et al. 2006), to potentially influencing the phenotype of skin tumours where Wnt signalling is pathogenic.

When we compared DKK2 high tumours (cylindromas) against DKK2 low tumours (spiradenomas), we found that the signalling networks that were overexpressed in spiradenomas were principally involved in cellular proliferation. Changes in Wnt/Beta-catenin signalling were seen in DKK2 low tumours. Recent characterisation of transcript changes over time of Wnt/Beta-catenin signalling pathway members in HEK-293 cells following stimulation of with Wnt3a also demonstrate the downregulation of APC transcripts in active Wnt/Beta-catenin signalling as seen in our model (Gujral and MacBeath 2010). Increased Wnt/Beta-catenin signalling has been shown to result in increased NFκB signalling, an effect mediated via increased transcription of beta transducing repeat-containing protein (βTrCP). This has been shown to reduce levels of IκB by ubiquitination (Spiegelman, Slaga et al. 2000) and may account for the increased expression of NFκB target genes seen in DKK2 low tumours such as *TNFAIP2*. DKK2 low tumours may thus have a proliferative advantage due to synergistic effects of oncogenic Wnt and NFκB signalling in a CYLD defective cellular context. Finally, it is interesting to speculate that the tissue tropism seen with CYLD defective tumours may be related to the dysregulation of pathways recognised to be important in embryological hair development.

5.4 Conclusions

Here we demonstrate dysregulated TRK and Wnt signalling in CYLD defective tumour following transcriptomic profiling. Validation of the TRK overexpression at the protein level confirmed overexpression of TRKB and TRKC in CYLD defective tumours. Furthermore, we examined sporadic skin cancers, and found that TRKC is overexpressed in 70% of BCC, making this a potential therapeutic target beyond *CYLD* mutation carriers.

By correlating the transcriptomic data against the level of organisation of tumours, we show that increasing disorganisation is associated with a reduction of expression of the Wnt signalling pathway inhibitor DKK2.

These data warrant further investigation in a cell culture model. In the next chapters, the derivation of primary cell cultures from CYLD defective tumours is used to investigate the functional consequences of targeting these pathways.

6 CHAPTER 6 : CYLD defective tumour primary cell culture

6.1 Introduction

Primary cell culture of CYLD defective tumours (CPCC) serve as an *in vitro* model to perform functional analysis of dysregulated pathways identified from the transcriptomic analysis of these tumours. They are also important for the screening of potential therapeutic targets. Derivation of primary cell culture has been described previously, and we chose to optimise the method of developing primary cell cultures from fresh tumour specimens (Weber, Wick et al. 1984; Bruckner-Tuderman, Pfaltz et al. 1991).

6.2 Methods

6.2.1 Microdissection , cellular disassociation and cell culture

Tumour tissue obtained following surgery was stored in transport medium, and processed within 2 hours. Cylindroma tumours that had a homogenous macroscopic appearance were used for primary cell cultures. Spiradenoma tumours with cystic or necrotic changes, or specimens with mixed features were excluded. Tumours were examined under a dissecting stereo microscope within a laminar flow hood, and microdissected, to ensure only tumour tissue and not perilesional tissue was used for primary cell culture (Figure 47). These pieces of tissue were maintained in the transport medium until dissection was complete. Tissue pieces were then cut using a scalpel till they were uniformly 1-2 mm in their longest dimension. Tissue pieces were then subject to enzymatic digestion with collagenase (Sigma, UK) for 90 minutes at 37 °C in a sterile centrifuge tube. Following this, the cells were spun down, and resuspended in trypsin (Invitrogen, UK) at 37 °C for 60 minutes. Cells were then resuspended in transport medium, to inhibit further enzymatic digestion, before being resuspended in KSFM for plating out, or in freezing medium for storage. Aliquots of tumour cells that were frozen down were placed in a cryogenic vessel that contained propranolol, that allowed the gradual cooling of cells at a rate of 1 °C per minute (Nalgene, UK). For cells that were used immediately for experiments, cell viability was assessed using Trypan Blue (Sigma, UK) and viable cells were counted and plated out at a

density of 600-25,000 cells per cm^2 depending on the application. Cells were plated on collagen coated (Type I Collagen- Invitrogen UK) tissue culture plasticware and grown in keratinocyte serum free medium (Invitrogen UK). Cells were maintained at 37°C at 5% CO_2 and 21% O_2 unless otherwise specified. Cultures were fed every 48 hours. Confluent cultures were passaged and replated at an appropriate density. The cells were washed in PBS, followed by a wash in Versene, before being incubated with Trypsin 0.5% with EDTA. Once cells had detached, the Trypsin was neutralised with soya bean Trypsin inhibitor (Sigma, UK). Cells were then pelleted and resuspended in KSFM, before viable cells were counted for plating. Cells that were grown on 3D polystyrene tissue culture scaffolds were prepared as above, before being plated onto scaffolds prepared in accordance with manufacturer's instructions. This involved rehydrating the scaffold with graded ethanols, washing with PBS, and finally coating with collagen (Type I Collagen - Invitrogen UK). Cells were plated at a density of 250,000-750,000 cells per cm^2 of scaffold material. Cells were grown as described above.

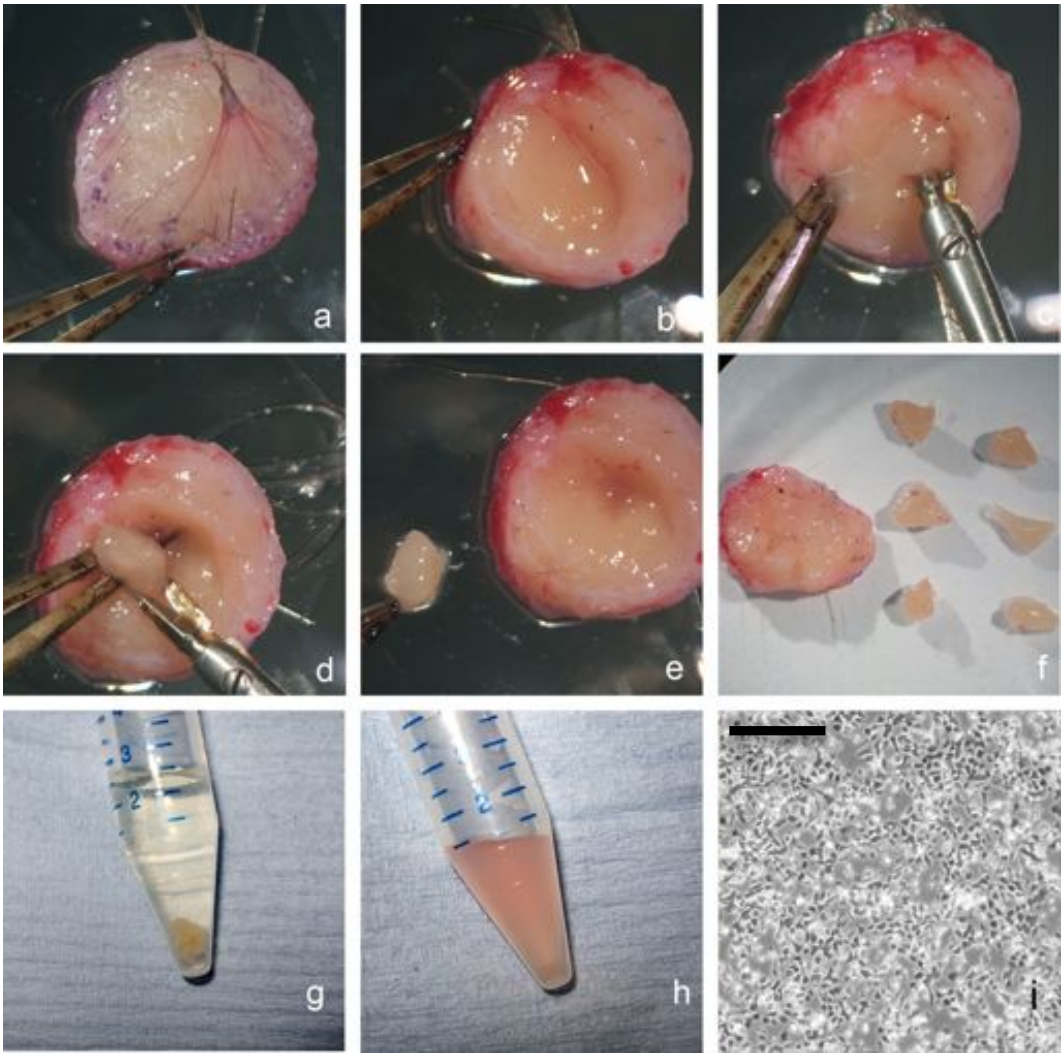

Figure 47 Microdissection technique and cellular disassociation.

(a) A fresh tumour specimen, demonstrating the external surface with overlying surface, and shave excision margins drawn in purple ink. (b) The reverse side of the same specimen, exposing the tumour tissue. (c-e) Microdissection with fine surgical instruments, and subsequent extraction of a piece of tumour tissue. (f) The sample after microdissection of the tissue. The 6 tumour samples are seen on the right and are used for enzymatic digestion, while the remaining tissue (on the left) is not used. (g) Before enzymatic digestion, and (h) after, when a single cell suspension is obtained. (i) Cells shown at 48 hrs after being plated on collagen coated tissue culture plastic; Scale bar indicates 100 μm.

6.3 Results

6.3.1 CPCC are an in vitro model of CYLD defective tumours

CPCC were derived from CYLD defective tumours obtained from patients with germline mutations undergoing surgical procedures to control tumour burden. Following a period of optimisation of protocols described in the literature, viable cell cultures were achieved. Cylindroma cells formed colonies of different sizes, and features of holoclones and meroclones were seen (Figure 48 a-b) (Barrandon and Green 1987). Cells that had grown to confluence demonstrated a classic cobblestone appearance (Figure 48 c-d), as seen by others (Weber, Wick et al. 1984). Two morphologies were seen; small cells typical of keratinocytes in culture were the predominant type, and large flat cells with increased nuclear size were occasionally seen.

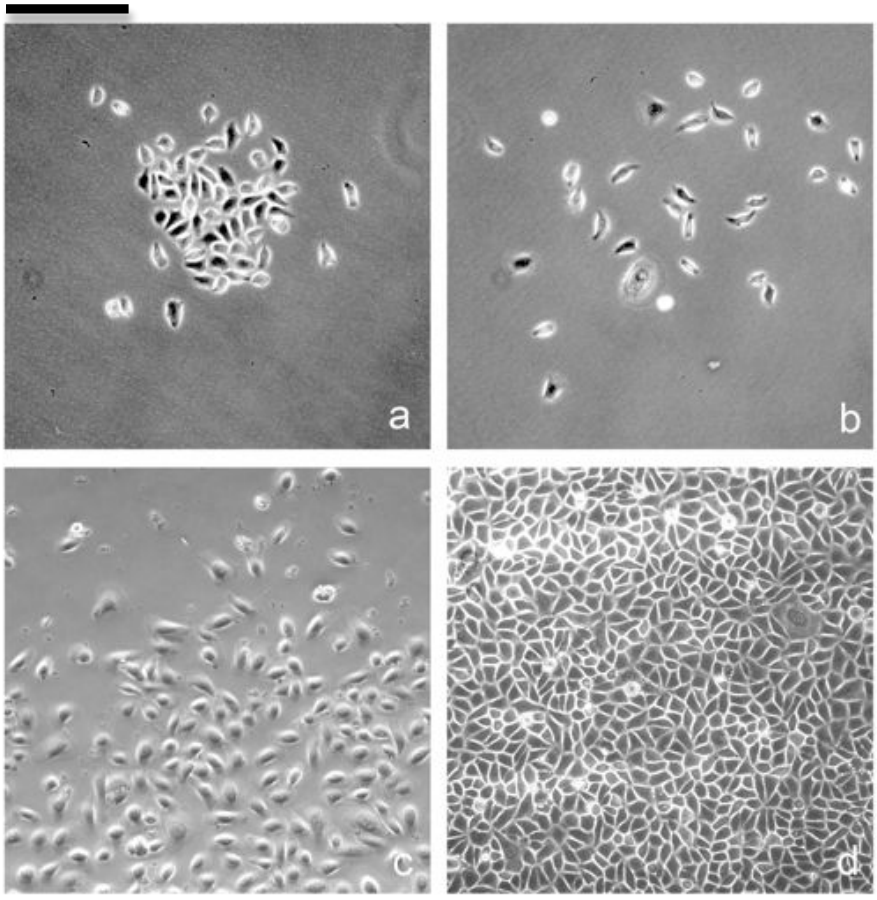

Figure 48 Primary cell culture of CYLD defective tumours (CPCC).
(a) Small tight colonies (meroclones), as well as cells that formed larger colonies (b) of widely distributed cells (holoclones) were both seen. (c) Cells at the edge of colonies were mobile and typically had a small cytoplasmic volume. (d) When cells became confluent, a classic cobblestone appearance was seen. Scale bar indicates 100 μm.

6.3.2 CPCC proliferate in low calcium serum free media

In the development of primary keratinocyte cultures without feeder layers, low calcium (<0.08mM) conditions have been shown to be important (Boyce and Ham 1983). We attempted culture in different media, which allowed for growth in different concentrations of calcium, as well as additives such as bovine pituitary extract, fibroblast growth factor, epidermal growth factor and insulin.

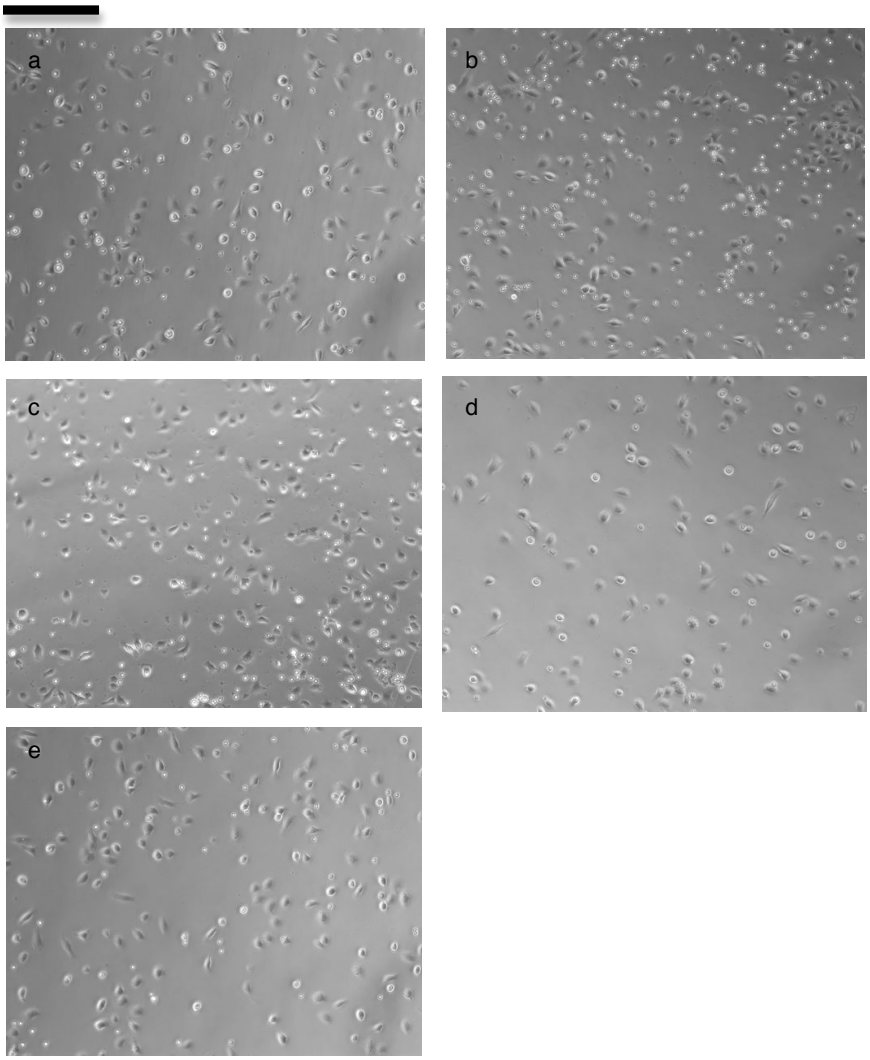

Figure 49 CYLD defective tumour CPCC maintained in different media, seen at 2 days after plating. (a) Keratinocyte differentiation medium (Low calcium, low BPE - Cnt-02), (b) Fully defined keratinocyte medium (Low calcium, No BPE - Cnt-07 PCT), (c) Keratinocyte non-defined medium (Low BPE, low calcium - Cnt-57 PCT) , (d) Keratinocyte fully defined medium (High calcium (1.2mM), serum and BPE free - Cnt-02 3D Prime), (e) Keratinocyte serum free medium, (Low calcium, no BPE), (Invitrogen KSFM). Scale bar indicates 100 μm.

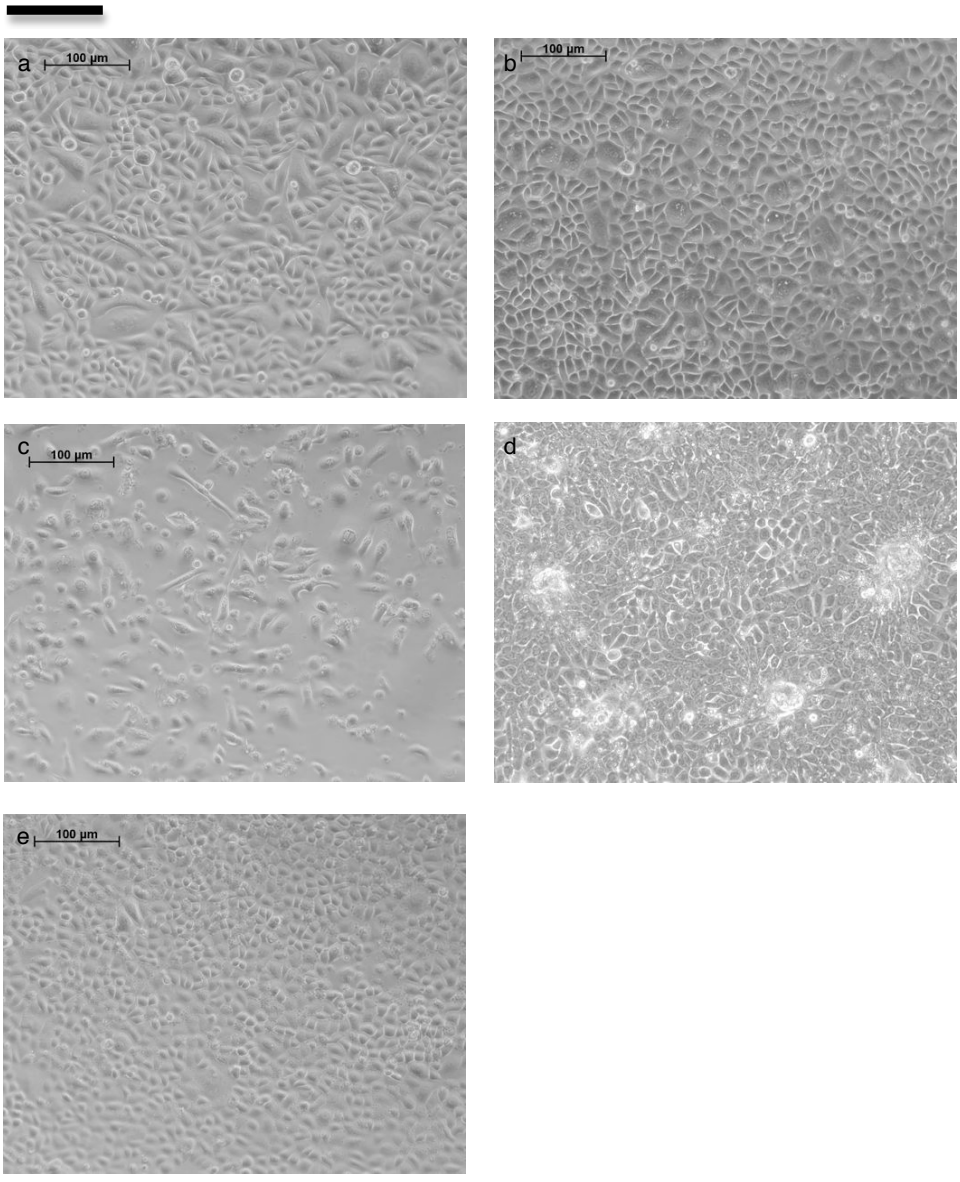

Figure 50 CPCC maintained in different media, seen at 1 week after plating.
(a) Keratinocyte differentiation medium (Low calcium, low BPE - Cnt-02), (b) Fully defined keratinocyte medium (Low calcium, No BPE - Cnt-07 PCT), (c) Keratinocyte non-defined medium (Low BPE, low calcium - Cnt-57 PCT), (d) Keratinocyte fully defined medium (High calcium (1.2mM), serum and BPE free - Cnt-02 3D Prime), (e) Keratinocyte serum free medium, (Low calcium, no BPE), (Invitrogen KSFM). Scale bar indicates 100 μm.

Following this period of optimisation, KSFM was selected as the medium for the subsequent experiments, as the cells appeared to proliferate, with few or no fibroblasts seen. This media was serum free, and had low calcium (0.08mM), and did not contain bovine pituitary extract. This was used for further characterisation of cells in different conditions.

6.3.3 Hypoxia retards growth of CPCC

Cells were grown in hypoxic conditions (pO_2 =5%) and normal oxygen tension (pO_2=21%) and colony sizes were monitored on a daily basis using photographs. Cells in each colony were then counted, and charted below (Figure 51).

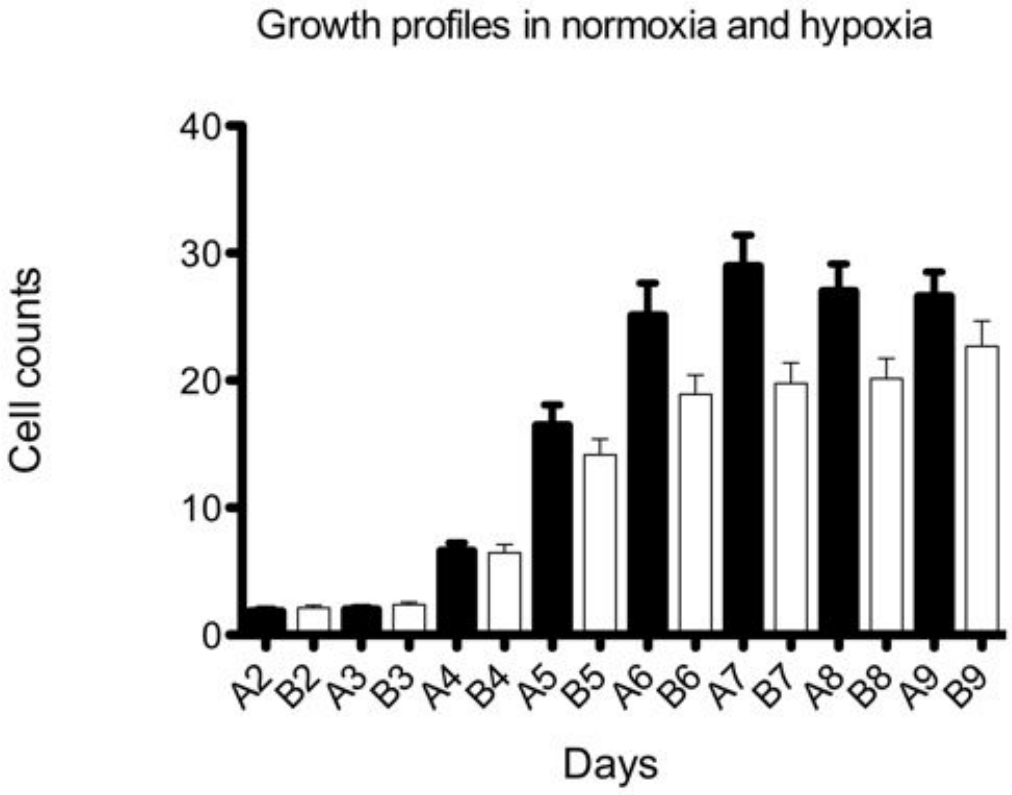

Figure 51 Growth of CPCC in normoxia and hypoxia.
Cell counts per colony was measured daily at 5% pO_2 (white bars, prefixed "B") and 21% pO_2 (black bars, prefixed "A") on uncoated plasticware. Photographs were taken of colonies and counted daily. Error bars indicate the standard error of the mean, Experiments were done in triplicate on one CPCC.

6.3.4 CPCC grow faster on Type I collagen coated plasticware

Cells were then grown at 21% pO_2 thereafter, and growth was compared between uncoated plasticware and Type I collagen coated plastic ware. Collagen coating resulted in increased colony sizes, and also loss of plateau of cell proliferation at day 7 (Figure 52).

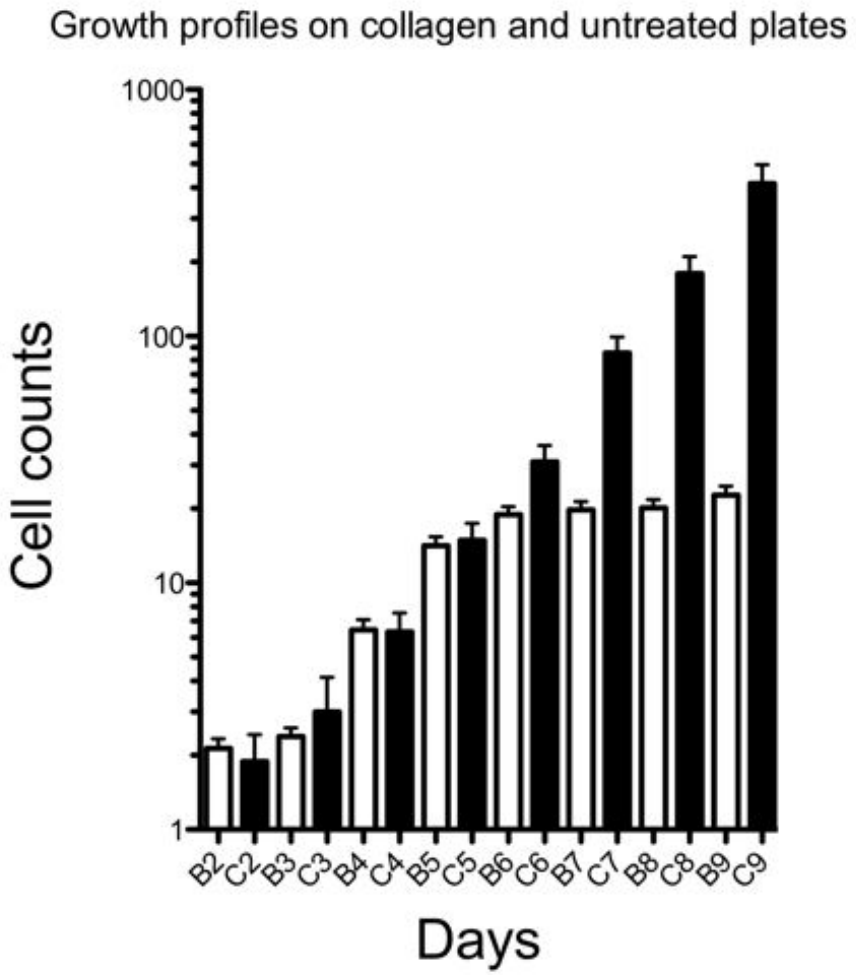

Figure 52 CPCC growth on coated vs. uncoated plasticware.
Comparison of growth profile on Type I collagen coated plasticware (black bars, prefixed "C") and uncoated plastic ware (white bars, prefixed "B") at 21% pO_2. Bars indicate cell counts per colony. The vertical axis has a logarithmic scale. Experiments were done in triplicate on one CPCC. Error bars indicate standard error of the mean.

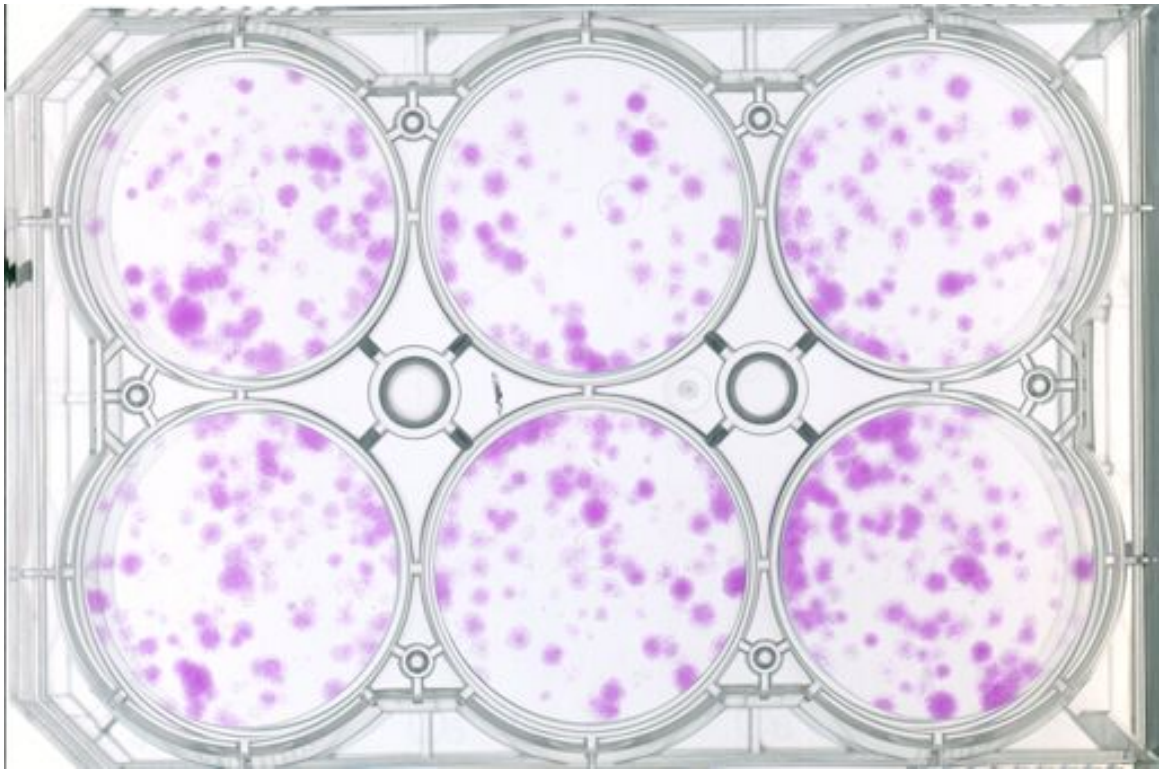

Figure 53 Colony forming assay.
CPCC were plated at a density of 1400 cells per well on Type I collagen coated plasticware and grown for 14 days. Cells were then fixed and stained with SRB, before colonies were counted. One plate, indicative of the triplicate is shown.

CPCC were grown on collagen coated plastic ware and passaged up to ten times. To clarify the longevity of these cultures, clonal cultures were established (Figure 53). In this CPCC, a mean colony forming rate of 71.67 cells (standard error of the mean - 9.77) per 1400 (5.2%) plated was seen when grown under standard culture conditions on collagen coated plasticware. Colonies were principally of two morphologies as previously seen in confluent cultures: the majority were smaller cells forming a variety of clones with some larger flatter cells with increased nuclear volume typically forming small clones. The predominant cell type was subject to serial subcloning. Serial subcloning was feasible for up to 5 times before cells did not proliferate in culture despite being maintained for two weeks presumably

having reached Hayflick's limit (HAYFLICK 1965).

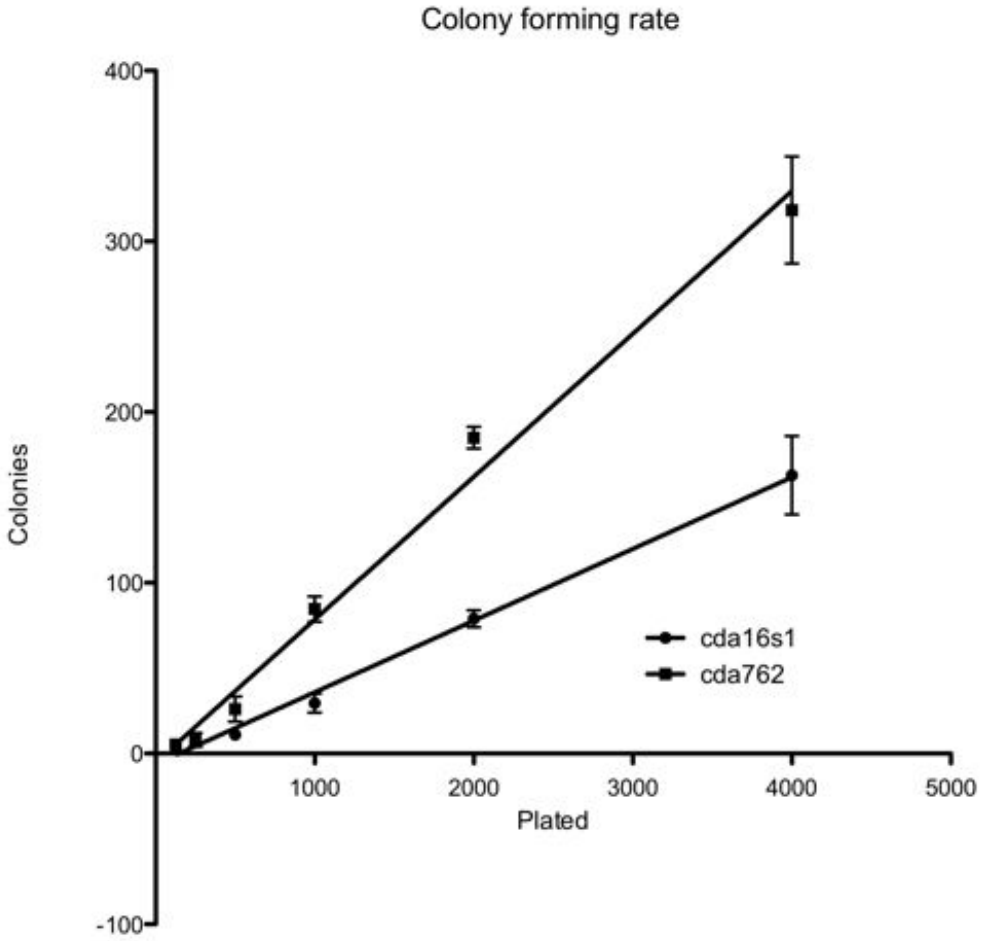

Figure 54 Colony forming assay with serial dilutions of plated CPCC.
CPCC were serially diluted 5 times and plated, and then grown for 2 weeks, before cells were fixed, stained and colonies counted. Each CPCC was plated in triplicate. Two CPCC are shown here, with different rates of colony formation, varying from 4-8%. Error bars indicate standard error of the mean.

CPCC appeared to display different rates of colony formation that varied between tumour samples. To clarify this, we performed a colony forming assay with serial dilutions of cells and found that cells formed colonies at a rate that varied between 4-8%.

When CPCC was grown in KSFM, there were rare clones of cells (<1 in a 1000) in some CPCC that were of a different morphology, consistent with the appearance of fibroblasts. These cells matched the appearance of cells grown from fibroblast cultures of perilesional dermis (Figure 55). Fibroblast cultures, developed to be used as a control cell culture, were grown in fibroblast culture medium, that contained 10% FBS. These cells had a linear shape, with

dendritic processes seen when subconfluent, and had a whorled, storiform appearance when confluent.

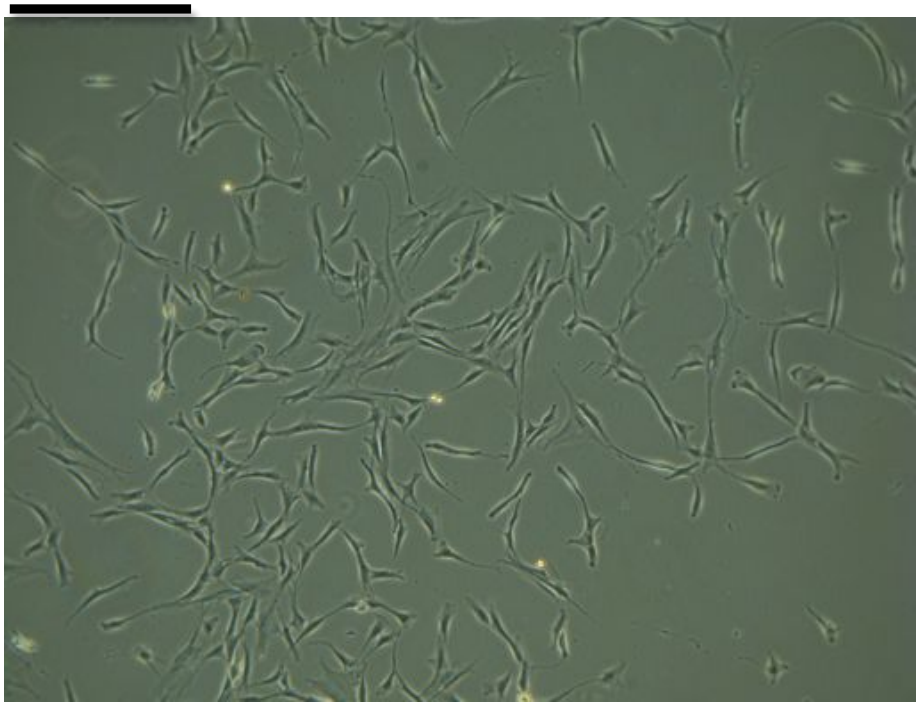

Figure 55 Fibroblast culture of perilesional dermis
Scale bar indicates 100 μm

6.3.5 CPCC lack full length CYLD

To confirm the purity of CPCC when grown in KSFM, we assayed expression of full length CYLD. We determined CYLD protein expression as a marker of purity of CPCC. CPCC lacked full length CYLD, whilst control HeLa and perilesional fibroblast cultures demonstrated CYLD expression (Figure 56).

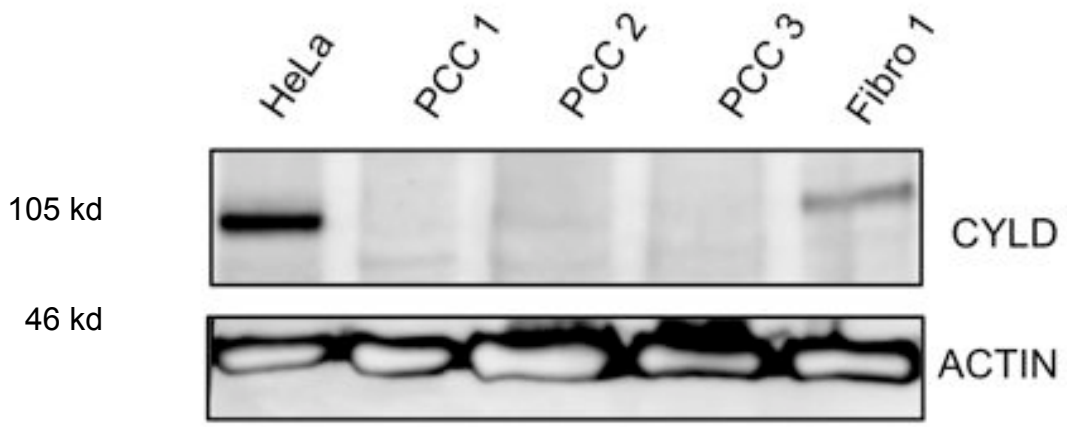

Figure 56 Expression of CYLD as a marker of purity in CPCC.
Total cell lysates were separated using SDS-PAGE, and subject to immunoblotting with anti CYLD antibody. Actin was used as a loading control.

6.3.6 Immunocytochemical characterisation of CPCC

CPCC were characterised using immunocytochemical techniques to confirm the presence of proteins seen *in vivo* (Figure 57). Cytokeratins 6, 14, 17 and smooth muscle actin were seen.

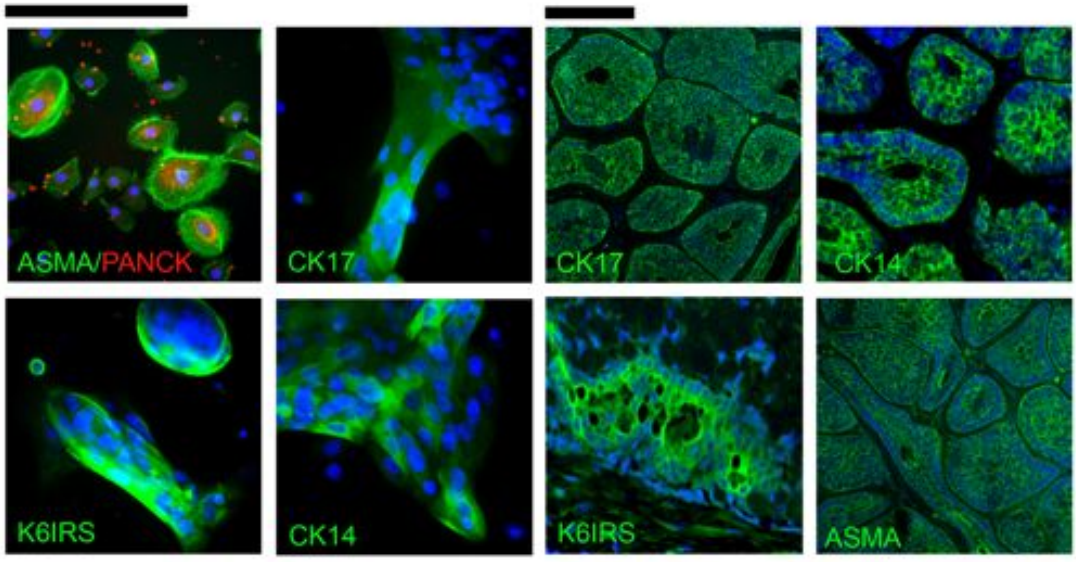

Figure 57 CPCC express markers that are seen *in vivo*.
CPCC were subject to fluorescent indirect immunocytochemistry, using the antibodies as labelled in the panels above. Cells in culture (4 left panels) expressed cytokeratins and smooth muscle actin as seen in tumour sections (4 right panels). Scale bars indicate 100 μm.

6.3.7 Reintroduction of full length CYLD results in reduced CPCC cell viability

CPCC were transfected with a lentiviral vector expressing CYLD under the control of the cytomegalovirus promoter. This resulted in reduced cell viability, with counts of cells reducing each day compared to cells transfected with empty vector.

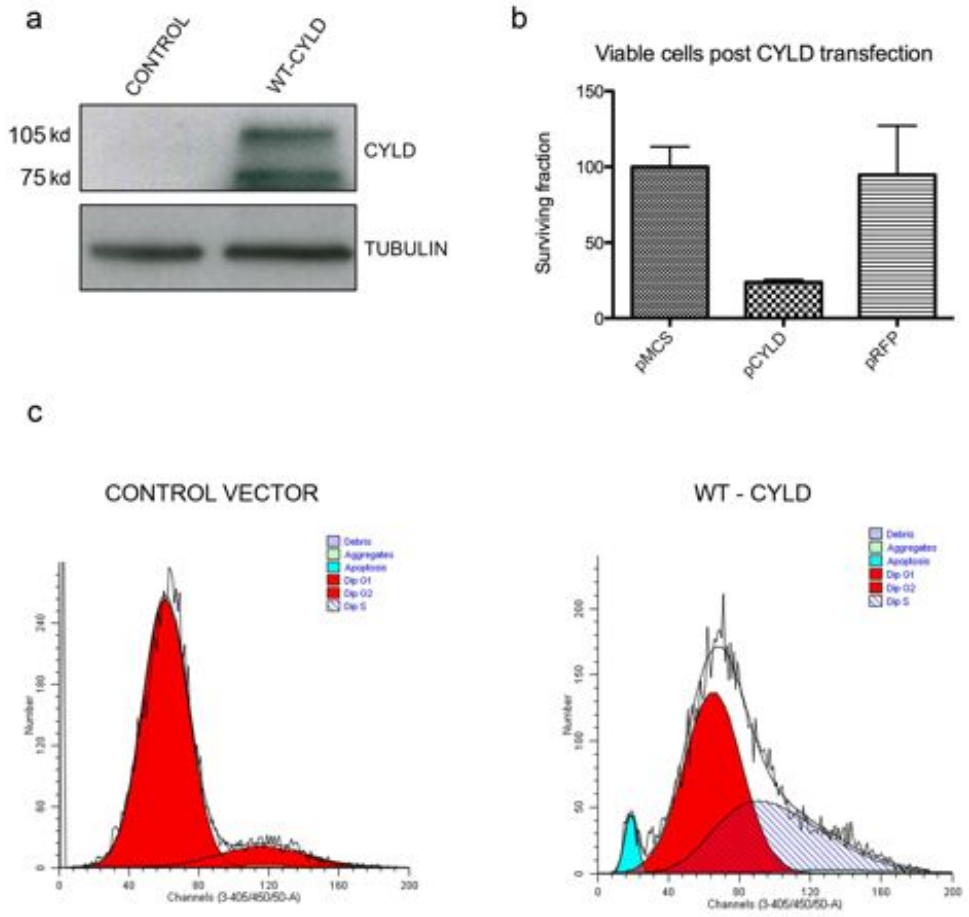

Figure 58 Reintroduction of wild type CYLD results in reduced cell viability.
Cells were plated in equal numbers and transfected with empty vector, wild type CYLD and red fluorescent protein, and selected with puromycin. At Day 5 post selection, cells were trypsinised and viable cells counted. **(a)** Expression of CYLD was assessed using immunoblotting, demonstrating full length CYLD (107kd) and a shorter natural splice variant (86kd) (Hövelmeyer, Wunderlich et al. 2007). **(b)** Small numbers of viable cells were seen with CYLD reintroduction. **(c)** FACS analysis was performed to determine changes in cell cycle and highlighted a sub G0/G1 peak suggestive of apoptosis. The experiments were performed in three different primary cell cultures derived from separate tumours.

Cell cycle analysis was performed using FACS, and this demonstrated a sub G0/G1 peak, suggestive of apoptosis. The reduced cell viability precluded further work with CPCC with reintroduced wild type CYLD.

6.3.8 CPCC on 3D tissue scaffolds

CPCC were plated and grown on 3D polystyrene tissue culture scaffolds to determine whether this would influence protein expression of TRK receptors. This was done as expression of TRKB and TRKC was high in tissue sections, but low in standard 2D culture. We hypothesised that the increased cell-cell interaction facilitated by 3D culture may influence the expression of membrane bound receptors. Cells were shown to maintain the same cytokeratin profiles seen in 2D culture (Figure 59). We found that expression of TRKB and TRKC were increased following 3D culture (Figure 60). The amount of TRKB and TRKC *in vivo* was significantly higher, and hence to allow for comparison with the 3D CPCC, only 5ug of tumour lysate was loaded versus the 20ug of lysate from 3D CPCC. Consistent with this, immunocytochemistry to demonstrate expression of TRKB and TRKC on 3D scaffolds gave poor results on preliminary attempts (data not shown).

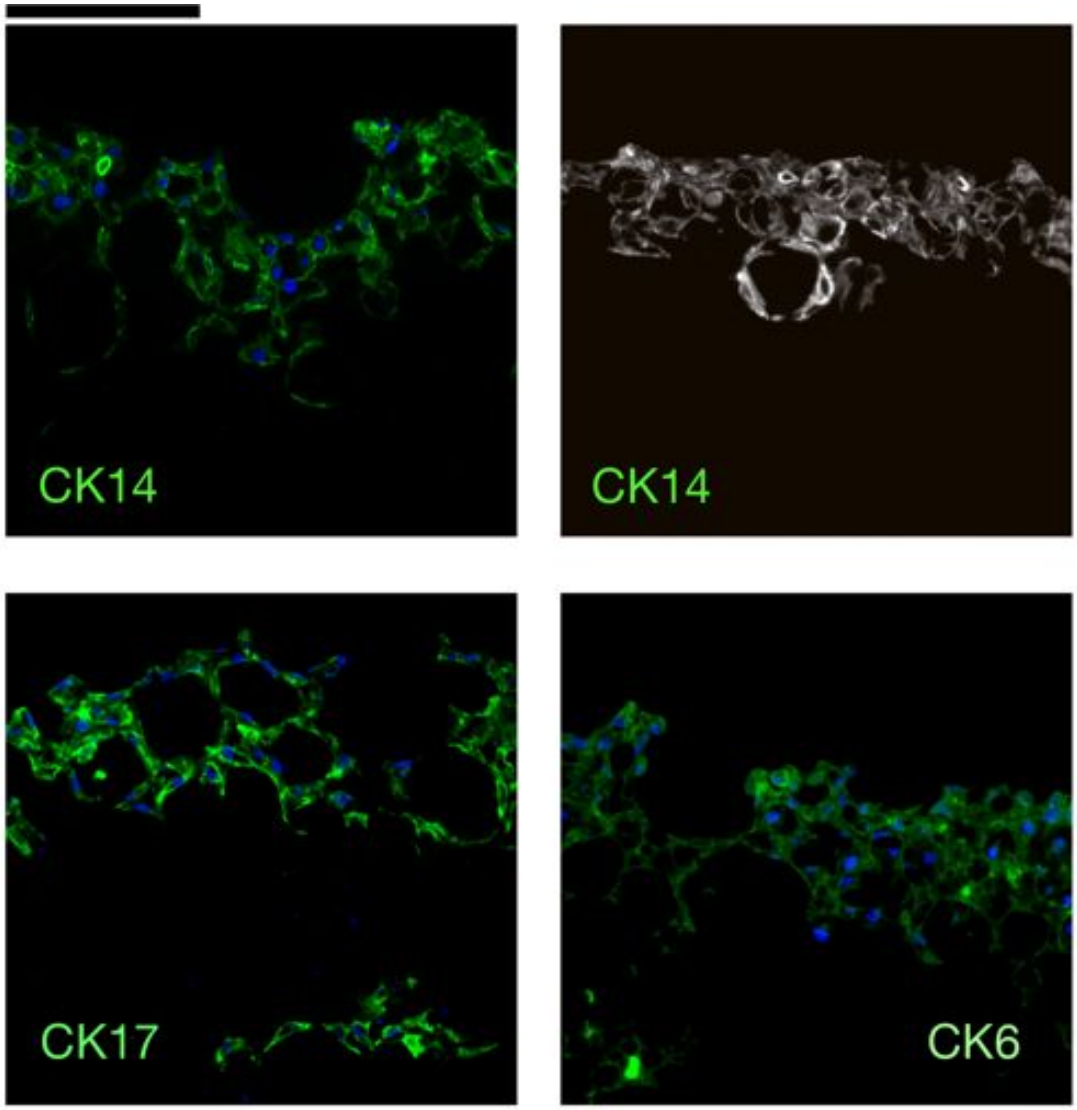

Figure 59 Immunocytochemistry demonstrates maintenance of expression of cytokeratins seen in 2D and *in vivo* in 3D CPCC.
Scale bars indicate 100 μm.

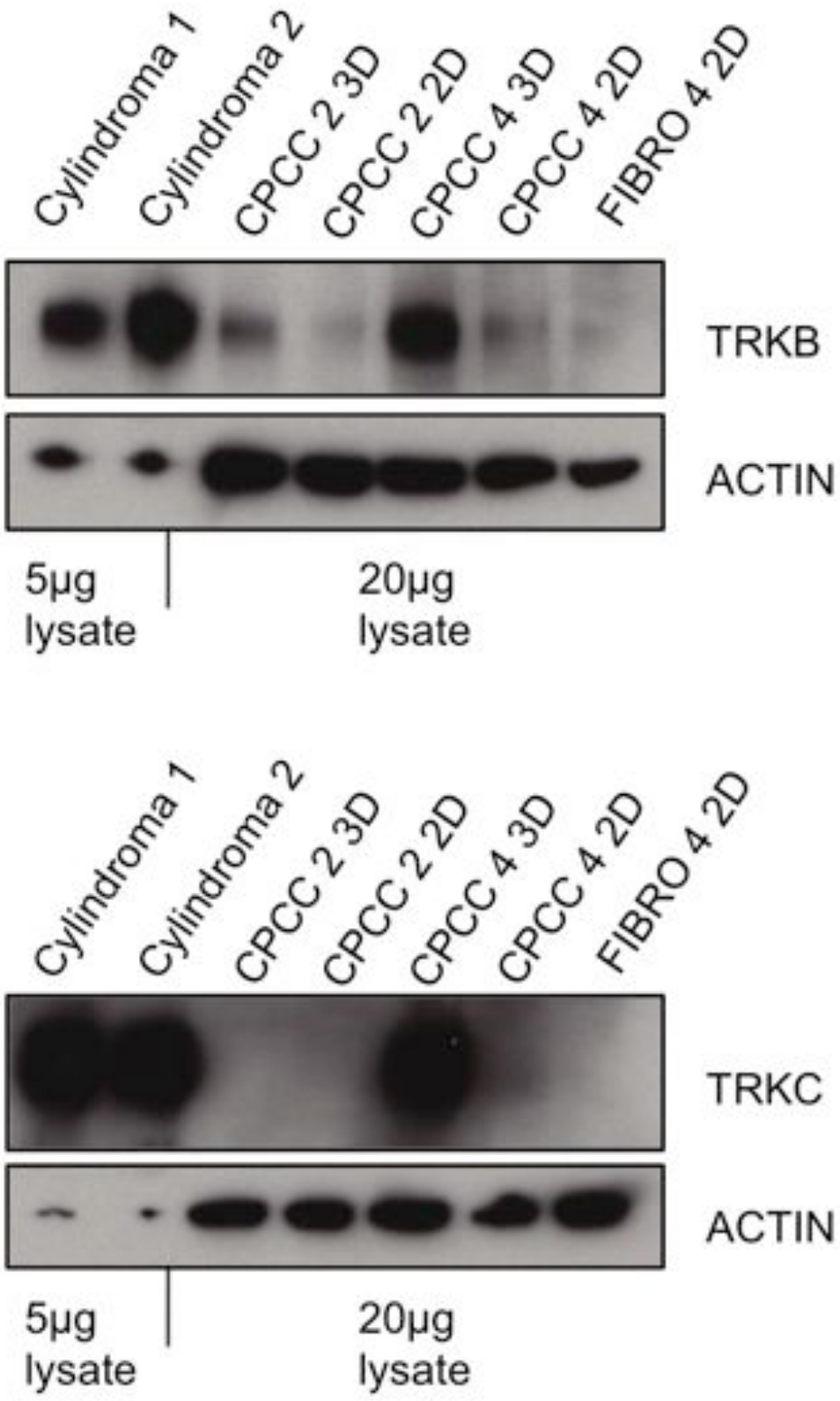

Figure 60 TRKB and TRKC expression in vivo compared with 3D and 2D culture.
Total cell lysates from fresh tumours, 3D and 2D cell cultures were separated using SDS-PAGE, and immunoblots were probed using TRKB and TRKC antibodies as indicated. Lanes 1 and 2 were loaded with 5µg of cell lysate from fresh tumours as TRK expression levels were significantly higher in tumour

tissue than the primary cultures, labelled “Cylindroma 1 and 2”, rest 20μg of lysate from primary cell cultures in 3D (CPCC 2,4 3D) and cultures in 2D (CPCC 2,4 2D). TRKB and TRKC were expressed at higher levels in 3D cell cultures (Lanes 3 and 5) compared to matched 2D cultures (Lanes 4 and 6).

6.3.9 Cell viability in 3D culture assayed using an ATP-dependent luminescent assay

Having developed a model where we were able to demonstrate increased expression of TRK, optimisation of a technique to determine cell viability was performed, with a view to determine the effect of inhibiting TRK. 3D cultures at 28 days were used. 2mm discs were punched out of the scaffold as shown in the sequence in Figure 61. These discs were placed individually in wells in a 96 well tissue culture plate, and maintained for two further weeks.

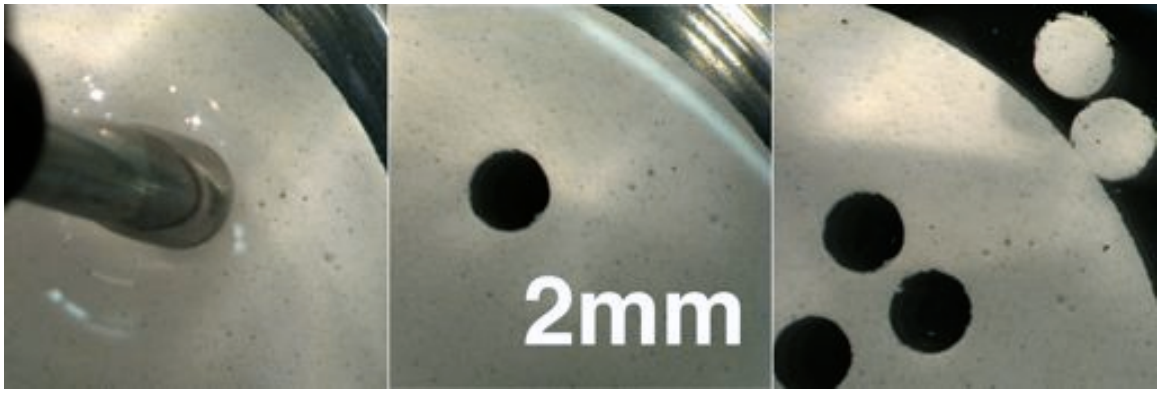

Figure 61 2mm disc 3D CPCC harvesting.

Cellular viability was assessed using an assay that lysed the cells, and produced a luminescent signal in direct proportion to the amount of available ATP (CellTiter GLO, Promega UK). This served as a readout of cell viability. CPCC grown on 2mm scaffold discs assayed in this manner at 2 weeks demonstrated a strong luminescent signal above background when read on a luminometer. Readings for each 2mm 3D CPCC disc were taken across three replicates (Figure 62). This demonstrated consistency in viable cells across triplicate discs, with a small standard error demonstrated.

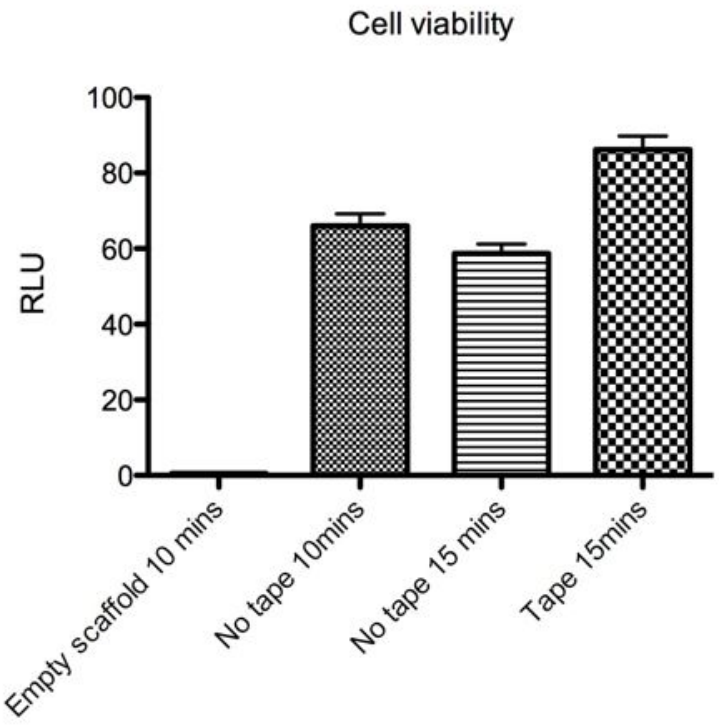

Figure 62 Assay of 3D CPCC cell viability using an ATP dependent luminescent assay.
2mm 3D CPCCs were assayed in triplicate, and error bars indicate standard error of the mean. Readings were taken in 96 well clear bottom plates, at the time points indicated after lysis of cells, with and without the bottom of the plate taped over with white tape. This optimization resulted in increased luminescence and was used subsequently.

6.4 Discussion

CPCC are an attractive model to study dysregulated pathways highlighted following transcriptomic profiling of CYLD defective tumours. By using CPCC from tumours derived from the same pedigrees, the genomic background is likely to be similar and homogeneous. Furthermore, by using primary cell cultures that are typically in the first passage for experiments, the likelihood for genomic change in the cells are minimised. Therapeutic targets discovered in this context are likely to remain pertinent to the *in vivo* context.
Primary cell cultures of aggressive skin tumours with a variety of genomic changes such as seen in melanoma or squamous cell carcinoma is well established, as are the development of cell lines from these tumours (Giard, Aaronson et al. 1973; Kondo and Aso 1981). Less aggressive but common tumours such as basal cell carcinoma, where mutations in the SHH pathway

appear to be sufficient to cause the tumour phenotype *in vivo* are difficult to establish in culture *in vitro*. Typically further mutations in other tumour suppressors such as p53 are needed to establish an *in vitro* line (So, Langston et al. 2006). Recent advances in the understanding of the dependence of such tumours on SHH signalling from peritumoural stroma may explain the difference seen *in vitro* vs. *in vivo* (Yauch, Gould et al. 2008). In keeping with this, sporadic basal cell carcinoma in humans is often intersposed with stroma.

As CPCCs are quickly established within hours of plating, it is likely that low passage tumours have a similar genomic profile to that demonstrated in tumours previously, i.e., LOH at 16q, rather than acquiring further genomic changes to allow *in vitro* proliferation. In humans, the tumours show remarkable growth, with lesions reaching up to 10 cm across *in vivo*, with little peritumoural stroma interspersed between tumour cells. It is interesting to speculate that it is this low dependence on stroma that allows development of *in vitro* CPCC.

CPCC are able to proliferate *in vitro* and are hence useful for investigating functional consequences of targeting pathways highlighted in the previous chapter. Whilst these cells are noted to stop proliferating typically after 5 serial subclones, preventing the development of cell lines, the tumours are of a sufficient size to generate significant amounts of CPCC. Characterisation of CPCC demonstrates consistent expression of cytokeratins seen in the hair follicle and related structures such as eccrine ducts. Theses features are retained in 2D as well as 3D culture. CPCC also do not express full length CYLD, indicating their purity. We attempted to reintroduce wild type CYLD into CPCC to develop an isogenic control, but found that this reduced cell viability. This suggests that the loss of functional CYLD in this cellular context is important to initiate the tumour phenotype and maybe the key driver mutation. Cell cycle analysis demonstrated a sub G0/G1 peak that is suggestive of apoptosis. Further characterisation was not pursued given the rarity of these samples.

CPCC were grown on 3D tissue culture scaffolds as to determine of this would alter the expression of TRK proteins. Lagadec *et al.* have found in that TRKA expression whilst high in breast cancer, was low in cell lines derived

from breast cancers (Lagadec, Meignan et al. 2009). Instead of overexpressing TRK artificially in the cell line, 3D growth alone was able to restore TRK expression, making this a model that was suitable to test the effects of TRK inhibition. The level of TRK expression however was not as high as seen in the tumours, and hence this model also has its own limitations.

6.5 Conclusions

Primary cell cultures are useful to investigate the functional consequences of gene knockdown. Furthermore they are useful for determining the utility of targeting dysregulated pathways with therapeutic agents. Here, CPCC are derived from fresh tumours and are characterised. In the following chapter, these cells are utilised for functional assays and drug testing, offering interesting insight into the biology of CYLD defective tumours.

7 CHAPTER 7: Functional studies in CYLD defective primary cell cultures

7.1 Introduction

CYLD transgenic murine models do not develop cylindroma tumours, precluding functional analysis *in vivo*. Using CPCC, we explore the role of targeting dysregulated TRK signalling using short hairpin RNA (shRNA) to silence TRKB and TRKC in altering cell viability. Furthermore, we can explore the functional effect of DKK2 knockdown. Given the precious nature of these CPCC, a variety of functional assays were performed to give insight into various biological aspects of this cell model. Here we describe the preliminary investigation of the effect of knockdown of TRK and DKK proteins in the assays described below.

7.2 Results

7.2.1 Functional TRK signalling in CPCC

To demonstrate functional TRK signalling in 3D CPCCs, we stimulated the cultures with recombinant human cognate ligands of TRK receptors. 3D CPCCs were stimulated with NGF (100ng/ml), BDNF (100ng/ml) and NT3 (50ng/ml) for up to 24 hours, and cells were assayed for levels of phosphorylated ERK and BCL2. Changes in phosphorylated ERK were seen within an hour (Figure 63), whilst BCL2 levels typically altered after 6 hours (Figure 64). The loading control used to compare the phosphorylated ERK was obtained by stripping and reprobing the membrane with total ERK. This suggested unequal loading of protein between lanes.

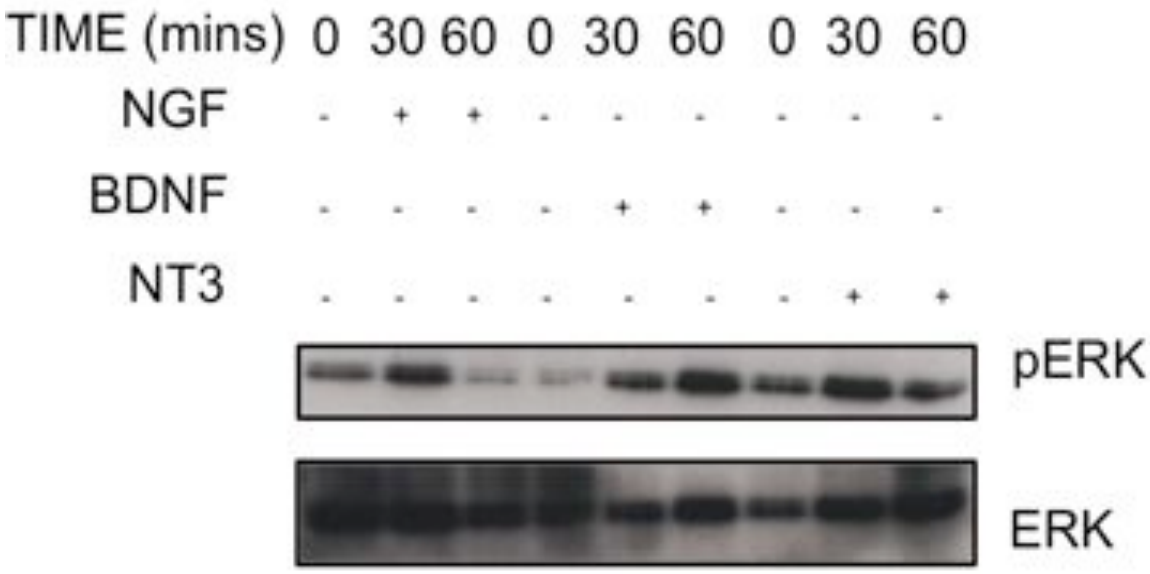

Figure 63 Stimulation of 3D CPCC with NGF, BDNF and NT3, with effect on phosphorylated ERK protein levels.

Cylindroma cells grown on 3D scaffolds and stimulated with NGF, BDNF and NT3 for the periods indicated, and then transferred to ice cold PBS, and cell lysates were extracted for immunoblotting. Membranes were probed with antibodies to phosphorylated ERK. All experiments were repeated at least three times.

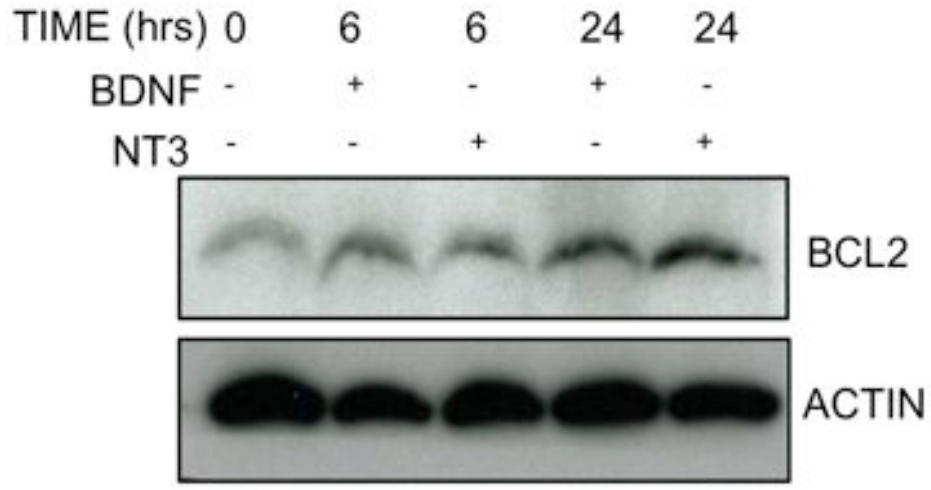

Figure 64 Stimulation of 3D CPCC with NGF, BDNF and NT3, with effect on BCL2 protein levels.

Cylindroma cells grown on 3D scaffolds and stimulated with NGF, BDNF and NT3 for the periods indicated, and then transferred to ice cold PBS, and cell lysates were extracted for immunoblotting. Membranes were probed with antibodies to BCL2. All experiments were repeated at least three times.

7.2.2 TRKB and TRKC silencing reduces cell viability and colony formation

To assess the functional significance of TRKB and TRKC in cylindromas, primary cell cultures were established from fresh tumour samples from the patients that contributed samples used for the molecular profiling and used for functional studies . These primary cells were transduced with lentiviruses expressing short hairpin (sh) RNAs targeting TRKB and TRKC. The shRNA vectors carried a GFP reporter allowing monitoring of delivery and a puromycin gene allowing selection - cells were grown in media containing puromycin for 48 hours post transfection resulting in cultures that were approximately 100% GFP positive when analysed (Figure 65).

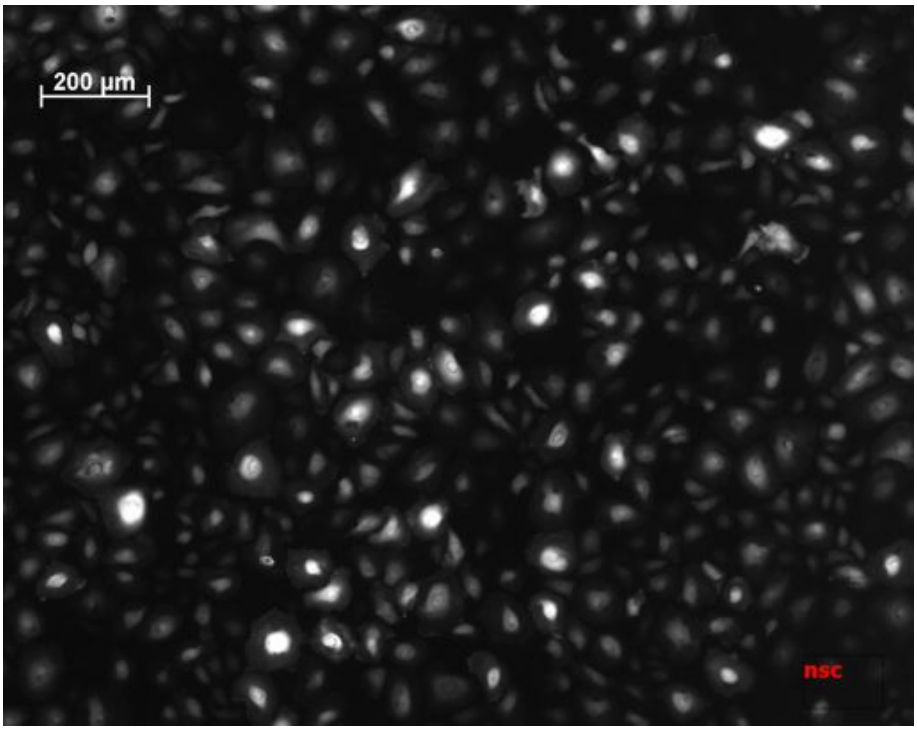

Figure 65 Lentiviral transfection of CPCC.
Cells seen after 3 days of puromycin selection. Transfection efficiency was monitored by GFP expression, and was between 90-100% following selection.

TRKB and TRKC knockdown was assayed using immunoblotting and corroborated with quantitative PCR, as the differences in protein expression particularly with TRKB were subtle (Figure 66,
Figure 67). After 10-14 days in culture, cells were fixed, stained and colonies were counted. Primary cells with knockdown of TRKB and TRKC demonstrated a modest reduction (20-40%; $p<0.05$) in colony formation (Figure 68).

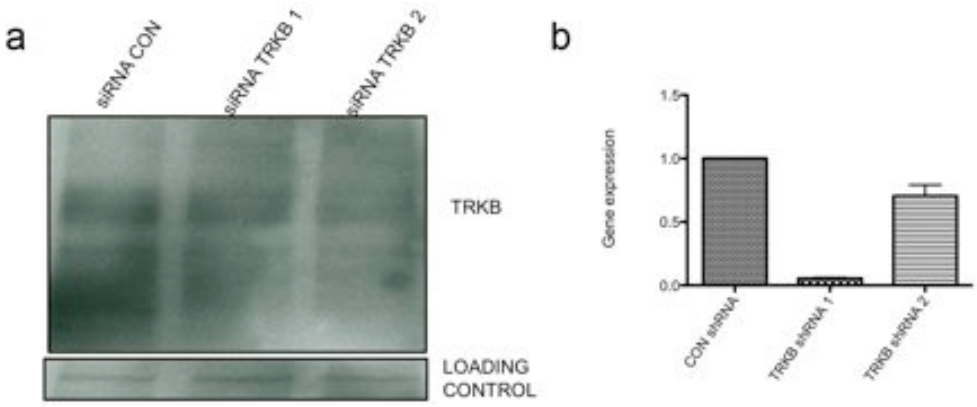

Figure 66 TRKB shRNA mediated silencing assessed by protein expression and transcript expression. CPCC cells were subject to lentiviral mediated short hairpin RNA knockdown of TRKB and these were compared against a control hairpin. (a) Knockdown was assessed at the protein level using immunoblotting, and (b) at the transcript level using quantitative PCR.

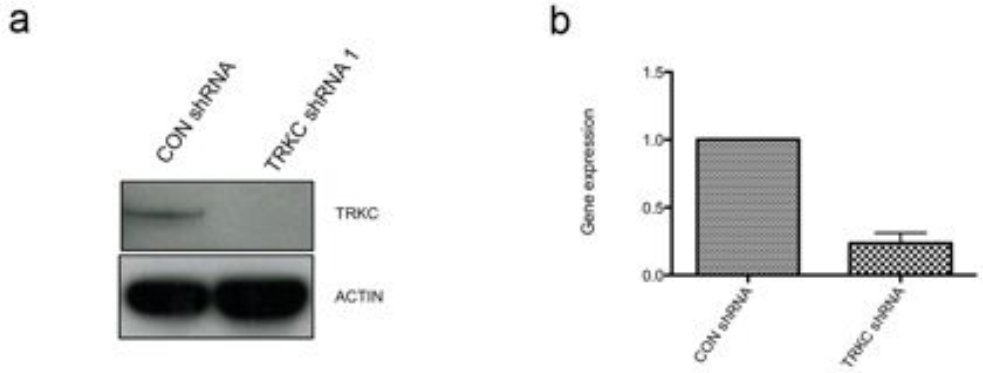

Figure 67 TRKC shRNA mediated silencing assessed by protein expression and transcript expression.. CPCC cells were subject to lentiviral mediated short hairpin RNA knockdown of TRKC and these were compared against a control hairpin. (a) Knockdown was assessed at the protein level using immunoblotting, and (b) at the transcript level using quantitative PCR.

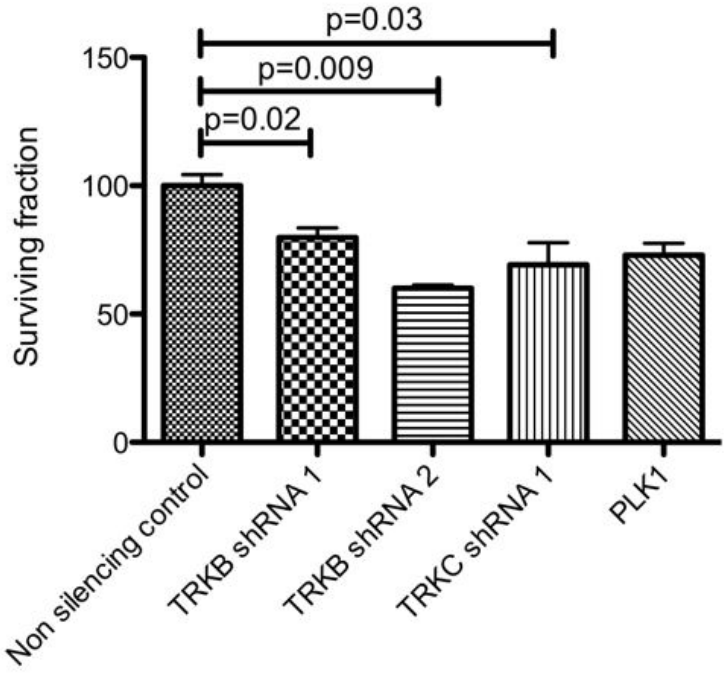

Figure 68 Lentiviral knockdown of TRKB and TRKC results in reduced viability.
Following puromycin selection, GFP positive cells were plated and grown over 12 days. TRKB and TRKC knockdown resulted in reduced colony formation. All experiments were repeated at least three times. Error bars indicate standard error of the mean

7.2.3 Three-dimensional primary cell cultures of cylindroma cells are sensitive to TRK inhibitors

To determine if these cultures were dependent on TRK signalling for survival, they were treated with small molecule TRK kinase inhibitors. These molecules inhibit all TRK receptors and feasibly cause a greater effect on cell viability than inhibition of individual TRKs by shRNA. As a control, CPCC were also exposed to salicylic acid which has previously been shown to effect survival in CYLD deficient cells (Brummelkamp, Nijman et al. 2003). Cells were only modestly sensitive to salicylic acid (surviving fraction (SF_{50}) 1.5mM), but were much more so to the panTRK inhibitors, lestaurtinib (CEP-701) (SF_{50}, 4.57μM), AG879 (SF_{50}, 4.21 μM) and K252a (SF_{50}, 366 nM) (Figure 69).

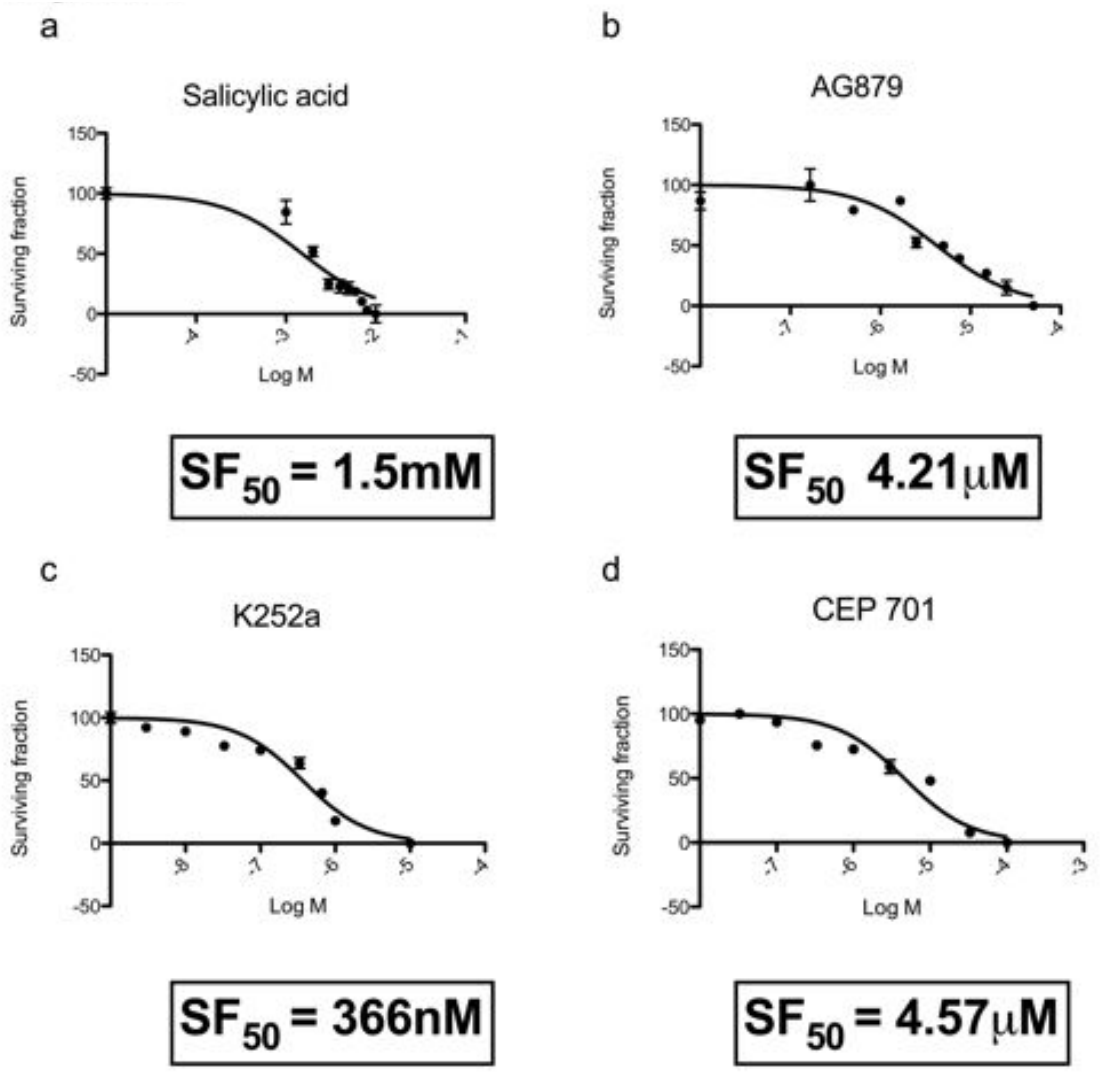

Figure 69 3D CPCC demonstrate an increased sensitivity to TRK inhibitors relative to aspirin. Cylindroma 3D cell cultures were grown for two weeks in the presence of salicylic acid, K252a, Tyrphostin AG879 and lestaurtinib (CEP-701) in triplicate in a 96 well format. This was repeated using at least three different tumours, from different body sites in three patients. Cell viability was assessed using a luminescent cell viability assay at the end of this period and dose response curves were generated. Cylindroma cells were sensitive to lestaurtinib at micromolar levels, whilst salicylic acid had a similar effect at milimolar levels.

7.2.4 Functional analysis of DKK2 knockdown in CPCC

To better understand how DKK2 expression contributes to tumourigenesis, we investigated the functional consequence of *DKK2* silencing in cylindroma tumour derived cells. Cells were grown both in adherent conditions (Figure 65) and in suspension (Figure 70). A GFP reporter linked by an internal ribosomal entry site to the targeting hairpins, allowed for monitoring of transfection efficiency and for puromycin selection. DKK2 silencing was assayed by immunoblotting (Figure 71).

One hairpin used (DKK2-1) had no effect on DKK2 protein expression levels. Cylindroma cells with silenced DKK2 demonstrated increased survival after growth for 96 hours on collagen coated tissue cultured plastic compared to controls (Figure 72). In addition to an increase in short term viability, DKK2 knockdown resulted in increased colony formation (Figure 73). In keeping with the differing efficiency of knockdown seen with the two shRNAs used, this effect was more convincing in shRNA DKK2-2. As the spiradenoma cells were highly disorganised and had fewer intercellular connections, we investigated if DKK2 knockdown was associated with anchorage independent growth. DKK2 knockdown resulted in increased trend towards anchorage independent growth when grown in suspension and compared to matched cells grown in adherent conditions, but this difference was not statistically significant (Figure 74). In addition, DKK2 knockdown resulted in increased migration when assayed using a scratch assay (Figure 75). Finally, we investigated if DKK2 knockdown resulted in an increased resistance to apoptosis when exposed to TNF; DKK2 knockdown resulted in a trend towards increased sensitivity to TNF induced apoptosis, though this was not statistically significant (Figure 76).

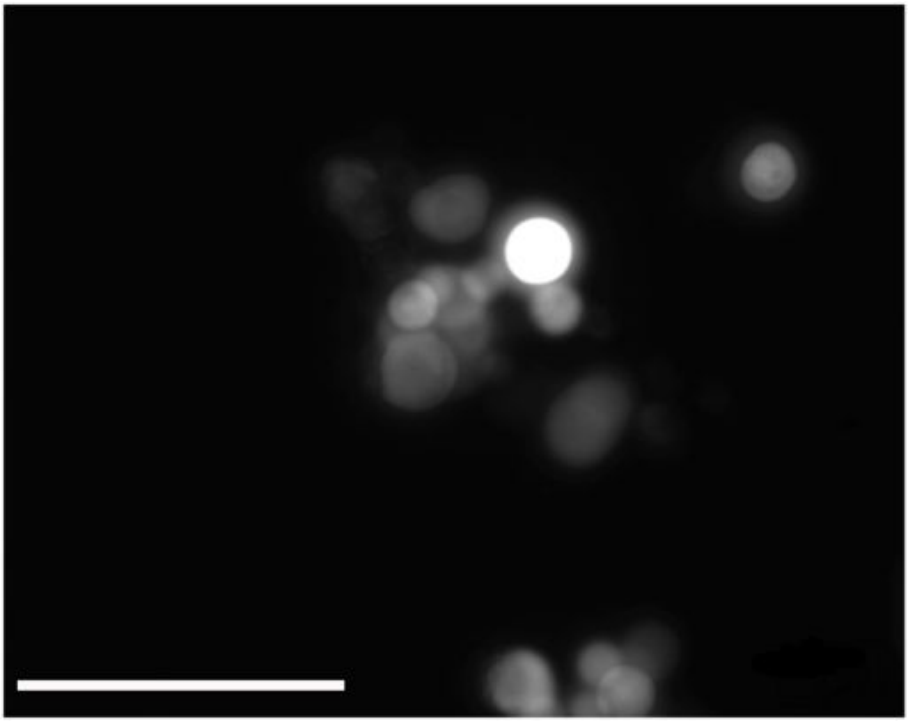

Figure 70 Transfected cylindroma primary cells growing in suspension.
Growth in suspension following treatment of tissue culture plastic with poly-HEMA coating (20x original magnification; scale bar indicates 100μm).

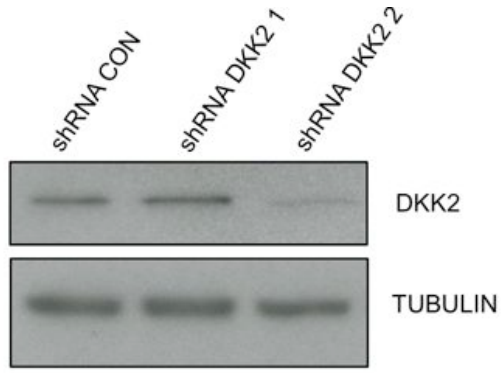

Figure 71 DKK2 shRNA mediated silencing assessed by protein expression.
Total cell lysate from GFP positive cells were separated by SDS-PAGE, immunoblotted and probed with antibodies against DKK2.

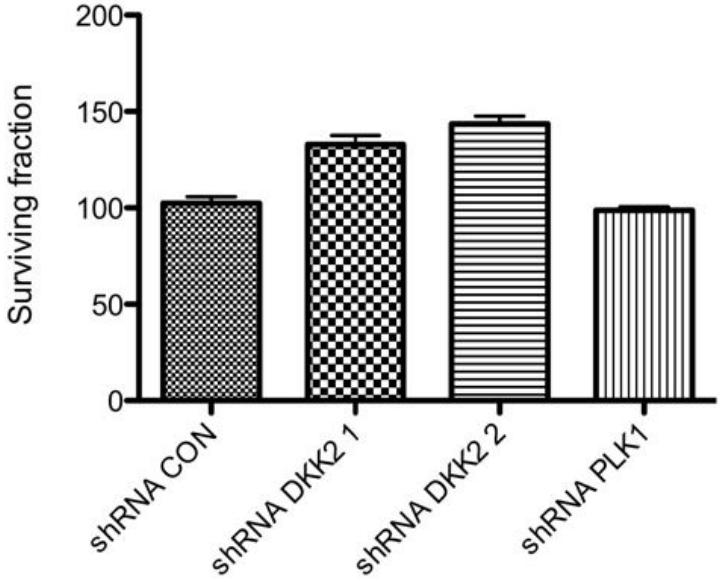

Figure 72 DKK2 silencing results in increased short term viability
Transfected cylindroma primary cells were plated in triplicate in a 96-well format, grown for 96 hours and the surviving fraction was assayed using a luminescent cell viability assay. All error bars indicate standard error of the mean.

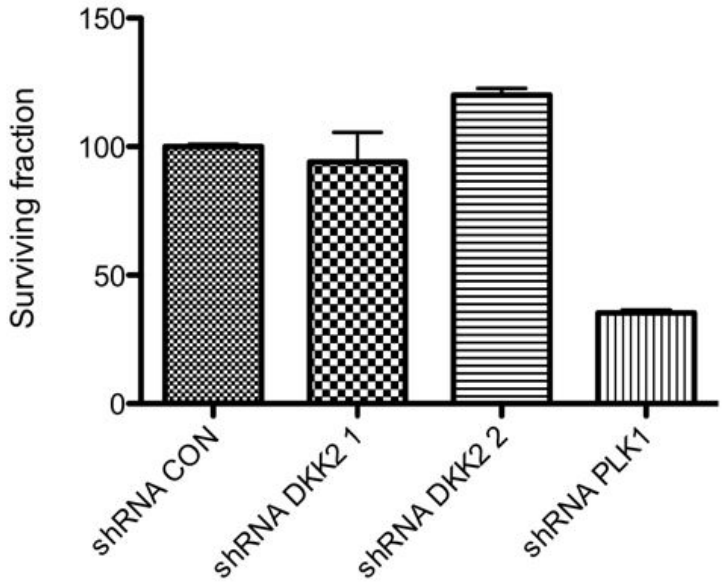

Figure 73 DKK2 silencing results in increased colony formation.
Transfected cylindroma primary cells were plated onto collagen coated tissue culture plastic and grown for 10-14 days. Colonies were fixed, stained and colonies were counted. All error bars indicate standard error of the mean.

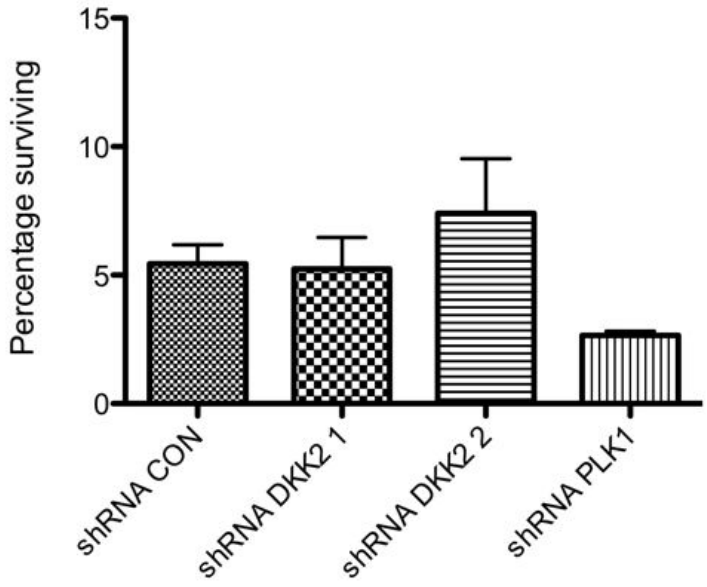

Figure 74 DKK2 silencing results in increased anchorage independent growth.
Transfected cylindroma primary cells were plated in triplicate in a 96 well format, in matched poly-HEMA and collagen coated wells, allowing for growth in suspension and in adherence to be compared. The percentage of surviving cells was then calculated as a ratio at 96 hours using a luminescent cell viability assay as a readout. All error bars indicate standard error of the mean.

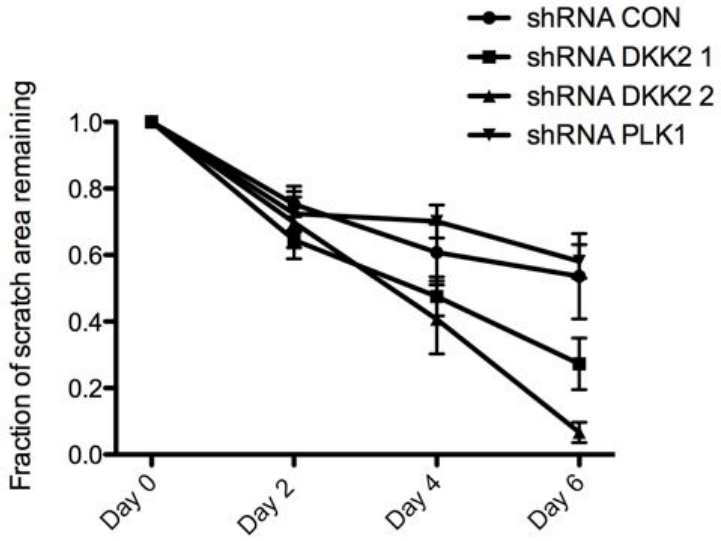

Figure 75 DKK2 knockdown results in increased migration.
Cylindroma primary cells were plated and grown to confluence, and the reduction in size of a scratch made in the centre of the tissue culture well monitored every 12 hours. Error bars indicate standard error of the mean.

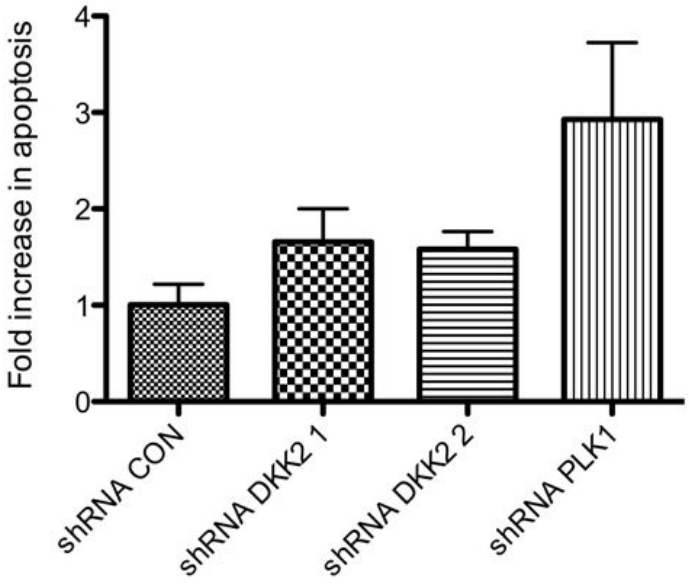

Figure 76 DKK2 knockdown results in an increased sensitivity to TNF induced apoptosis.
Cells were plated in 96 well format, grown for 48 hours, and TNF (50ng/ml) was added. Cleaved caspase 3 was assayed using a luminescent assay that served as a readout for apoptosis, and the fold increase was compared to control treated cells in triplicate. All error bars indicate standard error of the mean.

7.3 Discussion

We established TRK signalling was effective in cylindroma primary cell culture using recombinant human BDNF and NT3 for TRKB and TRKC respectively, and demonstrated increased expression of phosphorylated ERK and BCL2. These experiments are preliminary, and ideally could be optimised further to allow for more consistent loading across lanes. To delineate the advantage conferred by TRKB and TRKC expression, we used a lentiviral mediated knockdown system. This demonstrated reduced colony formation in TRKB and TRKC deficient cells supporting the pathogenic role of these receptors. Protein expression as a means to assess knockdown of TRKB suggested a small level of knockdown seen, which was supported by quantitative PCR at the transcript level. Further optimization of shRNA design in future work to target TRKB in particular would allow for greater level of knockdown and potentially clarify the consequence of more effective TRKB knockdown.

To investigate whether dysregulated TRK signalling in patients with truncating CYLD mutations represented a druggable pathway, we employed a 3D primary cell culture model. As seen in breast cancer (Lagadec, Meignan et al. 2009), TRK expression in vitro was low when 2D cylindroma cell culture was compared to tumours. 3D culture was associated with an increase in expression of TRKB and TRKC, allowing us to use this as an in vitro model to assay cell viability in the presence of TRK inhibitors. The reduction in viability at micromolar concentrations of TRK inhibitors is encouraging, particularly as these tumours are amenable to transcutaneous or intralesional drug delivery. We attempted to determine whether the mechanism of action of TRK inhibition in our primary cell culture model was mediated by ERK or BCL2. This analysis proved not to be possible because of the high sensitivity of the primary cells to TRK inhibitors, resulting in only very few live cells after TRK inhibitor exposure. The result seen with lestaurtinib is particularly interesting as this agent was recently found in a screen of 2800 compounds to be a potent inhibitor of NFκB, suggesting it may target two key pathways in CYLD mutant tumours (Miller, Huang et al. 2010). Lestaurtinib is currently in phase 3 clinical trials (Shabbir and Stuart 2010), and serum levels in patients on a 80 mg oral dose twice a day was 17- 25 μm after

taking the drug for 28 days (Marshall, Kindler et al. 2005), suggesting that the sensitivity of CYLD deficient tumours suggested by our model may be achievable in patients. This is in contrast to aspirin, where millimolar amounts appear to be necessary to obtain an equivalent effect, whilst patients typically achieve peak serum levels of 0.36mM after high doses of 800mg orally (Cerletti, Bonati et al. 1984). As novel agents with increased pan TRK specificity such as AZ-23 become available (Thress, Macintyre et al. 2009), patients with truncating CYLD mutations may be another step closer to non-surgical alternatives for this disfiguring disease.

We then went on to determine if reduced DKK2 expression in CYLD defective tumour primary cell cultures conferred a survival advantage to tumour cells. We demonstrated trends towards increased cellular proliferation, anchorage independent growth and cellular migration. We found a slight increased sensitivity to apoptosis in these cells, suggesting DKK2 loss may result in increased tumour volume predominantly via an increased proliferative drive. Further work, potentially with optimized shRNA targetting DKK2 may yield more conclusive results.This data corroborated the transcriptome analysis of DKK2 low tumours, where signalling networks that were overexpressed in spiradenomas were principally involved in cellular proliferation, and the increased Ki 67 positivity seen in spiradenomas.
Increased Wnt/Beta-catenin signalling has been shown to result in increased NFκB signalling, an effect mediated via increased transcription of beta transducing repeat-containing protein (βTrCP). This has been shown to reduce levels of IκB by ubiquitination (Spiegelman, Slaga et al. 2000) and may account for the increased expression of NFκB target genes seen in DKK2 low tumours such as *TNFAIP2*. DKK2 low tumours may thus have a proliferative advantage due to synergistic effects of oncogenic Wnt and NFκB signalling in a CYLD defective cellular context.

These data support a model where epigenetic changes influencing Wnt/Beta-catenin signalling may be a key player in specification of cutaneous tumour organisation in CYLD defective tumours. Contiguous growth in CYLD defective tumours, DKK2 modulation by methylation and the resulting proliferative

phenotype seen in DKK2 low models *in vivo* and *in vitro* led us to refine the model described in Chapter 3, that may account for the different histological phenotypes seen in CYLD defective tumours (Figure 77).

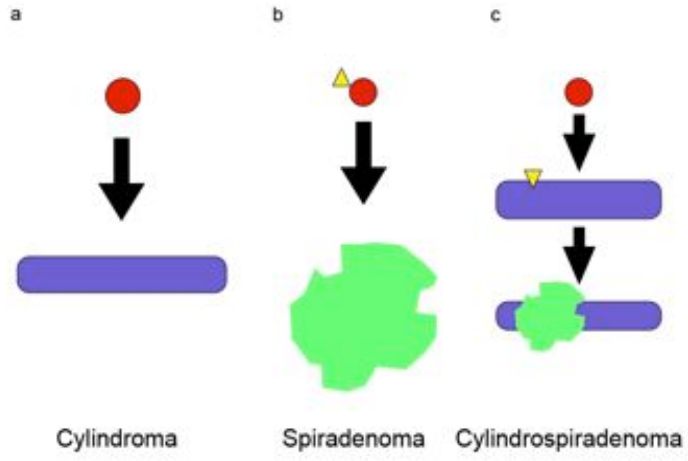

Figure 77 A model of epigenetic specification of tumours.
Given the contiguous growth of cylindromas and spiradenomas, and the finding the DKK2 expression was altered with change of organisation, we propose a model where perturbation of patterning by altered Wnt signalling may specify tumour phenotype in CYLD mutation carriers. (a) Loss of heterozygosity in a putative pluripotent hair follicle cell results in exclusive expression of mutant CYLD, conferring a growth advantage for these cells, (indicated by the red sphere). The cells are restricted to a tubular growth pattern due, giving rise to a structure where growth by extension, branching and budding is feasible (indicated by the purple column). This structure when folded gives rise to the finding that the tumour cells are seen organised as cylinders irrespective of the way the tumour is sectioned. (b) Loss of patterning associated with reduced expression of DKK2 may arise due to an epigenetic event (indicated by the yellow triangle) such as methylation, giving rise to a disorganised mass of tumour cells (indicated by the green mass), with no restriction to grow in a tubular pattern. (c) A late event that results in loss of DKK2 may result in a tumour that has already grown as a cylindroma to develop a region that is poorly organised, a finding supported by clinical and pathological observations of the coexistence of two tumour types in the same specimen.

This model is one where the timing of an epigenetic event such as *DKK2* methylation accounts for the different histological patterns seen in CYLD defective tumours. Whilst this remains to be validated in an *in vivo* model, it raises the possibility that the prevention of progression of cylindromas to painful spiradenomas may be feasible with methylation inhibitors such as azacitadine. A further intriguing prospect that is yet to be explored is the role of epigenetic silencing of Wnt inhibitors in other sporadic skin tumours where Wnt signalling is pathogenic, such as basal cell carcinoma (Hoseong Yang, Andl et al. 2008; Kriegl, Horst et al. 2009).

7.4 Conclusions

Here we demonstrate in CPCC, functional consequences of targeting two pathways highlighted from transcriptomic analysis of CYLD defective tumours. Firstly, dysregulated TRK is amenable to targeting with in human TRK inhibitors such as lestaurtinib, and use of such an agent may have the added benefit of activity against NFκB . Secondly, modulation of dysregulated Wnt signalling by DKK2 is supported by these data, and in some cases, this may be mediated by an epigenetic mechanism.

8 Concluding remarks

Herein we describe exciting data of direct translational relevance. CYLD cutaneous syndrome is a disease with severe impact on quality of life. Using a genomic approach, we characterised the genomic and transcriptomic changes in CYLD defective tumours. Dysregulated TRK and Wnt signalling are demonstrated, consequent to LOH at 16q, and functional effects are characterised in a primary cell culture model derived from CYLD defective tumours. Importantly, TRK inhibitors, which are currently in use in humans with demonstrated safety profiles, have an effect in this *in vitro* model. In addition to the translational implications of the TRK data, this model also offers insight into cutaneous tumour patterning via modulation of Wnt/Beta-catenin signalling. The implications of both these findings may bear relevance for sporadic skin cancer such as basal cell carcinoma, the commonest human cancer. TRKC, a target highlighted by this work in CYLD defective tumours, is shown to be overexpressed in 70% of BCC. This finding is intriguing and warrants further investigation. BCC is also dependent on pathogenic Wnt signalling, and the epigenetic influences on the different histological patterns seen in BCC remain to be explored. These data from the characterisation of CYLD defective tumours may hence be important in improving the understanding of common skin cancer.

9 References

Adly, M. A., H. A. Assaf, et al. (2005). "Human scalp skin and hair follicles express neurotrophin-3 and its high-affinity receptor tyrosine kinase C, and show hair cycle-dependent alterations in expression." Br J Dermatol **153**(3): 514-20.

Aguilera, O., M. F. Fraga, et al. (2006). "Epigenetic inactivation of the Wnt antagonist DICKKOPF-1 (DKK-1) gene in human colorectal cancer." Oncogene **25**(29): 4116-21.

Albores-Saavedra, J., S. C. Heard, et al. (2005). "Cylindroma (dermal analog tumor) of the breast: a comparison with cylindroma of the skin and adenoid cystic carcinoma of the breast." Am J Clin Pathol **123**(6): 866-73.

Alvarez-Rodríguez, R., M. Barzi, et al. (2007). "Bone morphogenetic protein 2 opposes Shh-mediated proliferation in cerebellar granule cells through a TIEG-1-based regulation of Nmyc." J Biol Chem **282**(51): 37170-80.

Andl, T., S. T. Reddy, et al. (2002). "WNT signals are required for the initiation of hair follicle development." Dev Cell **2**(5): 643-53.

Annunziata, C. M., R. E. Davis, et al. (2007). "Frequent engagement of the classical and alternative NF-kappaB pathways by diverse genetic abnormalities in multiple myeloma." Cancer Cell **12**(2): 115-30.

April, C., B. Klotzle, et al. (2009). "Whole-genome gene expression profiling of formalin-fixed, paraffin-embedded tissue samples." PLoS ONE **4**(12): e8162.

Arévalo, J. C., J. Waite, et al. (2006). "Cell survival through Trk neurotrophin receptors is differentially regulated by ubiquitination." Neuron **50**(4): 549-59.

Bahta, A. W., N. Farjo, et al. (2007). "Premature Senescence of Balding Dermal Papilla Cells In Vitro Is Associated with p16(INK4a) Expression." J Invest Dermatol.**128**(5):1088-94

Barrandon, Y. and H. Green (1987). "Three clonal types of keratinocyte with different capacities for multiplication." Proc Natl Acad Sci USA **84**(8): 2302-6.

Berk DR, B. S. (2010). "Milia: A review and classification." Journal of American Dermatology **59**(6): 1050-1063.

Biggs, P. J., P. Chapman, et al. (1996). "The cylindromatosis gene (cyld1) on chromosome 16q may be the only tumour suppressor gene involved in the development of cylindromas." Oncogene **12**(6): 1375-7.

Biggs, P. J., R. Wooster, et al. (1995). "Familial cylindromatosis (turban tumour syndrome) gene localised to chromosome 16q12-q13: evidence for its role as a tumour suppressor gene." Nat Genet **11**(4): 441-3.

Bignell, G. R., W. Warren, et al. (2000). "Identification of the familial cylindromatosis tumour-suppressor gene." Nat Genet **25**(2): 160-5.

Blake, P. W. and J. R. Toro (2009). "Update of cylindromatosis gene (CYLD) mutations in Brooke-Spiegler syndrome: novel insights into the role of deubiquitination in cell signaling." Hum Mutat **30**(5): 1-12.

Blasing, H., S. Hendrix, et al. (2005). "Pro-inflammatory cytokines upregulate the skin immunoreactivity for NGF, NT-3, NT-4 and their receptor, p75NTR in vivo: a preliminary report." Arch Dermatol Res **296**(12): 580-4.

Bollag, G., P. Hirth, et al. (2010). "Clinical efficacy of a RAF inhibitor needs broad target blockade in BRAF-mutant melanoma." Nature **467**(7315): 596-9.

Boyce, S. T. and R. G. Ham (1983). "Calcium-regulated differentiation of normal human epidermal keratinocytes in chemically defined clonal culture and serum-free serial culture." J Invest Dermatol **81**(1 Suppl): 33s-40s.

Bruckner-Tuderman, L., M. Pfaltz, et al. (1991). "Cylindroma overexpresses collagen VII, the major anchoring fibril protein." J Invest Dermatol **96**(5): 729-34.

Brummelkamp, T. R., S. M. Nijman, et al. (2003). "Loss of the cylindromatosis tumour suppressor inhibits apoptosis by activating NF-kappaB." Nature **424**(6950): 797-801.

Butti, M. G., I. Bongarzone, et al. (1995). "A sequence analysis of the genomic regions involved in the rearrangements between TPM3 and NTRK1 genes producing TRK oncogenes in papillary thyroid carcinomas." Genomics **28**(1): 15-24.

Cerletti, C., M. Bonati, et al. (1984). "Plasma levels of salicylate and aspirin in healthy volunteers: relevance to drug interaction on platelet function." J Lab Clin Med **103**(6): 869-77.

Chan, E. F., U. Gat, et al. (1999). "A common human skin tumour is caused by activating mutations in beta-catenin." Nat Genet **21**(4): 410-3.

Chen, G. and D. V. Goeddel (2002). "TNF-R1 signaling: a beautiful pathway." Science **296**(5573): 1634-5.

Chen, Z. J. (2005). "Ubiquitin signalling in the NF-kappaB pathway." Nat Cell Biol **7**(8): 758-65.

Chen-Tsai, C. P., M. Colome-Grimmer, et al. (2004). "Correlations among neural cell adhesion molecule, nerve growth factor, and its receptors, TrkA, TrkB, TrkC, and p75, in perineural invasion by basal cell and cutaneous squamous cell carcinomas." Dermatologic surgery : official publication for American Society for Dermatologic Surgery [et al] **30**(7): 1009-16.

Coe, B. P., B. Ylstra, et al. (2007). "Resolving the resolution of array CGH." Genomics **89**(5): 647-53.

Crain, R. C. and E. B. Helwig (1961). "Dermal cylindroma (dermal eccrine cylindroma)." Am J Clin Pathol **35**: 504-15.

DECIPHER. (2009). "DatabasE of Chromosomal Imbalance and Phenotype in Humans using Ensembl Resources." Retrieved 20/03/09, 2009, from https://decipher.sanger.ac.uk/perl/application/patient/2856.

Demchenko, Y. N., O. K. Glebov, et al. (2010). "Classical and/or alternative NF B pathway activation in multiple myeloma." Blood **115**(17): 3541-52.

Donovan, J. (2009). "Review of the hair follicle origin hypothesis for basal cell carcinoma." Dermatologic surgery : official publication for American Society for Dermatologic Surgery [et al] **35**(9): 1311-23.

Dutton, R., T. Yamada, et al. (1999). "Regulation of spinal motoneuron differentiation by the combined action of Sonic hedgehog and neurotrophin 3." Clin Exp Pharmacol Physiol **26**(9): 746-8.

Ermolaeva, M., H. Sebban, et al. (2006). Early postnatal lethality in knock-in mice expressing a truncated catalytically inactive form of CYLD NF-kB: 20 Years on the Road from Biochemistry to Pathology Keystone Symposium.

.

Flaherty, K. T., I. Puzanov, et al. (2010). "Inhibition of mutated, activated BRAF in metastatic melanoma." N Engl J Med **363**(9): 809-19.

Friedman, C. S., M. A. O'Donnell, et al. (2008). "The tumour suppressor CYLD is a negative regulator of RIG-I-mediated antiviral response." EMBO Rep **9**(9): 930-6.

Fuchs, E. (2007). "Scratching the surface of skin development." Nature **445**(7130): 834-42.

Fuchs, E. and S. Raghavan (2002). "Getting under the skin of epidermal morphogenesis." Nat Rev Genet **3**(3): 199-209.

Gao, J., L. Huo, et al. (2008). "The tumor suppressor CYLD regulates microtubule dynamics and plays a role in cell migration." J Biol Chem **283**(14): 8802-9.

Geetha, T., J. Jiang, et al. (2005). "Lysine 63 polyubiquitination of the nerve growth factor receptor TrkA directs internalization and signaling." Mol Cell **20**(2): 301-12.

Geetha, T., M. L. Seibenhener, et al. (2008). "p62 serves as a shuttling factor for TrkA interaction with the proteasome." Biochem Biophys Res Commun **374**(1): 33-7.

Gerretsen, A. L., S. C. van der Putte, et al. (1993). "Cutaneous cylindroma with malignant transformation." Cancer **72**(5): 1618-23.

Ghazizadeh, S. and L. B. Taichman (2001). "Multiple classes of stem cells in cutaneous epithelium: a lineage analysis of adult mouse skin." EMBO J **20**(6): 1215-22.

Giard, D. J., S. A. Aaronson, et al. (1973). "In vitro cultivation of human tumors: establishment of cell lines derived from a series of solid tumors." J Natl Cancer Inst **51**(5): 1417-23.

Given, K., K. Pickrell, et al. (1977). "Dermal cylindroma (turban tumor). Case report." Plast Reconstr Surg **59**(4): 582-7.

Goette, D. K., M. A. McConnell, et al. (1982). "Cylindroma and eccrine spiradenoma coexistent in the same lesion." Arch Dermatol **118**(4): 274-4.

Goldstein, A. M., S. J. Bale, et al. (1993). "Sun exposure and basal cell carcinomas in the nevoid basal cell carcinoma syndrome." J Am Acad Dermatol **29**(1): 34-41.

Gujral, T. S. and G. MacBeath (2010). "A system-wide investigation of the dynamics of Wnt signaling reveals novel phases of transcriptional regulation." PLoS ONE **5**(4): e10024.

Gunnarsson, R., J. Staaf, et al. (2008). "Screening for copy-number alterations and loss of heterozygosity in chronic lymphocytic leukemia--a comparative study of four differently designed, high resolution microarray platforms." Genes Chromosomes Cancer **47**(8): 697-711.

Harwood, C. A., J. M. McGregor, et al. (2003). "High frequency and diversity of cutaneous appendageal tumors in organ transplant recipients." J Am Acad Dermatol **48**(3): 401-8.

Hayflick, l. (1965). "The limited in vitro lifetime of human diploid cell strains." Exp Cell Res **37**: 614-36.

Hellerbrand, C., E. Bumes, et al. (2007). "Reduced expression of CYLD in human colon and hepatocellular carcinomas." Carcinogenesis **28**(1): 21-7.

Hirata, H., Y. Hinoda, et al. (2009). "Wnt Antagonist Gene DKK2 Is Epigenetically Silenced and Inhibits Renal Cancer Progression through Apoptotic and Cell Cycle Pathways." Clinical Cancer Research **15**(18): 5678-5687.

Hoseong Yang, S., T. Andl, et al. (2008). "Pathological responses to oncogenic Hedgehog signaling in skin are dependent on canonical Wnt/β-catenin signaling." Nat Genet **40**(9): 1130-1135.

Hövelmeyer, N., F. T. Wunderlich, et al. (2007). "Regulation of B cell homeostasis and activation by the tumor suppressor gene CYLD." J Exp Med **204**(11): 2615-27.

Hu, Y. F., Z.-J. Zhang, et al. (2006). "An Epidermal Neural Crest Stem Cell (EPI-NCSC) Molecular Signature." Stem Cells **24**(12): 2692-2702.

Huang, E. J. and L. F. Reichardt (2001). "Neurotrophins: roles in neuronal development and function." Annu Rev Neurosci **24**: 677-736.

Jenner, Leone, et al. (2007). "Gene mapping and expression analysis of 16q loss of heterozygosity identifies WWOX and CYLD as being important in determining clinical outcome in multiple myeloma." Blood **110**(9): 3291-300.

Jin, W., W. R. Reiley, et al. (2007). "Deubiquitinating enzyme CYLD regulates the peripheral development and naive phenotype maintenance of B cells." J Biol Chem **282**(21): 15884-93.

Jin, W., C. Yun, et al. (2007). "TrkC binds to the bone morphogenetic protein type II receptor to suppress bone morphogenetic protein signaling." Cancer Res **67**(20): 9869-77.

Jungehülsing, M., M. Wagner, et al. (1999). "Turban tumour with involvement of the parotid gland." The Journal of laryngology and otology **113**(8): 779-83.

K Moriwaki, D., K Sugawara, H Kobayashi, R Massoumi and M Ishii (2007). "A role of CYLD in hair cycling mouse " Journal of Investigative Dermatology **127**(s107): s107.

Kariya, Y., T. Moriya, et al. (2005). "Sex steroid hormone receptors in human skin appendage and its neoplasms." Endocr J **52**(3): 317-25.

Katayama, H., W. R. Brinkley, et al. (2003). "The Aurora kinases: role in cell transformation and tumorigenesis." Cancer Metastasis Rev **22**(4): 451-64.

Katoh, M. and M. Katoh (2007). "WNT signaling pathway and stem cell signaling network." Clin Cancer Res **13**(14): 4042-5.

Kazakov, D. V., R. Soukup, et al. (2005). "Brooke-Spiegler syndrome: report of a case with combined lesions containing cylindromatous, spiradenomatous, trichoblastomatous, and sebaceous differentiation." Am J Dermatopathol **27**(1): 27-33.

Kazakov, D. V., S. Thoma-Uszynski, et al. (2009). "A case of Brooke-Spiegler syndrome with a novel germline deep intronic mutation in the CYLD gene leading to intronic exonization, diverse somatic mutations, and unusual histology." Am J Dermatopathol **31**(7): 664-73.

Keats, J., R. Fonseca, et al. (2007). "Promiscuous Mutations Activate the Noncanonical NF-κB Pathway in Multiple Myeloma." Cancer Cell **12**(2): 131-144.

Kerscher, O., R. Felberbaum, et al. (2006). "Modification of proteins by ubiquitin and ubiquitin-like proteins." Annu Rev Cell Dev Biol **22**: 159-80.

Kikuno, N., H. Shiina, et al. (2008). "Genistein mediated histone acetylation and demethylation activates tumor suppressor genes in prostate cancer cells." Int J Cancer **123**(3): 552-60.

Knudson, A. G., Jr. (1971). "Mutation and cancer: statistical study of retinoblastoma." Proc Natl Acad Sci U S A **68**(4): 820-3.

Komander, D., C. J. Lord, et al. (2008). "The structure of the CYLD USP domain explains its specificity for Lys63-linked polyubiquitin and reveals a B box module." Mol Cell **29**(4): 451-64.

Kondo, S. and K. Aso (1981). "Establishment of a cell line of human skin squamous cell carcinoma in vitro." Br J Dermatol **105**(2): 125-32.

Kovalenko, A., C. Chable-Bessia, et al. (2003). "The tumour suppressor CYLD negatively regulates NF-kappaB signalling by deubiquitination." Nature **424**(6950): 801-5.

Kriegl, L., D. Horst, et al. (2009). "LEF-1 expression in basal cell carcinomas." Br J Dermatol **160**(6): 1353-6.

Lagadec, C., S. Meignan, et al. (2009). "TrkA overexpression enhances growth and metastasis of breast cancer cells." Oncogene **28**(18): 1960-70.

Lamb, J. (2006). "The Connectivity Map: Using Gene-Expression Signatures to Connect Small Molecules, Genes, and Disease." Science **313**(5795): 1929-1935.

Lang, P. G., A. C. McKelvey, et al. (1987). "Three-dimensional reconstruction of the superficial multicentric basal cell carcinoma using serial sections and a computer." Am J Dermatopathol **9**(3): 198-203.

Lee, J., Y. S. Yoon, et al. (2008). "Epigenetic silencing of the WNT antagonist DICKKOPF-1 in cervical cancer cell lines." Gynecol Oncol **109**(2): 270-4.

Leonard, N., R. Chaggar, et al. (2001). "Loss of heterozygosity at cylindromatosis gene locus, CYLD, in sporadic skin adnexal tumours." J Clin Pathol **54**(9): 689-92.

Lim, J. H., B. Stirling, et al. (2007). "Tumor suppressor CYLD regulates acute lung injury in lethal Streptococcus pneumoniae infections." Immunity **27**(2): 349-60.

Lin, K. K., V. Kumar, et al. (2009). "Circadian clock genes contribute to the regulation of hair follicle cycling." PLoS Genet **5**(7): e1000573.

Liu, H.-H., M. Xie, et al. (2006). "Essential role of TAK1 in thymocyte development and activation." Proc Natl Acad Sci USA **103**(31): 11677-82.

Lodygin, D., A. S. Yazdi, et al. (2003). "Analysis of 14-3-3sigma expression in hyperproliferative skin diseases reveals selective loss associated with CpG-methylation in basal cell carcinoma." Oncogene **22**(35): 5519-24.

Luo, J., N. L. Solimini, et al. (2009). "Principles of cancer therapy: oncogene and non-oncogene addiction." Cell **136**(5): 823-37.

Manning, A. M. and R. J. Davis (2003). "Targeting JNK for therapeutic benefit: from junk to gold?" Nat Rev Drug Discov **2**(7): 554-65.

Marchio, C., R. Natrajan, et al. (2008). "The genomic profile of HER2-amplified breast cancers: the influence of ER status." J Pathol **216**(4): 399-407.

Marshall, J. L., H. Kindler, et al. (2005). "Phase I trial of orally administered CEP-701, a novel neurotrophin receptor-linked tyrosine kinase inhibitor." Invest New Drugs **23**(1): 31-7.

Martin-Zanca, D., S. H. Hughes, et al. (1986). "A human oncogene formed by the fusion of truncated tropomyosin and protein tyrosine kinase sequences." Nature **319**(6056): 743-8.

Martins, C. and E. Bartolo (2000). "Brooke-Spiegler syndrome: treatment of cylindromas with CO2 laser." Dermatol Surg **26**(9): 877-80; discussion 881.

Massoumi, R. (2006). "Cyld Inhibits Tumor Cell Proliferation by Blocking Bcl-3-Dependent NF-κB Signaling." Cell **125**(4): 665-677.

Massoumi, R., S. Kuphal, et al. (2009). "Down-regulation of CYLD expression by Snail promotes tumor progression in malignant melanoma." Journal of Experimental Medicine **206**: 221-232.

Massoumi, R. and R. Paus (2007). "Cylindromatosis and the CYLD gene: new lessons on the molecular principles of epithelial growth control." Bioessays **29**(12): 1203-14.

Massoumi, R., M. Podda, et al. (2006). "Cylindroma as tumor of hair follicle origin." J Invest Dermatol **126**(5): 1182-4.

Matsumoto, K., R. K. Wada, et al. (1995). "Expression of brain-derived neurotrophic factor and p145TrkB affects survival, differentiation, and invasiveness of human neuroblastoma cells." Cancer Res **55**(8): 1798-806.

Meybehm, M. and H. P. Fischer (1997). "Spiradenoma and dermal cylindroma: comparative immunohistochemical analysis and histogenetic considerations." Am J Dermatopathol **19**(2): 154-61.

Michal, M., J. Lamovec, et al. (1999). "Spiradenocylindromas of the skin: tumors with morphological features of spiradenoma and cylindroma in the same lesion: report of 12 cases." Pathol Int **49**(5): 419-25.

Miller, S. C., R. Huang, et al. (2010). "Identification of known drugs that act as inhibitors of NF-kappaB signaling and their mechanism of action." Biochem Pharmacol **79**(9): 1272-80.

Monteiro, A. N. A. (2003). "BRCA1: the enigma of tissue-specific tumor development." Trends Genet **19**(6): 312-5.

Natrajan, R., B. Weigelt, et al. (2009). "An integrative genomic and transcriptomic analysis reveals molecular pathways and networks regulated by copy number aberrations in basal-like, HER2 and luminal cancers." Breast Cancer Res Treat **121**: 575-589.

Nilsson, M., A. B. Undèn, et al. (2000). "Induction of basal cell carcinomas and trichoepitheliomas in mice overexpressing GLI-1." Proc Natl Acad Sci USA **97**(7): 3438-43.

O'Blenes, C. A. E., J. P. Lee, et al. (2010). "An unusual case of turban tumor syndrome treated with total scalp excision and advancement flap and skin graft reconstruction." Ann Plast Surg **65**(1): 107-9.

Ohyama, M., A. Terunuma, et al. (2006). "Characterization and isolation of stem cell-enriched human hair follicle bulge cells." J Clin Invest **116**(1): 249-60.

Oosterkamp, H. M., H. Neering, et al. (2006). "An evaluation of the efficacy of topical application of salicylic acid for the treatment of familial cylindromatosis." Br J Dermatol **155**(1): 182-5.

Orentreich, N. (1959). "Autografts in alopecias and other selected dermatological conditions." Ann N Y Acad Sci **83**: 463-79.

Oshima, H., A. Rochat, et al. (2001). "Morphogenesis and renewal of hair follicles from adult multipotent stem cells." Cell **104**(2): 233-45.

Perez-Losada, J. and A. Balmain (2003). "Stem-cell hierarchy in skin cancer." Nat Rev Cancer **3**(6): 434-43.

Qiao, W., A. G. Li, et al. (2006). "Hair follicle defects and squamous cell carcinoma formation in Smad4 conditional knockout mouse skin." Oncogene **25**(2): 207-17.

Rajan, N., J. A. A. Langtry, et al. (2009). "Tumor mapping in 2 large multigenerational families with CYLD mutations: implications for disease

management and tumor induction." Archives of dermatology **145**(11): 1277-84.

Randall, V. A. (2008). "Androgens and hair growth." Dermatologic therapy **21**(5): 314-28.

Randall, V. A., N. A. Hibberts, et al. (2000). "The hair follicle: a paradoxical androgen target organ." Horm Res **54**(5-6): 243-50.

Rasband, W. S. "ImageJ, U. S. National Institutes of Health, Bethesda, Maryland, USA, http://rsb.info.nih.gov/ij/, 1997-2009.".

Reiley, W. (2004). "Negative Regulation of JNK Signaling by the Tumor Suppressor CYLD." Journal of Biological Chemistry **279**(53): 55161-55167.

Reiley, W. W., W. Jin, et al. (2007). "Deubiquitinating enzyme CYLD negatively regulates the ubiquitin-dependent kinase Tak1 and prevents abnormal T cell responses." J Exp Med **204**(6): 1475-85.

Reiley, W. W., M. Zhang, et al. (2006). "Regulation of T cell development by the deubiquitinating enzyme CYLD." Nat Immunol **7**(4): 411-7.

Ricci, A., S. Greco, et al. (2001). "Neurotrophins and neurotrophin receptors in human lung cancer." Am J Respir Cell Mol Biol **25**(4): 439-46.

Saggar, S., K. A. Chernoff, et al. (2008). "CYLD mutations in familial skin appendage tumours." J Med Genet **45**(5): 298-302.

Saha, R. N., X. Liu, et al. (2006). "Up-regulation of BDNF in astrocytes by TNF-alpha: a case for the neuroprotective role of cytokine." J Neuroimmune Pharmacol **1**(3): 212-22.

Salhi, A., D. Bornholdt, et al. (2004). "Multiple familial trichoepithelioma caused by mutations in the cylindromatosis tumor suppressor gene." Cancer Res **64**(15): 5113-7.

Sandbank, M. and D. Bashan (1978). "Multiple trichoepithelioma and breast carcinoma. Simultaneous appearance of epithelioma adenoides cysticum and infiltrating lobular carcinoma of the breast." Archives of dermatology **114**(8): 1230.

Sato, H., H. Suzuki, et al. (2007). "Frequent epigenetic inactivation of DICKKOPF family genes in human gastrointestinal tumors." Carcinogenesis **28**(12): 2459-66.

Scala, S., K. Wosikowski, et al. (1996). "Brain-derived neurotrophic factor protects neuroblastoma cells from vinblastine toxicity." Cancer Res **56**(16): 3737-42.

Scheibe, P., U.-D. Braumann, et al. (2010). "Image-processing chain for a three-dimensional reconstruction of basal cell carcinomas." Exp Dermatol **19**(7): 689-91.

Schmidt-Ullrich, R., T. Aebischer, et al. (2001). "Requirement of NF-kappaB/Rel for the development of hair follicles and other epidermal appendices." Development **128**(19): 3843-53.

Schmidt-Ullrich, R. and R. Paus (2005). "Molecular principles of hair follicle induction and morphogenesis." Bioessays **27**(3): 247-61.

Shabbir, M. and R. Stuart (2010). "Lestaurtinib, a multitargeted tyrosine kinase inhibitor: from bench to bedside." Expert Opin Investig Drugs **19**(3): 427-36.

Sick, S., S. Reinker, et al. (2006). "WNT and DKK determine hair follicle spacing through a reaction-diffusion mechanism." Science **314**(5804): 1447-50.

Snippert, H. J., A. Haegebarth, et al. (2010). "Lgr6 marks stem cells in the hair follicle that generate all cell lineages of the skin." Science **327**(5971): 1385-9.

So, P.-L., A. W. Langston, et al. (2006). "Long-term establishment, characterization and manipulation of cell lines from mouse basal cell carcinoma tumors." Exp Dermatol **15**(9): 742-50.

Spiegelman, V. S., T. J. Slaga, et al. (2000). "Wnt/beta-catenin signaling induces the expression and activity of betaTrCP ubiquitin ligase receptor." Molecular Cell **5**(5): 877-82.

Stegmeier, F., M. E. Sowa, et al. (2007). "The tumor suppressor CYLD regulates entry into mitosis." Proc Natl Acad Sci U S A **104**(21): 8869-74.

Stokes, A., C. Wakano, et al. (2006). "TRPA1 is a substrate for de-ubiquitination by the tumor suppressor CYLD." Cell Signal **18**(10): 1584-94.

Subramanian, A., P. Tamayo, et al. (2005). "Gene set enrichment analysis: a knowledge-based approach for interpreting genome-wide expression profiles." Proc Natl Acad Sci U S A **102**(43): 15545-50.

Suzuki, H., M. Toyota, et al. (2008). "Frequent epigenetic inactivation of Wnt antagonist genes in breast cancer." Br J Cancer **98**(6): 1147-56.

Suzuki, R. and H. Shimodaira (2006). "Pvclust: an R package for assessing the uncertainty in hierarchical clustering." Bioinformatics **22**(12): 1540-2.

Tan, D. S., M. B. Lambros, et al. (2007). "Getting it right: designing microarray (and not 'microawry') comparative genomic hybridization studies for cancer research." Lab Invest **87**(8): 737-54.

Tauriello, D. V. F., A. Haegebarth, et al. (2010). "Loss of the tumor suppressor CYLD enhances Wnt/beta-catenin signaling through K63-linked ubiquitination of Dvl." Mol Cell **37**(5): 607-19.

Tellechea, O., J. P. Reis, et al. (1995). "Dermal cylindroma. An immunohistochemical study of thirteen cases." Am J Dermatopathol **17**(3): 260-5.

Thress, K., T. Macintyre, et al. (2009). "Identification and preclinical characterization of AZ-23, a novel, selective, and orally bioavailable inhibitor of the Trk kinase pathway." Mol Cancer Ther **8**(7): 1818-27.

Timpl, R., S. Fujiwara, et al. (1984). "Laminin, proteoglycan, nidogen and collagen IV: structural models and molecular interactions." Ciba Found Symp **108**: 25-43.

Trompouki, E., E. Hatzivassiliou, et al. (2003). "CYLD is a deubiquitinating enzyme that negatively regulates NF-kappaB activation by TNFR family members." Nature **424**(6950): 793-6.

Trompouki, E., D. Kontoyiannis, et al. (2006). Targeted inactivation of the cylindromatosis tumor suppressor gene causes perinatal lethality in mice. NF-kB: 20 Years on the Road from Biochemistry to Pathology Keystone Symposium.

Trompouki, E., A. Tsagaratou, et al. (2009). "Truncation of the catalytic domain of the cylindromatosis tumor suppressor impairs lung maturation." Neoplasia **11**(5): 469-76.

Tsichritzis, T., P. C. Gaentzsch, et al. (2007). "A Drosophila ortholog of the human cylindromatosis tumor suppressor gene regulates triglyceride content and antibacterial defense." Development.**134**(14):2605-14.

Tunggal, L., J. Ravaux, et al. (2002). "Defective laminin 5 processing in cylindroma cells." Am J Pathol **160**(2): 459-68.

Turner, N., M. B. Lambros, et al. (2010). "Integrative molecular profiling of triple negative breast cancers identifies amplicon drivers and potential therapeutic targets." Oncogene **29**(14): 2013-2023.

Venza, I., M. Visalli, et al. (2010). "FOXE1 is a target for aberrant methylation in cutaneous squamous cell carcinoma." Br J Dermatol **162**(5): 1093-7.

Vernon, H. J., E. A. Olsen, et al. (1988). "Autosomal dominant multiple cylindromas associated with solitary lung cylindroma." J Am Acad Dermatol **19**(2 Pt 2): 397-400.

Volter, C., G. Baier, et al. (2002). "[Cylindrocarcinoma in a patient with Brooke-Spiegler syndrome]." Laryngorhinootologie **81**(3): 243-6.

Weber, L., G. Wick, et al. (1984). "Basement membrane components outline the tumour islands in cylindroma." Br J Dermatol **111**(1): 45-51.

Weeraratna, A. T., J. T. Arnold, et al. (2000). "Rational basis for Trk inhibition therapy for prostate cancer." Prostate **45**(2): 140-8.

Welch, J. P., R. S. Wells, et al. (1968). "Ancell-Spiegler cylindromas (turban tumours) and Brooke-Fordyce Trichoepitheliomas: evidence for a single genetic entity." J Med Genet **5**(1): 29-35.

Wolf, B. A., J. L. Gluckman, et al. (1985). "Benign dermal cylindroma of the external auditory canal: a clinicopathological report." Am J Otolaryngol **6**(1): 35-8.

Workman, C., L. J. Jensen, et al. (2002). "A new non-linear normalization method for reducing variability in DNA microarray experiments." Genome Biol **3**(9): research0048.

Wright, A., W. W. Reiley, et al. (2007). "Regulation of Early Wave of Germ Cell Apoptosis and Spermatogenesis by Deubiquitinating Enzyme CYLD." Dev Cell **13**(5): 705-16.

Wu, C., A. Ramirez, et al. (2007). "A functional dynein-microtubule network is required for NGF signaling through the Rap1/MAPK pathway." Traffic **8**(11): 1503-20.

Yang, W.-L., X. Zhang, et al. (2010). "Emerging role of Lys-63 ubiquitination in protein kinase and phosphatase activation and cancer development." Oncogene **29**(32): 4493-4503.

Yauch, R. L., S. E. Gould, et al. (2008). "A paracrine requirement for hedgehog signalling in cancer." Nature **455**(7211): 406-10.

Yin, M. J., Y. Yamamoto, et al. (1998). "The anti-inflammatory agents aspirin and salicylate inhibit the activity of I(kappa)B kinase-beta." Nature **396**(6706): 77-80.

Yoshida, H., H. Jono, et al. (2005). "The tumor suppressor cylindromatosis (CYLD) acts as a negative regulator for toll-like receptor 2 signaling via negative cross-talk with TRAF6 AND TRAF7." J Biol Chem **280**(49): 41111-21.

Young, A., R. Kellermayer, et al. (2006). "CYLD mutations underlie Brooke–Spiegler, familial cylindromatosis, and multiple familial trichoepithelioma syndromes." Clin Genet **70**(3): 246-249.

Zhang, G., Y. Huang, et al. (2006). "Diverse phenotype of Brooke?Spiegler syndrome associated with a nonsense mutation in the CYLD tumor suppressor gene." Exp Dermatol **15**(12): 966-970.

Zhang, J., B. Stirling, et al. (2006). "Impaired regulation of NF-κB and increased susceptibility to colitis-associated tumorigenesis in CYLD-deficient mice." J Clin Invest **116**(11): 3042-3049.

Zheng, G., L. Hu, et al. (2004). "CYLD mutation causes multiple familial trichoepithelioma in three Chinese families." Hum Mutat **23**(4): 400.

Zhong, S., C. R. Fields, et al. (2007). "Pharmacologic inhibition of epigenetic modifications, coupled with gene expression profiling, reveals novel targets of aberrant DNA methylation and histone deacetylation in lung cancer." Oncogene **26**(18): 2621-34.

Zhu, F., X. Xia, et al. (2007). "IKKalpha shields 14-3-3sigma, a G(2)/M cell cycle checkpoint gene, from hypermethylation, preventing its silencing." Molecular Cell **27**(2): 214-27.

10 Appendix A

Online video supporting information

To access the videos, please enter the URL addresses indicated in blue below into a web browser.

Supplementary video 1 **Cylindroma tumours are contiguous.** A video of a virtual flight through one column of tumour cells (green) to a distinctly formed column (purple) via a connecting bridge of tumour cells found further in the block. (http://www.youtube.com/watch?v=95biz3YEDhU).

Supplementary video 2 **Cylindromas and spiradenomas are part of the same tumour mass.** An organised region of tumour shown in purple was followed 490μm and was shown to be connected to a disorganised region of tumour. Three organised areas (highlighted in red, blue and green) are also shown extending from the disorganised structure. (http://www.youtube.com/watch?v=WcUSHk9NavI).

Supplementary video 3 **A spiradenoma with a central focus of cylindroma.** A spiradenoma (light blue) with a central organised column of cells indicated in purple. http://www.youtube.com/watch?v=NT7USIzcZPo)